PERFORMANCE-BASED SEISMIC DESIGN OF POST-TENSIONED CONCRETE COLUMNS

by

Qi Zhang

M.A.Sc., The University of British Columbia, 2016

A THESIS SUBMITTED IN PARTIAL FULFILLMENT OF

THE REQUIREMENTS FOR THE DEGREE OF

DOCTOR OF PHILOSOPHY

in

The College of Graduate Studies

(Civil Engineering)

THE UNIVERSITY OF BRITISH COLUMBIA

(Okanagan)

April 2021

The following individuals certify that they have read, and recommend to the College of Graduate Studies for acceptance, a thesis/dissertation entitled:

PERFORMANCE-BASED SEISMIC DESIGN OF POST-TENSIONED CONCRETE COLUMNS

submitted by Qi Zhang in partial fulfillment of the requirements of the degree of Doctor of Philosophy.

M. Shahria Alam, School of Engineering

Supervisor

Solomon Tesfamariam, School of Engineering

Supervisory Committee Member

Kasun Hewage, School of Engineering

Supervisory Committee Member

Anas Chaaban, School of Engineering

University Examiner

Mohamed Elgawady, Missouri University of Science and Technology

External Examiner

Abstract

Bridge structures are critical components of transportation networks. The seismic resistance of bridges not only determines the user safety during earthquakes but also decides the economic recovery of a region after earthquakes. Making bridges earthquake-resistant to provide continuous post earthquake serviceability has been a focus in the industry. In the meantime, accelerated bridge construction is playing an increasingly important role as the construction industry tries to reduce the on-site construction time to minimize traffic interruption. Thus, developing a seismic resilient bridge system becomes a focus of researchers and practicing engineers. To achieve this goal, post-tensioned precast concrete columns in various forms are proposed by researchers. Yet no systematic studies cover various design parameters, which poses difficulty in proposing a design guideline for practicing engineers.

This research first presents an overview of the performance-based design methodology and the post-tensioned rocking column system. Based on the literature review and available testing data, preliminary design guidance is developed and further research need is identified. Equations for calculating viscous damping are proposed. Then, this study examines the dynamic behaviors of post-tensioned rigid columns analytically using Lagrange's method solved with the Fourth-Order Runge-Kutta method. The effects of rocking impacts, tendon stiffness, post-tensioning force, and characteristics of applied loadings on the dynamic behaviors are investigated. Thereafter, finite element models for deformable rocking structures are developed and validated with experimental results. The effect of several factors including concrete strength, post-tensioning force, aspect ratio, axial load ratio, and reinforcement ratio on the seismic performance is presented. Regression analysis is performed to propose equations for calculating the global yielding and stiffness of columns. Under the design philosophy of performance-based design, maximum instantaneous drift-based design criteria are proposed for engineering design. Simplified design charts correlating damage states and drifts are presented

to assist in engineering practice. In the end, case studies using fragility analysis are performed to demonstrate the superior performance of the rocking column system compared with traditional reinforced concrete columns.

Lay Summary

To build seismic-resistant bridges, researchers and engineers started shifting away from the traditional design of reinforced concrete columns with plastic hinges. The post-tensioned rocking column is introduced as a prominent option to make bridges more resilient under earthquake loadings. Existing research projects suggested that this type of system can self-center and reduce permanent deformation compared to traditional fixed-base reinforced concrete columns. However, there is no adequate information on how to design such a system and some of its seismic behavior may not be fully understood. This study aims to fully investigate the seismic performance of post-tensioned concrete columns and provide design guidelines from the perspectives of performance-based design. Comparison with the traditional reinforced concrete column is conducted and its superior performance is demonstrated using a case study.

Preface

A portion of this work has been submitted to peer-reviewed journals and conference proceedings for publication. All literature review, calculations, and numerical models presented in the following publications have been solely carried out by the author. The academic supervisor was only responsible for the guidance and review of the work produced.

Publications related to this thesis include:

Journal papers

1. Zhang, Q., and Alam, M. S. (2016). Evaluating the seismic behavior of segmental unbonded post-tensioned concrete bridge piers using factorial analysis. Journal of Bridge Engineering, 21(4), 04015073, DOI: https://doi.org/10.1061/(ASCE)BE.1943-5592.0000851
2. Zhang, Q., and Alam, M. S. (2019). Performance-based seismic design of bridges: a global perspective and critical review of past, present and future directions. Structure and Infrastructure Engineering, 15:4, 539-554, DOI: https://doi.org/10.1080/15732479.2018.1558269
3. Zhang, Q., and Alam, M. S. (2020). State-of-the-art review of seismic resistant precast bridge columns. Journal of Bridge Engineering. 25(10), 03120001. DOI: https://doi.org/10.1061/(ASCE)BE.1943-5592.0001620
4. Zhang, Q., and Alam, M. S. (2021). Drift-based damage states for reinforced concrete columns and hybrid rocking columns. Journal of Bridge Engineering, to be submitted.

Conference papers

5. Zhang, Q., and Alam, M. S. Performance-based design of highway bridges: a state-of-the-art review. 10th International Conference on Short and Medium Span Bridges, July 30 – August 3, 2018, Quebec City, Canada.
6. Zhang, Q., and Alam, M. S. The dynamics of precast post-tensioned rocking columns. Structures Congress, ASCE, April 19–21, 2018, Fort Worth, Texas, USA.
7. Zhang, Q., and Alam, M. S. State-of-the-art review of seismic-resistant precast bridge columns. 12th Canadian Conference on Earthquake Engineering, June 17-20 2019, Quebec City, Canada.
8. Zhang, Q., and Alam, M. S. Drift-based design criteria for reinforced concrete columns and hybrid rocking columns. IABSE-JSCE Conference on Advances in Bridge Engineering-IV, 26-27 August 2020, Dhaka, Bangladesh.
9. Zhang, Q., and Alam, M. S. Performance-based seismic design of hybrid rocking bridge column. 17th World Conference on Earthquake Engineering, September 27 to October 2, 2021, Sendai, Japan.

Table of Contents

List of Tables

List of Figures

List of Notations

a	Constant implying overall earthquake rates
A_g	Area of column cross-section
A_p	Area of prestressing tendon
A_s	Area of ED bars/mild steel
ASR	Aspect ratio
ALR	Axial load ratio
$ADLR$	Axial dead load ratio
$APLR$	Axial post-tensioning load ratio
ADT	Average daily traffic
$ADTT$	Average daily truck traffic
ADE	Average daily traffic remaining on the damaged bridge
b	A constant determined by the specific earthquake magnitudes or half of the rocking column width
C	Damping coefficient
C_{car}	Rates per distance for operating cars
C_{truck}	Rates per distance for operating trucks
C_{AW}	Average hourly wage for car drivers
C_{ATC}	Average compensation per hour for truck drivers
C_{goods}	Time value of the goods transported in the cargo
D	Column diameter
d	Damage level
DL	Dead load
d_b	Longitudinal reinforcement diameter
DM	Damage measure
e	Elongation of prestressing tendons
$e'(t)$	Translational velocity of the damper
EDP	Engineering demand parameter
ED	Engineering demand, or energy dissipation
EAL	Expected annual loss
k	Tendon stiffness
f_c'	Concrete compressive strength
f_{pi}	Tendon initial prestressing stress

f_{pu}	Tendon ultimate strength
f_{ys}	Yield strength of steel
F_d	Damping forces
g	Gravity acceleration
G	Performance index
h	Height of concrete segment
H	Height of the center of gravity
F	Cumulative distribution function
I	Moment of inertia, route segment length containing a bridge
i	Discount rate
IM	Ground motion intensity measurement
L	Distance from column base to the point of contraflexure, or Lagrange equation
LF	Live load capacity factor
m	Earthquake magnitude, or mass
M_r	Re-centering moment
N	Number of segments
O_{car}	Average vehicle occupancies for cars
O_{truck}	Average vehicle occupancies for trucks
P	Probability, or axial load
PT	Post-tensioning
PV	Present value
P_0	Initial prestressing force
PGA	Peak ground acceleration
PGV	Peak ground velocity
Q	External force
R	Earthquake distance, or dimension parameter, or strength reduction
S_o	Average speed on the intact route
S_d	Average speed on the damaged route
r	Moment arm
r_k	Damage rate
t	Time in year
T	Kinetic energy
V	Potential energy

$\ddot{x}_g$	Horizontal ground acceleration
$\ddot{y}_g$	Vertical ground acceleration
$y(s)$	Expected value of loss given shaking magnitude of s
V	Replacement cost
ρ	Reinforcement ratio
σ	Standard deviation
θ	Rocking rotation, or median value
$\dot{\theta}$	Angular velocity
θ_{peak}	Peak drift ratio
$\theta_{residual}$	Residual drift ratio
$\dot{\theta_{t1}}$	Velocities before the impact
$\dot{\theta_{t2}}$	Velocities after the impact
β	Standard deviation
λ_m	Rate of the seismic event with magnitude greater than m
λ_{re}	Self-centering/re-centering ratio
αD	Distance from the center of the column to the centroid of the compression area
α	A parameter representing the slenderness of the rocking column
ε_s	Steel strain
ε_c	Concrete strain
ε_{cu}	Ultimate concrete strain
$\emptyset$	Standard normal cumulative distribution function

Acknowledgements

I would like to express my gratitude to Prof. M. Shahria Alam, who supervised both my Master's and Ph.D. research. His guidance and support helped me complete my study, gain knowledge, and also confidence in my life. Besides my advisor, I would like to thank the rest of my thesis committee members: Prof. Solomon Tesfamariam and Prof. Kasun Hewage for their insightful comments and encouragement, but also for the challenging questions which incented me to widen my research from various perspectives. I would like to thank Prof. Mohamed ElGawady for being the external examiner of my thesis and for his guidance on the research. I would also like to thank members of the ALAMS research group for providing valuable feedbacks on my study.

I am grateful for the support and guidance from colleagues and managers at WSP, especially Dr. Jianping Jiang and Mr. Keith Holmes for giving me the opportunities to perform research and contribute to the design of major bridge projects. I would also like to thank NSERC, UBC Okanagan and Canadian Precast Prestressed Concrete Institute for providing an excellent platform and research funding.

My appreciation also extends to the Taiji family. Thanks to Bruce, Jane, Nicole, and Sian for creating an environment that I could learn and enjoy when I first came to Canada. Thanks to Beatrice and Susumu, and Cheryl, Jocelyn, Wayne and many other Taiji families for hosting the best and warmest Christmas I ever had.

Last but not the least, I would like to thank my family: my parents, and my fiancée for supporting me spiritually throughout writing this thesis and my life in general.

Dedication

To my parents Wenge Zhang and Lili Jiang

and my fiancée Aizhe Xu

Chapter 1: Introduction and thesis organization

1.1 Background

Bridges are one of the most important infrastructural components. To improve the resilience of infrastructures, the seismic design of bridges is shifting from a simple ductility factor-based design to a sophisticated performance-based design (PBD), which aims at not only preventing collapses but also providing continuous service to the public after earthquakes. The concept of PBD originated several decades ago and has been evolving since. As PBD is relatively new in many design codes, several jurisdictions published guidelines to regulate design practices, such as the guidelines published by the Association of Professional Engineers and Geoscientists of the Province of British Columbia (EGBC 2018). PBD in its current form aims at achieving one or more predicted performance levels after predefined hazards and it does not have to follow the traditional prescribed design procedures. Under the PBD framework, the post-earthquake performance of bridges becomes more important than ever. To meet this challenge, post-tensioned rocking columns were proposed, which are expected to experience less permanent damage compared to that of the traditional cast-in-place (CIP) columns. The PBD framework brings excellent opportunities for novel structural systems that cannot be designed simply using forced based method and force-reduction/ductility factors. The post-tensioned rocking column is a novel structural system that can achieve better seismic performance as well as acceleration construction, thus it has been gaining popularity in the research communities.

Precast concrete elements are frequently used as a technique to accelerate bridge constructions. Precast concrete girders have been successfully used in bridges for many decades. Precast concrete has also been used for bridge deck construction in the form of partial precast deck panels and full-depth panels. In recent years, applications of precast elements have been extended to substructures such as abutments, columns, pier caps, and footings. However, the use of precast substructure elements is still relatively rare in high seismic regions.

This is mainly due to the fact that seismic behavior is highly sensitive to the characteristics of the connections of the earthquake-resisting systems. In seismic design, superstructures are designed elastically; however, substructures are typically designed to take plastic deformations, which require special seismic detailing.

1.2 The objective of the study

The overall objective of this study is to provide essential design guides that facilitate the design of post-tensioned rocking columns under the PBD framework, which makes bridge structures more resilient under earthquake events.

The overall objective can be accomplished through the following individual objectives:

- Review existing testing data and propose regression equations for basic design parameters such as viscous damping calculation and re-centering capacity calculation
- Develop equations of motion for rigid rocking columns and investigate the influence of different components (e.g. tendon stiffness and initial post-tensioning force) on the overall performance
- Evaluate seismic behavior of deformable post-tensioned rocking column and the individual effects and interactions of design parameters
- Develop drift-based design criteria based on the strain-based design criteria in design code
- Evaluate the fragility and loss estimate of the hybrid rocking column and compare it with a traditional reinforced concrete column

1.3 The scope of this research

This study addresses important design issues of the post-tensioning rocking column. This research thoroughly reviews and investigates the use of the post-tensioned rocking column as

the earthquake resist load path following a PBD approach. The scope of this research and its significance are listed below

a. Literature review and data analysis

PBD is a relatively new design methodology and a post-tensioned rocking column is a rapidly evolving system that can be used in seismic regions. A review of the PBD methodology around the world is first conducted. Then the development and especially available experimental testing of the post-tensioned rocking column are also reviewed. Based on the collected experimental test parameters and results from multiple research projects covering a wide range of post-tensioned rocking columns, regression analysis is conducted to propose equations that will facilitate engineering designs.

b. Analytical study of rocking column

Equations of motion for rocking columns are developed considering various parameters. The scope is limited to rigid columns that have one single rocking surface.

c. Finite element analysis of rocking column

Finite element models of the rocking columns are developed using general-purpose finite element software and structural design software. The models are validated based on experimental studies and are further used to perform in-depth analysis and parametric studies.

d. Drift-based damage states and loss estimate

Maximum drift-based damage states of post-tensioned rocking columns are developed and compared with traditional reinforced concrete columns. Fragility analysis and loss estimate of the two systems are also conducted and compared.

1.4 Thesis organization

This thesis consists of eight chapters. **Chapter 1** presents an introduction, objective, and scope of the research. Brief descriptions of the rest of the chapters are presented below:

In Chapter 2, a literature review on PBD is presented, covering its fundamentals, evolutions, current practices, and future directions. The review focuses on damage states proposed by researchers, design criteria used in different jurisdictions, along with loss estimate methodologies. The design criteria from different jurisdictions are compared and discussed.

In Chapter 3, a review and further analysis of rocking columns testing results are conducted. The chapter first provides a summary of the research development and challenges for both researchers and practitioners. Then, based on a large amount of available testing data, regression analysis is performed to propose several design equations such as the equation for calculating viscous damping.

Chapter 4 examines the dynamic behaviors of post-tensioned concrete columns under seismic excitations by developing equations of motion using Lagrange's method and solved using the Fourth-Order Runge-Kutta method. The effects of impacts, tendon stiffness, initial post-tensioning force, and characteristics of applied loadings on the dynamic behaviors are investigated.

Chapter 5 studies the effect of several factors including concrete strength, post-tensioning force, aspect ratio, axial load ratio on the seismic performance. Finite element models are developed and validated with experimental results. Both full factorial analysis and fractional factorial study are performed. Based on the lateral load-displacement responses of the columns, regression analysis is performed to propose equations for calculating the global yielding and stiffness of columns.

Chapter 6 investigates maximum instantaneous drift-based design criteria for both cantilevered reinforced concrete columns and rocking columns by using material strain limits defined in the Canadian Highway Bridge Design Code. Finite element models covering various column aspect ratios, reinforcement ratios, and axial load ratios are used to correlate drifts with damage states. Simplified design charts correlating damage states and drifts are presented to assist in engineering designs.

In Chapter 7, time history analyses of reinforced concrete and hybrid rocking column are performed under near-fault ground motions. Fragility functions for three damage states are developed using residual drift-based damage states. The maximum likelihood method is used for the fragility function fitting. Loss analysis is performed assuming seismic hazards in two regions. Expected annual losses and their present values are calculated to study the cost-benefit of using hybrid rocking columns.

Chapter 8 presents the research conclusions and recommendations for future research.

Chapter 2: State-of-the-art review on performance-based design of bridges

2.1 Background

Performance-based design (PBD) was originated in New Zealand in the 1970s (Priestley 2000) and evolved in the United States in the 1980s (Hamburger et al. 2004). It has been incorporated into several bridge design codes in recent years (CSA 2014; CSA 2019; NZT 2018) and is expected to be adopted by more design codes (Murphy et al. 2020). PBD uses quantitative as well as qualitative design criteria, such as limits in reinforcing steel strain, concrete strain, drift, and descriptive requirements such as no observable damage to connection components. It is a design methodology that explicitly demonstrates the performance of structures (Gibson 1982) and can be applied to various structural systems rather than limited to traditional structural systems. One of the most important features of PBD is that it explicitly connects structural performance with the design process and eliminates intrinsic risks (Lehman et al. 2004; Priestley 2000). The uncertainties of traditional seismic design can be caused by several unrealistic assumptions. For example, the equal displacement assumption is usually used under traditional force-based design, however, this assumption is not valid for structures with very short and long periods. Also, the structural ductility factor is dependent on many factors such as column axial load, lateral confinement, and foundation flexibility, therefore, the force reduction factor from traditional design code may not be appropriate. PBD not only eliminates many unrealistic assumptions but also leads to better risk control and management. Under PBD, the demands and capacities are based on probabilistic models (Mackie and Stojadinović 2005). With the application of PBD, probabilistic life-cycle cost analyses incorporating multiple hazards and continuous deterioration becomes possible (Akiyama et al. 2013; Gidaris et al. 2016; Kameshwar and Padgett 2014; Wen 2001). Therefore, PBD will facilitate decision-makers and stakeholders to allocate funding based on more realistic information (Marsh and Stringer 2013).

A flowchart showing the PBD process is presented in Figure 1. The design starts with the probabilistic hazard analysis and seismic fragility analysis at different hazard levels. Meanwhile, specific PBD criteria are selected. Then, the structural member sizes and material properties are determined to satisfy the performance criteria. From the bridge fragility analysis, structural damage such as reinforcing steel yielding, concrete spalling, bearing failure, and the corresponding losses are estimated. Based on the structural performance and transportation demand, the indirect losses caused by traffic delay and such can be predicted. For important and irregular bridges, project-specific performance design criteria may be needed to optimize the usage of available resources. Therefore, the iteration between cost analysis and design criteria selection may be necessary. For regular bridges, this step is not necessary since the criteria in design codes are well-calibrated for standard highway bridges.

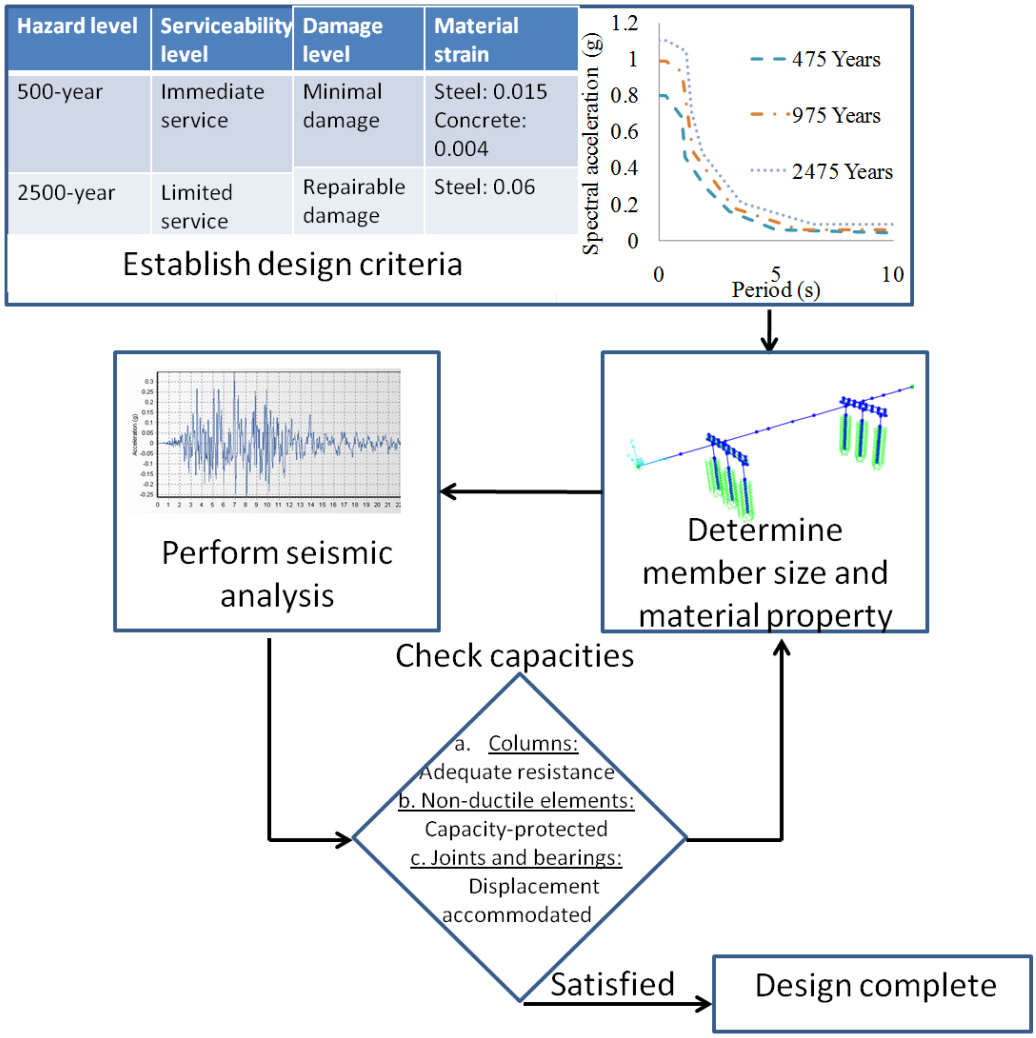

Figure 1 Performance-based design process

2.2 Development of performance-based design

Numerous efforts have been made over the last several decades to develop PBD. ATC-13 (ATC 1985) is one of the earliest reports focused on PBD. This report introduces the methods and data for loss estimates on building evaluation and repair cost in the California area. It is a guideline for estimating death, injuries, economic losses, and repair time. As a follow-up, ATC-36 (Rojahn et al. 1997) published a report on damage and loss estimation methodology and data for Salt Lake County, Utah. The successful experience from ATC-13 (ATC 1985) in California was passed to other states and worldwide. A few years later, FEMA-356 (FEMA 2000)

was published to provide seismic rehabilitation guidelines for buildings. Per FEMA-356 (FEMA 2000), most of the buildings that are rehabilitated as per the guideline would meet the performance level at the design earthquakes. The above-mentioned documents founded the basis of PBD in structural engineering. Although these documents were mainly developed for buildings, the methodologies and conclusions are as well applicable to bridges. PBD for bridges was extensively studied by Priestley (2000), Mackie & Stojadinović, (2007), and other researchers (Billah and Alam 2014; Floren and Mohammadi 2001; Mackie and Stojadinović 2003; Marsh and Stringer 2013; Shamsabadi et al. 2007) which systematically consider the demand and capacity of a system. The development of PBD for bridges is elaborated in the following sections.

2.3 Probabilistic seismic hazard analysis

The first study of probability dates back to mid-1600s and only after that could people make decisions and forecast the future with the help of probability (Long and Narciso 1999). Probability is the central component of risk management. One great advantage of PBD is that it incorporates better risk analysis than traditional design methodologies. Unlike other frequent disasters such as floods and frequent accidents such as vehicle collisions, earthquakes are relatively rare. It is not straightforward to determine what level of seismic loads should be used for the design. Therefore, probabilistic seismic hazard models are needed to predict the uncertainty of the earthquake location, size, and intensity for PBD (Shome 1999). The process of probabilistic seismic demand analysis is presented in (Baker 2008) and briefly discussed in this section.

The first step of probabilistic hazard analysis is to determine all sources of the earthquakes. The sources could be either natural such as a tectonic earthquake or manmade such as explosions and reservoir-induced earthquakes (Bormann et al. 2002). The second step is to determine the magnitude with the corresponding probabilities of earthquake sources based on the prediction

model. An example prediction model of earthquake rate is the Gutenberg-Richter recurrence law (Gutenberg and Richter 1944), which is described in Equation 1,

$$\log \lambda_m = a - bm \quad \text{Equation 1}$$

where λ_m is the rate of the seismic event with a magnitude greater than m, a is a constant denotes overall earthquake rates and b is a constant determined by the specific magnitudes. Based on Gutenberg-Richter law (Gutenberg and Richter 1944), the cumulative distribution function $F_M(m)$ and the probability $P(m)$ of an earthquake with magnitudes between m_j to m_{j+1} can be calculated using Equation 2 and Equation 3 respectively,

$$F_M(m) = \frac{1 - 10^{-b(m-m_{min})}}{1 - 10^{-b(m_{max}-m_{min})}} \quad \text{Equation 2}$$

$$P(m) = F_M(m_{j+1}) - F_M(m_j) \quad \text{Equation 3}$$

where m_j is a set of magnitude, m_{max} and m_{min} are maximum magnitude from an earthquake source and minimum magnitude without engineering importance. The minimum magnitude generally does not have any impact on civil structures. The third step is to determine earthquake distances which can be epicenter or hypocenter depending on the prediction models. The probability of an earthquake occurring within a certain distance to the site can be calculated based on the geometry of the sources. The fourth step is to predict the intensity of the earthquake to the site. Many prediction models have been developed in different regions. One example is the prediction model for eastern North America developed by Atkinson and Boore (2006). A general form of the model can be represented as Equation 4 (Baker 2008),

$$\ln IM = \overline{\ln IM}\,(M, R, \theta) + \sigma(M, R, \theta)\varepsilon \quad \text{Equation 4}$$

where IM is the ground motion intensity measurement, $\overline{\ln IM}\,(M, R, \theta)$ is the mean value of the prediction results, $\sigma(M, R, \theta)$ is its standard deviation, M is the magnitude, R is the distance, θ represents other parameters such as faulting mechanism, and ε is a standard normal random variable. The natural logarithm of intensity measurement is usually assumed to be normally

distributed and therefore, the probability of exceeding this intensity can be computed. The last step is to calculate the rate of exceeding an $IM(x)$ caused by n sources using the total probability theorem using Equation 5 (Baker 2008),

$\lambda(IM > x) = \sum_{i=1}^{n_{sources}} \lambda(M_i > m_{min}) \sum_{j=1}^{n_M} \sum_{k=1}^{n_R} P(IM > x | m_j, r_k) P(M_i = m_j) P(R_i = r_k)$ Equation 5

where λ is the annual rate of occurrence, M is the magnitude, m_{min} is the smallest intensity of interest, R is the distance. The rate of occurrence can be represented by the average return period, which is the reciprocal of the annual rate of occurrence. Also, the description of an earthquake event can be expressed in terms of exceeding a probability in a certain time following the Poisson model. The assumptions under the Poisson model are that earthquake events are independent and the probability of having multiple events in a short period is negligible. The probability P of the earthquake happening at least once in t years is computed as Equation 6,

$$P = 1 - e^{-\lambda t} \qquad \text{Equation 6}$$

where λ is the rate of occurrence.

2.4 Damage states

Damage state is an important component of PBD. Several damage states for PBD have been proposed by researchers (Billah and Alam 2016; Lehman et al. 2004; Mackie et al. 2008). Three commonly used limit states are serviceability, damage control, and collapse prevention (Ghobarah 2001; Kowalsky 2000). Serviceability means that no repair is needed. Damage control means that the damage is repairable. Collapse prevention implies that damage may not be repairable but collapse has to be avoided (Kowalsky 2000). Priestley et al. (1996) defined serviceability based on the column concrete crack width and steel strains. It was suggested that concrete crack should remain small (1mm) so that remedial action is not required. Under serviceability state, reinforcing steel tensile strain should not exceed 0.015 and concrete

compressive strain should not exceed 0.004. A repairable damage limit state was defined by Kowalsky (2000). It was suggested that concrete damage control strain of 0.018 can be conservatively assumed for columns with 1% lateral reinforcement which yields at 450 MPa. For reinforcing steel, Kowalsky (2000) suggested that reinforcement damage control strain is 0.06, which is the rupture strain under cyclic loadings. As well as preventing reinforcement rupture, it is equally important to prevent reinforcement from buckling. Feng et al. (2014) proposed equations to determine reinforcement buckling based on seismic displacement.

Although material strains are the most direct indicators of structural damages, they are not readily available in the field and are difficult to obtain. Therefore, researchers have been seeking other parameters to measure structural damages. Ghobarah (2001) proposed a series of damage states based on drifts. The proposed damage states and drift limits are no damage (drift<0.2%), repairable damage (drift<0.5%), irreparable damage (drift<1.5%), near collapse (drift<2.5%), and collapse (drift>2.5%). Berry and Eberhard (2003) proposed equations relating drifts with longitudinal rebar buckling and concrete cover spalling. The regression equations were based on the studies of about 300 rectangular columns and 170 circular columns. The drift ratio at longitudinal reinforcement buckling is estimated by Equation 7 and 8, and the drift ratio at concrete cover spalling is estimated by Equation 9. These equations have been adopted (Mackie et al. 2008) for developing an integrated performance-based evaluation methodology.

$$\frac{\Delta_{bb}}{L}(\%) = 3.25\left(1 + k_e \rho_{eff}\frac{d_b}{D}\right)\left(1 - \frac{P}{A_g f_c}\right)\left(1 + \frac{L}{10D}\right) \quad \text{Equation 7}$$

$$\rho_{eff} = \rho_s \frac{f_{ys}}{f_c} \quad \text{Equation 8}$$

$$\frac{\Delta_{spall}}{L}(\%) = 1.6\left(1 - \frac{P}{A_g f_c}\right)(1 + \frac{L}{10D}) \quad \text{Equation 9}$$

where k_e is 50 for a rectangular section and 150 for a circular column reinforced with spirals. ρ_s is the transverse reinforcement volumetric ratio, f_{ys} is the yield strength of transverse reinforcement, f_c is the concrete compressive strength, d_b is the longitudinal reinforcement diameter, D is the column diameter, P is the axial load, A_g is the column gross section area and L is the distance from column base to the point of contraflexure.

A ductility-based damage state definition was presented by Hwang et al. (2001). The proposed damage states are no damage, slight damage, moderate damage, extensive damage, and complete damage. The limits for the damage states are first yield displacement ductility, global yield displacement ductility, displacement ductility when concrete strain equals 0.002, and maximum displacement ductility. A summary of column damage states and limits proposed by researchers is listed in Table 1.

There are limited studies defining damage states using residual/permanent drifts. Residual drift-based damage prediction models for shape memory alloy reinforced concrete columns were proposed by Billah and Alam (2016). The proposed equations were able to estimate the drifts corresponding to cracking, yielding, and strength degradation. Based on the observation of the study by Sadrossadat-Zadeh et al. (2007), Billah and Alam (2016) suggested that a residual drift within 0.25% would meet the serviceability requirement, and a residual drift greater than 1% would be a collapse damage state. A design example was presented in (Billah and Alam 2016) based on the PBD methodology.

Table 1 Damage states and definition limits

Reference	Damage states	Limits
Priestley et al. (1996) and Kowalsky (2000)	Serviceability	Rebar strain<0.015 Concrete strain<0.004
	Repairable damage	Rebar strain<0.06 Concrete strain<0.018
Hwang et al. (2001)	Slight damage	First yield displacement ductility
	Moderate damage	Global yield displacement ductility
	Extensive damage	Displacement ductility when concrete strain equals 0.002
	Complete damage	Maximum displacement ductility
Ghobarah (2001)	No damage	Drift < 0.2%
	Repairable damage	Drift < 0.5%
	Irreparable damage	Drift < 1.5%
	Near collapse	Drift ≤ 2.5%
	Collapse	Drift > 2.5%

The performance of bridges is not only determined by the response of columns, it is also affected by many other components such as bearings, foundations, decks, and many other structural and non-structural elements. Some damage states of components other than columns were discussed by Mackie et al. (2008). For instance, although the deck is supposed to behave elastically, Mackie et al. (2008) suggested defining damage states of the deck according to the deck concrete strains. When concrete strain is below 2% spalling strains, no repair is needed. However, when 25% spalling strain is reached, small cracks would occur; and when 50% of spalling strain is reached, large cracks would happen and needs to be repaired with epoxy. (Murphy et al. 2020) proposed damage limits for superstructure-to-abutment vertical offset and defining it as the operational level if the offset is within 9 inches and fully operational when the offset is less than 1 inch. Under a PBD framework, many limits discussed above should be checked by the designers to ensure that the bridges provide satisfactory performance. The design requirements in different codes are discussed in the next section.

It should be noted that most design guidelines specify damage states of substructures based on flexural damage, shear damage should always be avoided at all costs. In the 1994 Northridge

earthquake (Mitchell et al. 1995), 1995 Hyogo-ken nanbu earthquake (Kawashima 2000) and 2008 Wenchuan earthquake (Han et al. 2009; Kawashima et al. 2009), a large number of bridges were damaged because of shear or combined flexural-shear failure. Ideally, bridge superstructures are capacity-protected. Yet, there were still cases that bridges were severely damaged due to failure in concrete girders, steel plate girders, and concrete decks (Kawashima et al. 2011; Schanack et al. 2012). Besides, bridges not only carry traffic but also pipelines and utilities. The utilities attached to bridges can be extensively damaged if they are not adequately flexible (Palermo et al. 2011). In PBD, designers should consider the performance of many components in addition to columns.

2.5 Design criteria

Two decades ago, Ghobarah (2001) recommended that there was a need for consensus on the definition of performance levels, corresponding to damage states, and design criteria. However, the consensus in the bridge community has not been achieved. Various PBD criteria are used by engineers and researchers. Here, a brief description of the design criteria in current design codes and literature are presented and compared. It should be noted that this is neither a complete list of all seismic codes nor complete code descriptions that cover all seismic design circumstances (e.g., specific criteria triggered by liquefaction or unique site conditions). The intent is to compare a few major design codes that are used in seismic zones for standard highway bridges. In this study, standard highway bridges are defined as key elements of a transportation system but are not unique structures that would impede the ongoing economy or security of the region if get damaged.

In Canada, PBD was introduced in the Canadian Highway Bridge Design Code in 2014 (CSA 2014) and continued to evolve in the 2019 code version (CSA 2019). For Major Route Bridges (standard highway bridges), the code requires a return period of 475 years for lower-level design and a return period of 2475 years for upper-level design. At the lower design level, no

rebar yielding is allowed. At the upper design level, extensive damage is permitted. However, the steel strain shall not exceed 0.05 and the core concrete shall not crush.

Following the publication of the Canadian Highway Bridge Design Code 2014 (CSA 2014), the British Columbia Ministry of Transportation and Infrastructure published the Supplement to CHBDC S6-14 (BCMOTI 2016). The British Columbia Supplement uses the same level of expected services for Major Route Bridges. However, the specific strain limits for each damage level are changed to reflect local practices. At the lower-level hazard (475-year return period), the concrete compressive strain is limited to 0.006 and the steel strain is limited to 0.01. At the upper-level hazard (2475-year return period), the core concrete strain is limited to 80% ultimate strain and steel strain is limited to 0.05. In 2019, the design criteria in BCMOTI 2016 were adopted by the 2019 version of the Canadian Highway Bridge Design Code (CSA 2019).

In the LRFD Specifications (AASHTO 2020) and the LRFD Guide Specifications for Seismic Design (AASHTO, 2013), only a single level design based on a 1000-year return period is required. When AASHTO (1981) first adopted the probabilistic method, the return period for the design was 500 years. Before changing the return period from 500 years to 1000 years, the National Cooperative Highway Research Program (NCHRP 2002) proposed two-level design criteria for AASHTO. In the proposed criteria, it was suggested that a 100-year return period is used for lower level (serviceability) design and a 2500-year return period be used for upper level (life safety) design. However, AASHTO rejected this proposal because the return periods were unjustified and were not consistent with the return periods of other hazards (FHWA-NHI 2014). It should be noted that although multiple-level design is not mandatory in AASHTO (2020), other return periods may be used for different performance targets depending on owners (FHWA-NHI 2014).

California Department of Transportation (Caltrans) was the first state to initiate performance-based criteria (Marsh and Stringer 2013). As per Caltrans (2013), California bridge categories are classified as important and ordinary bridges according to the required post-earthquake response. Bridges are defined as important if they: a) provide access to the emergency facility and protect post-earthquake life safety; b) cause major economic impact if closed; c) are critical elements in the local emergency plan. Ordinary bridges are further divided into standard or nonstandard according to their structural regularity. The Caltrans Seismic Design Criteria only apply to ordinary standard bridges. Caltrans uses both probabilistic and deterministic design spectra. The design spectrum is defined as the governing case of 1) a probabilistic spectrum with a return period of 975 years; 2) a deterministic spectrum of any fault near the bridge site with the largest median response resulting from the maximum rupture; 3) a statewide minimum spectrum. Under the design earthquake load, the bridge shall not collapse, however, there may not be access to traffic, and significant damage is permitted.

Oregon Department of Transportation (ODOT) uses a two-level design (life safety and operational) for new bridges and bridges in certain regions (e.g. on or West of US97) (ODOT 2016). For life safety level, 1000-year seismic loading with the force reduction factor for “other” bridges in AASHTO shall be used (e.g. R=3.0 for vertical reinforced concrete pile bents, R=5.0 for vertical steel pile bents). For operational design level, Cascadia Subduction Zone Earthquake seismic loading with the R factor for “essential” bridges shall be used (e.g. R=2.0 for vertical reinforced concrete pile bents, R=3.5 for vertical steel pile bents). Additionally, in Seismic Design Category (SDC) D, ODOT requires material strain within limits for the two-level design. At the 1000-year design level, concrete strain shall not exceed 90% of the ultimate concrete strain (ε_{cu}) computed by Mander’s model. Steel strain shall not exceed the Reduced Ultimate Tensile Strain defined by AASHTO Guide Specifications for LRFD Seismic Bridge Design (AASHTO 2013). The Reduced ultimate tensile strain varies from 0.04 to 0.09

depending on different bar sizes and diameters. For operational design level, the concrete strain shall be limited within 0.005, and steel strain shall not exceed two times the strain hardening strain. The onset of strain hardening varies from 0.005 to 0.015.

The South Carolina Department of Transportation (SCDOT 2008) requires two-level designs which have 462-year and 975-year return periods. The bridge importance is classified into three types from I to III, where I stands for the most important bridges and III stands for the least important bridges. Type I bridges are located on the interstate system or along certain roads. For type I bridges, under 462-year seismic load, the damage shall be limited to minimal damage. Under 975-year seismic loading, the damage should be limited to repairable. The South Carolina Department of Transportation defined specific drift and displacement limits for different damage levels. For example, under 462-year seismic loading, the displacement limit for type I bridges at interior bent with fixed bearing is 0.075H inches (the unit of H is in feet). Under 975-year earthquake event, this limit is 0.3H inches (the unit of H is in feet). Along with the displacement criteria, the SCDOT also provides maximum ductility factors that can be used. For single-column type I bridges, the ductility factor at 462-year and 975-year events are 2.0 and 3.0 respectively.

New York State Department of Transportation (NYSDOT 2015) only requires a two-level design for Critical Bridges. Critical Bridges are defined as bridges on the critical route without readily accessible detours. These bridges shall be functional under seismic load with 1000 years return period and life safety should be protected under seismic load with 2500 years return period. In the case of essential bridges, only a single-level design is required. Essential bridges shall experience repairable damage under seismic load with 1000 years return period. A similar practice is also adopted by the Washington State Department of Transportation (WSDOT 2016).

The Japanese Design Specifications for Highway Bridges uses multi-level seismic design (Kuwabara et al. 2013). The Japanese specification defines two levels of earthquake ground motions (Level 1 and Level 2). Level 1 earthquakes are highly likely to happen during the design life of the bridge and the design criterion is to have no damage. Level 2 earthquake is an event with high intensity and less probability of occurrence. The design criteria are to limit the damage to highly important bridges and to prevent the collapse of standard important bridges. Level 2 earthquake includes two types of earthquakes (Type 1 and Type 2). Type 1 earthquake represents large-scale subduction-type earthquakes and Type 2 represents near-field shallow earthquakes. In the Japanese Design Specifications for Highway Bridges, the seismic hazard is analyzed using deterministic methods, whereas most of the design codes from the U.S.A., Canada, EU, and China use probabilistic methods. Deterministic systems assume that the entire rule is known at any given time in the past and future (Kirchsteiger 1999). Deterministic methods are often used to check the worst scenario earthquakes, which have the largest magnitude and closest distance (McGuire 2001). The deterministic method usually considers a single scenario whereas, the probabilistic method considers multiple scenarios with associated probabilities. Although the probabilistic method is the dominant seismic risk analysis method, the deterministic method plays an important role in high seismic regions such as Japan, where the largest earthquake might occur every 300 years. The deterministic method allows the designer to consider more detailed effects from rupture propagation (McGuire 2001).

China initiated the two-level bridge design in 2008 (China-MOC 2008). The bridge importance is classified into four categories from Class A to Class D. Class A bridges have more than 150 m for single-span lengths, Class B bridges are within 150 m length for single spans. Class C and D are the bridges on less important highways with shorter spans. In the Chinese bridge design code, Class B bridges are designed for a 75 to 100-year return period without damage at the lower design level. At the upper design level, Class B bridges are designed for a 1000 to 2000-

year return period without collapse. In Eurocode (de Normalisation 1998), a 475-year return period is used for the upper-level design which aims at life safety. At the lower level design, the Eurocode does not specify a return period, however, it is suggested that a 95-year return period is used for the lower level design (JRC-Ispra 2012).

In addition to the design codes, many research reports also suggested various design criteria. ACI-341 (2014) suggested using a 50-year return period for the lower-level design and a 2500-year return period for the life safety design. It can be seen that the design criteria between different codes and guidelines are not consistent. Among all the guidelines and codes, Canadian Highway Bridge Design Code 2014 has the strictest criteria at the lower design level. A summary of the design criteria from different codes is presented in Table 2.

Table 2 Performance-based design criteria from various codes

Reference	Hazard levels	Performance requirements
LRFD Specifications (2014)	1000-year seismic load	Life safety
Eurocode (1998)	475-year seismic load	Life safety
Chinese Guidelines (2008)	1000 to 2000-year seismic load	Life safety
	75 to 100-year seismic load	No damage
Canadian Highway Bridge Design Code (2014)	2475-year seismic load	Extensive damage
	475-year seismic load	Minimal damage
Japanese Design Specifications for Highway Bridges (2012)	Large scale subduction-type earthquakes (deterministic)	Life safety
	Major near-field shallow earthquakes (deterministic)	Life safety
	Frequent earthquake (deterministic)	No damage
California DOT (2013)	Probabilistic spectrum with a return period of 975 years	Life safety
	Deterministic spectrum of any fault near the bridge site	
	Statewide minimum spectrum	
Oregon DOT (2016)	1000-year seismic load	Life safety
	Cascadia Subduction Zone Earthquake seismic load	Remain operational
South Carolina DOT (2008)	975-year seismic load	Life safety
	462-year seismic load	Repairable damage
New York DOT (2015) & Washington DOT (2016)	1000-year seismic load	Life safety

2.6 Soil structure interaction

The study on soil-structure interaction (SSI) started in the late 19th century and developed rapidly in the late 20th century due to the demands in nuclear power and offshore industries (Kausel 2010). In the past, seismic design mainly focused on the response of columns. However, in the events of the Kobe and Christchurch earthquake, many structures were demolished because of the foundation level damages (Millen et al., 2014). Traditionally, soil-structure interaction (SSI) was regarded as one factor that benefits structural seismic response. However, it was proved that the increase in fundamental periods due to SSI does not necessarily lead to a mitigated structural response (Mylonakis and Gazetas 2000).

Soil structure interaction is one of the key components in performance-based seismic design (Finn and Fujita 2002; Priestley 2000; Shamsabadi et al. 2007). A thorough review of soil-structure interaction can be found in NEHRP (2012) and Turner (2006). Detailed procedures of incorporating SSI in PBD have been presented by several researchers (Mekki et al. 2014; Roberts et al. 2010; Stewart et al. 2004; Zhang et al. 2016). The flowchart of incorporating soil-structure analysis into response spectral analysis is shown in Figure 2. One of the common practices of incorporating SSI to seismic design is using p-y curves (Boulanger et al. 1999; Zhang et al. 2016), where p stands for lateral soil pressure per unit length of the pile and y stands for the lateral deflection of the pile. The extensive usage of the p-y method is due to its simplicity and ability to incorporate linear and non-linear analyses (Dash et al. 2008). Although there are commercial programs available that can handle both structural analysis and nonlinear soil continuum, the computational time is too long for most of the designers (Finn et al. 2011). It should be noted that special attention is needed for bridges constructed on liquefiable soil. Soil liquefaction can lead to significant damages to foundations which may lead to failure of the bridge (Maheshwari and Sarkar 2011; Tang et al. 2010). Some guidance is provided by Caltrans (2013) on liquefiable soil-structure interaction analysis. Liquefied soil springs should be used for

the liquefiable layer and no spring should be used above the liquefied soil layer if the liquefied soil is near the ground surface. It is also suggested that non-liquefied soil springs should be used for shear design.

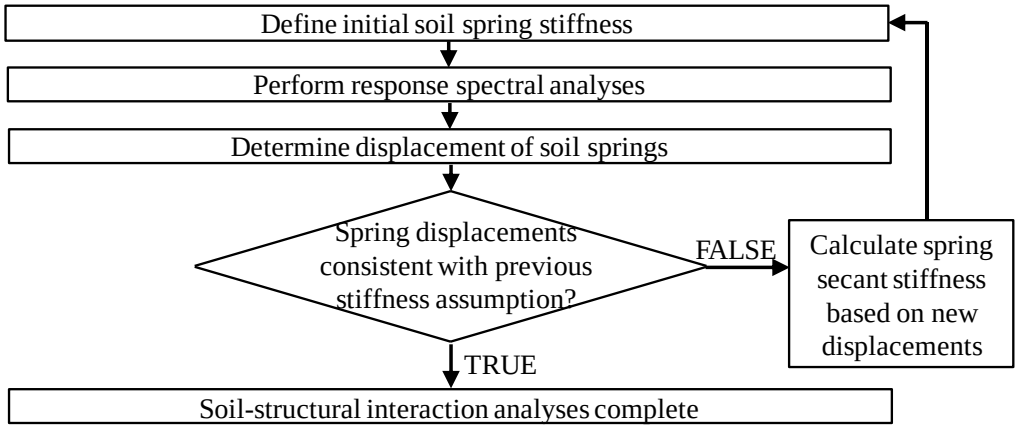

Figure 2 Soil-structure interaction in response spectral analyses

Similar to p-y curves, the vertical soil friction can be modeled using t-z curves, where t stands for vertical friction and z stands for vertical displacement. The vertical soil end bearing resistance can be modeled using q-z curves, where q stands for bearing resistance and z stands for vertical displacement. It should be pointed out that the commonly used axial ultimate capacities of the deep foundation are usually based on the assumption that significant settlement occurs. It is preferable to design the foundation for tolerable settlements at different limit states based on PBD methodology (Roberts and Misra 2010). For example, GangaRao and Moulton (1981) concluded that an average settlement of 1.6 inches of deep foundation did not require costly maintenance and repair. This was based on the evaluation of 280 concrete and steel bridges. Therefore, this settlement may be used to predict geotechnical resistance under repairable damage states. Although this may increase the efforts of analysis and design, it is likely to save a significant amount of budgets for large-scale projects.

2.7 Loss estimate

In the past, seismic designs were focused on collapse prevention while neglecting the fact that significant repair cost and repair time may be needed although life safety is protected (Ghobarah 2001). Under the PBD framework, not only life safety is to be considered but also the repair cost and repair time are taken into account, and to be minimized. A PBD framework that consistently considers overall systemic design issues was developed by Moehle and Deierlein (2004). The framework not only addresses seismic demands and damages but also tracks social demand and losses. An overall probabilistic model (Mackie and Stojadinović 2005) for earthquake demand is integrated from several sub-models that incorporate different levels of probabilities (Equation 10). Using the proposed methodology, decision-makers will be able to distribute resources based on social demands with the help of more realistic models (Marsh 2013).

$$P(D > dv|IM = im) = \int_{dm}\int_{edp}\int_{im} G_{DV|DM}(dv|dm) \cdot \left|dG_{DM|EDP}(dm|edp)\right| \cdot \left|dG_{EDP|IM}(edp|im)\right| \cdot |dG\_IM\ (im)|$$

Equation 10

where P is the total probability of a structure exceeding limit states, DM is the damage measure, EDP is the engineering demand parameter, IM is the seismic intensity measure, DV is the decision variables. In this model, the intensity measure is directly related to engineering demand. The damages are categorized into two levels; structural level and transportation level. The structural level damage triggers the losses from the bridge repair cost. This damage can be described as residual displacement, residual strain, and maximum strains of bridge components. The transportation level damage indicates the bridge serviceability, which results in indirect losses. The damage to transportation level can be described as traffic carrying capacity and lane closures. In many situations, the indirect losses are likely greater than the direct losses.

Under the PBD framework, fragility curves are frequently used to present the design results. Fragility curves present the probabilities of exceeding criteria at various hazard levels (Mackie and Stojadinović 2005). Numerous researchers have used fragility curves to describe the seismic behavior of structures (Billah and Alam 2015; Billah et al. 2012; Choi et al. 2004; Hedayati Dezfuli and Alam 2016; Hwang et al. 2001; Kim and Feng 2003; Padgett and DesRoches 2009; Shinozuka et al. 2000; Shinozuka et al. 2000). Details of seismic fragility assessment of highway bridges can be found in Billah and Alam (2015). The first generation of fragility curves was mostly based on empirical studies, especially based on the damages in the 1994 Northridge and 1995 Hyogo-ken Nanbu earthquakes (Gardoni et al. 2002; Mackie and Stojadinović 2005). However, the data from past experience is very limited and as a result, it is difficult to predict future structural fragilities based on the empirical method. Therefore, the second generation of fragility analysis is largely based on analytical studies. Analytical studies provide more insight into both existing bridges and new designs that have not experienced any earthquakes (Billah and Shahria Alam 2014). Extensive research has been performed to relate engineering demand parameters with damage measures (Lu et al. 2011; Mackie and Stojadinovic 2004). A computer program BridgePBEE based on the PBD methodology was developed (Lu et al. 2011). BridgePBEE not only performs nonlinear structural analysis, but also tracks the triggered indirect losses after earthquakes. The losses can be presented in terms of repair time and repair cost. Additionally, earthquake loss models of regional areas were also proposed by many research teams (Hazus 1997; Lu et al. 2014; Moore et al. 2002).

The loss analysis model by Mackie and Stojadinović (2005) provides guidance on loss estimation. However, it is not easy to conclude the decision variable from damage measurement. After earthquakes, the indirect losses to the transportation system largely depend on the live load capacity of the bridge (i.e. the number of lanes that can be open to traffic). Therefore, an additional parameter in the loss analysis model will be needed, which is the live load capacity

factor. The concept of live load capacity factor can be found in bridge evaluation sections of many codes, such as the Canadian Highway Design Bridge Code (CSA 2014), although it has not been used for seismic evaluation. The modified loss estimate model can be represented by Equation 11

$$\mathrm{P}(\mathrm{D} > dv|\mathrm{IM} = \mathrm{im}) = \int_{lf}\int_{dm}\int_{edp}\int_{im} |\, G_{DV|LF}(dv|dlf)\,| \cdot |\, G_{\mathrm{LF}|DM}(dlf|dm)\,| \cdot |\, dG_{DM|EDP}(dm|edp)\,| \cdot |\, dG_{EDP|IM}(edp|im)\,| \cdot |dG\_IM\ (im)|$$

Equation 11

where LF is the live load capacity factor and all other terms remain the same as defined in Equation 10. In general, the live load capacity factor can be calculated as

$$LF = \frac{Resistance - Dead\ loads - Other\ loads}{Live\ load}$$ Equation 12

Very limited research work (Mackie and Stojadinovic 2004; Terzic and Stojadinovic 2010) have investigated the relationship between seismic damages and residual live load capacity after earthquakes. Maeda et al. (2004) suggested using residual displacement to predict column damage after earthquakes. However, the dispersions of the prediction model were large. Elwood and Moehle (2005) investigated the axial capacity of columns after shear damage. It was reported that for columns with low axial load and high transverse reinforcement ratio, shear damaged columns can maintain axial loads beyond a drift of 2%. Terzic and Stojadinovic (2010) investigated the column axial capacity after earthquake damages through both experimental and numerical studies. It was concluded that specimens loaded up to displacement ductility level of 4.5 lost about 20% axial load capacity. The authors also concluded that bridges designed according to Caltrans SDC would not experience significant axial capacity loss under the design earthquake. However, this conclusion was limited to

columns without residual displacement. Currently, there is no established methodology to quantitatively connect axial live load capacity to damages such as strain and drift. Much research efforts are needed in order to better implement the loss estimate model in practice.

With the application of PBD, the cost associated with the seismic event can be incorporated into life cycle cost analysis. Life cycle cost is defined as the present value of total cost from construction to the end of the service life (Chang and Shinozuka 1996). A framework for life cycle cost analysis with natural hazards was proposed by Chang and Shinozuka (1996). The incorporation of PBD may change the life-cycle maintenance of bridge structures that are subjected to seismic hazards. For example, Figure 3 illustrates the impact that could be brought in by seismic events on maintenance. Three bridge condition curves are plotted in Figure 3. Curve 1 represents the bridge condition when seismic risk is not considered. The corresponding target maintenance time is in Year C. Curve 2 represents a potential bridge condition when a moderate earthquake happens. At the time of Year A, a moderate earthquake can cause damages that prevent serviceability. Thus, a retrofit is needed before Year A if the bridge has to remain in service after moderate earthquakes. Curve 3 represents the potential bridge condition when a major earthquake happens. In Year B, a major earthquake can bring the bridge performance down to collapse prevention level. Therefore, a retrofit is likely to be necessary to prevent collapse before Year B. Therefore, in this situation, a bridge retrofit is required in year A if serviceability has to be maintained after an earthquake. Otherwise, if only collapse prevention is required, the retrofit can be delayed to Year B. However, either case would require earlier rehabilitation than the situation without considering earthquake risks.

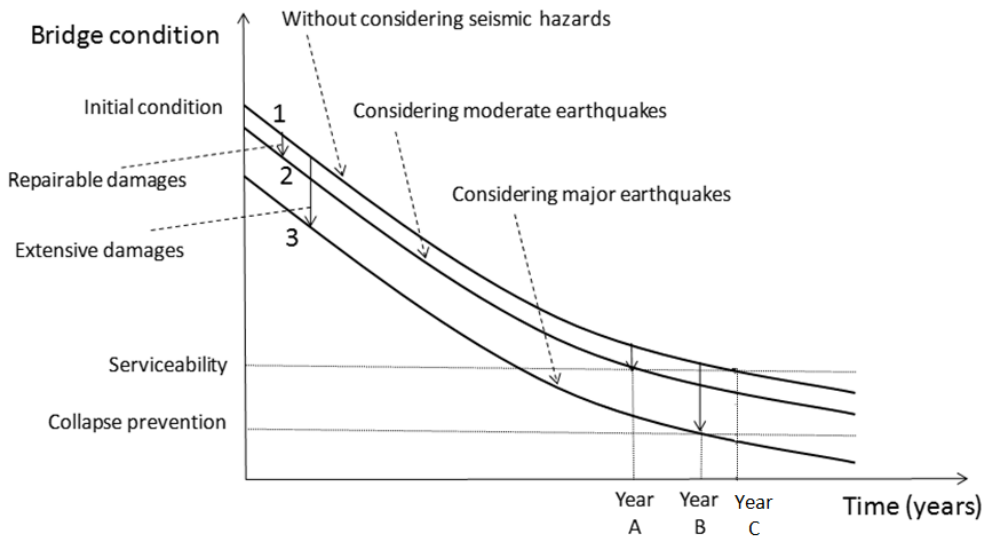

Figure 3 Bridge maintenance considering seismic hazards

2.8 Comparison of design criteria

Various PBD criteria are used in different design codes. It is not straightforward to determine whether these criteria are consistent with each other. In this section, a typical bridge column is analyzed using pushover analysis, and the design criteria from the Canadian and U.S. codes are compared. The pushover analysis was performed using SeismoStruct (SeismoSoft 2020) and a concrete column model was verified based on an experimental study by Petrini et al. (2008). The comparison between the backbone curve from the experimental study and the predicted response from SeismoStruct is shown in Figure 4. A similar numerical model was also developed by Priestley et al. (2007). The simulation and the experimental results match well in the negative quadrant. But in the positive quadrant, the numerical results are lower than the experimental result. It was explained that this may be caused by the eccentricity of the reinforcement cage in the test or higher flexural strength in the initial loading direction (Priestley et al. 2007).

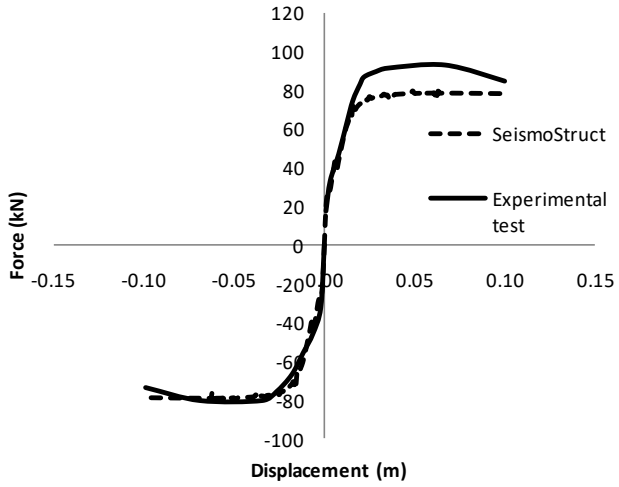

Figure 4 SeismoStruct & Experimental test results

For the comparison of different design code criteria, a six-meter high reinforced concrete column is considered. The column is fixed at the base and the top is free. A constant axial load is applied at the top of the column to simulate superstructure dead load. An incremental displacement load is applied at the top of the column in the lateral direction. The parameters of the column under investigation are shown in Table 3 **Column parameters**. The pushover results are shown in Figure 5. Various design limits from codes are marked on the pushover curve for comparison. It should be noted that this is not an exhaustive comparison of design results but rather a general comparison of conservatism in the different codes. There are many other variables in the design codes affecting design results that cannot be compared in this study, such as the resistance factors for capacity calculation. However, Figure 5 provides important information regarding damage states and gives the readers an idea of how these limits are compared to each other. When plotting the criteria from CSA (2014) and BCMOTI (2016), the material strains specified in the codes were used. For Caltrans (2013), SCDOT (2008), ODOT (2016) and AASHTO (2020), the limits defined by ductility factors were used.

Table 3 Column parameters

Concrete strength, MPa	35
Column height, m	6
Column diameter, m	1
Longitudinal rebar diameter, mm	25
No. of longitudinal rebar	24
Rebar yielding strength, MPa	400
Plastic hinge length, m	0.722
Transverse rebar spacing, mm	75
Axial load, kN	1374

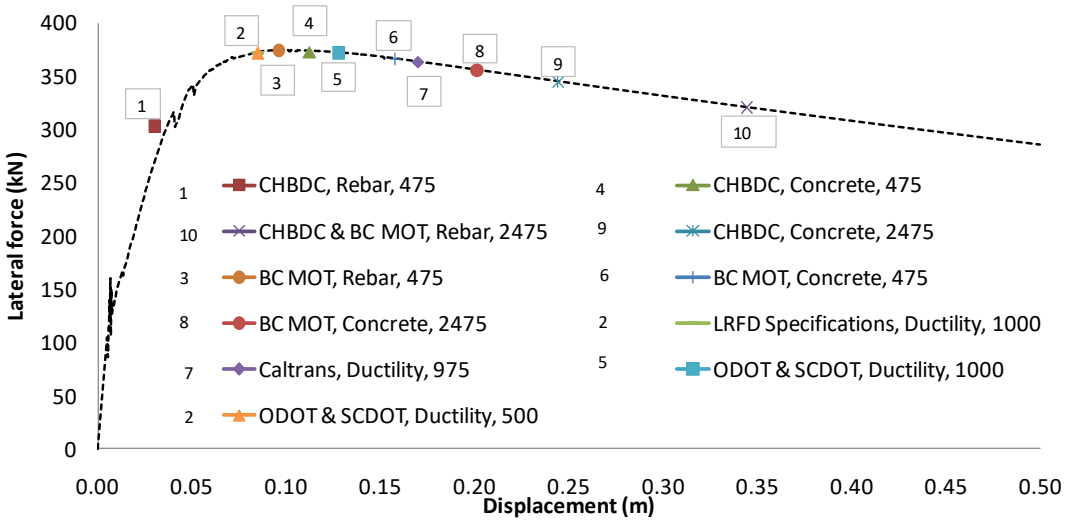

Figure 5 Damage states in various codes

From Figure 5 (Label 1), it is clear that the first yielding limit defined by CSA (2014) is very conservative in comparison with other codes at 475 years return period. This may become a challenge for bridges in high seismic zones. Label 2 represents the damage states at 1000 years return period defined by AASHTO (2020) based on ductility. The same damage state is used by SCDOT (2008) and ODOT (2016) but for a lower return period, which is 500 years. Label 3 is the damage state defined by BCMOTI (2016) at 475 years return period. At 475 to 500 years return period, the design criteria from BCMOTI (2016), SCDOT (2008) and ODOT (2016) are generally consistent (label 2 and 3), where the damage state is only beyond the

elastic limit slightly. The structure is still in an essentially elastic state and no strength reduction is observed. Label 4 and label 6 represent the concrete damage limit at 475 years return period from CSA (2014) and BCMOTI (2016). In this example, these two strain values are not governing the lower-level design.

Label 5 represents the damage limit at 1000 years return period required by SCDOT (2008) and ODOT (2016). Label 7 represents the damage limit at 975 years return period required by Caltrans (2013). In this example, Caltrans (2013) is less conservative than the other two DOTs. Label 8 and Label 9 mark the concrete damage stated defined by BCMOTI (2016) and CSA (2014) at 2475 years return period. These two values are related to the concrete core crushing strain. Label 10 defines the steel strain at 2475 years return period by BCMOTI (2016) and CSA (2014). A comparison of these codes in terms of column drift ratios is presented in Table 4.

Table 4 Code comparison in terms of column damage states and drifts

Sequence	Code	Drift
1	CHBDC, Rebar, 475 years	0.50%
2	ODOT & SCDOT, Ductility, 500 years	1.42%
2	LRFD Specifications, Ductility, 1000 years	1.42%
3	BC MOT, Rebar, 475 years	1.60%
4	CHBDC, Concrete, 475 years	1.87%
5	ODOT & SCDOT, Ductility, 1000 years	2.13%
6	BC MOT, Concrete, 475 years	2.63%
7	Caltrans, Ductility, 975 years	2.83%
8	BC MOT, Concrete, 2475 years	3.35%
9	CHBDC, Concrete, 2475 years	4.07%
10	CHBDC & BC MOT, Rebar, 2475 years	5.74%

As discussed earlier in this chapter, columns must have the adequate axial load capacity to carry traffic to provide serviceability after earthquakes. An example of the investigation of the residual axial load capacity of earthquake-damaged columns is performed using the column described in Table 3. In the analysis, the column is first pushed to a displacement and re-centered. Then a vertical displacement is applied to the top of the column to calculate the axial

load resistance. The assumption is that after earthquakes the columns do not have residual displacement or are re-centered manually before traffic is allowed to be resumed. The process of the analysis is presented in Figure 6 to Figure 8.

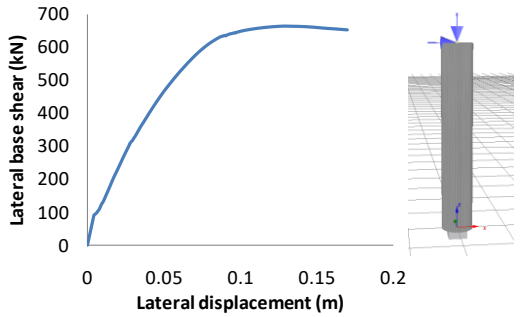

Figure 6 Apply dead and lateral load

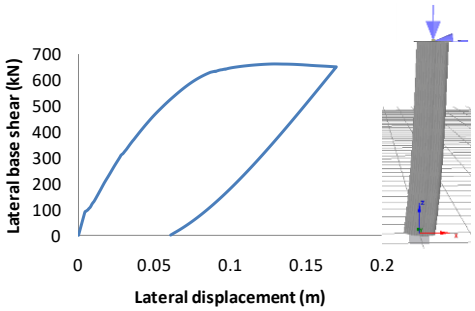

Figure 7 Maintain dead load and re-center column

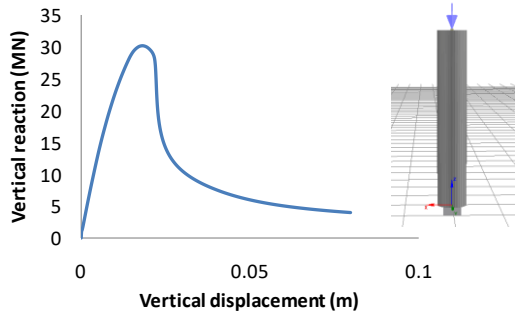

Figure 8 Apply vertical displacement until column fails

Figure 9 presents the column axial compression resistance before and after earthquake damages. Before applying any lateral load, the column resistance is 38,255 kN. After applying a lateral displacement corresponding to less or equal to 2 times ductility, the resistance is only reduced slightly to 37,600kN. However, if the displacement ductility is equal to or greater than 3, the resistance is reduced to 30,000kN, and the column failure becomes more brittle. From this single-column study, it can be seen that using a ductility factor of 2 is adequate for the serviceability state of design. A ductility factor of 3 or beyond can only be used for life safety

level design since significant stiffness, resistance, and ductility reduction are expected. This observation matches the code requirements mentioned earlier.

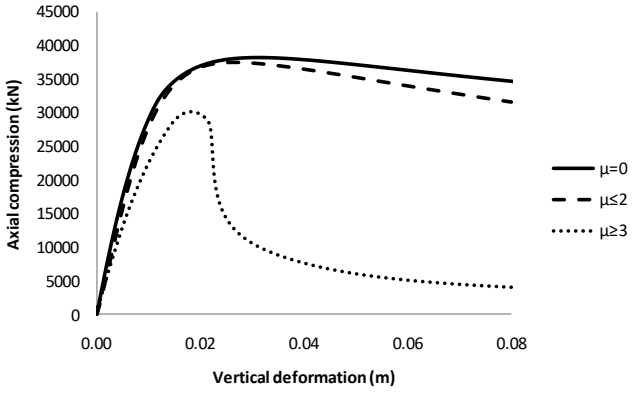

Figure 9 Column axial compression resistance

2.9 Summary

PBD is a promising and sophisticated design methodology that can be applied to both traditional ductile design and innovative structural systems. Significant achievements have been made with efforts from pioneers in the past several decades. Many design codes have adopted the PBD as a major design methodology. The section presents the core elements of PBD including damage limit states, performance targets, and appropriate loss estimates.

When comparing the PBD criteria among different codes based on the simple case study, the Canadian Highway Bridge Design Code 2014 (CSA 2014) is the most stringent as it does not allow steel yielding for major route bridges under 475-year earthquake loads. For the 475 to 500 years return period, the design criteria from BCMOTI (2016), the Canadian Highway Bridge Design Code 2019 (CSA 2019), South Carolina Department of Transportation (SCDOT 2008) and Oregon Department of Transportation (ODOT 2016) are generally consistent. Among the reviewed codes, seismic hazards based on the probabilistic method are used by most jurisdictions. However, Japan and some US DOTs also use deterministic methods.

Damage states of bridge columns are well defined in codes and can be easily checked by designers. The software currently available in the market can adequately predict the nonlinear response of structures. PBD is diversified by using different criteria based on ductility, transient/residual drift and material strain. However, the damage states of other structural and non-structural components are not well defined in most of the codes. It is agreed that columns are critical elements for life safety protection. But consideration of repair cost and repair time for many other components such as bearings, expansion joints, road barriers, etc. cannot be ignored. To properly estimate the repair cost and repair time, a large amount of research data has to be made available. This would need more cooperation between researchers and engineers.

The review suggests that limited information on the residual axial load capacity of earthquake-damaged columns is provided in the codes, although initial concepts have been developed in previous research. Based on the case study, the column axial load capacity decreases significantly when the maximum lateral displacement is equal or greater than three times yielding displacement.

Last but not the least, PBD is not limited to ductile structures, it applies to novel structural systems as well. PBD facilitates the communications between designers and owners, so that final performance targets can be achieved without necessarily following prescriptive procedures of code defined for traditional structures. It opens the door to innovative structures that can perform better than codified structures.

Chapter 3: Review of experimental studies on precast columns

3.1 Background

Accelerated bridge construction (ABC) is playing increasingly important roles as authorities are trying to reduce the traffic interruption of transportation networks. The philosophy of accelerated construction is “get in, get out and stay out” (Khaleghi 2005). Reducing construction time and costs are the main incentives for using ABC. Although costs on small ABC projects may be higher than conventional construction at some stages (Burak and Seraderian 2010), this is expected to be changed as more projects are built with ABC. The benefits of ABC also include improvements in safety, quality, durability, social costs and environmental impacts (FHWA 2017). ABC has been used in the U.S. (Ahn et al. 2006; Culmo 2011; Doolen et al. 2011; Mashal et al. 2017; PCI 2006), Canada (Fowler and Eng 2006), New Zealand (Palermo and Mashal 2012) and many other countries (Khan 2014). Design guidelines and examples of ABC were also published by many Departments of Transportation in the U.S. (Iowa-DOT 2009; Massachusetts-DOT 2013; Michigan-DOT 2013; ODOT 2016; UDOT 2015; WisDOT 2017; WSDOT 2017).

Precast concrete is frequently used as a technique to accelerate bridge constructions. Precast concrete girders have been widely used in bridge superstructures for many decades (Freyermuth 1969). Precast concrete has also been used for deck construction in the form of partial precast deck panels (PCI 2017) and full-depth panels (Issa et al. 1995; PCI 2011; Yamane et al. 1998; Yousif 1995). In recent years, applications of precast elements have been extended to substructures such as abutments, columns, pier caps, and footings (PCI 2006; Tobolski et al. 2006). Precast pier caps are typically connected with columns using pocket connections (Tazarv and Saiidi 2015). However, the use of precast columns is still relatively rare, especially in high seismic regions. This is mainly because seismic behavior is highly

sensitive to the characteristics of the connections (Kurama et al. 2018). In seismic design, superstructures are designed elastically, however, substructures are typically designed to undertake plastic deformations, which require special seismic detailing. Therefore, the use of precast concrete columns has to take into consideration of special joint design. Among the 100 ABC projects recorded on ABC-UTC Project Database (FIU 2018), 28 projects used precast pier components (e.g. columns and caps), 73 projects used precast abutments or walls, 74 projects used precast girders or deck panels.

This section categorizes precast columns into three types based on their connections: emulative column, simple rocking column, and hybrid rocking column. Emulative columns are designed to achieve responses comparable to that of cast-in-place (CIP) monolithic columns with full bending moment connections (Kurama et al. 2018; Mashal and Palermo 2015). Simple rocking columns are designed to rotate without any restraint from continuous rebar at the joints. Hybrid rocking columns (Palermo et al. 2005) are designed to achieve a balance between emulative and simple rocking columns. The hybrid rocking column is characterized by both unbonded PT tendon and continuous rebar at the rocking interface, therefore, named as “hybrid”. At the rocking interface, the rebar, which is designed to yield under design earthquake, is typically unbonded for a short length to avoid strain concentration. Many researchers named the yielding rebar as energy dissipating (ED) bar (Ou et al. 2010). The advantages of hybrid rocking columns are the improved energy-dissipating capacity resulted from ED bars, and relatively small residual displacement due to the re-centering force from the elastically designed tendons. The three types of precast columns can be comprised of a single precast element or multiple segments. In situations where there is transportation or pre-fabrication constrain for large columns, segmental constructions can be the solution. However, it is normally preferred to use as few segments as possible to accelerate on-site construction. Segmental PT columns in the forms of simple rocking and hybrid rocking are illustrated in Figure 10 and Figure 11.

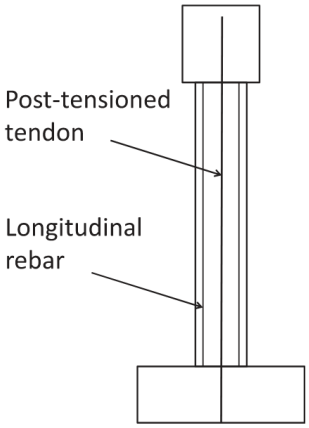

Figure 10 Simple rocking

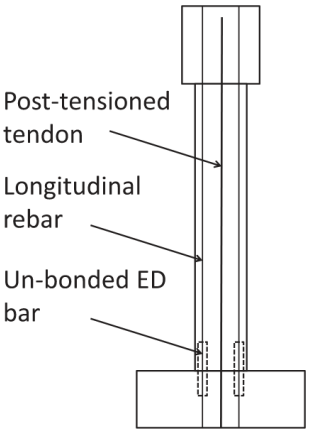

Figure 11 Hybrid rocking

Relevant fields to precast column systems are precast wall systems and precast beam-column in building structures, which were extensively investigated by many researchers, (Holden et al. 2003; Kurama et al. 1999; Kurama and Shen 2004; Marriott et al. 2008; Perez et al. 2007). Similar to precast columns, unbonded PT walls and beam-column connections can undergo large deformation with little damage because the opening along horizontal joints provides nonlinear-elastic behavior. Several large-scale research projects, as well as individual component tests, have taken place. For instance, some of the large research projects are the testing of a five-story precast concrete building (PRES project) in the U.S. (Priestley et al. 1999), testing of two full-scale building structures in Japan (Nagae et al. 2012), and testing of a full-scale 3-story precast concrete building (SAFECAST Project) in Europe (Negro et al. 2013). The design requirements of hybrid rocking walls are contained in ITG-5.1 (2008) and ITG-5.2 (2009). The design requirements of the special moment frame are specified in ACI-550.3 (2013). The development of earthquake-resistant precast structures in bridges lags behind buildings (Kurama et al. 2018). This is partially due to the vast application of precast elements in building structures.

3.2 Emulative columns

Emulative columns are designed to perform essentially like monolithic CIP columns. PT tendons may or may not be used in emulative columns. Several emulative connections suitable for ABC were evaluated by Marsh (2011). The connections are typically in the form of grouted, socket and coupled connections (Ameli et al. 2016; Haraldsson et al. 2013; Tazarv and Saiidi 2015; White and Palermo 2016). Emulative connections can be further categorized into ductile and strong connections. Structures with ductile connections are expected to yield in the connection regions. Structures with strong connections are expected to yield outside the connection regions. In the design of emulative connections, special attention should be given to the development length of reinforcement, ductility and strain concentrations. Figure 12 and Figure 13 illustrate typical grout-fill and socket connections. Ductile and strong connections using couplers are shown in Figure 14 and Figure 15.

Researchers have tested many types of construction details of emulative columns (Eom et al. 2015; Haraldsson et al. 2013; Popa et al. 2015; Tazarv and Saiidi 2013; Tran et al. 2013). Emulative column response can be achieved as long as the bending moment can be fully transferred between joints in a ductile manner. Two emulative segmental columns were tested by Mashal et al. (2013), one square section with grouted connections. and one circular section with socket connections. It was found that although both connections showed slightly pinched hysteresis loops, the energy dissipation met the expectation of emulative connections. When achieving emulative connection, ultra-high performance concrete (UHPC) is frequently used due to its high strength and bonding behavior. Tazarv and Saiidi (2015), Shafieifar et al. (2018), Ameli et al. (2014), and Parks et al. (2016) investigated UHPC and grouted splice sleeves in achieving emulative behaviors that are close to CIP concrete. In addition to using grout and socket connections, couplers are promising alternatives as well. It is noted that most of the jurisdictions do not permit using couplers in plastic hinge regions with only the exception of the Utah Department of Transportation (Ebrahimpour et al. 2016). Saiidi et al. (2015) suggested that

the prohibition of couplers in plastic hinge regions should be relaxed based on their study on five types of coupler: shear screw, headed bar, grouted sleeve, threaded and swaged. Coupler connections can also be used when smart materials such as shape memory alloy are used in the plastic hinge regions connected with mild steel used elsewhere (Alam et al. 2009; Alam et al. 2010; Billah and Alam 2012). The connections may be located either in the column portion or footing portion (Ebrahimpour et al. 2016; Haber et al. 2014).

In addition, the application of the precast column is not limited to shallow foundations, it can also be used in deep foundations (Kapur and Khaleghi 2009). Tran et al. (2014) tested the deep foundation splice shown in Figure 16 under quasi-static loads. It was concluded that if adequate transverse steel is provided in the splice zone, the plastic hinge would form in the column as expected. Researchers also tested columns that include both CIP and precast elements. For example, Ou et al. (2013) tested a tall segmental PT column that has a lower CIP portion and a prefabricated upper portion. The segments were assembled using U-loop PT anchored in CIP concrete. It was found that the damage was governed by a plastic hinge mechanism of the CIP region. Flexural failure was reached then followed by fracture of the transverse reinforcement and buckling of longitudinal reinforcement at 5.6% drift.

The design philosophy of emulative columns is similar to traditional CIP monolithic columns. The research and design code on emulative structures are relatively newly established. Design guidelines on emulative connections are well documented in references such as ACI-318 (2014). Guidelines specifically for bridge elements can be found in Steuck et al. (2008), Culmo (2009), Roddenberry (2012), Kapur et al. (2012), and Tazarv and Saiidi (2015).

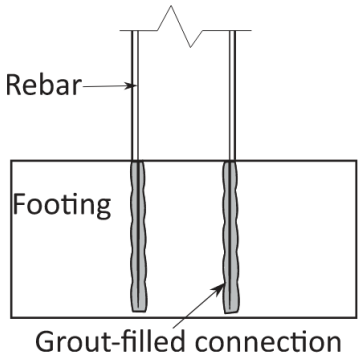

Figure 12 Grout-filled connection (Tazarv and Saiid Saiidi 2016)

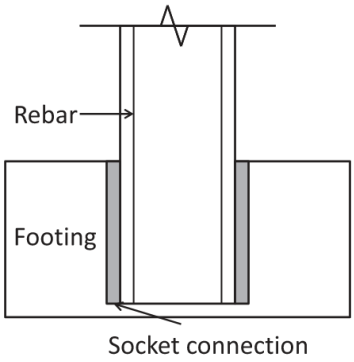

Figure 13 Socket connection (Mashal et al. 2013)

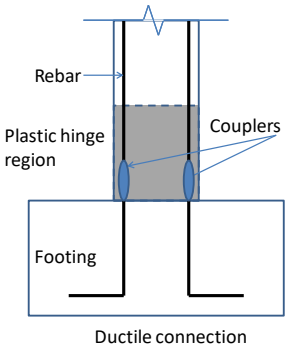

Figure 14 Ductile coupler connection (Kurama et al. 2018)

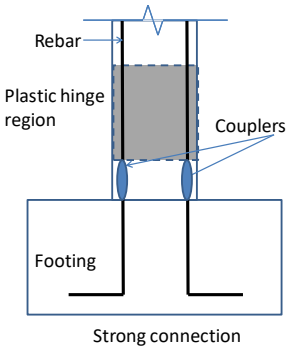

Figure 15 Strong coupler connection (Kurama et al. 2018)

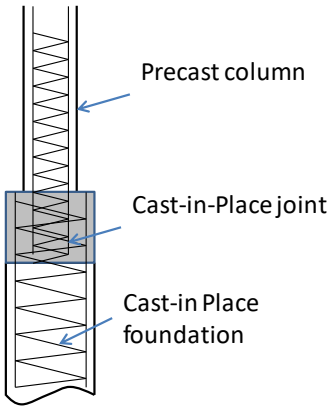

Figure 16 Deep foundation connection (Tran et al. 2014)

3.3 Simple rocking columns

Simple rocking columns can be divided into two types, which are unrestrained simple rocking columns and restrained simple rocking columns. This thesis refers free-standing column as an unrestrained simple rocking column (Figure 17). Columns with PT tendons (but without ED bar) are referred to as restrained simple rocking columns (Figure 18). Unrestrained simple rocking columns were first studied by Housner (1963), who proved that blocks with larger geometry were more stable. Subsequently, rocking behaviors were investigated by several researchers (Aslam et al. 1980; DeJong and Dimitrakopoulos 2014; Hogan 1990; Ishiyama 1982; Palmeri and Makris 2008; Psycharis and Jennings 1983; Shenton III 1996; Spanos and Koh 1984; Zhang and Makris 2001). Unrestrained rocking columns have many distinct characteristics that cannot be represented by Single-Degree-of-Freedom (SDOF) structures, as demonstrated by Makris and Konstantinidis (2003). For unrestrained rocking columns, the restoring force is provided by gravity, the stiffness is negative when rocking is initiated. Whereas for an SDOF system, the elastic stiffness from bending and shear is always positive. The dynamic behavior of unrestrained rocking columns is completely determined by the geometry and gravity acceleration. For flexible rocking columns, the rocking response is coupled with flexural deformations. Vassiliou et al. (2015) studied responses of deformable rocking columns and suggested that the stability of large cantilever columns would not be reduced by deformability. In AASHTO (2013), rocking foundations are defined in the category of Permissible Earthquake-Resisting Elements that require the owner's approval. A set of design criteria is described in the appendix of AASHTO (2013). It should be noted that rocking foundations are not commonly used in new structures, but may be used in seismic retrofits as a cost-effective (Dowdell and Hamersley 2000).

To make unrestrained rocking columns more stable, vertical tendons anchored to the foundation can be used to increase the stiffness of the rocking column and delay the initiation of rocking

response. The formulations of restrained rocking responses were studied by several researchers (Barthes 2012; Vassiliou and Makris 2015; Zhang and Alam 2018). The condition to initiate restrained rocking column rotation is expressed in Equation 13

$$m|\ddot{x}_g|H > mgb + bP_0 \qquad \text{Equation 13}$$

where m is mass, $\ddot{x}_g$ is horizontal ground acceleration, g is gravity acceleration, P_0 is the initial PT force, b is half of the column width and H is the height of the center of gravity. The geometry definitions of a rocking column are shown in Figure 18. Based on Equation 13, it is apparent that PT force delays the initiation of rocking compared with the unrestrained rocking column. In addition, the PT force provides re-centering force and the axial stiffness of the tendon increases the rocking vibration frequency. Makris and Vassiliou (2015) demonstrated that the use of vertical tendons can change the stiffness of the rocking column from negative to positive. However, the effectiveness of tendons reduces as the geometry of the column becomes larger. This is because rotational inertia is proportional to the square of the column size, which would provide most of the re-centering force for large columns under dynamic loadings.

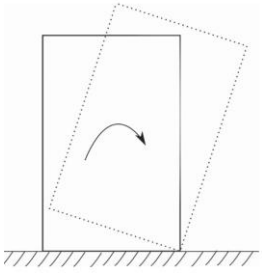

Figure 17 Unrestrained rocking column

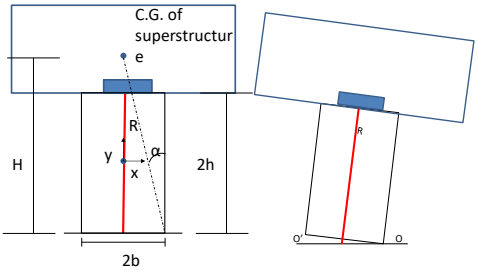

Figure 18 Restrained rocking column

Similar to monolithic frame structures, multiple rocking columns can be used to form a frame. The analytical model of a simple rocking column in a frame is studied by Roh and Reinhorn (2009), who pointed out that the rocking column boundary varies continuously from fixity to cracking, yielding, and crushing before rocking starts. The response of an array of an

unrestrained rocking column with a rigid cap beam was studied by Makris and Vassiliou (2013). It was concluded that the rocking response of an array of columns was identical to the response of a single column but in a larger size. It was also found that the weight of the cap beam increased the stability of the rocking frame.

Experimental research of simple rocking columns was performed by several researchers. Mander and Cheng (1997) performed theoretical and experimental studies of restrained simple rocking columns. The authors used steel plates at the column-footing interface to prevent impact damage. They suggested limiting the axial load ratio to 10% (including gravity and prestressing effects) to delay damages. Cheng (2008) conducted shaking table tests of a simple rocking frame with two columns. Similarly, steel plates were used at the base of the column. It was reported that up to at least 5% rotation, there was little damage or residual deformation. Hewes and Priestley (2002) tested four segmental concrete columns and each of the columns was tested twice. Steel jackets were used to confine the bottom segments to delay compression damage. The concrete segments were only connected by unbonded tendons and relied on friction for shear transfer. In the first set of tests, cyclic loads were applied to specimens with a low PT force. Then, the specimens were repaired and tested again with a higher PT force. It was found that specimens with thin jackets showed higher energy dissipation, which might be contributed by concrete crushing in thin jackets. The authors concluded that a high axial load ratio is not desirable as it will result in a negative post-elastic stiffness and poor ductility. It was suggested that the axial load ratio should be limited to 20%. Rocking columns using pin connections were studied by Mehrsoroush and Saiidi (2014), where connection consisted of two layers of steel pipes for shear force transfer and threaded bars for uplift force transfer. Hollow rectangular segmental columns in shaking table tests were carried out by Yamashita & Sanders (2009). Limited concrete spall and negligible residual drift were observed. Rocking behavior only occurred in the bottom segment. Shaking table tests of segmental columns were also tested by

Zhang et al. (2014). The authors stated that there was no residual displacement even when the PGA reached as high as 0.8g. Sideris et al. (2014) performed shaking table tests and quasi-static cyclic testing of segmental columns with sliding-rocking (HSR) joints. In the tests, both sliding and rocking at the joints were allowed. It was observed that the rocking dominant joints provided better re-centering capacity than sliding dominant joints. It was also found that near-fault motions resulted in larger deformations compared with far-field motions (Sideris et al. 2015). The capacity spectrum seismic design methodology for sliding-rocking columns was investigated by Madhusudhanan and Sideris (2018). It was found that simplified analysis models were in good agreement with the experimental data. The parametric study suggested that increasing post-tensioning force and dead load resulted in a slight increase in lateral strength.

The disadvantages of using simple rocking columns are the low energy dissipation capacity associated with high displacement demand, less reliable shear transfer mechanism and less redundancy comparing with CIP monolithic columns. The low energy dissipation is due to the flag-shaped hysteretic behavior since the structure essentially remains elastic. In such situations, oscillations may continue after earthquakes causing low-cycle fatigue effects (ACI-374 2014). The excessive displacement demand may significantly damage bridge joints, adjacent structures as well as non-structural components such as barriers and utilities. In terms of shear transfer relying on friction, it is not reliable when frame action significantly reduces compression at exterior columns. It is also less reliable during vehicular impact or when vertical acceleration causes uplifts. In ACI-318 (2014), it is specified that connections that rely solely on friction caused by gravity shall not be permitted. Hence, it is challenging to meet current code requirements using simple rocking columns.

3.4 Hybrid rocking column

Hybrid rocking columns are characterized by both unbonded tendons and energy-dissipating bars (ED bars) at the rocking interface as previously shown in Figure 11. The unbonded tendons provide re-centering capacity and the ED bars provide energy dissipation capacity. The amount of ED bars should be sufficient to provide energy-dissipating capacity, at the same time, the strength of ED bars should be smaller than the tendons such that the columns show self-centering behavior. The first and so far the only constructed bridge with hybrid rocking columns is the Wigram-Magdala Link Bridge (Routledge et al. 2016) in New Zealand. The bridge is about 99 m long with three spans of prestressed concrete girders supported on hybrid rocking column bents. The columns are concrete-filled steel tubes funded on pile footings. The columns have base plates that are connected to the footing using ED bars. The bridge has been seen as a success for a step-change in seismic design philosophy.

Limited design guidelines can be found in NZS (2006) and fib (2010) which are based on the Monolithic Beam Analogy method assuming the deformation of a hybrid rocking column would be similar to that of a CIP monolithic column. Although the design of s hybrid rocking column is not contained in North American codes, ACI-318 (2014) permits novel column designs if the test results meet ACI-374 (2014) criteria. ACI-374 (2014) specifies the detailed testing procedures for structures not fully satisfying the prescriptive requirements of ACI-318 (2014). The main criteria for cyclic loading up to 3.5% drift are: a) strength degradation shall be within 25%; b) relative energy dissipation ratio shall not be less than 1/8; c) secant stiffness from a drift of -3.5% to +3.5% shall not be less than 5% initial stiffness. It should be noted that even structures designed as per ACI-318 (2014) may not meet the requirement of ACI-374 (2014), the latter has more stringent requirements. Hybrid connections for buildings are defined in ACI-550.3 (2013), which specifies design requirements for special frames with beams post-tensioned to columns. In this structural system, rocking occurs at beam-column joints. ED bars are used at the joints and are unbonded to avoid strain concentration. ACI-550.3 (2013) stipulates that the bending

moment contribution from ED bars should be less than 50% of total capacity. This hybrid connection and its deformed shape are shown in Figure 19 and Figure 20 respectively. The anchor of the tendon would be located at the exterior column which is not shown in Figure 19 and Figure 20.

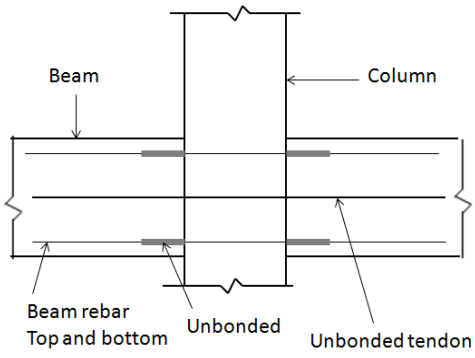

Figure 19 PT moment frame Jeong et al. (2008)

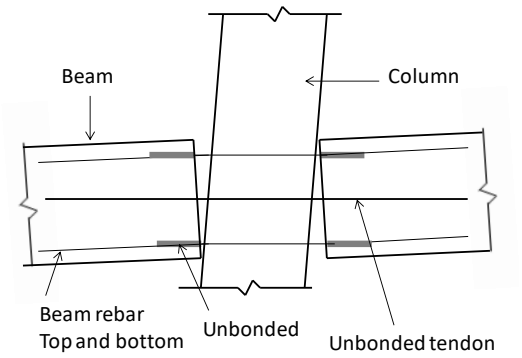

Figure 20 Deformed PT moment frame

Researchers have performed a large number of experimental tests on hybrid rocking columns (Bu et al. 2015; Bu et al. 2016; Cheng 2008; Hieber et al. 2005; Metelli et al. 2011; Motaref 2011; Sakai and Mahin 2004; Shim et al. 2008; Thonstad et al. 2016), as well as analytical and numerical studies (Bu et al. 2016; Chou et al. 2013; Chou and Hsu 2008; Rahmzadeh et al. 2018). The supplemental energy dissipation of the hybrid rocking column was achieved using internal unbonded bars or external replaceable devices (Marriott et al. 2009). Hybrid rocking columns under cyclic loadings were tested by Cohagen et al. (2008), Ou (2007), Wang et al. (2008), and Larkin et al. (2012) and other researchers. In these experiments, the axial load ratios range from 6% to 25%. The ED bar ratios (ED bar area to concrete section area ratio) range from 0 to 1.4% and the tendon area ratios (tendon area to concrete section area ratio) range from 0.15% to 1%. The locations of tendons may be at the center of cross-sections or around the parameter. A number of possible details are shown from Figure 21 through Figure 24 (Hung et al. 2017; Marriott et al. 2009; Saiidi et al. 2017; Thonstad et al. 2016). Figure 21

and Figure 22 show hybrid columns using pre-tensioned and post-tensioned tendons. Figure 23 shows a column with external mild steel energy dissipaters, which can be replaced after earthquake events. Figure 24 shows a segmental construction with shear keys in between segments.

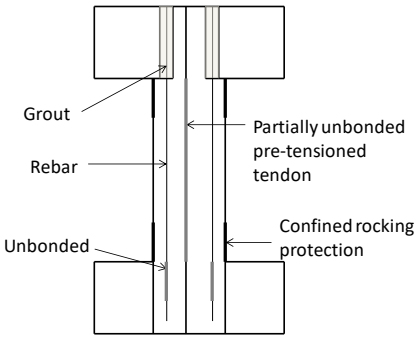

Figure 21 Pre-tensioned hybrid rocking column (Thonstad et al. 2016)

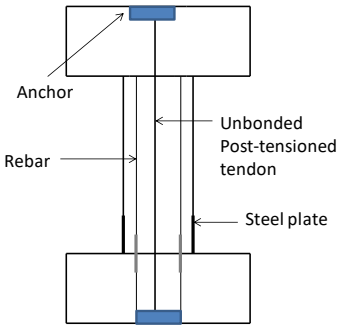

Figure 22 Post-tensioned hybrid rocking column (Saiidi et al. 2017)

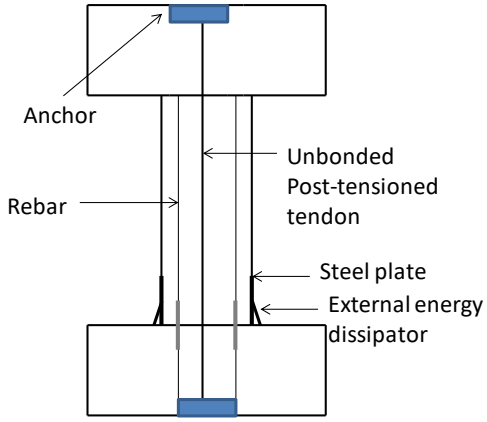

Figure 23 Hybrid rocking column with external dissipator (Marriott et al. 2011)

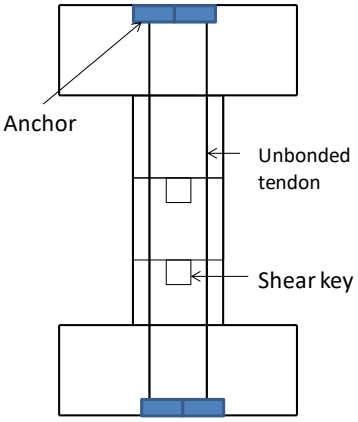

Figure 24 Hybrid rocking column with shear key (Hung et al. 2017)

The effects of ED bar ratios were investigated by several researchers. Ou et al. (2007) tested seven large-scale segmental rectangular concrete columns with ED bar ratios of 0%, 0.5%, and 1%. It was observed that with the increase in energy dissipation capacity, the residual displacement increased. Three of the seven specimens were tested under pseudo-dynamic

loading and then followed by cyclic loading to investigate residual strength. Specimens showed decreased stiffness, strength and energy dissipation capacity and even smaller residual drifts. It was explained that the decrease of residual drift might be caused by the crushing of the concrete cover and further softening of the reinforcement, which reduced the force to re-center the column. Therefore, residual drift cannot be the only criteria for the seismic performance of rocking columns. It can be misleading when the residual displacement is very small while the column residual strength is significantly decreased. Analytical model and finite element analysis of the column with ED bars were also developed by Ou et al. (2007). Wang et al. (2008) tested four large-scale segmental columns comprised of nine to ten segments under cyclic loadings. The authors suggested that large openings and high strength ED bars should be avoided to obtain satisfactory energy dissipation. Cohagen et al. (2008) tested two unbounded PT columns with different ED bar ratios. It was found that the column with PT force experienced damage earlier than the column without PT forces. The damage was mostly due to a high compression force. Marriott et al. (2011) tested columns with external replaceable ED bars. A number of biaxial moment-interaction diagrams as a function of mechanical and geometric section properties were proposed. White and Palermo (2016) compared the performance of one emulative with two hybrid rocking columns. These two hybrid rocking columns were detailed using couplers and socket connections. After the first round of the test, the columns were repaired and tested again. The authors indicated that the repair methodology requires further improvement to avoid ED bars pullout in subsequent earthquakes. Hung et al. (2017) tested segmental columns with concrete keys and steel dowels as shear connections. With the shear key connections, the authors found that relatively low PT force would be needed to maintain re-centering capacity. In addition to post-tensioned columns, pre-tensioned columns were also studied by researchers (Davis et al. 2017; Thonstad et al. 2016). Thonstad et al. (2016) conducted multi-shaking table tests of a two-span bridge with a pre-tensioned hybrid rocking column. It was found that residual drift was within 0.2% when the maximum drift achieved 221%

of design motion. The damage was limited to longitudinal rebar fracture and bulging of the column confining tube at 6% drift.

PT columns are normally subject to higher compression compared to traditional CIP columns due to the rocking impact and PT forces. The compression is particularly high at the compression toe under rocking response. A number of details were used to reduce compression damages, such as using steel plates at the column-footing interface, providing confinement reinforcement to protect the core concrete, and using external jacketing tubes. Chou and Chen (2006) tested double steel tube confined segmental columns under cyclic loads. Each of the columns was comprised of four segments. The bottom segment was attached with an ED device comprised of a steel plate and stiffeners. It was found that the column achieved 6% drift with little residual displacement and strength degradation. The authors converted hysteretic energy dissipation to equivalent viscous damping and reported that the column with the energy dissipation device has a 9% viscous damping whereas the column without the dissipation device only achieved 6.5% viscous damping. In subsequent research, Chou and Hsu (2008) presented a flag-shaped hysteretic model based on the tests. A two-plastic-hinge model was also proposed by Chou et al. (2013) for a segmental rocking column. The investigated column has two rocking surfaces located at the base of the column and top of the bottom segment. The proposed analytical model can capture the force-displacement relation of the investigated segmental column. The hysteretic model of segmental columns with ED bars was also studied by Ou et al. (2018).

Design guidelines of hybrid rocking bridge columns have been proposed by researchers from various perspectives. Kwan and Billington (2003) proposed two-level design criteria for the hybrid rocking column. For the functional level displacement, it was a) displacement at yielding of unbonded PT; b) displacement leading to 1% residual drift; c) 0.7 times survival-level displacement. It was suggested that the yield strain is 0.007 for PT bars and 0.01 for PT

strands. The proposed criterion for life safety is the displacement at which the capacity decreases by 10% compared to its peak capacity. In a subsequent study, Kwan and Billington (2003) suggested that the force reduction factor may be used to simplify the design similar to the traditional force-based design for monolithic columns. Ou et al. (2009) suggested that the ED bar contribution to the column strength should be within 35% of overall strength to limit the residual drift to 1%. Saiidi et al. (2017) proposed AASHTO guidelines for the design and construction of FRP-confined hybrid rocking columns. It was suggested that the AASHTO (2013) equation for analytical plastic hinge length of monolithic columns still applies. For columns with more than 1% ED bar ratio, the damping was taken as 5%, which was consistent with the monolithic column design (AASHTO 2013; CSA 2014). When the ED bar ratio was less than 1%, Saiidi et al. (2017) suggested reducing damping to 3.2% since a flag-shaped hysteretic behavior is expected. The overall design, modeling, and experimental response of the PT column were discussed in Palermo et al. (2007). Sectional analysis equations based on the global deformation compatibility of rebar, PT tendon and concrete can be found in (Palermo and Pampanin 2008; Pampanin et al. 2001; Rahmzadeh et al. 2018). The displacement based design approach was presented in Ou et al. (2010).

3.5 Novel materials in rocking column

Many novel materials with better strength and ductility have been tested to improve the seismic performance of rocking bridge columns (Saiidi et al. 2015; Zohrevand and Mirmiran 2011). Billington and Yoon (2004) tested seven precast columns with ductile fiber-reinforced concrete (DFRCC) in the plastic hinge region. After lateral loading with the maximum drift of 4%, the residual drift was less than 0.2%. The column with DFRCC showed more distributed cracking, higher peak loads and energy dissipation. The authors also found that columns with longer socket lengths showed better energy dissipation and delayed localization of cracks. The columns had negligible residual displacement even if the tendons were located at the corners of

the section. Fiber-reinforced concrete was also used in the shake table test by Trono et al. (2014) and the cyclic load test by Nguyen et al. (2017). Lee (2007) and Mehrsoroush and Saiidi (2016) investigated the design issues and simulation of precast columns with Engineered Cementitious Composites (ECCs) in plastic hinge regions. It was found that ECC could prevent significant spalling, however, using ECC with high tensile strength could lead to cracking and failure outside of the expected plastic hinge segment. Mohebbi et al. (2018) carried out a shake table test of rectangular PT column with Carbon Fiber Reinforced Polymer (CFRP) tendons and Ultrahigh-performance concrete (UHPC) in the plastic hinge region. The column was socket connected to the footing with unbonded ED bars. Results showed that the column had a ductility capacity of 6.9 and a drift ratio of 13.8%. PT UHPC columns were also tested by Mohebbi et al. (2018), Yang and Okumus (2017), and Wang et al. (2018) and (Wang et al. 2018). Ou et al. (2010) compared the cyclic behavior of segmental columns using high-performance (HP) steel with conventional steel as ED bars. The HP steel had higher strength, ductility, and superior corrosion resistance. Results showed that the column with HP ED bars had better drift capacity, lateral strength, and energy dissipation compared to conventional rebar when the bonding conditions are the same. Tazarv and Saiid Saiidi (2016) studied three advanced materials in precast column including UHPC, ECC, and Shape Memory Alloy (SMA). Studies on segmental column with SMA bars were also carried out by Roh & Reinhorn (2010), Nikbakht et al. (2015), Moon et al. (2015), Varela and Saiidi (2017) and Li et al. (2017). In the shaking table tests by Motaref et al. (2013), ECC, elastomeric pad and unidirectional carbon fiber reinforced polymer (CFRP) were used in the plastic hinge regions. Precast columns with polyurethane (PU) as base segment were studied by Nikoukalam and Sideris (2017). Precast columns with fiber tube and steel tube systems were also tested (ElGawady et al. 2010; ElGawady and Sha'lan 2010; Moustafa and ElGawady 2018). A performance based design approach of concrete-filled GFRP columns was proposed by Dawood and ElGawady (2013). Guerrini et al. (2014) tested columns

comprised of double steel cylindrical shells with concrete cast in between. A satisfactory seismic performance was reported from quasi-static tests.

3.6 Seismic damage and re-centering capacity

As there is a large amount of testing data available, this section provides some discussions based on observation and analysis of existing data. It is worthwhile to emphasize again that rocking columns are designed to self-center after earthquakes. The self-centering bending moment is provided by the tendons and gravity, which are designed to be greater than the plastic strength of ED bars. In other words, while ED bars are the fuses, the tendons should be capacity protected to reduce the residual drift. Thus, important parameters include ED bar ratios, axial load ratios, and PT force, which determine the seismic damage under earthquake loadings.

Residual drift is an important seismic performance indicator for post-earthquakes, which can be used for seismic evaluations (Christopoulos et al. 2003; Ghobarah 2004). Hieber et al. (2005) proposed a self-centering/re-centering ratio (λ_{re}) parameter, which is defined as the ratio of the self-centering moment to resisting moment (Equation 14). The expressions of M_{re} and M_y are presented in Equation 15 and Equation 16. The value of M_{re} should be higher than M_y to obtain self-centering capacity. In fact, to be consistent with capacity design requirements in most of the design codes, the overstrength of ED bars may need to be used, rather than the nominal strength. The self-centering ratio will be used as an input to predict other crucial parameters such as damping in this study.

$$\lambda_{re}=\frac{M_{re}}{M_y}=\frac{D+A_p f_{pi}}{A_s f_y} \quad \text{Equation 14}$$

$$M_{re}=\left(DL+A_p f_{pi}\right)\alpha D \quad \text{Equation 15}$$

$$M_y=\left(A_s f_y\right)\alpha D \quad \text{Equation 16}$$

where DL=Dead load; A_p = Tendon area; f_{pi} =Tendon initial stress; A_s =Total area of ED bars/mild steel; f_y=yield strength of ED bars/mild steel; αD=distance from the center of the column to the centroid of the concrete compression area.

Several rocking column testings are selected and used for data analysis. The testing parameters and results are presented in Table 5, including peak (transient) drifts, residual (permanent) drifts, and some other important parameters. Specimens in Hewes and Priestley (2002) were simple rocking segmental columns without ED bars. Tests by Chou and Chen (2006) were concrete segments confined by steel jackets. Specimens in Ou (2007) were segmental hybrid rocking columns using PT strands and ED bars. Hollow sections with ED bars were tested by Wang et al. (2008). Specimens in Cohagen et al. (2008) were continuous hybrid rocking columns with Williams PT bars and ED bars. The specimens P3 and P4 in Wang et al. (2008) were strengthened to avoid opening at the bottom of the column, therefore, will not be included in further analysis in this study. Similarly, two specimens in Bu et al. (2015) used bonded PT bars, which are also excluded in further analysis. Numerous experimental studies were done by researchers and only a limited number of them are listed in Table 5, with their highlights summarized in the last column. Due to the limit in space, not all experiments are described in detail in this section.

Table 5 Test parameters and residual drifts

Reference	Specimen	ASR	N	D	λ_{re}	ρ_{ed}	θ_{peak}	$\theta_{residual}$	ALR	Highlights
Hewes and Priestley (2002)	JH11	6.0	4	610	NA	0.00	3.00	0.14	25.4	No ED bar, bottom segment confined by steel jacket, static cyclic loading
	JH21	6.0	4	610	NA	0.00	4.00	0.30	20.4	
	JH31	3.0	2	610	NA	0.00	4.00	0.10	17.6	
	JH41	3.0	2	610	NA	0.00	4.00	0.05	17.5	
Chou and Chen (2006)	1	4.9	4	500	NA	0.00	6.00	0.61	N/A	All circular segments confined by steel jacket
	2	4.9	4	500	NA	0.00	6.00	0.80	N/A	
Ou (2007)	C0C	4.7	4	860*860	NA	0.00	5.00	0.20	15.4	Hollow square sections, static cyclic and dynamic loading
	C5C	4.7	4	860*860	2.18	0.50	5.00	0.40	6.1	
	C8C	4.7	4	860*860	1.09	1.00	5.00	2.90	11.3	
	C5C-1	4.7	4	860*860	1.54	0.50	5.00	0.90	11.4	
Wang, et al. (2008)	P1	7.9	10	1200*1800	NA	0.00	4.00	0.05	N/A	Hollow rectangular sections, ED bar ratios vary along the height, static cyclic loading
	P2	7.9	10	1200*1800	0.90	0.57	4.00	0.40	N/A	
	P3	7.9	9	1200*1800	0.80	1.41	5.00	1.60	N/A	
	P4	7.9	9	1200*1800	1.33	0.85	5.00	1.30	N/A	
Cohagen, et al. (2008)	LB6-PT	3.0	1	508	1.60	0.84	6.80	1.36	12.1	Circular sections, static cyclic loading
	LB7-PT	3.0	1	508	1.20	1.15	9.80	3.14	12.6	
Jeong et al. (2008)	PRC-2	6.2	1	406	1.22	0.66	10.71	2.08	11.6	Circular sections, dynamic loading
	PRC-U	6.2	1	406	1.17	0.66	11.09	0.30	11.5	
	PRC-U2	6.2	1	406	1.56	0.66	9.99	0.94	14.9	
	PRC-UJ	6.2	1	406	1.19	0.66	9.78	0.61	11.7	
Marriott, et al. (2009)	PT	4.6	1	350*350	NA	0.00	3.50	0.00	N/A	Square sections, static cyclic and dynamic
	HBD3	4.6	1	350*350	6.37	0.26	3.50	0.00	N/A	
	HBD4	4.6	1	350*350	4.98	0.33	3.50	0.50	N/A	
Larkin, et al. (2012)	PT-LL	4.5	1	610	1.51	0.69	7.00	2.70	14.0	Circular sections, static loading
	PT-HL	4.5	1	610	0.89	1.33	7.00	3.65	16.0	
Hung, et al.	SSKP0	6	4	600*	0.6	1.26	7.00	3.80	10.0	

(2017)				600	3					Steel dowels and reinforced concrete shear keys, static cyclic loading
	SSKP1	6	4	600*600	1.04	0.94	7.00	2.70	12.5	
	SSKP2	6	4	600*600	1.25	0.94	7.00	1.50	15.0	
	RCSKP0	6	4	600*600	0.72	1.26	7.00	4.10	10.0	
	RCSKP1	6	4	600*600	1.19	0.94	7.00	3.70	12.5	
	RCSKP2	6	4	600*600	1.43	0.94	7.00	3.00	15.0	
Li, et al. (2018)	5seg	10	5	100*100	NA	0.00	7.00	1.40	10.1	Slender square sections, static cyclic loading.
	5segED	10	5	100*100	2.75	0.25	7.00	1.40	10.1	
	7seg	10	7	100*100	NA	0.00	7.00	0.60	10.1	
	5segkey	10	5	100*100	NA	0.00	7.00	0.60	8.7	
	7segkey	10	7	100*100	NA	0.00	6.00	2.75	10.1	
Li, et al. (2019)	S1	6.0	3	100	0.69	1.44	5.00	0.12	11.2	Bidirectional earthquake motions
White and Palermo (2016)	SC-N	5	1	500	1.60	1.3	3	0.5	13.0	ED bars can be effectively replaced.
	CC-N	5	1	500	1.29	1.6	3	0.75	12.0	
Wang, et al. (2018)	R-1	4	3	500*500	1.88	0.88	6.00	0.40	6	UHPC shell for the bottom segment
	R-2	4	3	500*500	2.42	0.88	6.00	0.40	8	
	R-3	4	3	500*500	0.99	1.67	6.00	0.40	6	
Bu, et al. (2015)	UPC	5.29	4	350	NA	0	7.00	0.20	7.49	PT bars are bonded in the last two specimen
	UPCE	5.29	4	350	1.23	0.7	7.00	0.90	7.49	
	BPC	5.29	4	350	NA	0	7.00	4.00	3.74	
	BPCII	5.29	4	350	NA	0	7.00	3.00	7.49	

Notes: ASR: aspect ratio; N: number of segments; D: diameter or dimension of the section; λ_{re}: recentering ratio, %; ρ_{ed}: ED bar ratio, %; θ_{peak}: peak drift ratio, %; $\theta_{residual}$: residual drift ratio, %; ALR: axial load ratio, %

Table 5 includes columns composed of 1 to 10 segments, with and without ED bars. It was found that when λ_{re} is higher than 1, the ratio of residual to max drift is generally small. When λ_{re} is lower than 1, significant residual displacement was observed in all the specimens. Equation 17 is proposed to correlate the self-centering ratios with the residual drift to the

maximum drift ratio. The proposed equation has an R square of 0.53 and the comparison between testing data and the prediction equation is shown in Figure 25. In addition to residual drift, viscous damping is also an important parameter in seismic design, especially when using the displacement-based design method. Based on the experimental results presented in Table 5, this study proposes an equation to predict the viscous damping of hybrid rocking columns as a function of ductility and self-centering ratio. The proposed relation is presented in Equation 18, which also has an R square of 0.53. It is noted that for both equations, the R square values are relatively low. This is mainly because the testing columns are not all consistent in detailing, and there are other variables that cannot be captured by the regression equations. For example, some columns had steel jackets confining the bottom rocking segment while others may not have such a high level of confinement thus having different residual deformation and damping. The two proposed equations are intended to help engineers for sizing columns and preliminary designs and cannot replace detailed analyses. More testing and numerical studies are needed to propose regression equations for various types of details.

$$\theta_{residual} = \left(\frac{0.2727}{\lambda_{re}} + 0.057\right) \times \theta_{max} \quad \text{Equation 17}$$

$$\text{Equivalent viscous damping} = 0.05 + \frac{0.16}{\lambda_{re}} \times \left(1 - \frac{1}{\sqrt{u}}\right) \quad \text{Equation 18}$$

To help gain more insight into the progressive damage process of rocking columns, the tests by Hewes and Priestley (2002), Cohagen et al. (2008), and Ou et al. (2007) are presented in Table 6 with more details. The simple rocking columns in Hewes and Priestley (2002) have higher concrete strength and also higher axial forces. The cracking drift of the simple rocking column is the drift at which the gaps open at segment interfaces. The reinforcement yielding drifts were not available in tests by Hewes and Priestley (2002). The ED bar yielding drifts were reported in Cohagen et al. (2008) and Ou et al. (2007) and the results are similar. The readers should

expect similar damage results and sequences in other columns that have similar axial load ratio, ED bar ratio, and column aspect ratio.

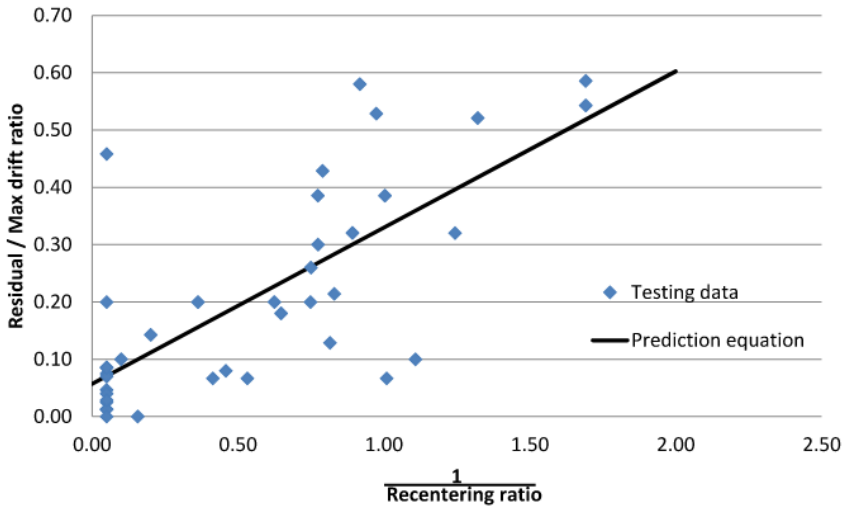

Figure 25. Residual to maximum drift ratio versus self-centering ratio

Table 6 Test parameters and damage states

References	Specimen	Cracking drift (%)	Yield drift (%)	Concrete crush drift (%)
Hewes and Priestley (2002)	JH11	0.3	N/A	2
	JH21	0.2	N/A	1.6
	JH31	0.3	N/A	1.2
	JH41	0.2	N/A	1.2
Cohagen et al. (2008)	LB6-PT	0.26	0.58	1.83
	LB7-PT	0.25	0.41	1.4
Ou et al. (2007)	C0C	N/A	0.2	4
	C5C	0.5	0.43	3
	C8C	0.38	0.56	3
	C5C-1	0.38	0.48	4

In terms of damage states used for PBD, for monolithic columns, Ghobarah (2001) suggested a drift limit of 0.2% for the lower-level design. For higher-level earthquakes, it is typically expected that the damage is repairable although there may be traffic interruptions. A drift limit of 0.5% was proposed by Ghobarah (2001) for repairable damage. Based on a review of available experimental results by Hewes and Priestley (2002), Cohagen et al. (2008), Ou (2007), Wang et al. (2008), and Larkin et al. (2012), two-level PBD criteria using drift limits of hybrid rocking

columns could be suggested. The concrete cracking and crushing drifts reported from the five projects are plotted in Figure 26. The average cracking drift is 0.32%, which can be the limit for serviceability design. For concrete crushing drifts, the values range from 1.2% to 4%, with an average of 2.3%. Currently, there is no clear recommendation on the design drift limits of hybrid rocking columns, more experimental and numerical studies are needed in the future. In addition to reviewing drift-related damage, based on several test results (Chou and Chen 2006; Cohagen et al. 2008; Hewes and Priestley 2002; Larkin et al. 2012; Ou 2007; Wang et al. 2008), this study determined the cracked stiffness of each specimen. It was found that the cracked stiffness to uncracked stiffness ratio was between 20% to 40% (shown in Figure 27). Early research (Itani 2003) might suggest using 100% unreduced stiffness for prestressed concrete members. However, this should not be applied to hybrid rocking column designs. A design example of a hybrid rocking column is presented in Appendix A. The example presents how the sizing of the column and tendon can be selected in the preliminary design.

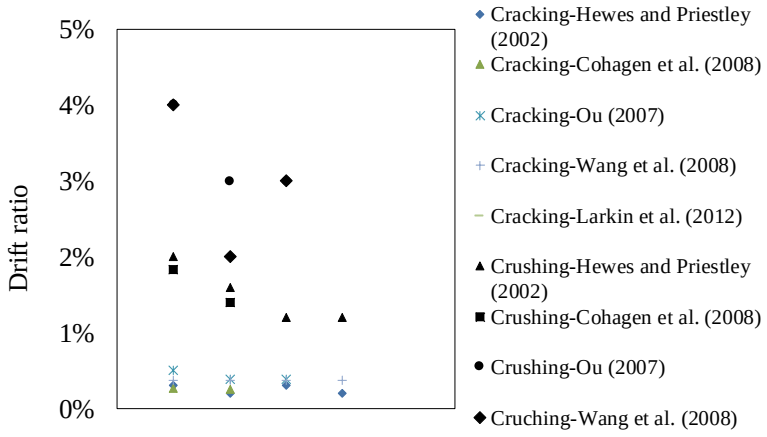

Figure 26 Concrete cracking and crushing drifts

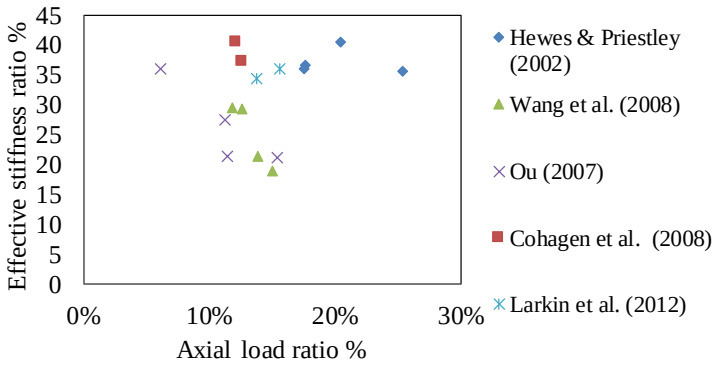

Figure 27 Cracked stiffness ratio

In terms of the seismic damage and re-centering capacity of the novel columns with advanced materials and structural types, they performed better than conventional reinforced concrete hybrid rocking columns. Table 7 presents test parameters and results of novel segmental columns with UHPC, ECC, SMA, and FRP tubes. In the tests by Tazarv and Saiid Saiidi (2016) and Wang et al. (2018), the maximum drift ratios range from 6% to 11% and the residual drifts range from 0.38% to 1.2%. The ratios of residual to maximum drifts are between 6% and 11%. In the test by ElGawady et al. (2010), the columns were pushed to a drift of 15%, which caused residual drifts of 2.53% to 6.78%. The residual drift to maximum drift ratios ranges from 17% to 44%. It should be noted that the specimens FRP1 to FRP4-S are much more slender than the other specimens listed in Table 7. In all these tests, the columns were pushed to a displacement significantly beyond the code requirements. In ACI-374 (2014), columns for seismic applications are only tested to a drift ratio of 3.5%. It can be seen that these novel columns do have superior seismic performance.

Table 7 Test parameters and results of novel segmental columns

References	Specimen	ASR	N	D	ALR	ρ_{ed}	θ_{peak}	$\theta_{residual}$	Notes
Billington and Yoon (2004)	SCon38	1.90	1	200*200	NA	0.00	4.00	0.30	Ductile Fiber-Reinforced Concrete
	SFrc76	1.90	2	200*200	NA	0.00	420.00	0.50	
	SFrc38	1.90	2	200*200	NA	0.00	4.20	0.60	
	TCon38	3.40	1	200*200	NA	0.00	4.00	0.20	
	TFrc76	3.40	2	200*200	NA	0.00	4.00	0.20	
	TFrc38	3.40	2	200*200	NA	0.00	4.20	0.60	
ElGawady et al. (2010)	FRP1	8.13	1	203	NA	0.00	15.30	2.53	Segmental columns consisting of precast post-tensioned concrete-filled fiber tubes
	FRP4	8.13	4	203	NA	0.00	15.40	6.78	
	FRP4-R	8.13	4	203	NA	NA	15.40	2.91	
	FRP4-S	8.13	4	203	NA	NA	15.30	3.27	
Motaref et al. (2013)	SC-2	4.51	4	406	20.00	1.00	11.60	0.40	Reinforced concrete segment
	SBR-1	4.51	4	406	20.00	1.20	14.00	3.00	Rubber base segment
	SF-2	4.51	4	406	20.00	1.00	14.90	0.10	FRP confined segment
	SE-2	4.51	4	406	20.00	1.00	10.70	1.00	ECC segment
	SC-2R	4.51	4	406	20.00	1.00	14.80	1.80	Repaired with FRP segment
Tazarv and Saiid Saiidi (2016)	HCS	4.49	1	610	10.00	2.80	11.00	1.20	Novel column with UHPC, ECC, reinforcing NiTi superelastic SMA bars and self-consolidating concrete (SCC).
Ichikawa et al. (2016)	RC-UHPC	4.57	2	300*300	NA	NA	6.50	5.00	Multiple UHPC rings are used to compose the bottom portion of the column, bilateral cyclic loading and hybrid testing
	PC-UHPC	4.57	2	300*300	NA	NA	3.50	2.80	
	HY-UHPC	4.57	2	300*300	NA	NA	4.00	3.00	
Moustafa and ElGawady (2018)	SEG	6.00	4	300	26.80	0.00	8.85	0.08	Hollow-core FRP-concrete-steel columns
	SEG-ED1	6.00	4	300	26.80	0.24	1.80	0.08	
	SEG-ED2	6.00	4	300	26.80	0.43	8.85	0.08	

Wang et al. (2018)	R-1	3.33	3	500	6.20	1.35	6.00	0.38	UHPC segmental columns with hollow square cross-section and replaceable dissipaters and cover plates.
	R-2	3.33	3	500	8.00	1.35	6.00	0.40	
	R-3	3.33	3	500	6.20	1.35	6.00	0.38	
Cai et al. (2019)	ED1N1	7.00	6	600*400	10.00	1.37	5.80	3.80	Mixed use of steel and basalt FRP reinforcement
	BFRP1N1	7.00	6	600*400	10.00	1.37	5.80	3.00	
	BFRP2N1	7.00	6	600*400	10.00	1.37	5.80	2.00	
	BFRP2N2	7.00	6	600*400	20.00	1.37	5.80	4.30	

Notation definitions see Table 5 notes.

3.7 Summary

Thanks to the trend in growing interests in accelerated bridge construction, applications of precast components have been extended from bridge superstructures to substructures in recent years. However, the use of precast columns is still mostly limited to low seismic regions. To expand the application to high seismic regions, substantial efforts have been made in the research of PT rocking columns. This review provides a summary of the research development and challenges for researchers and practitioners.

This study categorizes precast columns into three types: emulative column, simple rocking column, and hybrid rocking column. Emulative columns are designed to behave like monolithic columns. The related research and design code developments are relatively comprehensive. The two types of rocking columns are both non-emulative. Simple rocking columns are anchored to the foundation only by tendons without supplemental energy dissipating bars. The drawbacks are the low energy dissipation and large displacement demand. Hybrid rocking columns are composed of both tendons and ED bars, which are designed to dissipate energy, improve lateral stiffness and meet serviceability requirements. ED bars are normally unbonded in the joint region to avoid strain concentration caused by large openings. The tendons are designed to remain elastic and capacity-protected so that columns show self-centering

behaviors. Hybrid rocking columns are the most prominent option as they seek a balance between monolithic columns and simple rocking columns.

Numerous tests have been performed on PT columns and several new materials were investigated. While most often strands and high strength steel bars were used as PT tendons, attempts were made using SMA and FRP as PT materials as well. Supplemental energy dissipating was achieved either using external or internal ED bars, with steel or smart materials such as SMA. Rocking columns are subject to higher compression compared with traditional columns due to the rocking impact as well as PT forces. To improve the ductility and to limit compression damage, advanced materials were considered replacing normal weight concrete at the plastic hinge regions, such as ultra-high performance concrete and engineered cementitious composites. In addition, steel and FRP jackets were also used to provide better confinement thus improved ductility.

Upon a review of existing test parameters and results, some design recommendations can be made for the hybrid rocking column design:

- Hybrid rocking columns with ED bar ratios up to 1.7% have been tested by researchers and showed less than 1% residual drift when tested to a 6% maximum column drift.
- Tendons should be designed as capacity-protected elements to ensure self-centering behavior. This can be achieved when the moment capacity contribution from the tendon is higher than that from ED bars. Based on existing literature, it is suggested that the moment contribution from the ED bar is between 35% to 50% of the total moment resistance.
- Based on the review of existing testing data, for columns with the ED bar ratio ranging from 0 to 1.4% and the tendon area ratio ranging from 0.15% to 1%, the cracked to uncracked stiffness ratio ranges from 20% to 40%. When a detailed analysis is not

performed, both the lower and upper bound stiffness may need to be checked by designers.

- To facilitate engineering designs, two regression equations are proposed to calculate residual to maximum drift ratio and to predict the equivalent viscous damping ratio. It should be noted that as long as the crushed concrete does not hinder the re-entering force of the tendon, the residual displacement could be small, which does not necessarily mean the column is undamaged. Therefore, residual displacement is only one of the criteria for evaluation purposes.

To fully transfer research results to applications, detailed design standards are to be developed for use by design professionals. Although hybrid PT columns may be used if meeting acceptance criteria in ACI-374 (2014) based on physical testing, this would require much effort from practitioners. A design standard that allows engineers to demonstrate the strength and toughness of the rocking column through analysis rather than experimental evidence would expand its applications in seismic regions. In addition, efficient and reliable methods are to be developed for the construction of hybrid rocking columns, and the repair of various supplemental energy dissipating systems. One of the most important incentives of using precast columns is accelerating the construction. Achieving this goal would require researchers to spend more effort investigating simpler details that allow practical construction tolerances.

Chapter 4: Dynamics of post-tensioned rocking columns

4.1 Background

A rocking column may be the simplest form of structure, yet its seismic response can be very complex. The equations of motion of rocking columns have been developed by several researchers as discussed in Chapter 3. However, there is limited existing literature revealing how various parameters affect the seismic performance of a rigid rocking column post-tensioned with tendons. It is not clear how much improvement can be achieved with the use of supplemental damping and tendons, or if they are always beneficial. This chapter examines the dynamic behaviors of post-tensioned concrete columns under seismic excitations. The equations of motion are derived using Lagrange's method and are solved using the Fourth-Order Runge-Kutta method. The effects of tendon stiffness, initial post-tensioning force, and supplemental damping on the dynamic behaviors are investigated.

Early studies of free oscillations of rocking blocks were conducted by Housner (1963) which was triggered by observations that some rocking and slender structures survived the Chilean earthquakes in May 1960 and Arvin-Tehachapi earthquakes in California in July 1952. Housner (1963) discovered an unexpected scale effect, which makes blocks with larger geometry more stable. Subsequently, several researchers investigated the rocking response of rigid blocks (Aslam et al. 1980; Hogan 1990; Ishiyama 1982; Psycharis and Jennings 1983; Shenton III 1996; Spanos and Koh 1984). Yim et al. (1980) further investigated the sensitivity of rigid blocks under earthquake loadings with different sizes. It was found that the stability of a block does not necessarily increase with the increase in size or decrease in slenderness. Overturning of a block by a specific ground motion does not imply that the block will overturn under a particular more intense motion. The rocking response of free-standing blocks under cycloidal pulses was studied by Zhang and Makris (2001). The rocking behavior assembly consisting of multiple

blocks was studied by a number of researchers (Andreaus and Casini 1999; Psycharis 1990; Spanos et al. 2001; Winkler et al. 1995). A methodology to derive equivalence between the single rocking block and multiple blocks was proposed by DeJong and Dimitrakopoulos (2014). The existing studies revealed the complexity of design rocking columns under seismic loads, further study is needed to investigate how different components of the post-tensioning system affect its performance.

4.2 Initiation of rocking response

Under lateral loads, rocking structures start rotating about pivot points once the lateral force reaches a threshold. Overturning of the structure does not occur if the re-centering moment is greater than the overturning moment. The response after rotation initiates and before overturning is called the rocking response. Consider a simple rocking column shown in Figure 28, with a width of 2b and a height of 2h. The center of gravity (C. G.) of the structure is at a height of H. The two pivoting points of the column are denoted as O (right-hand side) and O' (left-hand side). The distance from C.G. to the pivoting points is R. The angle between the vertical direction and the distance R radius is denoted as α, which describes the slenderness of the column geometry. The mass of the structure is defined as m located at a height of H. The directions of positive axes x and y are shown in Figure 28. The condition for the initiation of rocking response is

$$\mathrm{H}m\left|\ddot{x}_g\right| > bmg + bm\ddot{y}_g \qquad \text{Equation 19}$$

where $\ddot{x}_g$ is horizontal ground acceleration, $\ddot{y}_g$ and g are vertical ground acceleration and gravity acceleration, respectively. A positive vertical ground acceleration would help increase the stability of the rocking column and vice versa. For simplicity, this study ignores the vertical component of earthquake excitations.

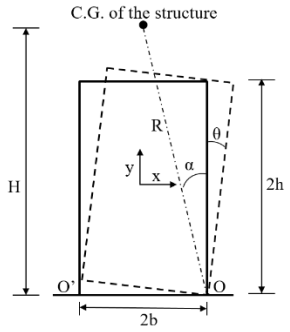

Figure 28 Schematic of rocking column

When the rocking column is comprised of multiple rigid blocks, there could be several rocking modes as presented in Spanos et al. (2001). An example of a rocking column with two identical blocks is shown in Figure 29. For simplicity, it is assumed that the C.G. of the structure is at the top center of the column. This is a reasonable assumption for most regular highway bridges. The column could rock in modes shown in Figure 29b or Figure 29c. When the two blocks have no differential rotation, the assembly behaves like a single block as shown in Figure 29b. When the two blocks rotate relative to each other, the mode is represented by Figure 29c. Assume the bottom block rotates about point O, and the top block rotates about point O''. For the top block, the re-centering moment about point O'' is shown in Equation 20.

$$M_r = mg[Rsin(\alpha - \theta) + hsin\theta] \quad \text{Equation 20}$$

$hSin\theta$ is the horizontal distance between O and O'', which represents an additional re-centering moment for the top block. Similarly, the overturning moment of top block about O'' is shown in Equation 21.

$$M_o = m\ddot{x}_g[RCos(\alpha - \theta) - hCos\theta] \quad \text{Equation 21}$$

The top block would start to rotate about point O'' when M_o is greater than M_r, which can be written as the following function (Equation 22).

$$f(\alpha, \theta) = M_r - M_o < 0 \quad \text{Equation 22}$$

A simple case study will show that this is unlikely to happen considering most regular bridge column geometries. Assume a peak ground acceleration equals gravity ($m\ddot{x}_g = \mathrm{mg}$), normalize $f(\alpha, \theta)$ with R gives Equation 23.

$$\frac{f(\alpha,\theta)}{\mathrm{R}} = \mathrm{Sin}(\alpha-\theta) - \mathrm{Cos}(\alpha-\theta) + \frac{\mathrm{Cos}\alpha(Sin\theta + Cos\theta)}{2} \qquad \text{Equation 23}$$

The function $f(\alpha,\theta)/\mathrm{R}$ is plotted in Figure 30, considering the ranges of α and θ up to 0.5 rad. It is observed that in the considered range, $f(\alpha,\theta)$ is always positive, which means that the two blocks do not have differential rotations and act as one rigid body. It is also seen that a higher value of α not only increases the stability of a single rocking block, but also increases the stability of an assembly of rocking blocks.

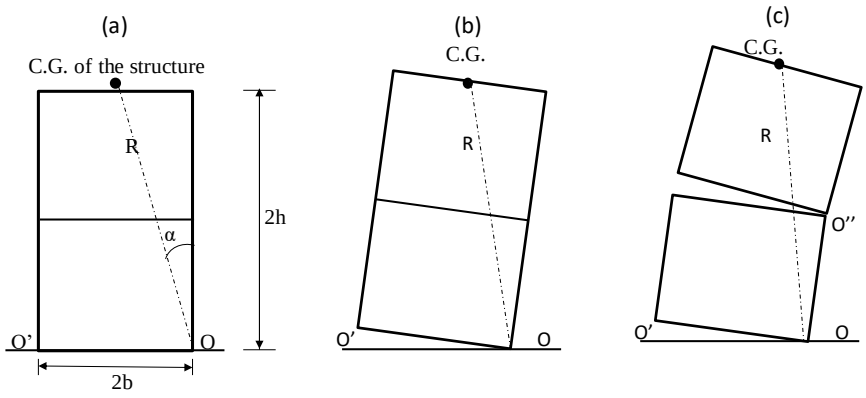

Figure 29 Schematic of multiple rocking blocks

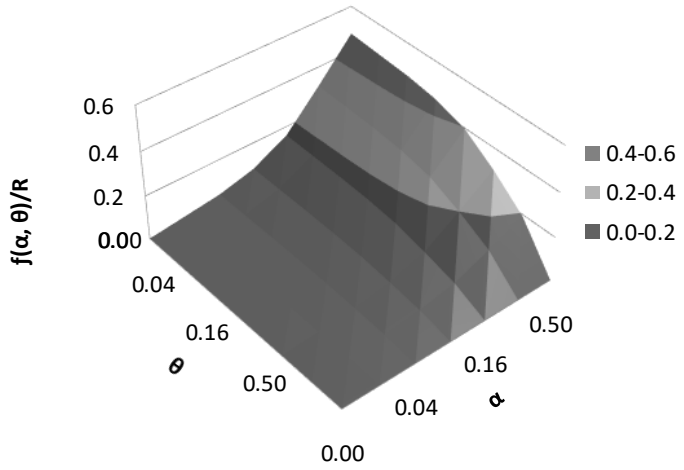

Figure 30 Relation of $f(\alpha,\theta)/R$, α and θ

4.3 Equations of motion

The rocking column system has several different components determining its dynamic response. In this chapter, the Lagrange method is used to derive the equations of motion, which are then solved using the Fourth-Order Runge-Kutta method. The equations of motion include the consideration of prestressing force, tendon stiffness and supplemental damping. This study focuses on the rocking behavior of a single column. Its kinetic energy is described in Equation 24.

$$T = \frac{1}{2}\mathrm{I}\dot{\theta}^2 \qquad \text{Equation 24}$$

where I is the moment of inertia and $\dot{\theta}$ is the angular velocity. For a simple unrestrained rocking column, when the column rotates about the O point ($\theta > 0$), the potential energy of the column is described in Equation 24.

$$V = \delta mg\Delta\mathrm{H} = \delta mgr[\cos(\alpha-\theta) - \cos(\alpha)] \qquad \text{Equation 25}$$

Lagrange method is described using Equation 26,

$$\frac{d}{dt}\left(\frac{dL}{d\dot{\theta}}\right) - \frac{dL}{d\theta} = \mathrm{Q} \qquad \text{Equation 26}$$

where L is the Lagrange equation (L=T-V) and Q is the external force. Considering ground motion acceleration, the external force that contributes to the rocking energy is $\mathrm{F(t)Rcos(\alpha-\theta)}$. $\mathrm{F(t)}$ is the seismic force in the horizontal direction ($\text{-}\ddot{x}_g mg$), $\mathrm{Rcos(\alpha-\theta)}$ is the moment arm about point O. Combining equations (6) through (8) yields Equation 27.

$$\mathrm{I\ddot{\theta} = -mgR\sin(\alpha-\theta)} + F(t)Rcos(\alpha-\theta) \qquad \text{Equation 27}$$

Similarly, when the column rotates about point O'($\theta < 0$), Equation 27 becomes Equation 28.

$$\mathrm{I\ddot{\theta} = mgR\sin(\alpha+\theta)} + F(t)R\cos(\alpha+\theta) \qquad \text{Equation 28}$$

To increase the stability of rocking columns, vertical tendons can be used to anchor them to the foundation (Figure 31). For a prestressed rocking column, its potential energy term in the Lagrange equation has an additional tendon strain energy.

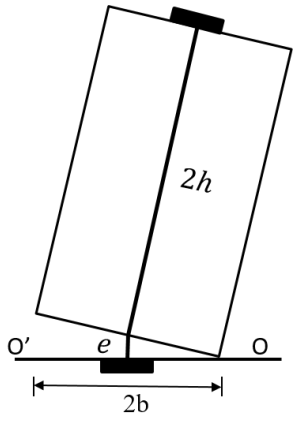

Figure 31 Schematic of a rocking column with tendons

For a rotation of θ, the elongation of the tendon caused by rocking is approximated by Equation 29.

$$e(\theta) = b\theta \qquad \text{Equation 29}$$

With an initial elongation e_0 for prestress force, the total strain energy in the tendon is described in Equation 30.

$$\mathrm{E(\theta)} = \frac{1}{2}\mathrm{k}(b\theta + e_0)^2 \qquad \text{Equation 30}$$

Thus, when the column rotates about point O, the potential energy of the column with tendons is described using Equation 31.

$$V = mgR[\cos(\alpha - \theta) - \cos\alpha] + \frac{1}{2}\mathrm{k}(b\theta + e_0)^2 \quad \text{Equation 31}$$

Applying Lagrange's method, the equation of motion becomes Equation 32.

$$\mathrm{I}\ddot{\theta} = -\mathrm{mgR}\sin(\alpha - \theta) - [\mathrm{bk}(\mathrm{b}\theta + e_0)] + \mathrm{F(t)Rcos}(\alpha - \theta) \quad \text{Equation 32}$$

The condition to initiate rocking is shown in Equation 33.

$$m|\ddot{x}_g|\mathrm{H} > mgb + bP_0 \quad \text{Equation 33}$$

where P_0 is the initial post-tensioning force. Similarly, when the rotation is about O', the equation of motion becomes Equation 34.

$$\mathrm{I}\ddot{\theta} = mgR\,sin(\alpha + \theta) - [\mathrm{bk}(\mathrm{b}\theta + e_0)] + F(t)Rcos(\alpha + \theta) \quad \text{Equation 34}$$

By introducing a rocking frequency parameter p^2 equals mgr/I and $sgn(\theta)$ function, the equation of motion can be written as Equation 35.

$$\ddot{\theta} = -p^2\left(sin(\alpha sgn(\theta) - \theta) + \frac{\ddot{x}_g}{g}cos(\alpha sgn(\theta) - \theta)\right) - sgn(\theta)\frac{\mathrm{bk(b}\,|\theta| + e_0)}{I} \quad \text{Equation 35}$$

When the post-tensioned column is subject to free rocking in the positive rotation, the equation of motion is shown in Equation 36.

$$\ddot{\theta} = -p^2(sin(\alpha sgn(\theta) - \theta)) - \frac{\mathrm{bk}(\mathrm{b}\theta + e_0)}{I} \quad \text{Equation 36}$$

For a small rotation, the re-centering moment component can be linearized as $\sin(\alpha - \theta)$ equals $\alpha - \theta$. When the column has no initial prestressing force, the rocking motion about O is described as Equation 37.

$$\ddot{\theta} + p^2\left(\frac{\mathrm{kb}^2}{mgr} - 1\right)\theta = -p^2\alpha \quad \text{Equation 37}$$

With the initial condition of $\theta = \theta_0$ and $\dot{\theta} = 0$ at time t=0, assuming a parameter of q is $\frac{\mathrm{kb}^2}{mgr}$, the solution is shown from Equation 38 to Equation 40.

When 1-q>0 Equation 38

$$\theta = \left(\theta_0 - \frac{\alpha}{1-q}\right)\cosh\left(pt\sqrt{1-q}\right) + \frac{\alpha}{1-q}$$

When 1-q=0 Equation 39

$$\theta = -\frac{p^2 t^2 \alpha}{2} + \theta_0$$

When 1-q<0 Equation 40

$$\theta = \left(\theta_0 - \frac{\alpha}{1-q}\right)\cos\left(pt\sqrt{q-1}\right) + \frac{\alpha}{1-q}$$

Assuming the period of the rocking column is T, at time T/4, the rocking column arrives at balanced position $\theta = 0$, thus when 1-q>0, T can be solved using Equation 41.

$$0 = \left(\theta_0 - \frac{\alpha}{1-q}\right)\cosh\left(pT/4\sqrt{1-q}\right) + \frac{\alpha}{1-q}$$ Equation 41

Similarly, T can be solved for the condition of q equals or greater than 1. The relationships among $\frac{\theta_0}{\alpha}$, parameter q and period T are plotted in Figure 32. As can be seen, when q is zero, which means there is no tendon, the period increases with the increases in rotation amplitude. When q is greater than 0, the period also increases with the increase in amplitude, but the slope is smaller. Furthermore, the increase of q has an effect on the increasing vibration frequency.

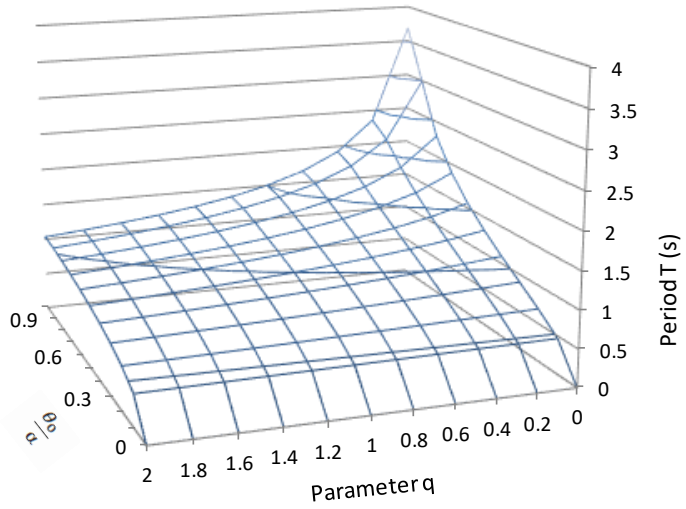

Figure 32 Relation between $\boldsymbol{\theta}$, parameter q and period T

In addition to improvements made by using tendons, engineers and researchers used supplemental damping devices to improve the seismic performance of rocking columns. In this case, the equation of motion includes an additional term representing the damping force as shown in Equation 42

$$\ddot{\theta} = -p^2\left(sin(\alpha sgn(\theta) - \theta) + \frac{\ddot{x}_g}{g}cos(\alpha sgn(\theta) - \theta)\right) - \frac{\mathrm{bk}(\mathrm{b}\theta + e_0)}{I} - \frac{\sum F_d r}{I} \qquad \text{Equation 42}$$

where F_d represents damping forces and r represents corresponding moment arms. A comprehensive and detailed formulation for supplemental hysteretic and viscous damping on rocking columns is presented in Makris and Aghagholizadeh (2019).

4.4 Effects of tendon and supplemental damping

As shown in Equation 42, the rocking response is affected by initial post-tensioning force, stiffness of the tendons and supplemental damping. In a recent study, it was proven that the addition of tendons and supplemental damping does not always improve the performance of the rocking column. Vassiliou and Makris (2015) conducted a comprehensive study on rocking columns with vertical tendons. It was concluded that when the column size R is greater than 5

m, their rocking response becomes independent of the tendons as the resistance primarily originates from the rotational inertia. In the study by Makris and Aghagholizadeh (2019), it was found that the effect of supplemental damping strongly depends on kinematic characteristics of the ground motion. In some cases, such as the Newhall ground motion recorded during the 1994 Northridge earthquake, the rocking rotation of damped columns exceeded that of undamped columns.

This study first re-visits some of the previous case studies, then further explores the effects of tendon and supplemental damping on the rocking response. In Makris and Aghagholizadeh (2019), the South Rangitikei Rail Bridge in New Zealand is used as an example rocking structure for dynamic analysis. This study starts with the same structure then expands to various parameters. Several important rocking parameters of the South Rangitikei Rail bridge are frequency parameter p = 0.38 (1/sec), slenderness parameter alpha = 0.146 (rad), half of column width b=6.75 (m), mass m=1900000 (kg), and column size R=46.36 (m). In the case of viscous dampers installed at the rotation pivot points, F_d can be calculated using Equation 43

$$F_d = Ce'(t) \qquad \text{Equation 43}$$

where C is the damping coefficient and $e'(t)$ is the translational velocity of the damper in the vertical direction.

Figure 33 presents the response of the rocking columns' free vibration considering four scenarios: 1. rocking column is unrestrained; 2. a tendon is used to restrain the rocking column; 3. prestress force is applied to the tendon; 4. in addition to tendon and prestress force, supplemental damping is added to the column. The undamped columns do not have the supplemental viscous damping but still have minimum damping to engage in rocking response as expressed in Equation 44. During the rocking response, it is assumed the shift between O and O' is smooth and the angular momentum is conserved. The angular velocities before and

after an impact can be computed based on the conservation of angular momentum as shown in Equation 44 (Housner 1963).

$$\mathrm{r} = \left(\frac{\dot{\theta_{t2}}}{\dot{\theta_{t1}}}\right)^2 = \left[1 - \frac{mR^2}{I}(1 - \cos 2\alpha)\right]^2 \qquad \text{Equation 44}$$

where $\dot{\theta_{t2}}$ and $\dot{\theta_{t1}}$are the velocities after and before the impact.

The initial conditions for all columns are 0.05 rad rotation and zero angular velocity. It is shown that the use of tendon reduces the rocking period and the addition of prestressing force further reduces the rocking period. It can also be seen that the supplemental damping reduces both the rocking period and rotation magnitude.

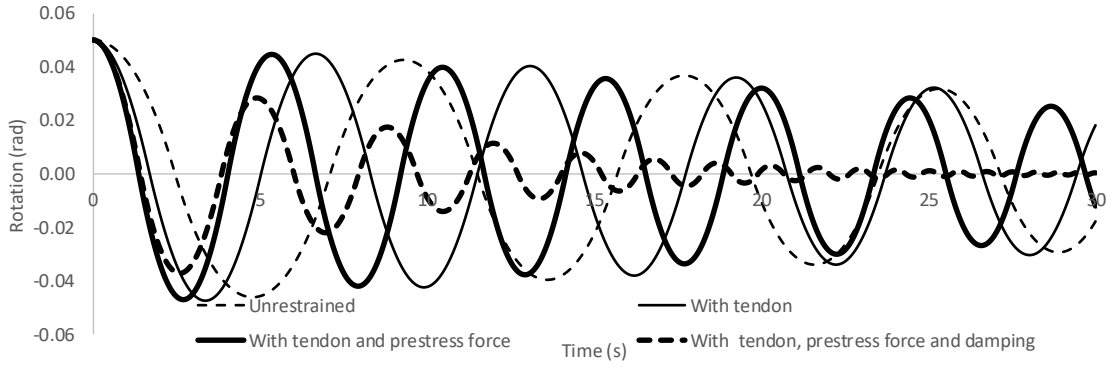

Figure 33 Free rocking response in different scenarios

However, observations similar to Figure 33 do not always happen when there are external excitations. Figure 34 shows a rare case where the rocking rotation of the damped structure is higher than the undamped structure when the Newhall ground motion recorded during the 1994 Northridge earthquake is applied to the structure. Included in Figure 34 is the acceleration time history of the ground motion, the normalized rotation time history of the column, and the angular velocity time history of the column. In the damped case, the damping constant C is 4444 kNs/m and the damper has zero length, which are the same assumptions in the study by Makris and Aghagholizadeh (2019), where the authors suggested that the damping forces possibly make the rocking column recover back to the balanced position slower, which lead to further rotation

in the next half cycle of the ground acceleration. The authors suggested that the phenomenon of damped response exceeding undamped response would occur when the ground motions show the characteristics that can be represented by antisymmetric Ricker wavelet.

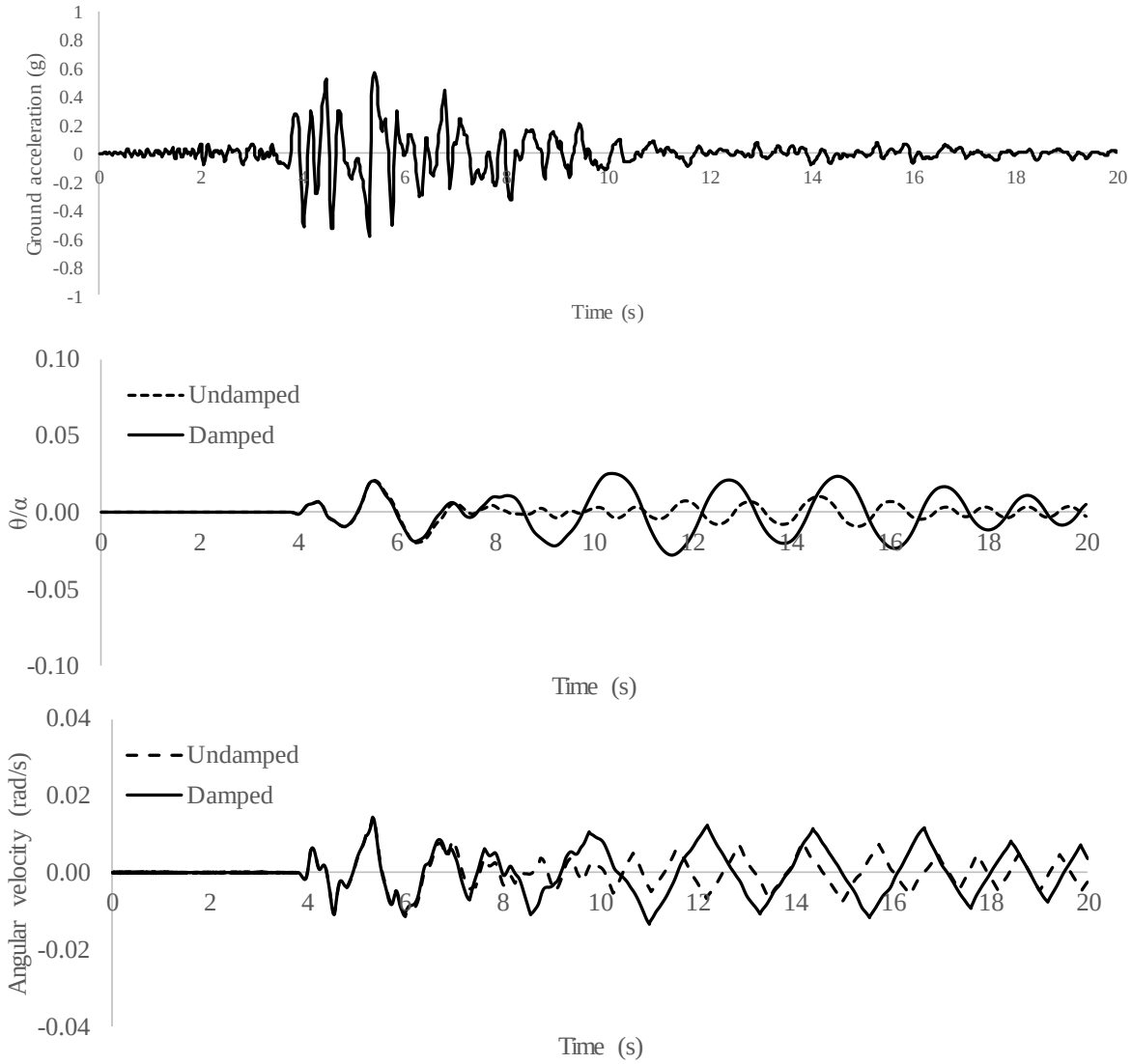

Figure 34 Rocking response of damped and undamped structure (Newhall ground motion)

The negative effects of supplemental damping observed in Figure 34 may be remediated by changing some other rocking parameters, such as using prestressed tendons. It is found that if a steel tendon with an area of 45,000 mm^2 prestressed to a strain of 0.003 is provided, the damped response would be reduced. The assumed steel tendon area is less than 1% of the column sectional area, which is acceptable in design practice. Figure 35 presents the

comparison between undamped column (previously studied), damped column (previously studied) and damped column with prestressing tendons (PT). The damped column with PT not only has a low magnitude of rocking rotation, but it also damps out the vibration the quickest among the three scenarios.

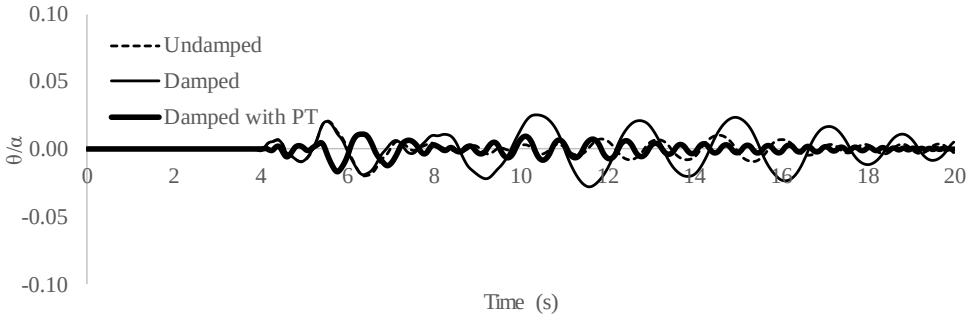

Figure 35 Rocking response of damped, undamped and PT structure (Newhall ground motion)

When the same structure is subject to the 1971 Pacoima Dam record, the response under undamped condition, damped condition and damped with PT are shown in Figure 36. In this case, as expected, the undamped structure has higher rotation and the damped structure with PT has the lowest rotation.

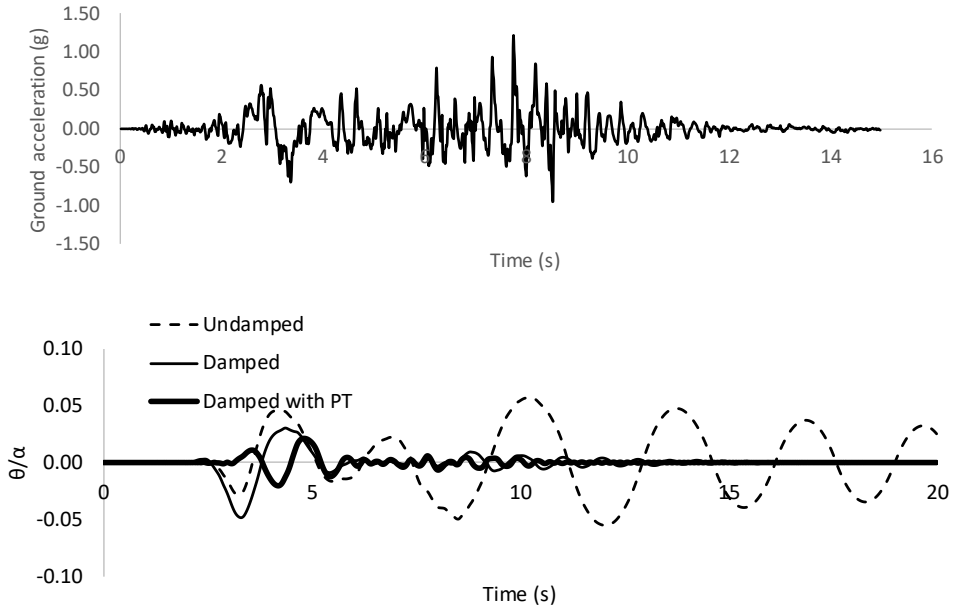

Figure 36 Rocking response of damped and undamped structure (Pacoima Dam motion)

4.5 Rocking spectrum analysis

Rocking spectrum is similar to response spectrum analysis and reveals important seismic response for a series of continuously changing parameters. In most cases, it is believed that the use of tendons, prestress force and supplemental damping is beneficial to the seismic performance. This section examines this understanding by using the rocking spectrum varying one parameter at a time. Rocking structures can be described by several parameters (Makris and Vassiliou 2013; Vassiliou and Makris 2015): p equals to $\sqrt{\mathrm{mgr}/\mathrm{I}}$, EA/mg representing the relative stiffness of tendon, P/mg representing the effect of prestress force and C/mp representing the damping effect.

This section presents the rocking response of a large column (presented in the previous section) and a small column (a typical highway bridge single column) under two ground motions, which are the Newhall ground motion recorded during the 1994 Northridge and the 1971 Pacoima Dam record. The Pacoima Dam record contains notable acceleration pulses (longer than 1 second) that impose high deformation demands on structures (Makris and Aghagholizadeh, 2019). Response spectra of the two motions are plotted in Figure 37. Response spectrum analysis is often used to estimate peak responses of essentially elastic single degree of freedom structures based on their structural periods. The response spectrum does not apply to rocking structures due to the different vibration mechanisms. However, from the response spectra plots, it can be seen that the structural peak response is non-linear and does not necessarily decrease with the increase in the structural period. From the standpoint of the response spectrum, the Newhall record creates high acceleration for vibration period ranges approximately between 0.2s to 0.4s.

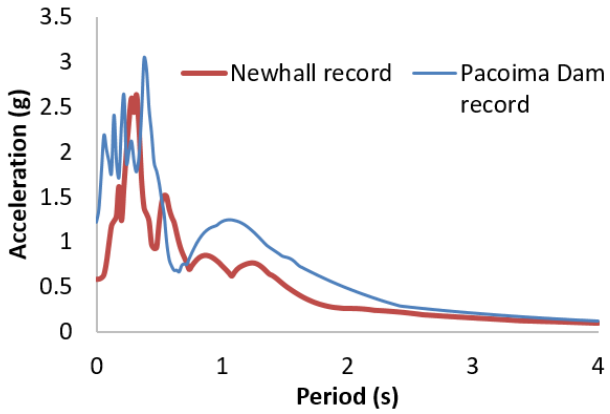

Figure 37 Response spectra

The rocking spectra of the two ground motions applied to structures based on the South Rangitikei Rail Bridge in New Zealand as a prototype are plotted in Figure 38. The spectra are plotted with one varying parameter at a time and a fixed column size R. The maximum rocking rotation is used as the structural response indicator. In Figure 38a, the maximum rotation generally reduces with the increase of 1/p. A small value of 1/p represents a slender column, which is more likely to be overturned. Figure 38b shows the effect of tendon stiffness. For the Pacoima Dam record, the peak rotation reduces with the increase in tendon stiffness until a certain level then increases again. For the Newhall record, the peak rotation increases with the increase in tendon stiffness. In Figure 38c, it is seen that the response under the Pacoima Dam record decreases first then increases with the increase in prestress force. The response under the Newhall record is a constant positive slop curve with the increase in prestress force. Figure 38d shows the effect of supplemental damping. It is seen that for both two ground motions, there are local peaks and lows, which means that the damping effect could improve or reduce the seismic performance depending on ground motion characteristics and rocking parameters.

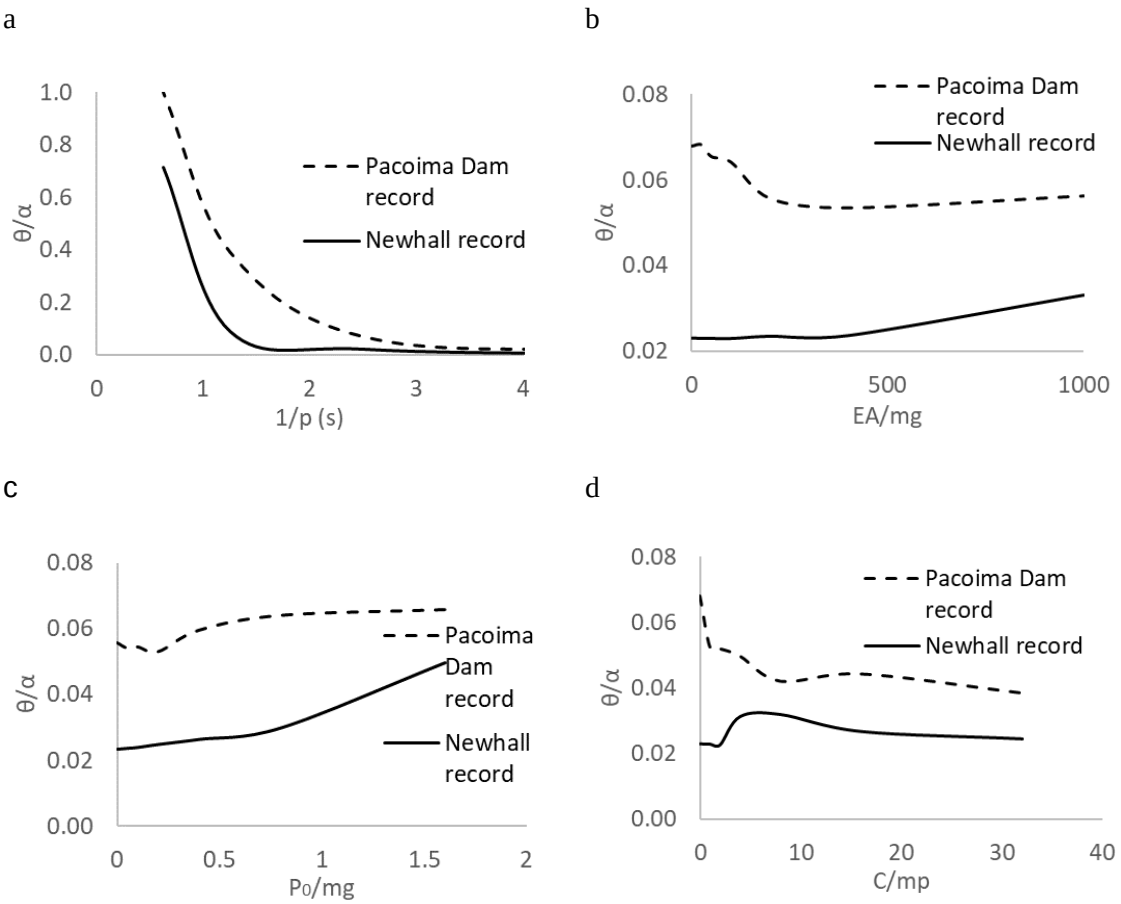

Figure 38 Rocking spectrum of a large column

Subsequent to the rocking spectrum analysis of the large rocking pier, a parallel analysis is performed on a typical highway bridge column with an R of 7.1m. The rocking spectra are plotted in Figure 39. Similar observations to the large column can be drawn from Figure 39 for the typical highway bridge column. The effects of the tendon, prestress force and damping are not always beneficial to the structural response. The parameter p has the most significant effect on the rocking rotation, the parameter EA/mg representing tendon stiffness may increase or decrease rocking rotation when it changes the structural stiffness. The parameter P_0 representing initial PT force is likely to increase rocking rotation magnitude, although it can delay the time for initial rocking. The parameter C/mp representing damping may occasionally increase rocking magnitude, however, in most situations, it decreases rocking rotation.

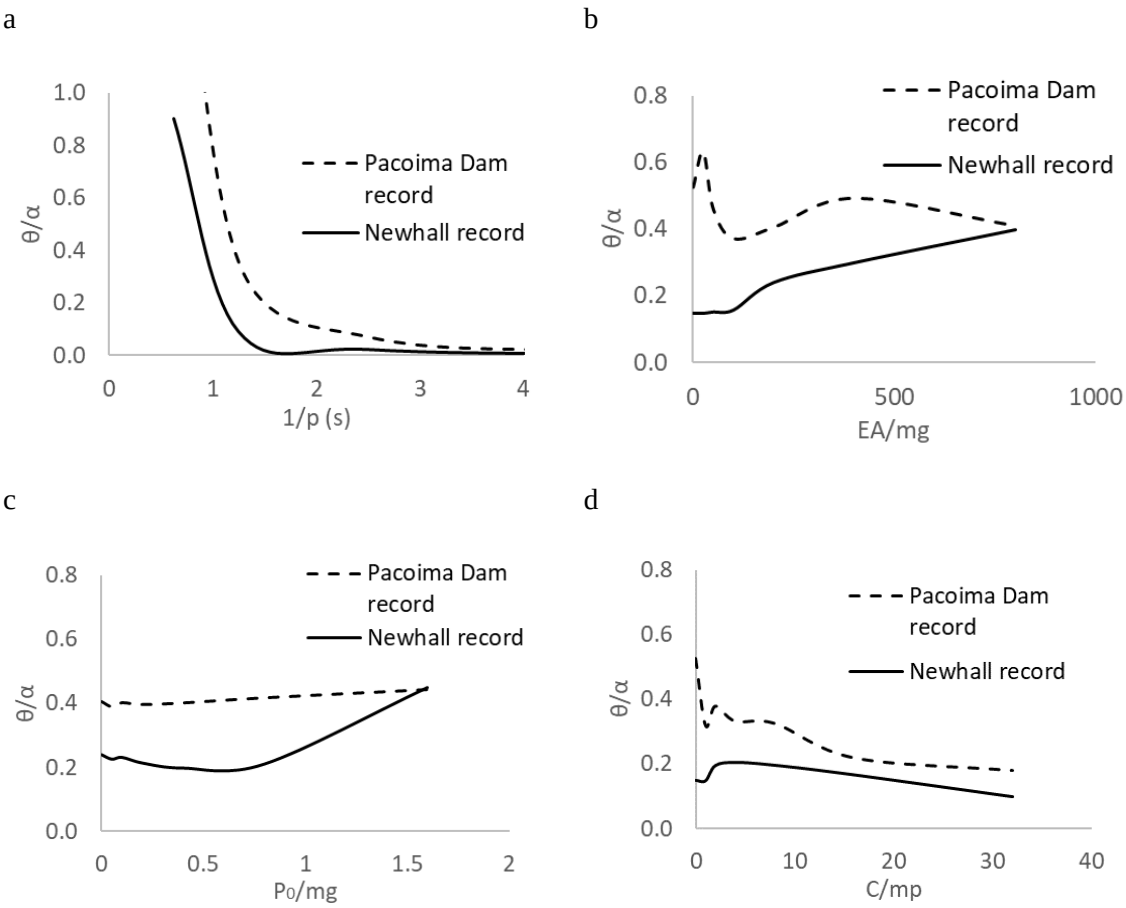

Figure 39 Rocking spectrum of a typical highway bridge column

4.6 Summary

This study derives the equations of motion of rocking columns using the Lagrange Method and investigates the effects of tendons and supplemental damping on the rocking response. The following conclusions can be drawn.

- A parameter q is defined to represent the stiffness of the tendon. When q is zero (no tendon condition), the period increases with the increases in initial rotation amplitude. When q is greater than 0 (with tendon condition), the period increases with the increase in initial rotation amplitude, but the rate is smaller. The increase in tendon stiffness has an increasing effect on the vibration frequency.

- This study confirms findings by Makris and Aghagholizadeh (2019) that the kinematic characteristics of ground motions determine the effectiveness of supplemental damping. Further study shows that the effectiveness of tendon stiffness and initial PT force also dependent on the kinematic characteristics. Although when in free vibration, tendon stiffness, initial PT force and supplemental damping are beneficial to the seismic performance, it is not always true when the structure is subject to ground motions.
- Existing literature suggests that using supplemental damping may adversely change the rocking response and increase maximum rocking rotation. This study finds that this effect can be eliminated by using supplemental damping and post-tensioning at the same time. When supplemental damping happens to increase the rocking response by changing its period, other measures such as post-tensioning should be used to further control the response.
- One large size and one small size columns are studied considering two ground motions. Rocking spectra are plotted for the two structures considering varying tendon stiffness, initial PT force, and supplemental damping. The use of supplemental damping may amplify peak rotation occasionally, in most cases, it reduces the peak rotation response.

Chapter 5: Evaluating the seismic behavior of segmental post-tensioned concrete columns using factorial analysis

5.1 Background

Segmental post-tensioned concrete columns are comprised of prefabricated concrete segments assembled by tendons. Unbonded post-tensioned concrete columns can provide a rapid construction method because they are manufactured in factories so that construction time can be reduced compared to that of cast-in-place construction. Precast columns also often have higher quality as they are fabricated in a better-controlled environment (Jacqueline 1999). On top of these benefits, these columns can achieve better seismic performance (Hewes and Priestley 2002; Ou et al. 2007).

In this chapter, detailed finite element models of the segmental post-tensioned concrete columns are developed. It involves the interaction of several structural elements and their inelastic behaviors. Thus, it is beyond the complexity of the equations can achieve in Chapter 4. Segmental unbonded post-tensioned concrete columns can resist large lateral drift and reduce residual deformation considerably. They show trivial residual deformation and may experience only minor damages near the compression toe close to the support under moderate earthquakes. As a result, the columns can be functional without major repairs (Hewes and Priestley 2002). Several researchers (ElGawady and Dawood 2012; Moon et al. 2015) have conducted finite element analysis on unbonded post-tensioned concrete piers. These studies cast light on many important issues of unbonded post-tensioned concrete piers. ElGawady and Dawood (2012) presented models that were under monotonic pushover loads using Abaqus (2012). Ou et al. (2007) developed models with energy dissipation bars that were subjected to cyclic loads. In this study, the model validations and fractional factorial analyses were conducted based on both cyclic load results (fractional factorial analysis) and single-direction

pushover analyses (preliminary 3-factor analysis). The seismic behavior of unbonded post-tensioned concrete columns depends on a number of factors, such as concrete strength, initial tendon stress and the aspect ratio of columns. The initial tendon stress plays an important role because the stress should be high enough to allow the transfer of lateral shear force, and it should avoid very high axial load. The initial stress of the tendon should be applied at a level that can avoid its inelastic response in earthquake to reduce the residual lateral displacement. Stress on tendons may also affect the stiffness of columns. Therefore, this study determines the interactions between different factors that affect the overall seismic performance of unbonded post-tensioned concrete columns.

5.2 Finite element model of unbonded post-tensioned concrete columns

In this chapter, ABAQUS (2012) is used to perform finite element analysis and the model is developed according to tests conducted by Hewes and Priestley (2002). In the finite element model, concrete was modeled using the C3D8R element, which is a general-purpose and fully integrated linear brick element (ABAQUS 2012). The Damaged Plasticity model was used for concrete material modeling. As for the confined concrete material, the spiral confined concrete model from Mander et al. (1988) and the steel tube confined concrete model from Han (2000) were incorporated. The concrete model can be used for both static and dynamic modeling (Dawood et al. 2011). Longitudinal steel rebar and tendon were modeled using truss elements T3D2. The steel jacket was modeled by shell elements S4R. The steel jacket was only used to confine the bottom segment, which was the segment directly connected with the foundation. The tendons were anchored in the foundation and loading head. The loading head was subjected to a vertical force that represented superstructure dead loads. Contact behaviors between segmental concrete, segmental concrete and foundation, segmental concrete and loading head, concrete and steel jacket were modeled using node to surface contact method. The contact properties were defined using the default constraint enforcement method and hard

contact, which meant that the contact surfaces cannot withstand tension. Tangential behavior between segments was modeled using a penalty method with a friction coefficient of 0.5 suggested by Dawood et al. (2011). Since the tendons were unbonded with concrete, the friction between concrete and tendons was negligible. The tangential friction coefficient was set to zero between tendons and concrete to simulate the unbonded behavior. In the simulation, loadings to the columns were divided into three steps. In the first step, the post-tensioning force was applied to the tendons by defining the tendon initial stress. Superstructure weight was applied to the columns in the second step, and the lateral force on the loading head was applied in the third step. All the loadings were the same as the tests (Hewes and Priestley 2002). Mesh sensitivity analysis was performed to generate accurate results while keeping the simulation computationally less expensive. The same mesh size (80 mm) was used for both steel tube and concrete. As an example, the JH11 specimen model had 14,032 elements in total, including 429 elements of S4R, 523 elements of T3D2 and 13,080 elements of C3D8R. All the models used similar mesh sizes. The finite element model is shown in Figure 40.

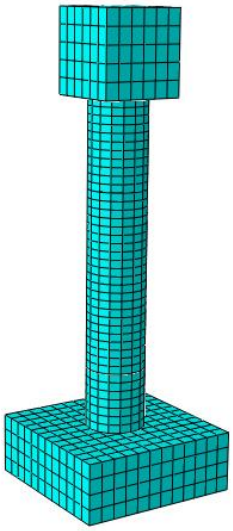

Figure 40 Finite element model in Abaqus (2012)

5.3 Model validation

The finite element model was validated with experimental results by Hewes and Priestley (2002). The tests were conducted at the University of California at San Diego (UCSD). The four columns used for validation were named JH11, JH21, JH31, and JH41. All columns were circular sections and the diameter of the section was 610 mm. The bottom segmental concrete was 610mm high and all other segmental concrete segments were 900 mm high. The first two columns were comprised of four segments. The bottom segment was confined by a steel tube to improve its compressive strength and ductility. The steel tube was not connected to the foundation. The bottom segment had no reinforcement and all other segments were reinforced. The longitudinal reinforcement was not connected between each segment. They were connected only by tendons and the tendons were anchored into the foundation and loading head. The ultimate strength of the tendon was 1860 MPa and the cross-section area of the tendon was 2665mm^2. The aspect ratio (column height divided by column diameter) of the two columns was 6. The specimens JH31 and JH41 were similar to the first two specimens, except that the aspect ratio of JH31 and JH 41 was 3.

The simulation results were compared with experimental results in Figure 41 (a), (b), (c) and (d). Simulation (a) and (b) were under cyclic loads; (c) and (d) were under pushover loads. Results show that the model can capture the stiffness, yielding, and residual displacements. The errors of the simulation in terms of stiffness, strength, and post-elastic stiffness are presented in Table 8. The errors were likely caused by the contact modeling between different components, stress loss, anchorage and foundation modeling. It should be noted that the residual displacements were very small in both test and simulation. In the tests, it was reported that the residual drifts were only 0.14% (JH11) and 0.3% (JH21) (Hewes and Priestley 2002). In the simulation, it was also observed that the residual drift was smaller than 0.3%.

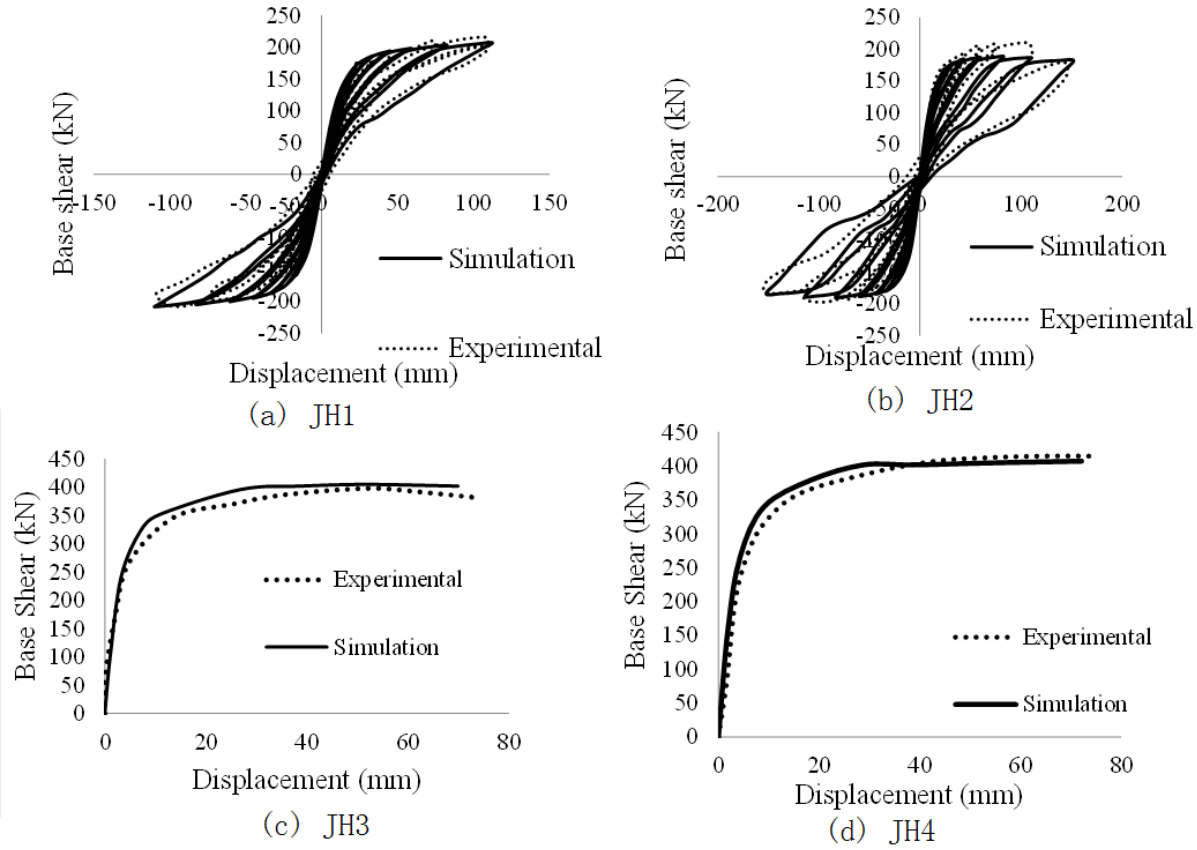

Figure 41 Finite element model validation

Table 8 Errors in predicting initial stiffness, maximum shear and post-elastic stiffness

Specimen	Initial stiffness	Max base shear	Post-elastic stiffness
JH11	10.10%	4.22%	0.71%
JH21	4.41%	10.40%	6.67%
JH31	12.36%	1.11%	7.7%
JH41	3.64%	2.51%	14.25%

5.4 Preliminary interaction study

The behavior of an unbonded post-tensioned concrete column can be affected by various factors, such as the concrete strength, reinforcement ratio of tendon and post-tensioning force (Dawood et al. 2011; Dawood and ElGawady 2013). The major difference between unbonded post-tensioned concrete columns and regular reinforced concrete columns is the existence of post-tensioning force. The preliminary study focuses on the investigation of the unique

characteristics of unbonded post-tensioned concrete columns, which is the post-tensioning force. The post-tensioning force is jointly determined by the tendon area and the tendon stress as the force is the product of the tendon area and initial stress. From existing research, it is not clear whether the two factors (post-tensioning level and post-tensioning ratio) have the same effects on the overall response of the pier or not. If the two factors work in the same manner to affect pier response, an increase in the initial stress would be a more economical way than the increase in the tendon area. Additionally, the post-tensioning force and concrete strength are important factors that determine axial load ratio. So that concrete strength was also included in the preliminary study to check potential interactions between post-tensioning elements and concrete strength. After the preliminary study, a more comprehensive study was performed for seven factors that determine the column response. The seven factors include the aspect ratio of the column, transverse reinforcement ratio, longitudinal reinforcement ratio, axial dead load ratio, the aspect ratio of segment, post-tensioning stress ratio and concrete strength.

In the preliminary study, the considered parameters are concrete compressive strength ($f_c^{'}$), the ratio of the tendon to concrete cross-section ($\mathrm{A_p}/\mathrm{A_g}$, defined as post-tensioning ratio, PT ratio) and post-tensioning force level defined as a ratio, between initial stress and ultimate strength (f_{pi}/f_{pu}, defined as post-tensioning level, PT level) of the tendon. A factorial design of 3×3×3 has been conducted to find the interactions among the three factors (compressive strength, PT ratio and PT level). Each of the factors was considered at three levels. The three levels of PT ratio were 0.44%, 0.90% and 1.20% of gross section area; three levels of post-tensioning force ratio were 10%, 30% and 70% of ultimate stress; three levels of concrete compressive strength were 30 MPa, 50 MPa and 70 MPa. There were 27 runs as a complete combination of three factors. Among the 27 runs, the dead load was the same for all but concrete strength and post-tensioning force varied, which led to varying axial load ratios ranging from 2% to 52%.

5.4.1 Simulation results

The first step in the loading was to apply post-tensioning force to the tendon. It was observed that with the increase of post-tensioning force, stress was higher on the concrete cover and the segments were shortened slightly. Figure 42 shows the stress distribution in a segment. The top and bottom concrete were subjected to more concentrated stress compared to the other segments. This was because the tendons were located at the center of the pier and were anchored through the top and bottom segments. In the second step, a compressive load was applied to the top of the loading head to represent the superstructure dead load. During this step, it was observed that the stress on the steel tube was higher than that on the concrete (Figure 43). In the third step, when lateral loading was applied, the column started to bend and stress increased significantly at the compression side. With further increase in the lateral load, the separation between the foundation and bottom concrete segment was observed since they were not connected by rebar. The deformed shape of the model is shown in Figure 44.

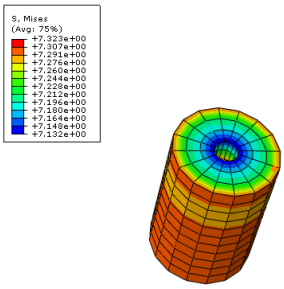

Figure 42 Stress contours in step 1

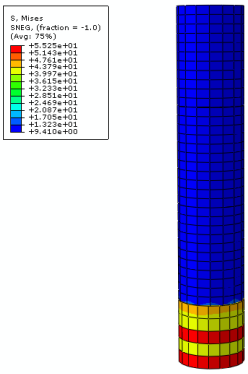

Figure 43 Stress contours in step 2

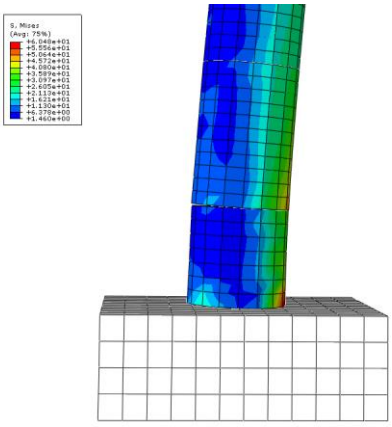

Figure 44 Separation between the foundation and bottom concrete

The pushover responses in terms of base shear-displacement curves of each bridge column model are shown in Figure 45. The maximum displacement in all the analyses is 200mm, which represents a 5.5% drift ratio. The specimen was named with 3 numbers where the first number represents concrete strength in MPa. The second number represents the PT ratio and the third number represents the PT level. The charts in Figure 45 were named from “a” to “i”.

Table **9** shows all the specimen names and what they represent. For example, a specimen with 30 MPa concrete strength, 0.44% PT ratio and 10% PT level is named 30-0.44-10. From Figure 45, it is concluded that yielding base shear increases with the increase in concrete strength, PT

level and PT ratio. Comparing graphs “a”, “b” and “c”, it can be seen that yielding base shear increases with the increase in concrete strength. Comparing graph “a”, “d” and “g”, it can be seen that the yielding base shear increase with the increase in PT level. Comparing plots with different concrete strengths, it can be seen that with the increase in concrete strength, not only the base shear capacity increases but also the post-elastic stiffness increases. With a high concrete strength, the column has better compressive resistance and stiffness which postpones the decrease of post-elastic stiffness. When comparing the three curves in the same plot, it can be seen that the post-elastic stiffness can decrease with the increase of PT level. This is because when the total axial load ratio of the pier is higher than a certain level, the compression side of the column can be damaged. Thus, this study suggests that the total axial load ratio be limited to 20% including dead load and PT load. This limit should decrease when multi-column bents are used since the frame action increases the compression.

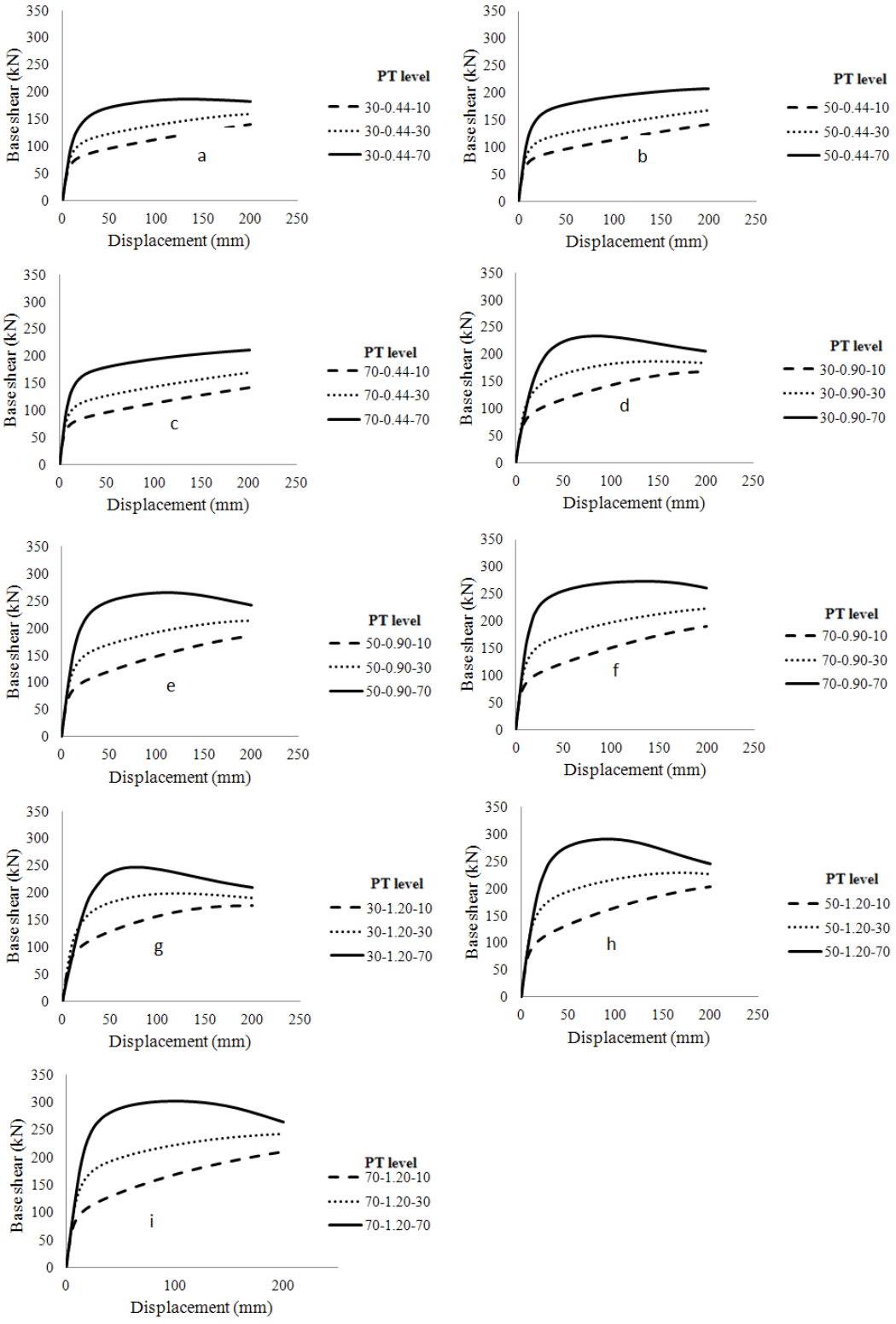

Figure 45 Pushover curves

Table 9 Denotation of specimens

Specimen	fc' (MPa)	PT Ratio	PT level	Specimen	fc' (MPa)	PT Ratio	PT level
30-0.44-10	30	0.44%	10%	50-0.90-70	50	0.90%	70%
30-0.44-30	30	0.44%	30%	70-0.90-10	70	0.90%	10%
30-0.44-70	30	0.44%	70%	70-0.90-30	70	0.90%	30%
50-0.44-10	50	0.44%	10%	70-0.90-70	70	0.90%	70%
50-0.44-30	50	0.44%	30%	30-1.2-10	30	1.20%	10%
50-0.44-70	50	0.44%	70%	30-1.2-30	30	1.20%	30%
70-0.44-10	70	0.44%	10%	30-1.2-70	30	1.20%	70%
70-0.44-30	70	0.44%	30%	50-1.2-10	50	1.20%	10%
70-0.44-70	70	0.44%	70%	50-1.2-30	50	1.20%	30%
30-0.90-10	30	0.90%	10%	50-1.2-70	50	1.20%	70%
30-0.90-30	30	0.90%	30%	70-1.2-10	70	1.20%	10%
30-0.90-70	30	0.90%	70%	70-1.2-30	70	1.20%	30%
50-0.90-10	50	0.90%	10%	70-1.2-70	70	1.20%	70%
50-0.90-30	50	0.90%	30%				

5.4.2 Factor interactions

Several tests and simulations of segmental unbonded post-tensioned columns have been performed by researchers (Chou and Chen 2006; Ou et al. 2007). Dawood et al. (2014) conducted a study using a one-factor-at-a-time strategy and analyzed some of the factors that affect the seismic behavior of segmental precast columns. One-factor-at-a-time strategy cannot consider the interaction between factors. If interactions exist, the effect of one factor may be different when the other factor is at different levels. A factorial analysis was conducted here to investigate the potential interactions between the three factors: concrete strength, PT level and PT ratio. Factorial analysis means that all the possible combinations of different levels of factors are investigated (Montgomery, 2008).

Figure 46 to Figure 48 show the interaction between PT ratio, concrete strength and PT level with the output of yielding base shear. Figure 49 to Figure 51 show the interaction between PT ratio, concrete strength, and PT level considering post-elastic stiffness as the output. In the interaction graphs, the differences in the slope of the curve indicate the extent of interaction. Parallel curves mean no interaction and vice versa. Response surface is also of help when one

is looking for optimized solutions. It shows the relationships between two variables and one output. From Figure 46 to Figure 48, it was concluded that PT level and PT ratio have notable effects on yielding force. Meanwhile, the increase in concrete strength also increased yielding force, especially when the PT ratio or PT level was at a higher level. This was because only when high-strength concrete was utilized, the columns could better benefit from the post-tensioning force while remaining an acceptable axial load ratio. The interactions were not significant in Figure 46 to Figure 48 since no negative slopes were observed. The P-Values of interactions were checked based on the method by Montgomery (2008). All the interactions have P-Values that were greater than 0.05. At the same time, from the response surfaces in Figure 46 to Figure 48, it can also be seen that none of the parameters results in decreased yielding force. Increase in the parameter of concrete strength, PT ratio, and PT level all improved yielding capacity. Therefore, the minimal interactions between factors will not be a concern for engineers when considering the yielding force of the column within the parameter ranges in this study.

From Figure 49, it can be concluded that the interactions are negligible between concrete strength and PT ratio. The same conclusion also applies to concrete strength and PT level (Figure 50). More significant interaction can be observed in Figure 51 for the interaction between PT level and PT ratio. The interaction P-Value was calculated based on the approach by Montgomery (2008) and it was smaller than 0.05. It shows that when the PT level is low, the post-elastic stiffness increases with the increase of the PT ratio. However, when the PT level is high, the post-elastic stiffness decreases with the increase in the PT ratio. This is due to the excessive axial load ratio caused by post-tensioning force.

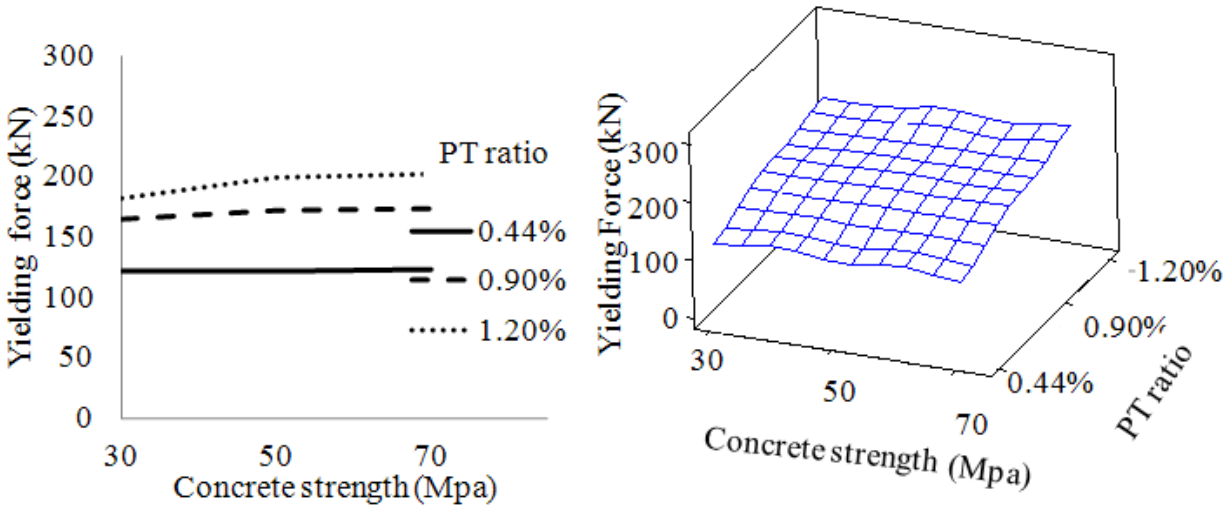

Figure 46 Concrete strength and PT ratio interaction considering yielding

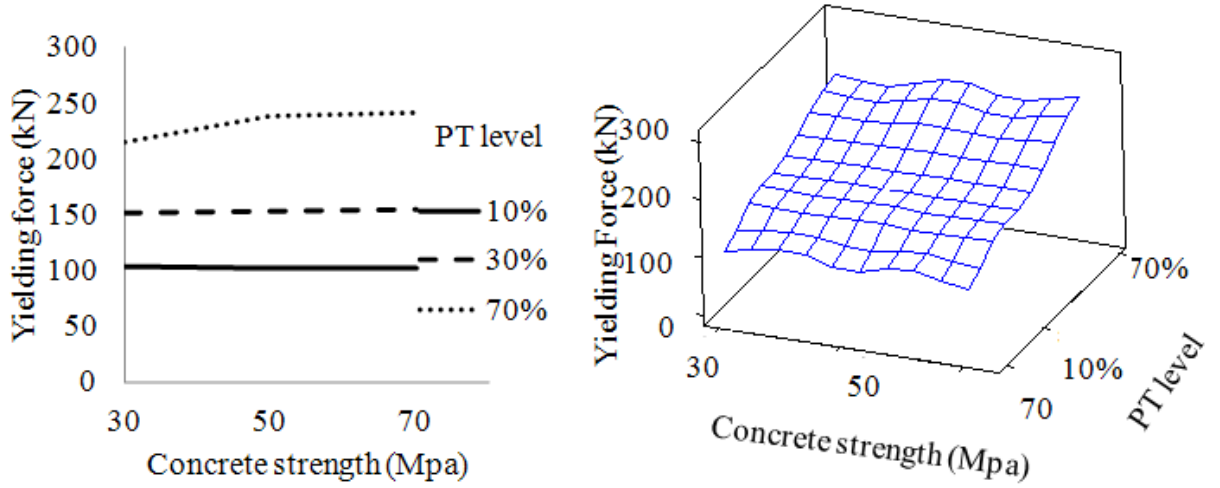

Figure 47 Concrete strength and PT level interaction considering yielding

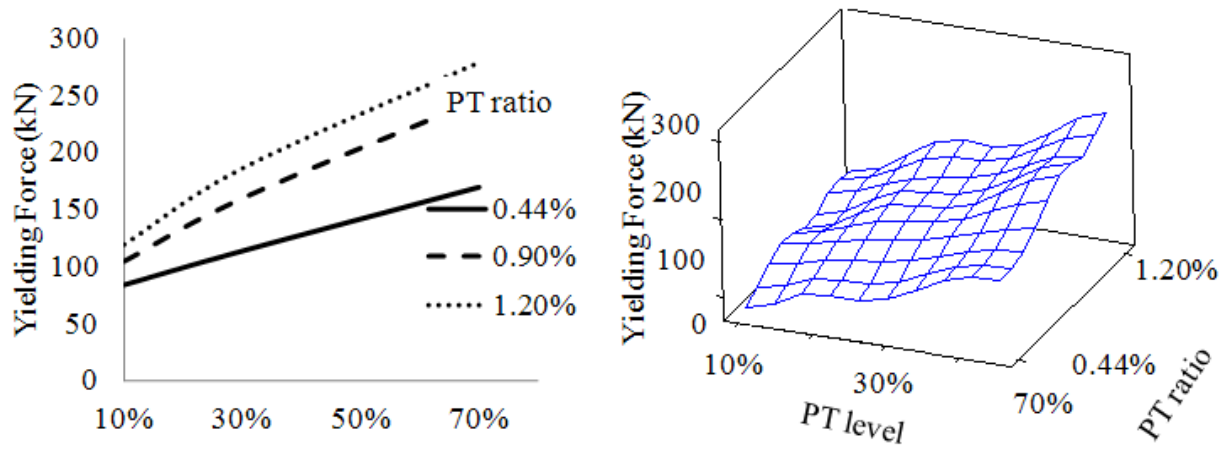

Figure 48 PT ratio and PT level interaction considering yielding

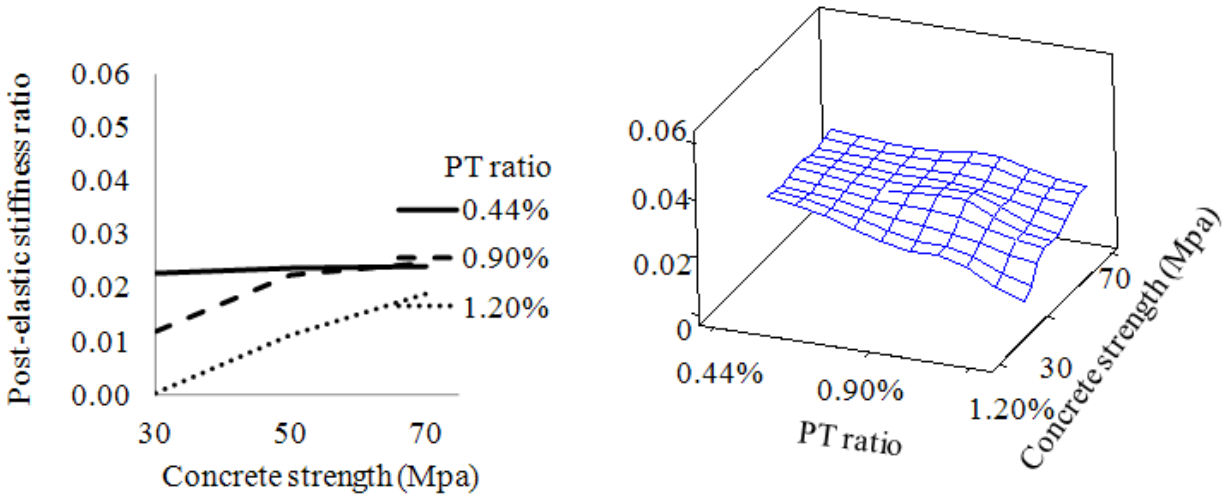

Figure 49 Concrete strength and PT ratio interaction considering stiffness

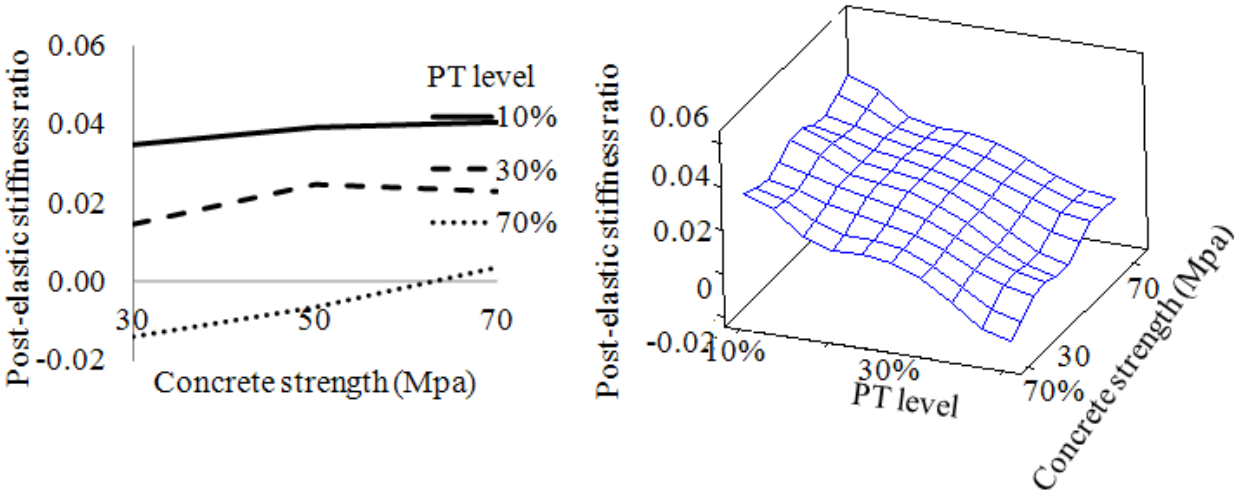

Figure 50 Concrete strength and PT level Interaction considering stiffness

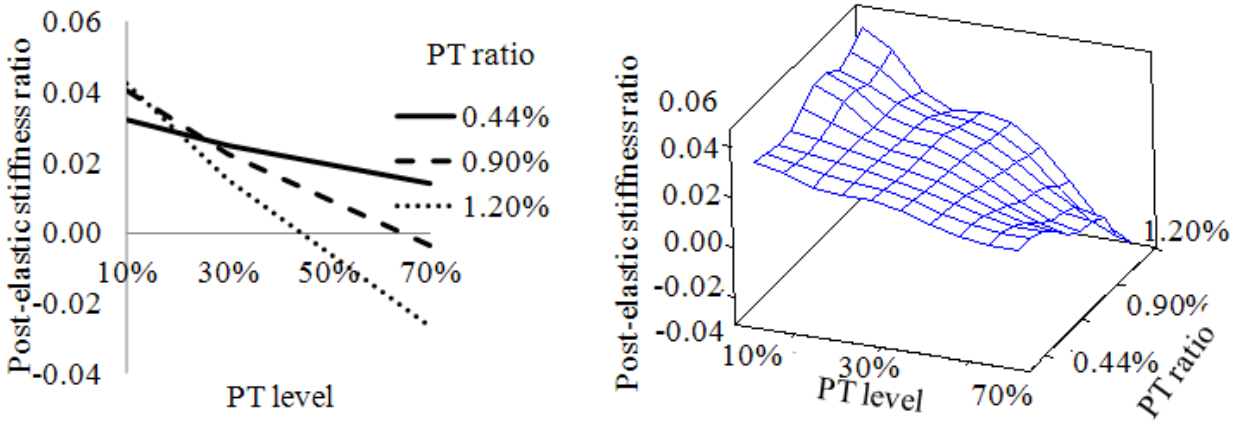

Figure 51 PT ratio and PT level interaction considering stiffness

5.5 Fractional factorial analysis

The purpose of this fractional factorial analysis is to evaluate all the relevant design parameters of the unbonded post-tensioned concrete column. Table 10 shows the parameters and the two levels of each parameter. The ranges of the factors were determined considering traditional bridge column design (Wang et al. 2014). These combinations resulted in a range of total axial load ratios from 5% to 30%, with different axial load ratios and concrete strengths. Axial load

ratio is defined as $P/(A_g f_c')$, where P is the total axial load including dead loads and post-tensioning loads, A_g is gross section area and f_c' is concrete strength. In all the following models, the columns were comprised of RC segments of equal height. All the segments were connected by tendons and no energy dissipation bars were considered. Reverse cyclic loads were applied in the analyses.

Table 10 Two levels of the considered factors

Parameter	H/D	ρ_s	ρ_l	ADLR	h/D	f_{pi}/f_{pu}	f_c' (MPa)
Level	A	B	C	D	E	F=ABCD	G=ABDE
-	3	0.01	0.01	0.03	1.5	0.3	40
+	6	0.03	0.03	0.2	1	0.7	70

H = Height of column, D = Diameter of column, ρ_s =Transverse reinforcement ratio, ρ_l= Longitudinal reinforcement ratio, f_{pi} = Initial post-tensioning stress, f_{pu}= Ultimate strength of tendon, ADLR = Axial dead load ratio, h = Height of segment, and f_c'= Concrete compressive stress.

Factorial analysis is often used when multiple factors exist in determining output. However, sometimes the full factorial analysis requires a very large number of runs, which may not be necessary or practical. For example, if the analysis includes seven factors and each factor has two levels, a complete replicate contains 128 runs. However, the main effects only have seven degrees of freedom. In the following study, a one-quarter fraction of the 2^k (k is the total number of parameters) analysis is performed. The analysis contains 2^{k-2} runs which are 32 runs in total.

Constructing a one-quarter fractional factorial analysis requires two steps. In the first step, a complete 2^{k-2} fractional factorial combinations are determined. Then, two generators (the last two columns in Table 10) are used to determine factors that are not included in the complete combinations. The generators are relations between the last two columns with previous five columns. Table 11 shows the combinations of the analysis. Each factor had two levels that were represented by – (low) or + (high), the levels of the first five factors were determined considering a full factorial analysis, the last two factors were determined by using generating relations (Montgomery 2008). Based on this approach, the total 2^7 runs were reduced to 2^5 runs.

Table 11 Combinations of different levels

		Basic design				Generated from Basic design	
Parameter	H/D	ρ_s	ρ_l	ADLR	h/D	f_{pi}/f_{pu}	f_c'
Run	A	B	C	D	E	F=ABCD	G=ABDE
1	-1	-1	-1	-1	-1	1	1
2	1	-1	-1	-1	-1	-1	-1
3	-1	1	-1	-1	-1	-1	-1
4	1	1	-1	-1	-1	1	1
5	-1	-1	1	-1	-1	-1	1
6	1	-1	1	-1	-1	1	-1
7	-1	1	1	-1	-1	1	-1
8	1	1	1	-1	-1	-1	1
9	-1	-1	-1	1	-1	-1	-1
10	1	-1	-1	1	-1	1	1
11	-1	1	-1	1	-1	1	1
12	1	1	-1	1	-1	-1	-1
13	-1	-1	1	1	-1	1	-1
14	1	-1	1	1	-1	-1	1
15	-1	1	1	1	-1	-1	1
16	1	1	1	1	-1	1	-1
17	-1	-1	-1	-1	1	1	-1
18	1	-1	-1	-1	1	-1	1
19	-1	1	-1	-1	1	-1	1
20	1	1	-1	-1	1	1	-1
21	-1	-1	1	-1	1	-1	-1
22	1	-1	1	-1	1	1	1
23	-1	1	1	-1	1	1	1
24	1	1	1	-1	1	-1	-1
25	-1	-1	-1	1	1	-1	1
26	1	-1	-1	1	1	1	-1
27	-1	1	-1	1	1	1	-1
28	1	1	-1	1	1	-1	1
29	-1	-1	1	1	1	1	1
30	1	-1	1	1	1	-1	-1
31	-1	1	1	1	1	-1	-1
32	1	1	1	1	1	1	1

Note: H = Height of column, D = Diameter of column, ρ_s: = Transverse reinforcement ratio, ρ_l = Longitudinal reinforcement ratio, f_{pi}: = Initial post-tensioning stress, f_{pu} = Ultimate strength of tendon, ADLR = Axial dead load ratio, h = Height of segment, f_c' = Concrete compressive stress.

A typical hysteresis curve of an unbonded post-tensioned concrete column is shown in Figure 52. The parameters of this column are shown in Table 12. It can be seen that the residual displacement was negligible. When the pier was pushed to 4% drift, the residual drift was only 0.3%. However, the energy dissipation capacity was poor because of the flag shape hysteresis.

Table 12 Example combinations of different levels

Basic design				Generated from basic design		
H/D	ρ_s	ρ_l	ADLR	h/D	f_{pi}/f_{pu}	f_c'
3	0.03	0.01	0.2	1.5	0.7	40

Note: H = Height of column, D = Diameter of column, ρ_s = Transverse reinforcement ratio, ρ_l = Longitudinal reinforcement ratio, f_{pi} = Initial post-tensioning stress, f_{pu} = Ultimate strength of tendon, ADLR = Axial dead load ratio, h = Height of segment, and f_c' = Concrete compressive stress.

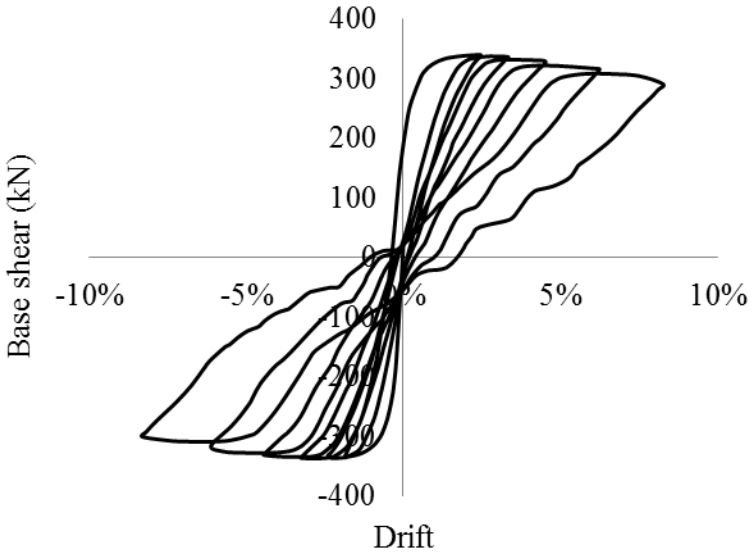

Figure 52 Example hysteresis response

5.6 Regression analysis

The purpose of the regression analysis is to provide equations that can help in preliminary designs. It should be noted that the equations are only applicable within the range that has been considered in the previous factorial analysis. The equations are only suitable for unbonded segmental concrete that is connected by tendons without ED bars. No energy dissipation devices and bars are incorporated in this chapter.

The regression equations are proposed based on the factors that are considered significant in determining the seismic response of the column in this chapter. The factors include aspect ratio (H/D), axial dead load ratio (ADLR), concrete strength (f'_c), and post-tensioned force (f_p). Comparisons of the effects of each factor are shown in Figure 53 and Figure 54. The effects are calculated based on how much contribution (percentage) each factor would contribute to the output considering the overall changes in the output resulted in all parameter changes (Montgomery 2008). From Figure 53, it can be seen that the most important factors are aspect ratio, axial dead load ratio, concrete strength, and post-tensioned force. From Figure 54, it can be concluded that the stiffness of the column is determined mainly by aspect ratio and concrete strength. The calculations of the contributions are presented in Appendix B.

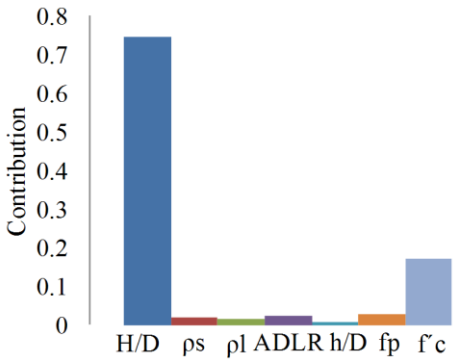

Figure 53 Contribution in determining yielding force

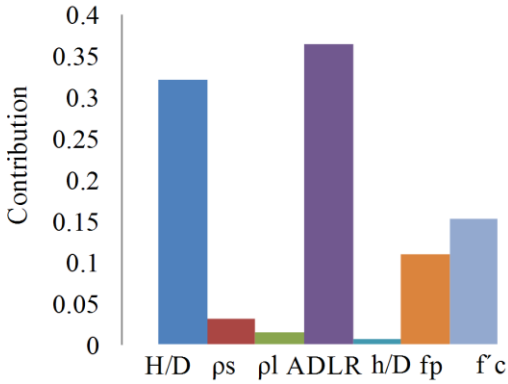

Figure 54 Contribution in determining the stiffness

The regression analysis focuses on two outputs from the finite element analysis. The two outputs are based on global response: yielding and stiffness. They are the most important factors that affect the seismic behavior of structures. To get the two global response, the backbone curves of each simulation was bilinearized. A regression equation (Equation 45) was proposed to calculate the yielding force, with an R^2 of 0.957. As suggested in this equation, the yielding force increases with the increase of axial load ratio (both axial dead load ratio and post-tensioning ratio), concrete strength and cross-section area, and decreases with the increase in column height. In the regression analysis of column stiffness, it followed the form of $3EI/H^3$, which is the stiffness of a cantilever column loaded at the top, where *E* is the modulus of elasticity, *I* is the moment of inertia and *H* is the column height. *E* is calculated as a function of $\sqrt{f_c'}$ and *I* is a function of D^3 for circular columns. So the regression equation of stiffness was simplified to Equation 46, considering the parameters used in this study. This regression equation resulted in an R^2 of 0.953.

$$F = \frac{0.0265 \times (ADLR + APLR) \times f_c' \times A_g}{H/D} \quad \text{Equation 45}$$

$$K = \frac{262.8 \times \sqrt{f_c'} \times D^4}{H^3} \quad \text{Equation 46}$$

where ADLR is axial dead load ratio, APLR is axial post-tensioning load ratio, f_c' is concrete compressive stress, A_g is column section area, H is the height of the column, and D is the column diameter.

In all simulations, it was found that the post-elastic stiffness ratio ranged from -1% to 10% and the average value was 3%. When the total axial load ratio was higher than 22%, the post-elastic stiffness ratio showed negative values. Therefore, it is suggested that the total axial load ratio should be less than 20% for unbonded post-tensioned column design. On the conservative side,

a post-elastic stiffness from 1% to 3% can be assumed when the total axial load ratio is less than 20%. Figure 55 shows a comparison between results from simulation and regression equation. The errors in predicting the stiffness and yielding force were within 10%.

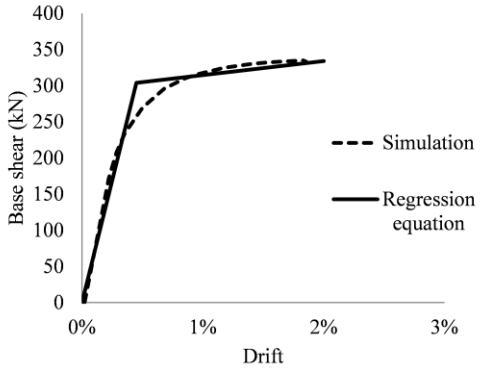

Figure 55 Comparison between simulation and regression results

5.7 Summary

In this chapter, the finite element model of segmental unbonded post-tensioned concrete columns was developed and validated with experimental results. The model could capture the stiffness, yielding and deformation of the column. A preliminary factorial analysis was conducted to investigate potential interactions between factors including concrete strength, PT ratios and PT levels. It was found that interaction exists between PT levels and PT ratios in determining post-elastic stiffness. This was due to the excessive axial load ratio when both the factors were at high levels. In turn, carefully choosing the two factors (PT ratios and PT levels) can improve the lateral behavior of the columns. As long as the total axial load ratio is within 20%, the increase of any of the factors does not generate negative effects on column performance.

After the preliminary analysis, a more comprehensive fractional factorial analysis was conducted considering factors including the aspect ratio of the column, transverse reinforcement ratio, longitudinal reinforcement ratio, axial dead load ratio, the aspect ratio of segment, post-tensioning stress ratio and concrete strength. Seven factors were considered in the analysis and

regression equations were suggested. It was found that the yielding force was determined by total axial load ratio, concrete strength, gross section area and aspect ratio. The initial stiffness was determined by concrete strength, diameter and height. The proposed regression equations include parameters that can predict lateral load capacity and stiffness of the columns well. Additionally, it is suggested that the total axial load ratio should not exceed 20% to get a positive post-elastic stiffness ratio and good ductility. This axial load limit is consistent with findings from ElGawady and Dawood (2012), which is higher than the limit for regular reinforced concrete columns (Caltrans, 2019). To summarize, the following findings can be concluded:

- The model developed in the study can predict the seismic behavior of segmental unbonded post-tensioned very well. The degradation and residual displacement can be captured under cyclic loads.
- The interaction exists between PT levels and PT ratios in determining post-elastic stiffness. This is due to the excessive axial load ratio when both the factors were at high levels.
- The column yielding force is determined by total axial load ratio, concrete strength, gross section area and aspect ratio. The column stiffness was determined by concrete strength, column diameter and height. The equations proposed in the study can be used to predict yielding force and stiffness with good accuracy.

Chapter 6: Drift-based damage states for reinforced concrete columns and hybrid rocking columns

6.1 Background

In PBD, various types of design criteria and engineering design parameters have been used around the globe. Three sets of example engineering design parameters and damage states are listed in Table 13. In the Canadian Highway Bridge Design Code (CSA 2019), material strains are used as the main seismic design criteria. The code requires most highway bridges to be designed for multiple levels of hazards with different return periods. At each level, a set of concrete and steel strains are given to limit the inelastic deformation of seismic critical components. In some other jurisdictions, displacement-based or drift-based damage states are used, where drift is the ratio of lateral deformation to member length. For example, in the South Carolina Department of Transportation, the displacement limit at interior bent with fixed bearing is 0.075 H inches (H is the column height in feet) for 462-year earthquakes (SCDOT 2008). Drift-related damage states are widely used in the building industry (Ghobarah 2001) but less common in the bridge industry. It is noted that in the AASHTO (2013) and AASHTO (2020), and most Departments of Transportation in the US, displacement ductility limits are used to determine the damage states and structural performance. Recently, a proposed PBD guideline for AASHTO was developed by Murphy et al. (2020), it was suggested that material strains are more direct engineering design parameters to reveal structural performance. However, the challenge is that nonlinear analysis is always needed to obtained inelastic strains.

Table 13 Damage states

Ghobarah (2001)		CSA (2019)		Hwang et al. (2001)	
Damage states	Drift	Damage states	Material strain	Damage states	Displacement
No damage	0.2%	Minimal damage	Concrete strains ≤ 0.006 Steel strains ≤0.01	Slight damage	First yield displacement
Repairable damage	0.5%	Repairable damage	Steel strains ≤0.025	Moderate damage	Global yield displacement
Irreparable damage	1.5%	Extensive damage	Concrete core ≤ 80% ultimate strain Steel strains ≤0.05	Extensive damage	Displacement when concrete strain equals 0.002
Near collapse	2.5%	Probable replacement	Crushing of concrete core Steel strains ≤0.075	Complete damage	Maximum displacement

Despite extensive research on the column drifts, there is yet a systematic study on the design drift limits of bridge columns corresponding to the Canadian Highway Bridge Design Code (CSA 2019) strain limits considering parameters of aspect ratios, reinforcement ratios, and axial load ratios. The purpose of this chapter is to propose design drift limits for different damage states that can be used by engineers. It is expected that using drift limits as damage states would greatly simplify the design process of most regular bridges. Although drift limits cannot replace strain limits when using the Canadian Highway Bridge Code (CSA 2019), drift limits can be simple and powerful tools in preliminary designs and for a cross-check on final designs. In the following study, the basis of the damage state definition is the material strains defined in the Canadian Highway Bridge Design Code (CSA 2019) shown in Table 13. To correlate drifts with material strains, static nonlinear pushover analyses are performed for the reinforced concrete column. For the hybrid rocking column, both static nonlinear pushover analyses and dynamic time-history analyses are performed. The time-history analysis is not performed for the reinforced concrete column because most design codes do not require such a sophisticated analysis for a regular cantilever column analysis, where pushover analysis should generate reliable results.

In this chapter, two types of bridge columns are studied: traditional reinforced concrete columns and hybrid rocking columns. While reinforced concrete columns are certainly the dominant earthquake-resistant system, hybrid rocking columns are gaining more attention both in the research community and the bridge industry. Hybrid rocking columns are usually composed of precast columns that are made continuous with adjacent members through post-tensioning tendons and energy dissipating (ED) bars. At the connections between the hybrid rocking column and footing, any longitudinal yielding rebar is often referred to as energy dissipating bars. They are usually unbonded to concrete for a certain length to allow the opening of a large gap and avoid stress concentration. The post-tensioning tendons are always unbonded to the concrete for the full length. Experimental and numerous studies have proved that hybrid rocking columns offer excellent seismic performance and have the potential to accelerate constructions (Bu et al. 2016; Dawood et al. 2011; Palermo et al. 2005; Sideris et al. 2014; Wang et al. 2018).

6.2 Column prototype and finite element model

Finite element analyses are performed to correlate strain-based damage states with drift-based damage states. Before using the finite element models for the parametric study, they are first validated against experimental studies. In this chapter, SeismoStruct (SeismoSoft 2020) is used to simulate both the reinforced concrete column and the hybrid rocking column. The software has been extensively used by other researchers in simulating traditional reinforced columns and columns with new materials including FRP and shape memory alloys (Billah and Alam 2012; Calvi et al. 2008; Zhang et al. 2016). The modeling of the reinforced concrete column is relatively straightforward; thus, this study does not elaborate more on the modeling of the reinforced concrete column. One model validation of reinforced concrete columns is presented in Chapter 2. The focus of this section is on the modeling of the hybrid rocking column, which can be quite sophisticated as has been done by several researchers depending on how the detailed modeling is conducted (Salehi and Sideris 2016; Trono 2014). This section uses a

relatively simple yet accurate approach, which can be achieved by general structural software without extensive calibrations on rocking springs. Two cantilever hybrid rocking column models are shown in Figure 56. In Figure 56a and b, steel and concrete are all modeled using fiber elements. In this model, a concrete column segment with no longitudinal rebar (ED bar) is created at the bottom of the column. ED bar elements are created separately outside of the concrete section. The top node of the concrete segment constrains the top node of the ED bars. The lengths of the unreinforced column segment and the ED bar equal to the length of unbonded longitudinal rebar in the tested column to simulate an unbonded ED bar condition. For the column section above the unbonded ED bar portion, it can be modeled as a regular reinforced concrete section or an elastic element with proper cracked stiffness as inelastic behavior is only of concern at the bottom section where ED bars are unbonded. An elastic element overlapped with the column element is used to simulate the unbonded tendons. In Figure 56b, nonlinear link elements are used to model the ED bars and concrete contact with the foundation.

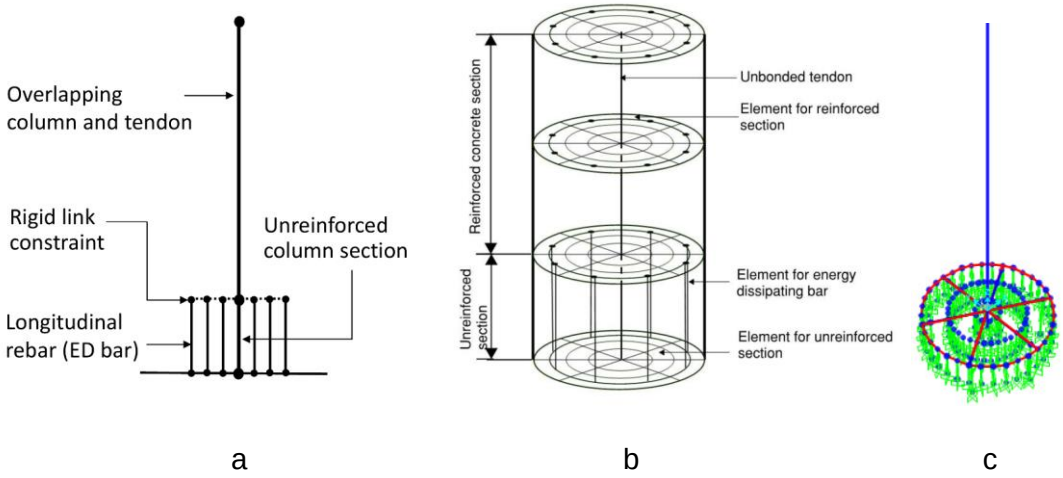

Figure 56. Finite element models of the hybrid rocking column

Finite element models are validated based on the experimental study by Cohagen et al. (2008) and Jeong (2007). Cohagen et al. (2008) tested hybrid rocking columns under reversed cyclic

static loading, in which columns were connected with footings using six large diameter bars as ED bars. The ED bars were unbonded from the column-footing interface to 203 mm depth into the footing. Unbonded post-tensioned Williams bar was used for post-tensioning to achieve self-centering behavior. Jeong (2007) conducted dynamic shake table tests of hybrid rocking columns by applying two horizontal components of an excitation recorded in Los Gatos during the 1989 Loma Prieta, California, earthquake (Somerville 1997) simultaneously in the two horizontal directions. They applied the dynamic loadings in four stages by scaling them to 10%, 25%, 50% and 75%, which corresponded to elastic, yield, design and maximum level of the design earthquakes. The major column parameters from both of the two research projects are presented in Table 14.

Table 14 Parameters of tested columns

Reference	Specimen	Height (mm)	Diameter (mm)	Total Axial Load Ratio	Unbonded Length of ED Bar (mm)
Cohagen et al. (2008)	LB7	1500	500	0.12	203
Jeong (2007)	PRC-U2	2440	406	0.15	813

The comparison between simulation and static testing results by Cohagen et al. (2008) is presented in Figure 57. The finite element model captures the initial and post-elastic stiffness as well as strength very well even at extreme deformation up to 10% drift. It is noted that the strength degradation is gradual and ductile, energy dissipation is satisfactory, and the hysteresis loop is stable. In the following sections, the models developed in SeismoStruct using fiber elements are used.

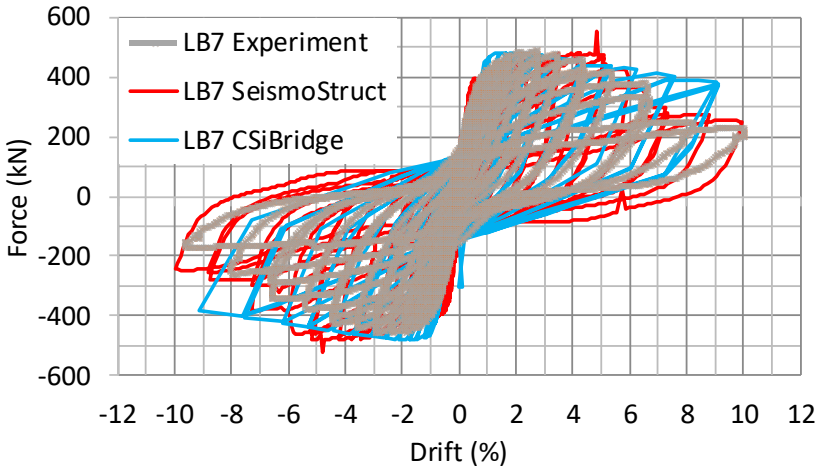

Figure 57. Hybrid rocking column response under static cyclic loads

The comparisons of hysteretic behaviors between simulations and experimental results by Jeong (2007) are shown in Figure 58, which include two horizontal directions and four loading stages (10%, 25%, 50% and 75% scaled motions) sequentially applied on the same column. The comparisons of displacement time history between simulation and experimental results are shown in Figure 59. When doing the finite element simulation, the motions recorded in Los Gatos during the 1989 Loma Prieta, California, earthquake (Somerville 1997) were used. More accurate simulation results could be achieved if the measured acceleration time history of the shaking table were available. While the measured acceleration time history was not available, it can still be seen that the numerical model can capture the stiffness, strength and accumulations of damage at all stages relatively well. At the elastic stage, the column behavior is generally linear. At the yield and design levels, there is apparent yielding, energy dissipation, and minor residual deformation. At the design level, the hysteresis loops show apparent energy dissipation. Its shape became asymmetric due to extensive damage. At the maximum level, the column maximum displacement is at about 8% drift. In the experimental study, it was observed that there were significant longitudinal rebar buckling and spiral fracture. At this level of damage, the simulation model is less accurate in capturing the force-displacement relation although the

displacement time history seems satisfactory. It should be noted that in actual designs, structures are most likely to be designed for a much smaller drift limit. Thus, finite element models in this study suffice the required accuracy for smaller design drifts.

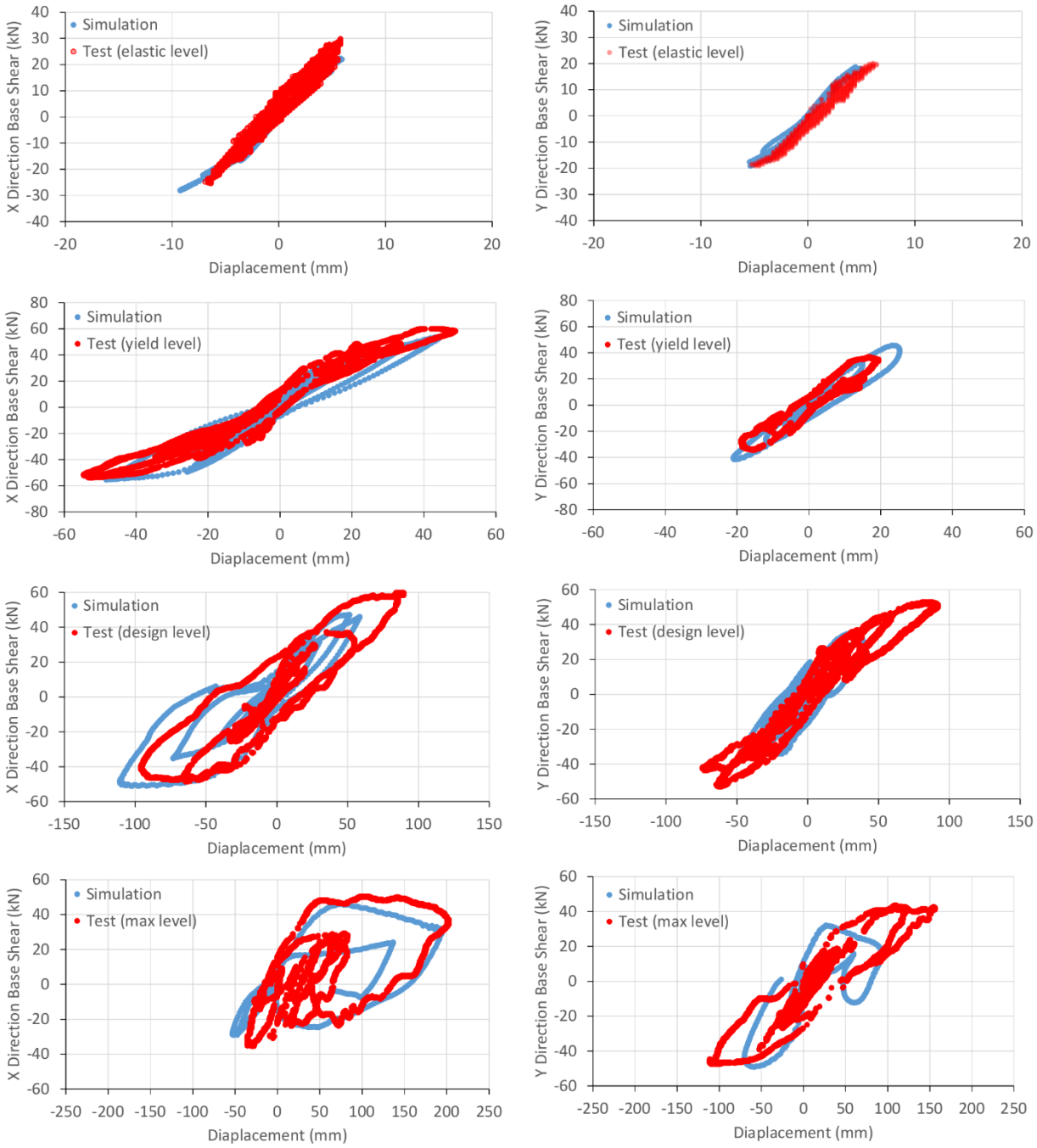

Figure 58. Hysteretic response of hybrid rocking column under dynamic loads

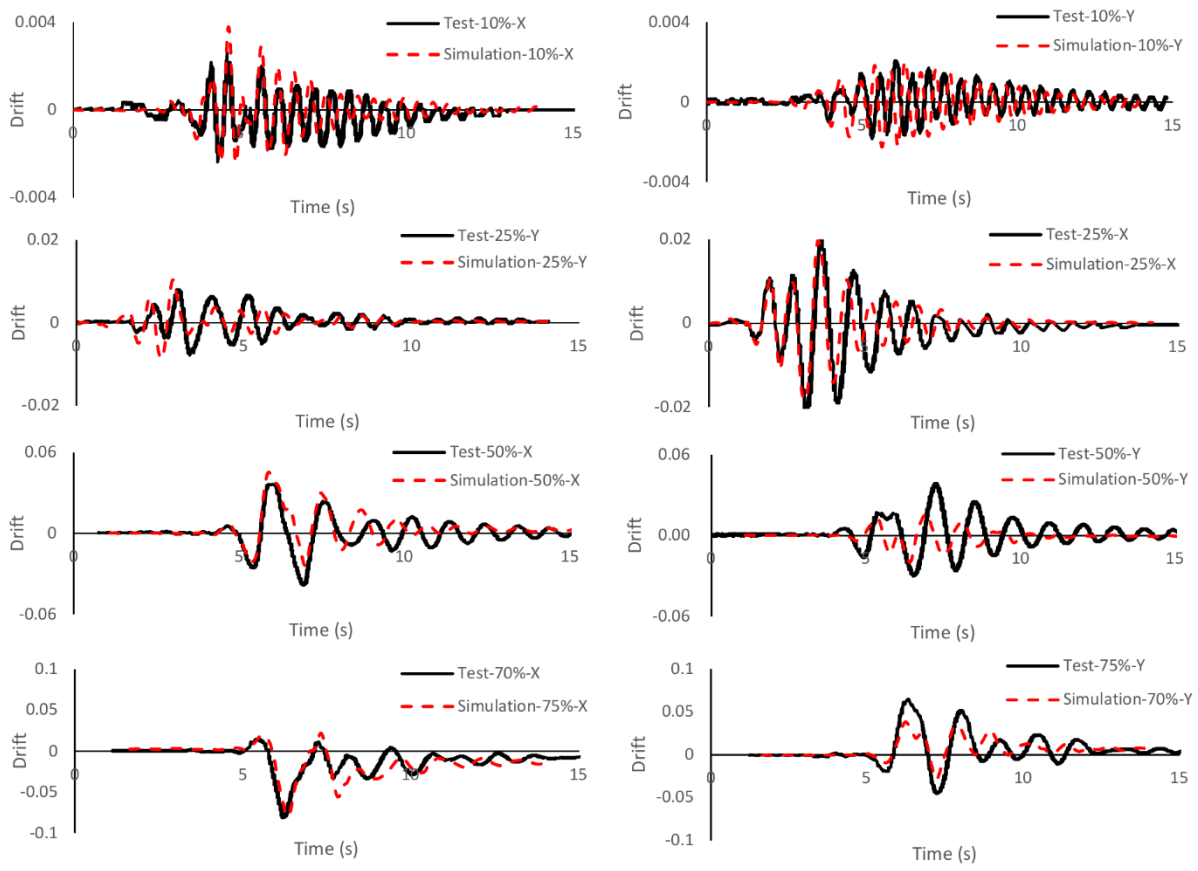

Figure 59. Displacement time history of hybrid rocking column under dynamic loads

6.3 Parametric study

The seismic performance of flexural members is largely dominated by a few normalized parameters: aspect ratio, reinforcement ratio, and axial load ratio. The aspect ratio is the ratio of column height to its diameter, which determines how slender the member is. Slender members usually have higher lateral deformation capability compared to squat members. The reinforcement ratio is the volumetric ratio of rebar to the concrete, which is an important factor deciding the bending moment capacity of the section. For hybrid rocking columns, the term reinforcement ratio does not include any considerations of the tendons. It is purely the ratio between longitudinal rebar (ED bar) area to column cross-section area. The axial load ratio is

defined as the ratio of axial load to the concrete section axial resistance. In the case of the hybrid rocking column, the term total axial load ratio is used when the axial load is caused by both dead load and initial post-tensioning force. Excessive axial load ratios tend to cause compressive damage and reduce ductility. By considering a range for each of the three parameters, this study proposes drift-based damage states for both reinforced column and hybrid rocking column.

Table 15 summarizes the parameters and their ranges studied in this chapter. For reinforced concrete columns, three parameters are examined at three levels that cover most of the typical bridge column designs. An aspect ratio of 10 represents a slender column and a ratio of 3 represents a short column. Axial load ratios of most bridges in moderate to high seismic regions are around 10%, and not less than 5% and not more than 20%. Caltrans SDC (Caltrans 2019) limits axial dead load ratio to 15% for columns with no frame overturning effect and 22% for columns with frame overturning effect. The rebar ratio of most bridge columns ranges between 1% to 2%. Overall, the three parameters at three levels represent 27 column designs. For hybrid rocking columns, the same three parameters are investigated, but at slightly different levels for axial load ratio and reinforcement ratio (ED bar ratio). Hybrid rocking columns are normally subjected to higher total axial load ratios because of the combination of dead load and post-tensioning force. Therefore, only two levels of total axial load ratios are studied, which are 10% and 20%. In this study, the dead load and post-tensioning force are set to equal, both of which contribute to half of the total axial load. For example, a total axial load ratio of 10% for hybrid rocking column means a 5% dead load combined with a 5% post-tensioning load. In terms of reinforcement ratio, hybrid rocking columns often have less rebar (ED bar) compared with the reinforced concrete columns. This is because the moment capacity is contributed by both the tendon and the ED bar. An excessive amount of ED bar would reduce the re-centering capacity of the column and increase construction costs. Thus, for hybrid rocking columns, this study

investigated aspect ratios at three levels and the other two parameters at two levels, the overall combinations generate 18 column designs.

Table 15 Column parameters

Column type	Aspect Ratio	Axial load ratio	Reinforcement ratio
Reinforced concrete column	3	0.05	0.01
	6	0.1	0.015
	10	0.2	0.02
Hybrid rocking column	3	0.1	0.005
	6	0.2	0.01
	10		

6.4 Drift-based damage states for reinforced concrete columns

The major benefit of using drift-based damage states is that they can simplify the structural design process, especially during the preliminary design stage. With drift limits in mind, engineers would not have to perform nonlinear analysis to obtain material strains to determine damage states. However, the challenge of using drift limits as damage states is that the limit varies with structural systems and several column design parameters. In this section, the drift limits correspond to different damage states defined in the Canadian Highway Bridge Design Code (CSA, 2019) are calculated based on nonlinear pushover analyses. For standard highway bridges, the design code (CSA, 2019) only requires nonlinear pushover analysis rather than time-history analysis. The analyzed columns are cantilevered and have varying parameters described in Table 15.

Based on the pushover analysis results, charts correlating drifts with damage states are produced. Figure 60 (a), (c) and (e) correlate drift to concrete damage states, considering aspect ratios of 10, 6 and 3. Figure 60 (b), (d), and (f) correlate drift to rebar damage states for the same three aspect ratios. In each of the charts, two other variables axial load ratio (P) and rebar ratios are included. Other notations included in the charts are ε_s: steel strain, ε_c: concrete

strain, ε_{cu}: 80% of ultimate concrete strain (0.008), ε_{su}: ultimate steel strain. In Figure 60 (a), (c) and (e), it is noted that the plotted lines are generally discrete in the vertical direction, whereas the lines in (b), (d), and (f) are grouped closely based on the level of damage (minimal, repairable and extensive damage). This shows that the concrete damage states (Figure 60 (a), (c) and (e)) are more sensitive to the axial load ratios. Thus, different axial load levels generate different drift limits. Axial load ratios do not seem to affect rebar damage states significantly (Figure 60 (b), (d), and (f)). Therefore, the drift limits corresponding to rebar damage with different axial load ratios seem to be similar. Another finding from Figure 60 is that all the lines representing concrete damage drift limits (Figure 60 (a), (c) and (e)) have zero or negative slope, meaning that increasing the rebar ratio from 1% to 2% would reduce the drift limit related to concrete damage (negative effect). However, from Figure 60 (b), (d), and (f), it can be seen that using more rebar can increase the drift limit related to rebar damage. Also, in most cases, the drift limit has less than 1% difference irrespective of the rebar ratio conditioned on the same axial load and aspect ratio. It is also noted that for columns with aspect ratios greater than 6, the extensive damage states of rebar occur only at very large drift levels.

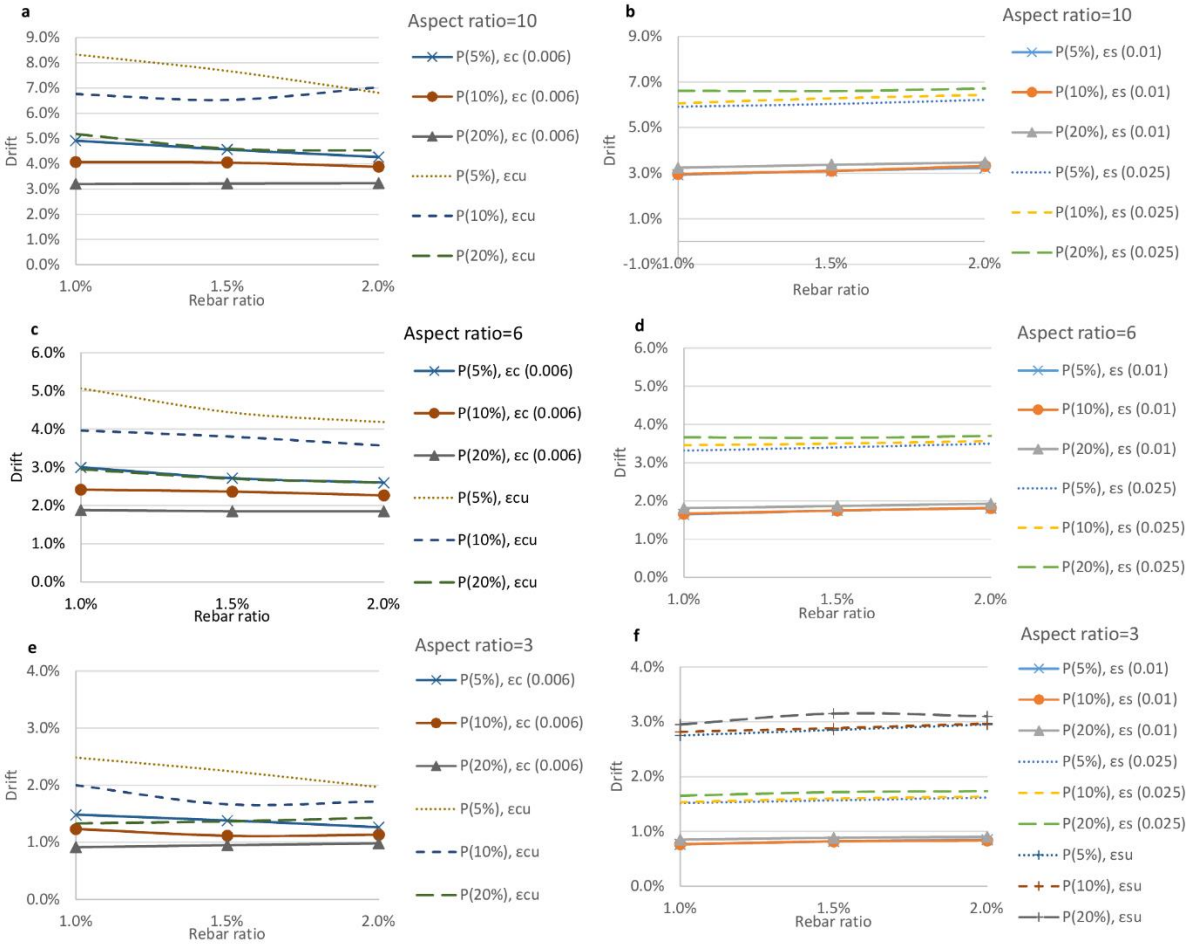

Figure 60 Drift – strain relations of reinforced concrete columns

It is noted that the aspect ratio is the most significant factor affecting the drift limits. In comparison, the effects of rebar ratio and axial load ratios are relatively smaller. Therefore, it may be appropriate to propose damage states solely based on aspect ratio and take the average effect of rebar ratio and axial load ratio. These simplified design limits may be used for preliminary design. Table 16 presents the drift limits for reinforced concrete columns with three levels of aspect ratios. The corresponding standard deviation resulted from various levels of axial load ratios and rebar ratios are also presented.

Table 16 Average reinforced concrete column drift limits in static analysis

Aspect ratio	Drift	Steel strain, εs: 0.01	Concrete strain, εc: 0.006	Steel strain, εs: 0.025	Concrete core strain, εc: 0.008
3	Average	0.83%	1.16%	1.62%	1.80%
	Standard deviation	0.04%	0.19%	0.07%	0.38%
6	Average	1.79%	2.33%	3.53%	3.70%
	Standard deviation	0.09%	0.39%	0.12%	0.78%
10	Average	3.19%	3.93%	6.32%	6.39%
	Standard deviation	0.17%	0.58%	0.27%	1.26%

In addition to researching drifts corresponding to various material strain levels, this study also investigates drifts corresponding to the maximum strength, 10% strength reduction, and 20% reduction of the base shear/base moment. The three levels of strength are of interest because it is usually expected that the strength reduction is within 10% for repairable damage and within 20% for extensive damage as indicated in the Canadian Highway Bridge Design Code (CSA 2014). Based on the pushover analysis results, Figure 61 plots the relation between drift and base shear strength levels. Three lines in each plot represent the drift at the maximum base shear, 10% and 20% reduction in base shear indicating repairable and extensive damage. The first chart in each row represents columns with 5% axial load ratios. The charts in the second and third columns represent columns with axial load ratios of 10% and 20%. In each row, the charts represent aspect ratios of 10, 6 and 3. The notation P represents axial load ratio, R10% is 10% strength reduction, R20% is 20% strength reduction.

Upon a careful examination of Figure 61 and a comparison with Figure 60, it is found that damage states in material strain do not always have a good correlation with strength reduction because the corresponding drifts are different. For example, in Figure 60 (a) and (b), the slender column (aspect ratio of 10) only reaches extensive damage states when the drift is beyond 6% and 4% respectively, for axial load less than 20% and equal to 20%. However, in Figure 61 (c),

it is shown that this column would already reach 20% strength reduction and extensive damage at a drift level of less than 3%. This indicates that engineers may not purely rely on material strains to predict the overall strength reduction, especially when the P-Delta effect becomes significant in slender columns. For columns with aspect ratios of 3 and 6, it was found that the strain-based damage states were conservative, meaning that drifts corresponding to specified strains were smaller than drifts corresponding to specified strength reductions.

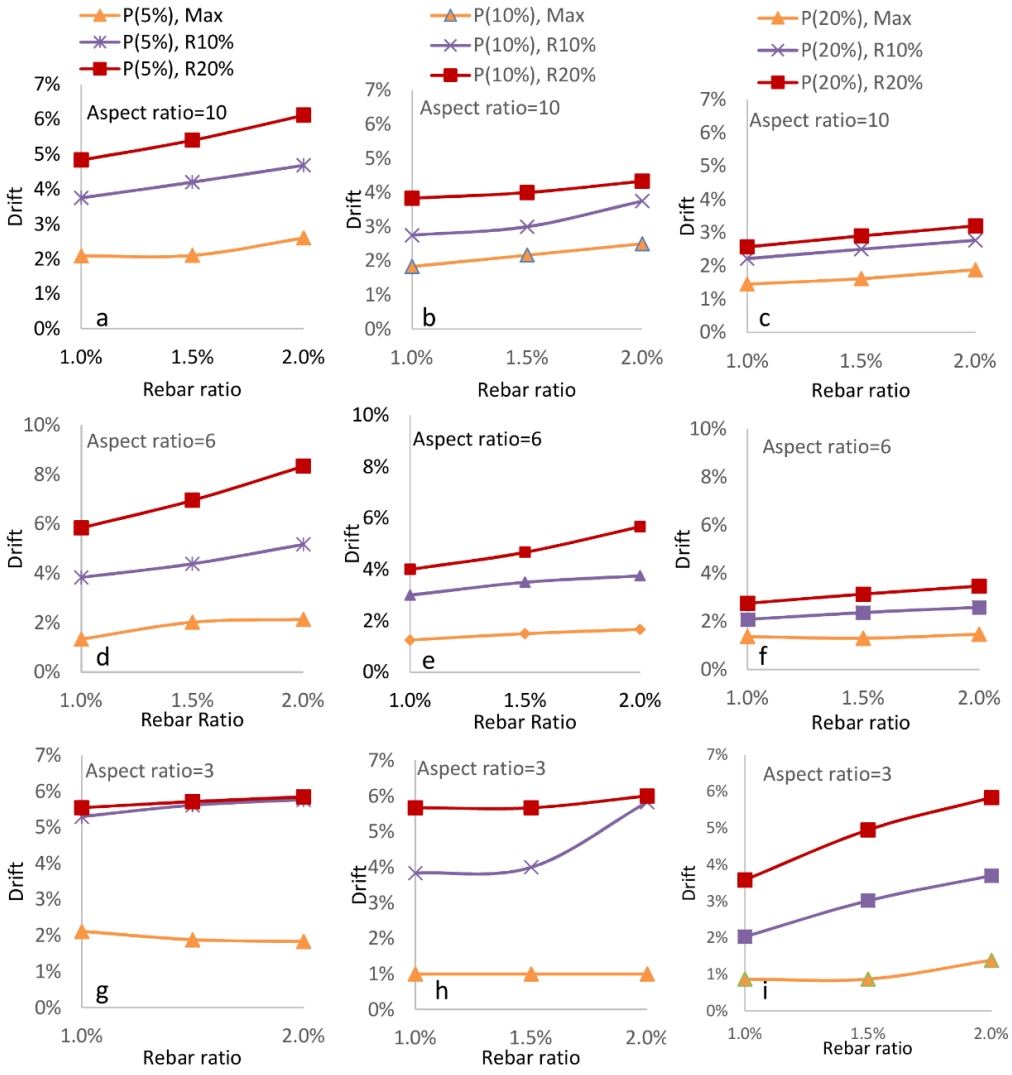

Figure 61. Drift – strength relations of reinforced concrete columns

6.5 Drift-based damage states for hybrid rocking columns

Several design methods of hybrid rocking columns were proposed by researchers (Pampanin et al. 2001; Rahmzadeh et al. 2018). The drift-based damage states proposed in this study are additional tools for checking structural performance. The drift limits are developed based on the strain-based criteria presented in Table 13. It should be noted that in the current Canadian Highway Bridge Design Code (CSA, 2019), there are no design provisions regarding hybrid rocking columns. Therefore, the same strain limits are used for both reinforced concrete columns and hybrid rocking columns in this study. In fact, since the energy dissipating bars of hybrid rocking columns can be located externally to the column to facilitate post-earthquake repair and replacement, its damage states based on material strain could be more relaxed. In the meantime, it should be noted that the damage states studied in this study do not include tendons and shear damage. Tendons are expected to behave elastic and the shear resistance of the column should be capacity protected. This is to ensure flexure damage occurs before brittle damage such as shear failure and tendon fracture.

In the analyzed hybrid rocking columns, it is assumed that the longitudinal reinforcement (ED bars) are unbonded for a length equal to the plastic hinge length of an equivalent reinforced concrete column. This approach has been used by researchers (Sakai et al. 2005) to reduce the maximum strain induced in the bars. If engineers decide to increase the unbonded length, it is possible to further reduce the damage in the ED bars as stress will be distributed to an even longer length. Besides, it is assumed that the axial dead load and initial post-tensioning force are equal in each column design. The reported axial load ratio is the total axial load ratio including both dead load and initial post-tensioning force after losses. Under these conditions, hybrid rocking column drift–strain relationships are presented in Figure 62. These results are based on the nonlinear static pushover analysis. Notations in the charts are P: axial load ratio, ε_s: steel strain, ε_c: concrete strain, ε_{cu}: 80% of ultimate concrete strain (0.008), ε_{su}: ultimate steel

strain. Similar to the charts for reinforced concrete columns, it is noted that the lines in Figure 62 also have relatively small slopes, which means that the effect of the reinforcement ratio (ED bar ratio) on the drift limit is small for a given axial load ratio.

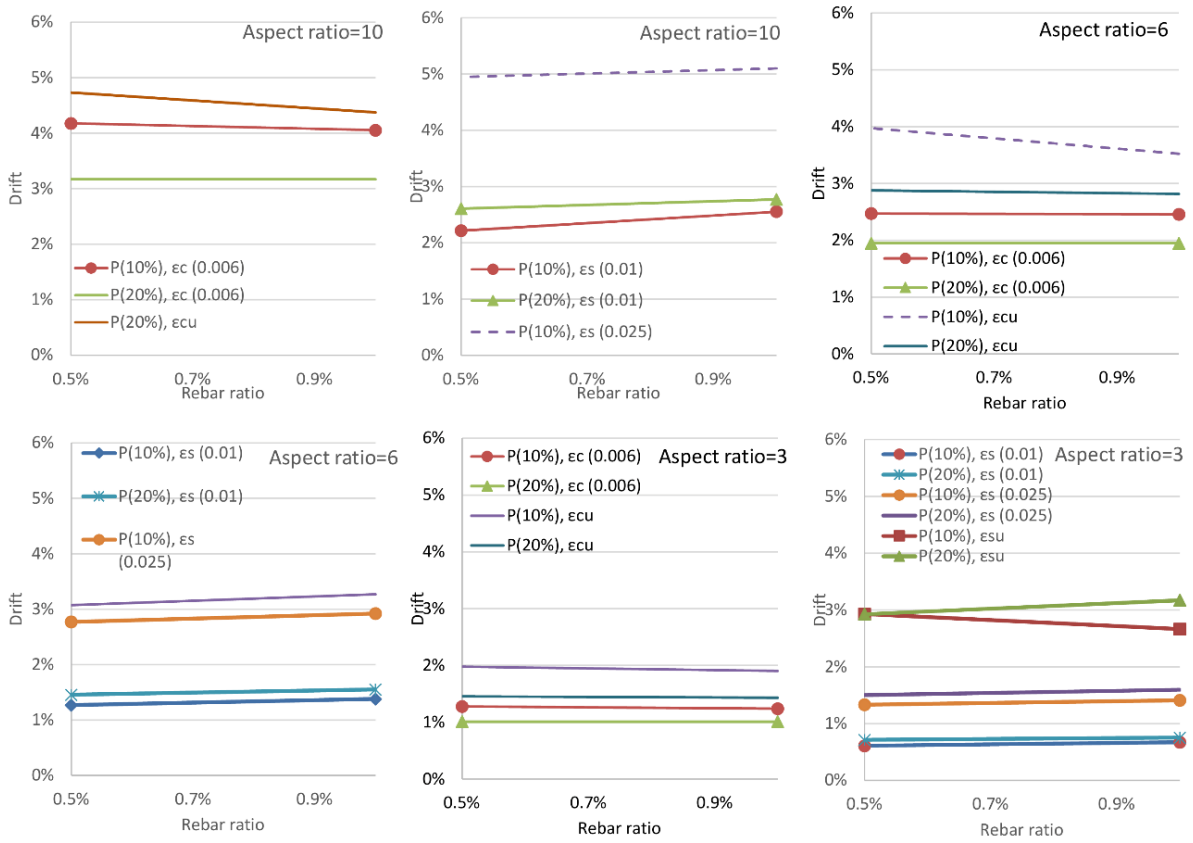

Figure 62. Drift – strain relationships of hybrid rocking column

To present hybrid rocking column drift results in a more consolidated way, by taking the average effects of axial load ratio and ED bar ratio, drift limits for three levels of aspect ratios are presented in Table 17. Standard deviations are also presented and they are relatively small compared to the average values.

Table 17 Average hybrid rocking column drift limits in static analysis

Aspect ratio	Drift	Steel strain, εs: 0.01	Concrete strain, εc: 0.006	Steel strain, εs: 0.025	Concrete core strain, εc: 0.008
3	Average	0.69%	1.14%	1.46%	1.69%
	Standard deviation	0.05%	0.12%	0.10%	0.25%
6	Average	1.41%	2.21%	3.01%	3.30%
	Standard deviation	0.10%	0.26%	0.18%	0.48%
10	Average	2.54%	3.64%	5.02%	4.55%
	Standard deviation	0.20%	0.48%	0.08%	0.18%

After completing the nonlinear static analysis, nonlinear dynamic time-history analyses were performed on hybrid rocking columns to examine and confirm the results from static analysis. In the time-history analysis, 11 motions are used and each of the motion is scaled to three levels. In cases where the original ground motions are not intense enough, they are scaled up to ensure that the interested damage states are reached. Table 18 presents the ground motions used in this study and Figure 63 plots the acceleration response spectra of original ground motions. In each time history analysis, the time steps of reaching specific material strains are recorded. Then based on the recorded time steps, maximum drifts prior to the recorded time step are extracted. In this way, the maximum strain and drift are correlated.

Table 18 Earthquake records

Event	Year	M	Station	R (km)	PGA (g)
Loma Prieta	1989	6.9	Agnews State Hospital	28.2	0.172
Northridge	1994	6.7	Canoga Park - Topanga Can.	15.8	0.489
Borrego Mountain	1968	6.8	El Centro Array #9	46	0.13
Loma Prieta	1989	6.9	APEEL 2E Hayward Muir Sch.	57.4	0.171
Coalinga	1983	6.4	Pleasant Valley P.P. - bldg	8.5	0.38
Imperial Valley	1979	6.5	Aeropuerto Mexicali	8.5	0.327
Northridge	1994	6.7	Bell Gardens - Jaboneria	46.6	0.098
Northridge	1994	6.7	LA - Pico & Sentous	32.7	0.186
Northridge	1995	6.7	LA - E Vernon Ave.	39.3	0.153
San Fernando	1971	6.6	LA - Hollywood Stor Lot	21.2	0.21
Superstition Hills	1987	6.7	El Centro Imp. Co. Cent	13.9	0.358

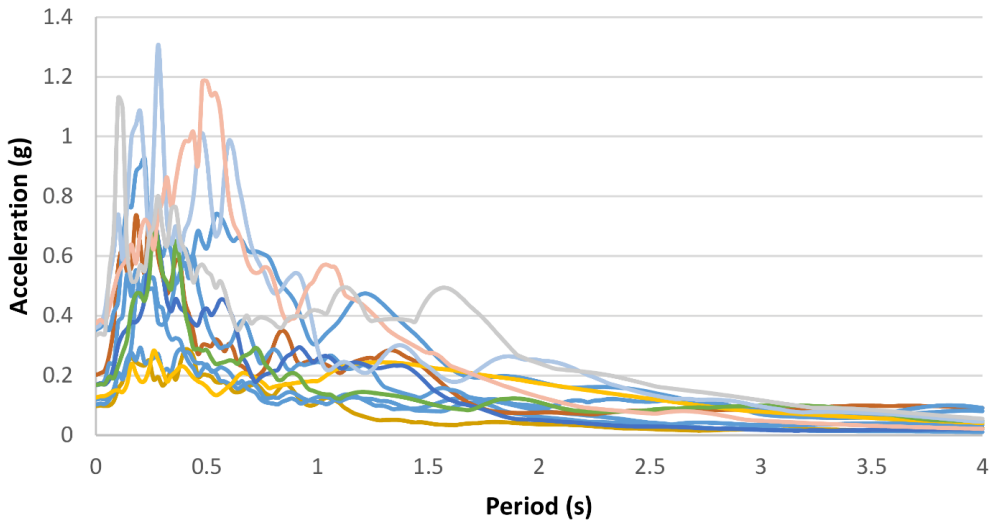

Figure 63. Acceleration response spectra

Similar to the data analysis for static analysis, upon extracting the drifts corresponding to different damage states, the effects due to axial load ratio and ED bar ratio are averaged to simplify the drift limits. The average drifts from all motions for different aspect ratios are summarized in Table 19. The results from Table 17 and Table 19 are consistent in most cases. The average difference of all damage levels is about 2% and the maximum difference for the individual damage stage is about 8%. Throughout the analyses, the steel strain limit of 0.05 is rarely reached, therefore no corresponding drift is included.

Table 19 Average hybrid rocking column drift limits in dynamic analysis

Aspect ratio	Drift	Steel strain, εs: 0.01	Concrete strain, εc: 0.006	Steel strain, εs: 0.025	Concrete core strain, εc: 0.008
3	Average	0.68%	1.10%	1.43%	1.62%
	Standard deviation	0.18%	0.13%	0.09%	0.21%
6	Average	1.31%	2.05%	2.91%	3.21%
	Standard deviation	0.48%	0.58%	0.98%	0.86%
10	Average	2.43%	3.46%	5.17%	4.90%
	Standard deviation	0.63%	1.36%	1.78%	1.77%

6.6 Design recommendations

Based on findings of the finite element analyses, this study proposes drift-based damage states for cantilevered reinforced concrete columns and hybrid rocking columns that can be used by practitioners. These drift limits are to be compared with the drift/displacement demands at various hazard levels to ensure columns are within the specified minimal, repairable and extensive damage states. As has been presented in previous sections, average drift limits for different axial loads and rebar ratios have small coefficients of variation. Thus simplified drift limits are proposed solely based on aspect ratios. The sequence of the damage is generally consistent in all the analyzed columns, from the beginning to the end, the steel strain of 0.01 occurs first, then the concrete strain of 0.006, followed by steel strain of 0.025 and concrete core crushing. The latter two damage definitions may exchange sequence depending on lateral confinement conditions. Better confinement would increase concrete core crushing strains and delay its damage. Throughout the analysis, the damage state with steel strain of 0.05 is rarely reached and should not be the governing case for the majority of bridge designs. Based on the static nonlinear pushover analysis of reinforced concrete columns and hybrid rocking columns, Figure 64 and Figure 65 are proposed for assisting engineering designs, which are average drift limits minus one standard deviation. In the two figures, the vertical axis is the design drift limit, damage states are identified on the horizontal axis. Each of the charts includes aspect ratios from 3 to 10. As the finite element models have only included aspect ratios of 3, 6 and 10, results for other aspect ratios are based on linear interpolations.

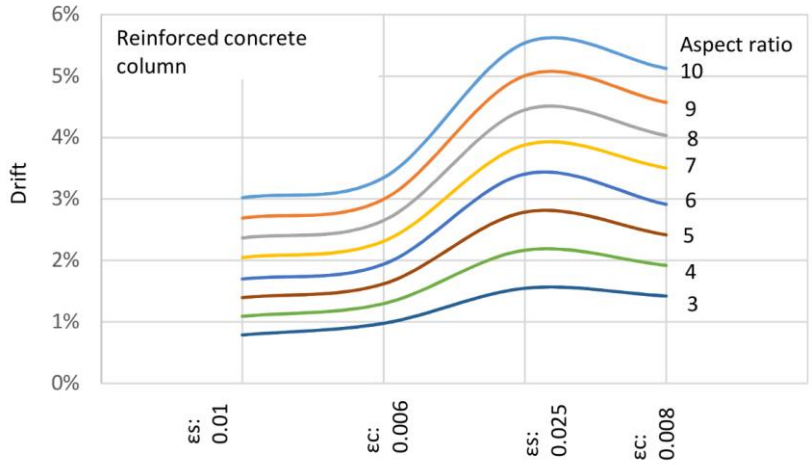

Figure 64. Reinforced column drift limit

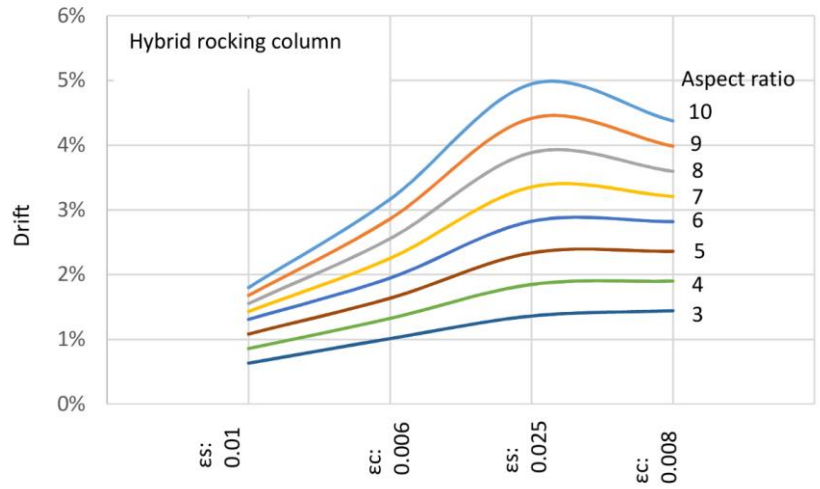

Figure 65. Hybrid rocking column drift limit

6.7 Summary

This chapter first validates finite element models based on two experimental studies. It is shown that the modeling approach is satisfactory in capturing the strength and stiffness of both the reinforced column and hybrid rocking column. Using the finite element models, a parametric study is performed on both types of columns. Charts correlating drift limits with damage states are presented based on the damage definitions in the Canadian Highway Bridge Design Code (CSA 2019). It is noted that aspect ratios have the most significant impact on drift limits for both

reinforced concrete and hybrid rocking columns. The influence of reinforcement ratio and axial load ratio is relatively small.

Besides, in reinforced concrete column design, it is often expected that when the material strains are limited to code specified values, the overall strength reduction is also guaranteed. For example, the strength reduction would be within 10% for repairable damage and 20% for extensive damage when the corresponding strain limits are reached. However, analysis results show that it is not true for slender columns. Using a column with an aspect ratio of 10 as an example, the column reaches extensive damage states at about 5% drift, while the 20% strength reduction already occurs at about 3% drift.

In the end, two design charts are proposed for performance-based preliminary engineering designs. The two charts are based on the average drifts of different rebar ratios and axial load, minus one standard deviation. Engineers would be able to determine design drift limits simply based on the damage states and the column aspect ratios.

Chapter 7: Residual drift and loss estimate of reinforced concrete and hybrid rocking columns

7.1 Background

Under the framework of PBD, structures are not only designed to avoid collapse but also to provide satisfactory post-earthquake serviceability. This chapter first presents the dynamic modeling and analysis of RC and hybrid rocking columns using finite element analysis. The residual drift results based on time history analyses are presented and analyzed statistically. Then, fragility functions of both types of columns are developed and compared using damage states defined by residual drifts. Based on the fragility functions, assumed seismic hazards, and repair costs, seismic losses and cost-benefit are discussed in the end.

Residual displacement is an important indicator of permanent damage and post-earthquake serviceability. To normalize the magnitude of displacement to structural height, the concept of residual drift is often used, which is the ratio of residual displacement over column height. PBD criteria based on residual drifts have been used by several researchers (Billah and Alam 2016; Mackie and Stojadinović 2005). Large residual drifts indicate severe structural damage and can cause additional secondary effects (P-Delta effects) on structures. It also presents challenging problems for post-earthquake retrofits. For instance, after the Hyogo-ken Nanbu earthquake of January 17, 1995, about 100 columns with drifts of more than 1.75% were demolished and replaced with new columns because of the difficulty in re-centering the columns and re-alignment of the superstructures (Kawashima et al. 1998). Another study in Japan suggested that for buildings with more than 0.5% permanent drift, it is more expensive to repair than to replace them (McCormick et al. 2008). Although this study was focused on building structures, the conclusions for bridges would be similar, as the repair of bridges usually causes significant disruptions to traffic and trigger associated indirect costs. In the study by Billah and Alam (2016), it was found that bridge columns with 0.24% to 0.33% residual drifts represent slight

damage, 0.48% to 0.62% represent moderate damage, 0.73% to 0.87% represent extensive damage and residual drifts over 1.04% to 1.22% represent collapse.

Near-fault ground motions have been known to cause large residual drifts (Ardakani and Saiidi 2018; Cheng et al. 2016; Choi et al. 2010). These motions contain high input energy and strong velocity pulses that may result in large lateral displacement which may not be predicted by typical methods such as response spectrum analysis (Ardakani and Saiidi 2018; Baker 2007). Under these ground motions, upon the reversal of the column displacement, the asymmetric column stiffness causes residual displacements that cannot be fully recovered. Kawashima et al. (1998) suggested that residual drift is significantly affected by a bilinear factor *r*, which is the ratio of post-yielding stiffness to initial elastic stiffness. Residual drifts of columns would be small when the ratio *r* is large. The authors also suggested that the dependence of residual drifts on the natural period, soil condition, and ductility is not significant. Phan et al. (2007) developed a hysteresis model that is specifically calibrated for near-fault earthquakes, which could capture residual drifts more accurately. However, due to the variabilities in ground motions and structures, researchers recognized that it is very difficult to estimate residual drifts accurately (Ardakani and Saiidi 2018; Lee and Billington 2010; Yazgan and Dazio 2011).

Modeling the residual displacement or residual drifts of columns with large deformation can be a challenging task. Lee and Billington (2010) investigated the modeling approaches that can improve the prediction of residual displacement. It was suggested that many fiber element models are unable to capture the residual displacement of RC columns due to pinching effects in the hysteretic response. The authors proposed a modified concrete constitutive model that could better predict residual displacement. When performing engineering analysis, residual drifts can be obtained through non-linear dynamic time history analysis. However, time history analysis is time-consuming and requires resources that may not be available in typical engineering consultant offices. Erochko et al. (2011) studied the residual drift response of

special moment-resisting frames (SMRFs) and buckling-restrained braced (BRB) frames. Prediction equations for residual drifts were developed as a function of peak drifts, initial elastic drift and the drift concentration factor of each system. Ardakani and Saiidi (2018) presented five approaches to estimate residual drift without running time history analysis. The first four approaches are based on earthquake and structural parameters such as maximum pseudo velocity, sinusoidal velocity pulse, and triangular velocity pulse. The fourth approach was developed empirically based on structural displacement ductility. ATC-58 (2019) provides simple rules to estimate the residual drift ratio from the peak transient drift ratios. For structures reaching one to four times story yielding drift ratio, the residual drift is 30% of the plastic drift. After the transient drifts reaching four times yielding drift, the residual drift equals transient drift minus three times yielding drift.

To reduce residual drifts of columns, prestressing tendons have been proposed by a number of researchers to equip columns with some self-centering capacity (Lee and Billington 2011; Marriott et al. 2009; Ou et al. 2009; Wang et al. 2018; Zatar and Mutsuyoshi 2002). The tendons act as additional reinforcement going through the center of the column and provide re-centering force. They are designed to remain elastic during earthquake events so that the residual drifts are minimized.

7.2 Model validation

Dynamic time history analysis of reinforced concrete column and hybrid rocking column is used to provide the data used for further fragility analysis and loss estimate. Before conducting time history analysis, finite element models are validated based on experimental results. The validation for the hybrid rocking column is not repeated in this section as it has been presented in Chapter 6. Here, a validation of the reinforced concrete column under a series of shake table testing is performed, which was done by Sakai et al. (2006). The reinforced concrete column was identical to the hybrid rock column PRC-U2 presented in Table 14, except that this column

does not have prestressing tendons. The column was tested under four levels of intensities: elastic, yield, design and maximum level. However, Lee and Billington (2010) suggested that the design level earthquake was the maximum level earthquake as the resulted displacement ductility was close to 8. Therefore, the validation is based on the first three levels of shake table testing. Figure 66 shows the comparison between testing results and simulation results. It can be seen that the model is satisfactory although not perfectly matching all testing results. At the elastic level and yield level loads, the average differences in x and y directions are within 10% between simulation and testing results. At the design level loads, there are more differences between simulation and testing results due to the damage of the structure and other reasons. One of the reasons includes the use of the original ground motions, rather than recorded motions of the shake table (not available in the literature), which could result in differences in the outputs.

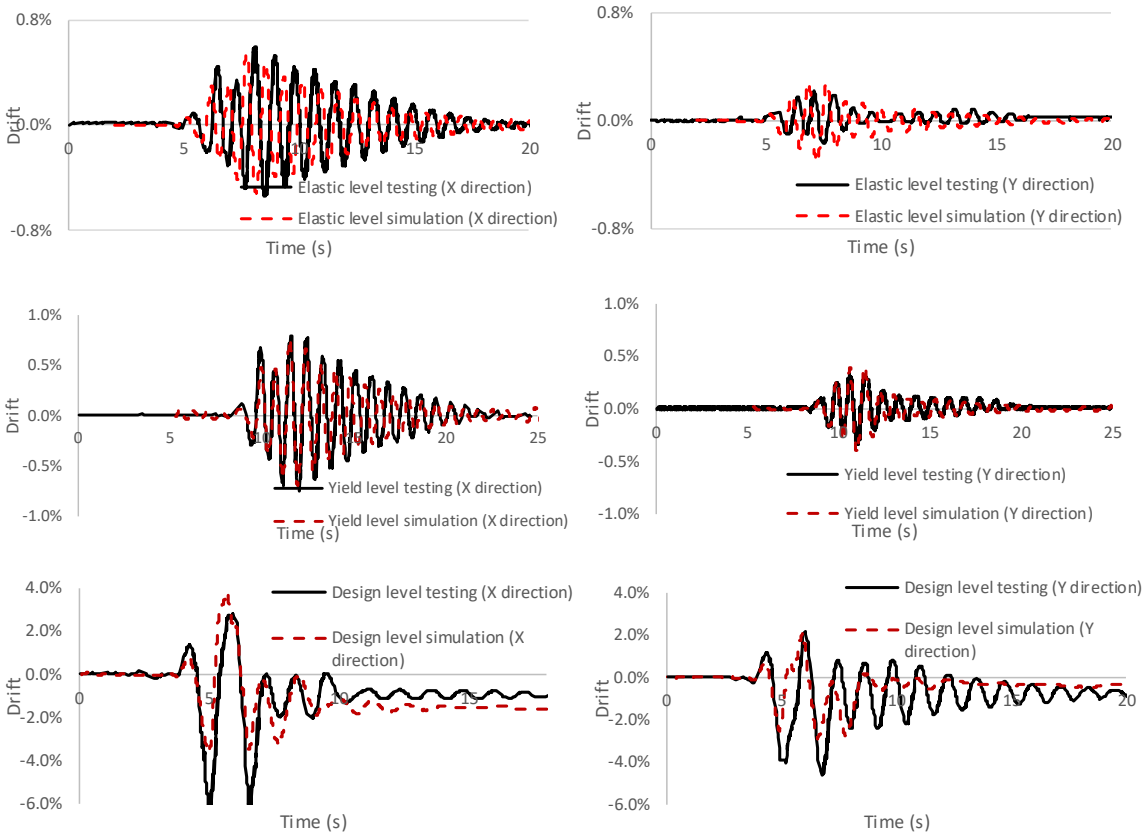

Figure 66 Displacement time history validation of RC column

7.3 Column parameters and analysis

One typical RC column and one hybrid rocking column are selected to conduct the case study. They are seen as typical because they represent a large portion of typical highway bridge columns in terms of aspect ratio, axial load ratio, and reinforcement ratio. The two columns have the same dimension, both of which are 6 m tall and 1 m diameter circular sections. The axial dead load ratios are 10% for both columns. The hybrid rocking column has another 10% axial load from the tendons. The hybrid rocking column has a 1% ratio of energy dissipating (ED) bar and a prestressing tendon. The tendon area is 0.18% of the column section area and its prestressed to about 17% of ultimate stress. The reinforced concrete column has 2% longitudinal reinforcement.

In the analysis, 11 sets of near-fault ground motions are selected from Mackie and Stojadinović (2005) as inputs for the time history analysis. In each of the analyses, two horizontal components of each set of motion are applied simultaneously to the columns. The time history analysis is performed using the software SeismoStruct (SeismoSoft 2020). To cover a wide range of PGAs, each set of the motions is scaled to 4 levels. Thus, there are 44 time-history analyses for each of the two columns. A summary of the selected motions is presented in

Table **20**. The acceleration response spectra of unscaled ground motions are presented in Figure 67. Since each set of records has two horizontal components, there are 22 spectra plotted in Figure 67. The plot of PGV vs PGA of the record is shown in Figure 68. When performing the time history analyses, a few seconds of zero acceleration is added to the end of each input motion to allow the column to damp out the vibration.

Table 20 Selected ground motions

Record	Event	Year	M	R	Station	Mechanism	PGA (g)	
							x	y
1	Coalinga	1983	6.4	8.5	Pleasant Valley	reverse-oblique	0.285	0.38
2	Imperial Valley	1979	6.5	8.5	Aeropuerto Mexicali	strike-slip	0.26	0.327
3	Imperial Valley	1979	6.5	2.5	Bonds Corner	strike-slip	0.775	0.588
4	Imperial Valley	1979	6.5	10.6	Calexico Fire	strike-slip	0.202	0.275
5	Loma Prieta	1989	6.9	12.7	Gilroy Array	reverse-oblique	0.322	0.367
6	Loma Prieta	1989	6.9	12.7	Gilroy	reverse-oblique	0.241	0.284
7	Morgan Hill	1984	6.2	3.4	Halls Valley	strike-slip	0.312	0.156
8	Northridge	1994	6.7	7.1	Rinaldi Receiving	reverse-slip	0.472	0.838
9	Northridge	1994	6.7	8.9	Sepulveda VA	reverse-slip	0.939	0.753
10	Whittier Narrows	1987	6	9.8	Bell Gardens	reverse-slip	0.212	0.219
11	Whittier Narrows	1987	6	10.5	West Covina	reverse-slip	0.179	0.137

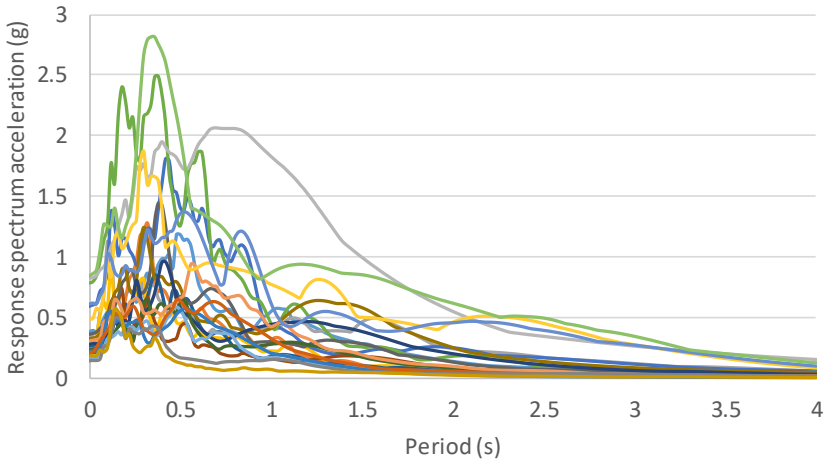

Figure 67 Acceleration response spectra

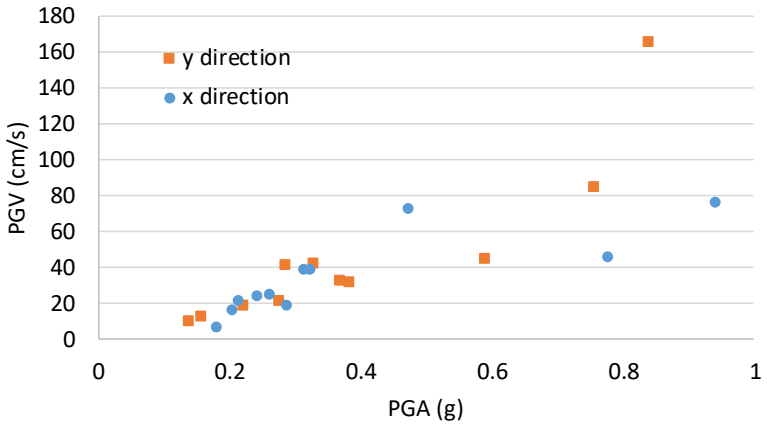

Figure 68 PGV vs PGA of selected records

7.4 Residual drift results

Residual drifts of each time history analysis are obtained at the end of the analysis. Then the data is used for further analysis. Figure 69 and Figure 70 are example results of the columns' hysteretic curves in the x and y direction under the loading of Record Number 6 in Table 18 with a scale factor of 2. The RC column has a reinforcement ratio of 2% and the hybrid rocking column has a reinforcement ratio of 1%. By comparison, when the columns show obvious inelastic behavior, the RC column has larger hysteretic loops which represent more energy dissipations. In the y-direction, the seismic demands are relatively lower thus the two columns show similar hysteresis. It should be noted that hybrid rocking columns would not always have negligible residual deformation since they have ED bars similar to rebars used in reinforced concrete columns.

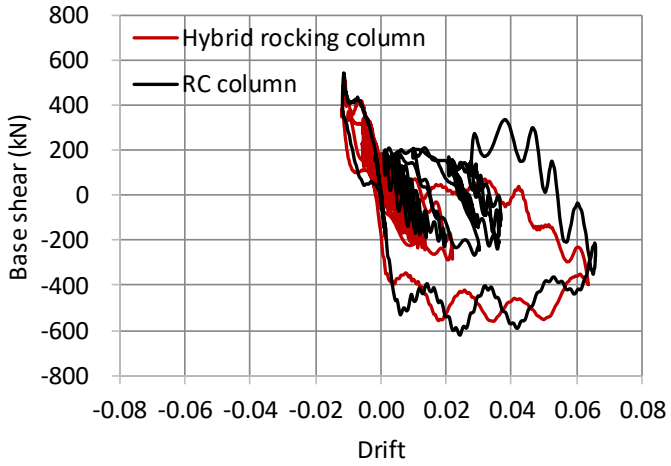

Figure 69 Hysteretic curves in the x-direction

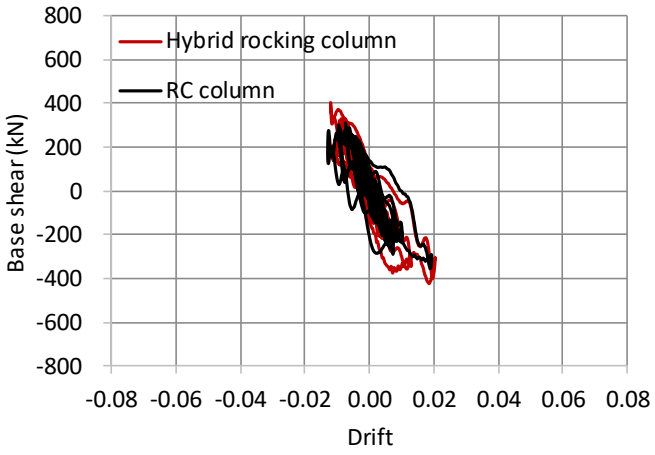

Figure 70 Hysteretic curves in the y-direction

Figure 71 plots the residual drift to maximum drift ratios with respect to PGA. And Figure 72 plots the residual drift with respect to the maximum drift ratio. The two variables PGA and maximum drift ratio are chosen because the residual drift increases with the increase in these two parameters and they are relatively easy to obtain during the design phase. During the design phase, PGA is always provided as part of seismic hazard input for seismic design. The maximum drift can be calculated through a linear response spectrum analysis. By observing these two figures, it is apparent that the RC column has a higher residual drift compared to the hybrid rocking column. The distribution of the data is generally fan-shaped, which means that at large inelastic deformations, the residual deformation varies more significantly. The residual to

maximum drift ratio increases with the increase in PGA and maximum drift. The dispersion of the data seems to increase when PGA and maximum drift are higher.

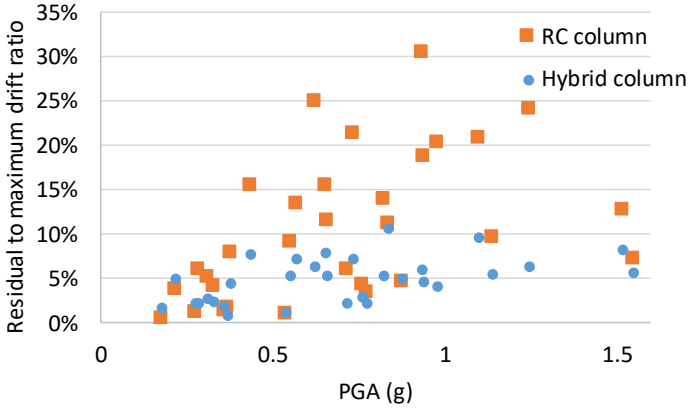

Figure 71 Residual to maximum drift ratio vs PGA

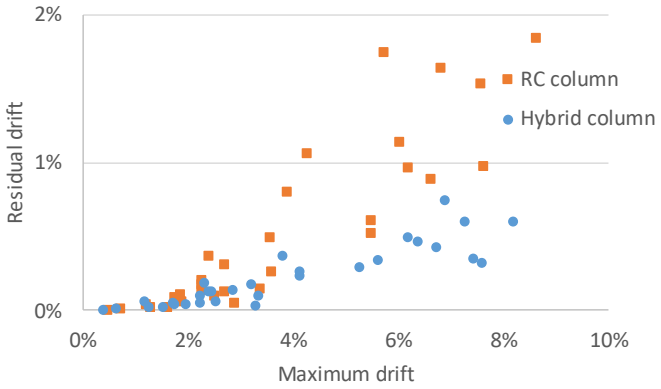

Figure 72 Residual drift vs maximum drift

To correlate the residual to maximum drift ratio to design parameters, a multi-linear regression is performed for both the RC column and hybrid rocking column. The regression equations for the RC column and hybrid column are shown in Equation 47 and Equation 48 having R-square values of 0.55 and 0.42, respectively. The coefficients for Max drift are 2.64 and 0.57 for the RC column and hybrid column, respectively. Thus, the residual drift of the RC column is more dependent on the max drift. The line fit plots of two regression equations are shown in Figure 73 and Figure 74. For the RC column, the predicted residual/max drift has a Mean Absolute Error (MAE) and Root mean squared error (RMSE) of 4.1% and 5.4%. The MAE and RMSE for hybrid rocking column predicated data are 1.5% and 1.9%.

$RC\ column$:

$$Residual\ drift = Max\ drift \times (0.007 + 0.0037 \times \mathrm{PGA} + 2.64 \times Max\ drift) \qquad \text{Equation 47}$$

Hybrid column:

$$Residual\ drift = Max\ drift \times (0.019 + 0.0130 \times \mathrm{PGA} + 0.57 \times Max\ drift) \quad \text{Equation 48}$$

where PGA is the peak ground acceleration in the unit of g.

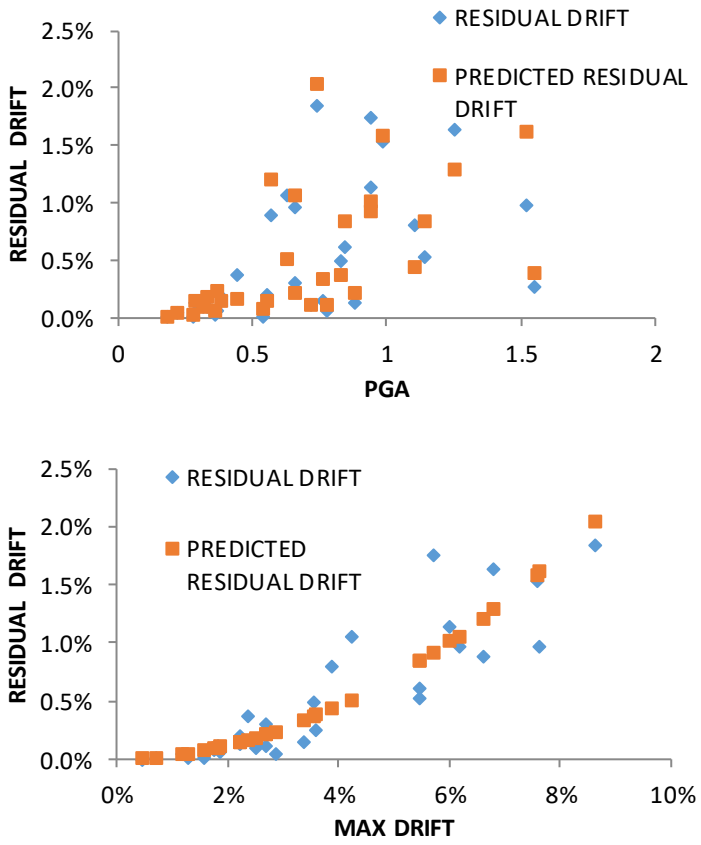

Figure 73 Regression equation evaluation for RC column

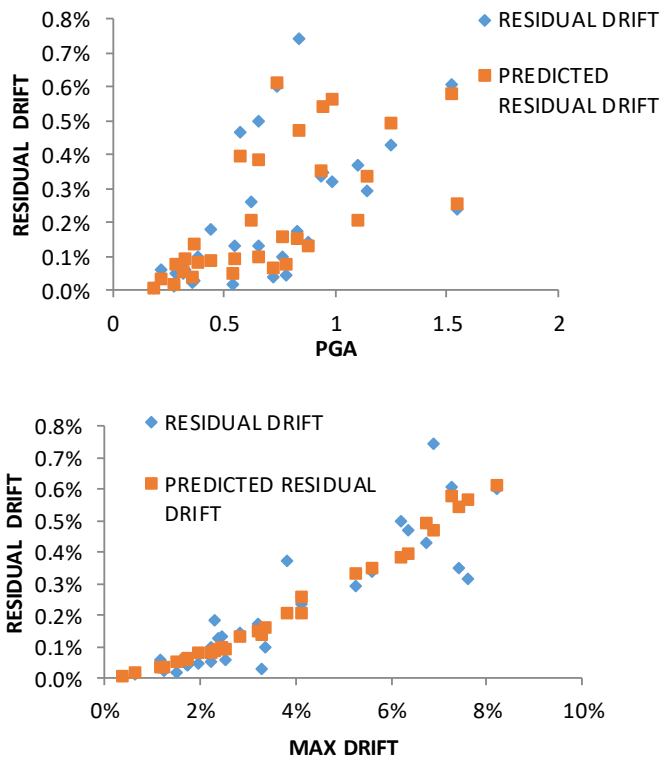

Figure 74 Regression equation evaluation for hybrid rocking column

7.5 Fragility functions

The previous sections have shown that the RC column generally has higher residual drifts than the hybrid rocking column. However, the difference cannot be quantified by simple observation. Thus, fragility functions are developed in this section to do a further comparison. The fragility function describes the probability of structures achieving a certain damage state of interest in a prescribed ground motion intensity measurement (Billah & Alam, 2014a). More precisely, Porter (2020) stated that a fragility function is the cumulative distribution of the capacity of an asset to resist an undesirable limit state. The probability of exceeding the limit states can be expressed using Equation 49:

$$Fragility = P\,(DS \mid IM = x) \qquad \text{Equation 49}$$

where $\mathrm{P}\ (\mathrm{DS}\ |\ \mathrm{IM}{=}\mathrm{x})$ is the probability that a ground motion with intensity measurement of x will cause damage states beyond DS. The intensity measurement can be any parameter describing

the ground motion severity such as PGA and PGV. When developing analytical fragility curves, time history analyses are usually first performed and then followed by statistical methods to estimate the fragility function parameters. To define the fragility function, a lognormal cumulative distribution is often assumed (Equation 50) as researchers confirmed that IM values causing structural damage are lognormally distributed (Li et al. 2020; Porter 2020; Xiang and Alam 2019).

$$\mathrm{P}\left(\mathrm{DS} \mid \mathrm{IM}=\mathrm{x}\right)=\emptyset\left(\frac{\ln\left(\frac{x}{\theta}\right)}{\beta}\right) \quad \text{Equation 50}$$

where $\emptyset$ is the standard normal cumulative distribution function, θ is the median and β is the standard deviation of ln(IM). To develop the fragility function, the values of θ and β need to be estimated. The estimated values of the two parameters are denoted as $\hat{\theta}$ and $\hat{\beta}$ in this study. One way of estimating the $\hat{\theta}$ and $\hat{\beta}$ is performing the incremental dynamic analysis (IDA) and then calculate the two parameters using Equation 51 and Equation 52. The required result from IDA is IM corresponding to the interested damage state for each ground motion. The analytical fragility function parameters are fitted by taking logarithms of each IM corresponding to the damage states, then calculating their mean and standard deviation.

$$ln\hat{\theta}=\frac{1}{n}\sum_{i=1}^{n}\ln IM_i \quad \text{Equation 51}$$

$$\hat{\beta}=\sqrt{\frac{1}{n-1}\sum_{i=1}^{n}\left(\ln\left(\frac{IM_i}{\hat{\theta}}\right)\right)^2} \quad \text{Equation 52}$$

Another way of estimating $\hat{\theta}$ and $\hat{\beta}$ is through performing multiple stripes time-history analysis and fitting the fragility function using the maximum likelihood method (Baker 2015). When using this method, some time-history analyses are performed at each intensity level x_j. The probability of z_j cases reaching interested damage states out of n_j motions at IM=x_j is given by a binomial distribution (Equation 53).

$$P\left(z_j \; cases \; damaged \; in \; n_j \; motions\right) = \binom{n_j}{z_j} p_j^{zj} (1 - p_j)^{nj - zj} \quad \text{Equation 53}$$

where p_j is the probability that at ground motion with IM=x_j will cause the damage state. The goal of the function fitting is to find parameters that maximize the likelihood of having the probability with the observed data in the time history analysis for a range of IM. The likelihood of multiple IM is the product of Equation 53, as shown in Equation 54.

$$Likelihood = \prod_{j=1}^{m} \binom{n_j}{z_j} p_j^{z_j} (1 - p_j)^{n_j - z_j} \quad \text{Equation 54}$$

It is known that p_j can be represented by Equation 50, the likelihood function can be re-written as Equation 55.

$$Likelihood = \prod_{j=1}^{m} \binom{n_j}{z_j} \emptyset \left(\frac{\ln (\frac{x_j}{\theta})}{\beta} \right)^{z_j} \left(1 - \emptyset \left(\frac{\ln (\frac{x_j}{\theta})}{\beta} \right) \right)^{n_j - z_j} \quad \text{Equation 55}$$

When maximizing Equation 55 to seek the greatest likelihood, it is equivalent to maximizing the logarithm of the likelihood function, as shown in Equation 56, which is much easier to optimize numerically.

$$f(\theta, \beta) = \sum_{j=1}^{m} \left\{ ln \binom{n_j}{z_j} + z_j \ln \emptyset \left(\frac{\ln (\frac{x_j}{\theta})}{\beta} \right) \; + (n_i - z_j) ln \left(1 - \emptyset \left(\frac{\ln (\frac{x_j}{\theta})}{\beta} \right) \right) \right\} \quad \text{Equation 56}$$

By using the fragility function fitting method for each damage state, Figure 75 and Figure 76 can be obtained considering different levels of damage states. Figure 75 is developed for a residual drift of 0.2% which corresponds to minimal damage slightly beyond the elastic stage (denoted DS1). Figure 76 is developed for a residual drift of 0.5% residual drift, which corresponds to a moderate damage state (denoted DS2). DS3 is developed considering a residual drift of 1%, which will be discussed later. These three damage states are determined based on FEMA 2012

(FEMA 2012; Hamburger et al. 2012), where a residual drift of 0.2% is used for the first damage state representing slight damage. A drift ratio of 0.5% is used for the second damage state, meaning that the realignment of structural frames and non-structural components is needed. The third level of damage state is signified by a 1% drift, where the repair of the structure may not be economically and practically feasible. Although these drift limits were originally developed for building structures, they should be generally applicable to standard highway bridges and for a comparison of two bridge columns.

From Figure 75 and Figure 76, it can be seen that the hybrid column has a smaller probability of being damaged than the RC column for both Damage State 1 and Damage State 2. The difference between the two systems is especially obvious at the damage level DS2. However, at Damage States 3, the data points would introduce a relatively high slope in the fragility curve due to small $\hat{\beta}$ value and make fragility curves cross each other. The solution to solve the issue was proposed by Porter (2020), who suggested using three different $\hat{\theta}$ values but single $\hat{\beta}$ throughout all damage states. In this way, the two non-zero points produce more reasonable fragility in the case of hybrid column DS3. The overall maximum likelihood method for fragility fitting allows using very limited data to produce results which are of great help in practice, as it significantly reduces the required number of time history analysis. In some situations, it is also possible that at the site the seismicity is not high enough to introduce the interested damage state and upscaling the excitations to an extremely high level may not be realistic. Therefore, producing fragility with limited data is essentially important. In this overall maximum likelihood calculation, the $\hat{\theta}$ and $\hat{\beta}$ values fitted for all three damage states can be obtained considering the likelihood of all PGAs and all damage states simultaneously, as expressed in Equation 57.

$$Likelihood = \prod_{j=1}^{m} \prod_{i=1}^{s} P_z(z) \qquad \text{Equation 57}$$

where m is the number of damage states and s is the sets of approximately equal excitations with similar PGAs, P_z is the probability that there will be z cases of damage in n analyses. By using Equation 57, the fragility functions of the hybrid column in Figure 77 and Figure 78 can be obtained. The $\hat{\theta}$ and $\hat{\beta}$ values of hybrid column and RC column using individual damage state likelihood fitting are shown in Table 21. The $\hat{\theta}$ and $\hat{\beta}$ values of the hybrid column using all damage states simultaneously for function fitting are shown in Table 22. When using a single $\hat{\beta}$ value and considering the maximum likelihood of all damage states, the hybrid column has less probability of being damage compared with the RC column in all damage states.

Table 21 Fragility fitting using each damage states separately

	Hybrid column			RC column		
Damage states	DS1	DS2	DS3	DS1	DS2	DS3
$\hat{\theta}$	0.810	1.189	1.192	0.673	0.810	1.027
$\hat{\beta}$	0.284	0.327	0.153	0.328	0.284	0.348

Table 22 Fragility fitting using all damage states simultaneously

	Hybrid column		
Damage states	DS1	DS2	DS3
$\hat{\theta}$	0.811	1.149	1.309
$\hat{\beta}$	0.272	0.272	0.272

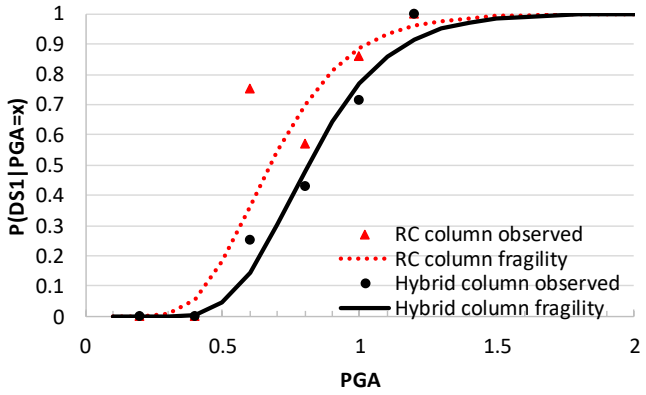

Figure 75 Fragility function for DS1

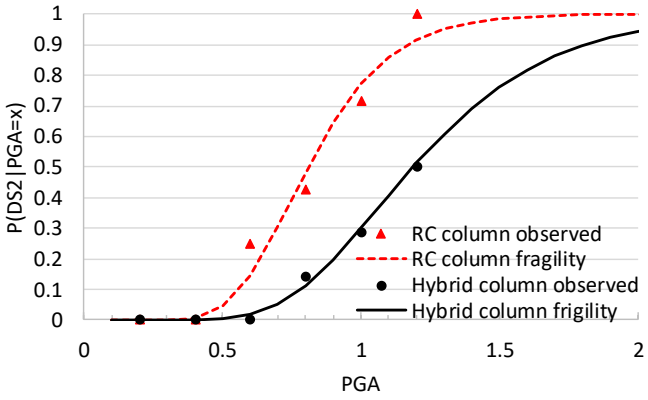

Figure 76 Fragility function for DS2

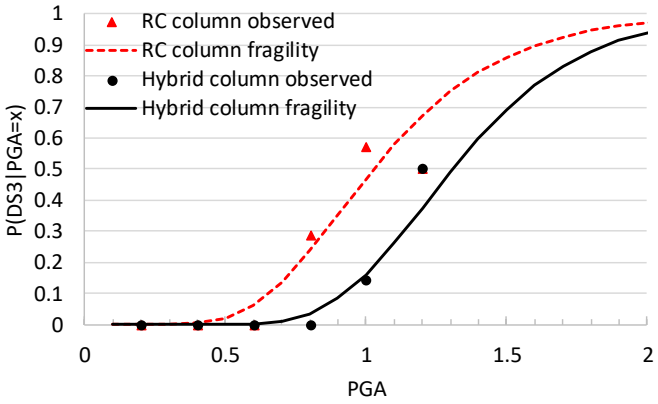

Figure 77 Improved fragility function for DS3

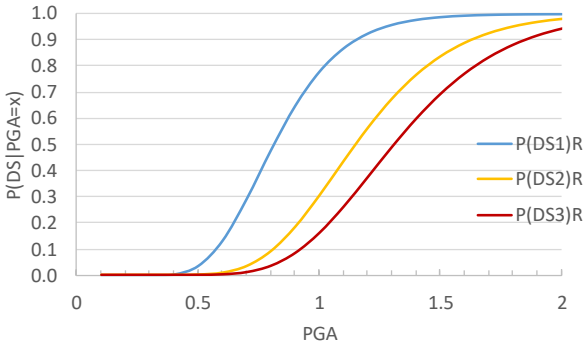

Figure 78 Hybrid column fragility (single $\widehat{\boldsymbol{\beta}}$)

7.6 Loss estimate

Minimizing earthquake losses is one of the major goals of PBD. Several models for seismic loss estimates were proposed by researchers (Bendimerad 2001; Mackie and Stojadinović 2007; McCormack and Rad 1997; Whitman et al. 1997). Mackie et al. (2008) presented a probabilistic performance-based evaluation of bridges in California introducing approaches to produce the probability of exceeding the decision limit state given an earthquake intensity. The basic form of the integrated probability can be expressed in Equation 58. Then, it is assumed that EDP has a lognormal distribution when conditioned on IM (Equation 59). Similarly, the relation of Engineering Demand Parameter (EDP) and Damage Measurement (DM), and Decision Variable (DV) are represented by Equations 60 and Equation 61 assuming lognormal distributions. The solution of the integrated probability is shown in Equation 62.

$$P\,(DV > dv^{LS} |\; IM = im) = \qquad \text{Equation 58}$$

$$\int\int G_{DV|\,DM}(dv^{LS} \mid dm)\left|\, dG_{DM|\,EDP}(dm|\; edp)\right| \left|\; dG_{EDP|\,IM}(edp|\; im)\right|$$

$$ln(\widehat{EDP}) = A + Bln(IM) \qquad \text{Equation 59}$$

$$ln(\widehat{DM}) = C + Dln(EDP) \qquad \text{Equation 60}$$

$$ln(\widehat{DV}) = E + Fln(DM) \qquad \text{Equation 61}$$

$$P\,(DV > dv^{LS} |\; IM = im) = 1 - \Phi\left[\frac{\ln\left(dv^{ls}\right) - (E + FC + FDA + FDBln(im))}{\sqrt{d^2 f^2 \boldsymbol{\sigma}^2_{EDP|\,IM} + f^2 \boldsymbol{\sigma}^2_{DM|\,EDP} + \boldsymbol{\sigma}^2_{DV|\,\mathbf{DM}}}}\right] \qquad \text{Equation 62}$$

Seismic loss and resilience of the rocking column were recently studied by Giouvanidis and Dong (2020). The study suggested that the rocking column bridge had considerably less seismic losses compared to the fixed base structures. The study focused on direct structural losses of simple rocking columns that do not have energy dissipating bars. The indirect economic losses resulted from bridge damage were studied by Stein et al. (1999) and Dong and Frangopol (2015). In the cases of bridges in urban areas, indirect losses could be much higher than direct structural losses. In addition to losses resulting from a single damaged structure, seismic loss estimates and risk analysis of a portfolio were investigated by several researchers (Park et al. 2007; Porter 2020; Weatherill et al. 2015).

In this section, loss analyses of the hybrid rocking column and RC column are performed considering the seismicity in Vancouver BC, Canada, and Salt Lake region, Utah, USA. PGAs are used as intensity measurements to describe the hazard curves. For the seismicity in BC, three PGA data points with the corresponding annual rates are obtained from NRC (2020). Seismic hazards with return periods of 475 years, 975 years and 2475 years are corresponding to the mean rates of shaking per year of 0.0021, 0.001, and 0.000404. The obtained data can be used to estimate a continuous hazard curve based on the Gutenberg-Richter recurrence law (Gutenberg and Richter 1944), which assumes that the magnitude or intensity and the log of annual rate are in a linear relationship (Baker 2008), as described in Equation 63. The seismic hazards for Utah are obtained from Wong et al. (2002). Sites with high seismicity are selected and the hazard curves are developed using Equation 63. Figure 79 shows the hazard curves for both regions. The seismic curve of BC has PGAs of 0.306g at the 475-year event and 0.578g at the 2475-year event. The seismic curve of Utah has PGAs of 0.5g and 0.9g at the 475-year event and 2475-year event, respectively.

$$log_{10}\lambda_m = a + \mathrm{b} \times \mathrm{IM} \qquad \text{Equation 63}$$

where a and b are constants that can be obtained from a linear regression analysis, λ_m is the rate of earthquakes with magnitudes greater than m.

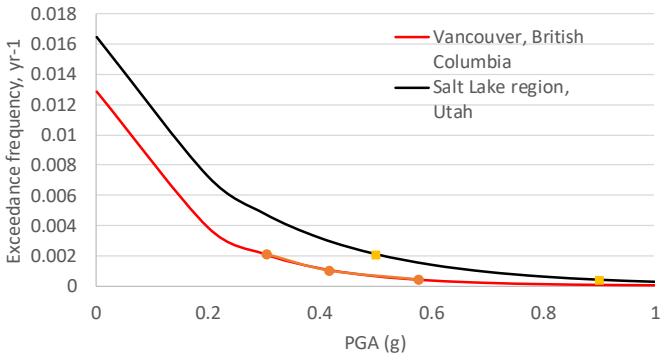

Figure 79 Hazard curves

With estimated rates of occurrence of earthquakes and fragility function of a structure conditioned on specific seismicity IM, the annual rate of structural damage can be calculated using Equation 64 (Porter 2020)

$$\lambda = \int_0^{\infty} -F(s)\frac{dG(s)}{ds}ds \qquad \text{Equation 64}$$

where λ is the mean rate or number per unit time the damage occurs, $F(s)$ is the fragility function for the damage state considering earthquake intensity of s. $G(s)$ is the mean rate of shaking per year with an intensity of not less than s. $\frac{dG(s)}{ds}$ can be seen as the mean number of earthquakes per year with intensity exactly s. Numerically, Equation 64 can be solved by solving Equation 65 (Porter 2020).

$$\lambda = \sum_{i=1}^{n-1}\frac{1}{2}\left(\emptyset\left(\frac{\ln\left(\frac{x_i}{\theta}\right)}{\beta}\right)+\emptyset\left(\frac{\ln\left(\frac{x_{i+1}}{\theta}\right)}{\beta}\right)\right)\left(G(x_i)-G(x_{i+1})\right) \qquad \text{Equation 65}$$

Bringing in the estimated hazards curves and the fragility functions to Equation 65, the annual rate of exceeding the three damage states are obtained and presented in Figure 80. The annual rate of exceedance of the RC column for DS1 is about 0.0002. All other damage state rates of exceedance are less than 0.00005. It should be noted that the annual frequency bridge collapse

under some other extreme loadings such as vessel collision is 0.0001 (AASHTO 2020; CSA 2019). Thus, the two types of columns both meet the minimal code safety requirements. Additionally, the probability of suffering damage within the structure's lifetime can be calculated using the Poisson equation shown in Equation 66. Considering a design life of 75 years for most highway bridges, Figure 81 presents the probability of being damaged in 75 years for both columns.

$$P = 1 - \exp(-\lambda t) \qquad \text{Equation 66}$$

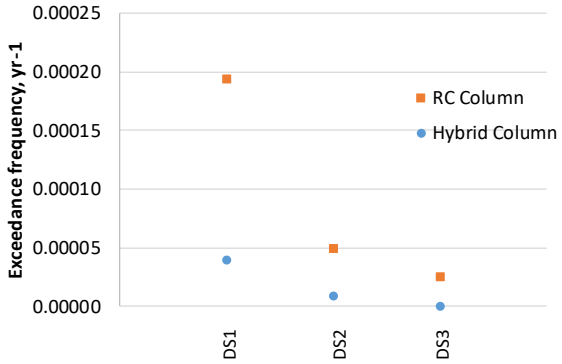

Figure 80 Exceedance frequency for three damage states

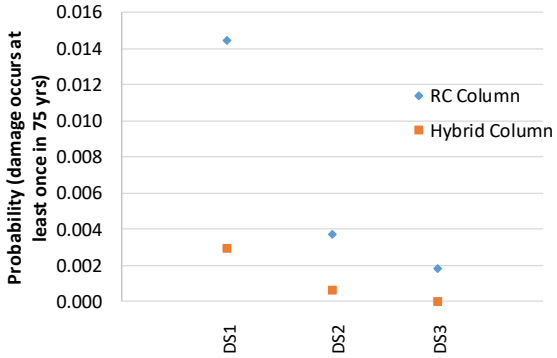

Figure 81 Probability of being damaged in 75 years

The above analysis quantifies the difference between the two systems in terms of the probability of being damaged. To make decisions considering limited resources, the comparison needs to be based on monetary terms considering cost and benefit. With known annual rates of exceeding the damage states, it is possible to compute the expected annual losses with

presumed repair costs. Similar to the damage occurrence annual rate, the expected annual loss (EAL) can be computed using Equation 67 (Porter 2020).

$$\mathrm{EAL} = V \int_0^{\infty} y(s) \frac{dG(s)}{ds} ds \qquad \text{Equation 67}$$

where V is the replacement cost of the bridge and $y(s)$ is the expected value of loss given shaking s as a fraction of V, which is also called damage ratio. Based on the expected annual loss, the present value of the annual loss can be computed using Equation 68.

$$PV = EAL \frac{\left(1 - e^{-ti}\right)}{i} \qquad \text{Equation 68}$$

where i is the discount rate and t is the number of years in which the expected annualized loss EAL occurs.

Based on the above-presented methodology, it is possible to compare the financial benefit of bridges using a hybrid rocking column to replace the RC column. The column presented in the previous section is adequate for supporting three lines of steel girders and concrete deck superstructure that is about 70 m long and 11 m wide with two lanes of traffic. For a bridge of this size, the approximate cost is about 2 million Canadian dollars based on the construction cost estimate provided by BCMOTI (2013). However, it should be noted that the construction cost of bridges can vary significantly based on the construction site. To assess the seismic losses, it is assumed that a specific amount of structural losses (damage ratios) and indirect economic loss (based on repair time) would occur with a 50% chance at PGAs corresponding to a 50% exceedance probability of the damage states in the fragility functions. The PGAs for the 50% exceedance probability at three damage states and their annual rates of shaking are summarized in Table 23.

The estimated repaired methods and time for the three damage states are based on several past studies and standards (CSA 2019; Dong and Frangopol 2015; Mackie and Stojadinović

2005). At the first level of damage state (DS1), it is expected that the bridge remains fully serviceable for normal traffic and the repair work does not cause traffic disruption. The repair work could be sealing cracks and minor removal and patching of concrete. At DS2, it is expected that the bridge is only open for emergency vehicles. Normal service would be restored in a longer time. Therefore, there would be indirect losses to the economy starting from DS2. The repair actions can be replacement of buckled rebar, major patching of concrete cover, installing steel casing, and other strengthening techniques. At DS3, major construction work may be needed such as replacing the column and re-centering the superstructure. The following calculation assumes that the direct structural losses at three damage states are 3%, 8% and 25% of the bridge replacement value for both the hybrid column and the RC column (HAZUS 2010). This should be a conservative assumption in comparing the benefit of using a hybrid rocking column. When designing the hybrid rocking column, the goal is to make it easier to repair within a short time, such as locating the ED bars externally to the column. Thus, assuming that the repair efforts of the two systems cost the same percentage of the initial cost is conservative. The required repair time is 1 day, 2.5 days and 75 days for the RC column supported bridge based on the average repair time in (HAZUS 2010). The required repair time for the hybrid column is assumed to be the time required for the RC column less than one standard deviation (HAZUS 2010). This is because researchers have extensively investigated the repair methods for the hybrid rocking columns and expected that hybrid rocking columns are much easier to repair, especially when the energy dissipater is located outside of the column section (Marriott et al. 2009).

The estimated repair time combined with traffic data is used to calculated indirect economic losses. The first type of indirect loss is called running cost, which is the cost of driving a vehicle through detours, as expressed in Equation 69. The second type of indirect loss is the monetary value of time loss expressed in Equation 70.

$$C_{Run} = (C_{\,car}(1-T) + C_{truck}T)D \times ADT \quad \text{Equation 69}$$

where $C_{\,car}$ and C_{truck} are rates per distance for operating cars and trucks (CAD/km), D is the additional distance of the detour (km); ADT is the average daily traffic, and T is the average daily truck traffic ratio (ADTT, %).

$$C_{TL} = \left(C_{AW}O_{car}(1-T) + \left(C_{ATC}O_{truck} + C_{goods}\right)T\right)\left(ADT\frac{D}{S} + ADE\left(\frac{l}{S_d} - \frac{l}{S_o}\right)\right) \quad \text{Equation 70}$$

where C_{AW} the average hourly wage for car drivers, C_{ATC} is the average compensation per hour for truck drivers, C_{goods} is the time value of the goods transported in cargo, ADE is the average daily traffic remaining on the damaged bridge; O_{car} and O_{truck} are the average vehicle occupancies for cars and trucks; l is the route segment containing the bridge (km); S_o and S_d represents the average speed on the intact route and damaged route (km/h); and S represents the average speed on a detour (km/h). When using Equation 69, this study assumes the ADE is zero as there would not be any vehicle on the damaged bridge. The assigned values for the parameters are presented in Table 24.

Table 23 PGAs corresponding to three damage states and rates of shaking

Column type	RC column			Hybrid rocking column		
Damage state	DS1	DS2	DS3	DS1	DS2	DS3
Earthquake intensity (PGA)	0.65	0.8	1.15	0.8	1.15	1.3
Mean rate of shaking, BC	0.00026	0.00010	0.00001	0.00010	0.00001	0.00001
Mean rate of shaking, Utah	0.00114	0.00061	0.00015	0.00061	0.00015	0.00008

A summary of the loss estimate is presented in

Table **25**. The initial costs of the bridge with RC column and hybrid rocking column are $2 million. The annual loss of the bridge with RC and hybrid rocking columns in BC are $1387 and $210, respectively. The initial costs plus present values of expected annual loss for bridges with RC and hybrid rocking column are $2.03 million and $2.12 million. Thus, there does not seem to be enough incentive to adopt the hybrid rocking column system considering the monetary benefits considering the difference is only 1%. When the site is at an extremely high seismic region such as the case of Utah, the initial costs plus present values of expected annual loss for RC and hybrid rocking column are $2.12 million and $2.03 million, which indicate a meaningful reduction in total project cost (5% savings). Therefore, it is more likely that the low damage system being adopted in very high seismic regions. It should be noted that in this example, the majority of the seismic losses result from indirect economic losses. For instance, shutting down a bridge with average daily traffic of 40,000 vehicles for 30 days would cost about a few times the replacement cost of the bridge.

Table 24 Parameters for indirect loss estimate

Average daily traffic	40,000
Average daily truck traffic ratio	25%
Bridge length (m)	80
Detour distance (km)	2
Cars occupancies	1.5
Trucks occupancies	1.05
Car driver wage ($/h)	12
Truck drivers Compensation ($/h)	30
Inventory cost ($/h)	4
Car operating cost ($/km)	0.4
Truck operating cost ($/km)	0.6
Detour speed (km/h)	50

Table 25 Loss estimate

Column type		RC column		Hybrid column	
Bridge replacement cost ($)		2,000,000		2,000,000	
Direct (structural) loss	Damage states	Damage ratio	Repair cost ($)	Damage ratio	Repair cost ($)
	DS1	0.03	60,000	0.03	61,200
	DS2	0.08	160,000	0.08	163,000
	DS3	0.25	500,000	0.25	510,000
Indirect loss	Damage states	Repair time (days)	Loss	Repair time (days)	Loss
	DS1	1	0	1	0
	DS2	2.5	6,060,000	1	3,030,000
	DS3	75	24,240,000	33	12,120,000
Annual loss	BC	1,387		210	
	Utah	6,014		1,186	
Present value of annual loss	BC	27,087		4,101	
	Utah	117,447		23,168	
Replacement cost plus present value of expected loss	BC	2,027,087		2,004,101	
	Utah	2,117,447		2,023,168	

7.7 Summary

Non-linear time history analyses of RC column and hybrid rocking columns are performed and the results in terms of residual drifts are obtained. 11 sets of bi-directional near-fault ground motions are selected and scaled to four intensity levels for the time history analysis. It is observed that the hybrid rocking column has less residual drift compared with the RC column. The residual drift to maximum drift ratios of both systems increases with the increase in PGA and maximum drifts. Regressions equations correlating residual/max drift ratio and PGA and maximum drift ratio are developed. The residual drift of the RC column is more dependent on the max drift compared with the hybrid rocking column.

Based on the time history analysis results, three damage states are identified. The fragility functions of both systems are developed using the maximum likelihood function fitting methods. For the hybrid rocking column, due to a lack of observed damage at the DS3, abnormal results could be reached. Thus, a likelihood function considering all three damage states is used. The

total likelihood function is maximized considering three different $\hat{\theta}$ values but single $\hat{\beta}$ value. Based on this approach, the fragility functions show that the hybrid column has less probability of being damaged under all intensity measurements and all damage states.

In the end, a loss estimate assuming a typical bridge construction cost and urban daily traffic is performed. The hazard curves from BC and Utah are used, which present a high seismic region and extremely high seismic region, respectively. It is shown that if the initial cost of the bridge with a hybrid rocking column is only 2% higher than the traditional RC column construction, it may not be financially beneficial to build the bridge with hybrid rocking columns. However, when the seismicity is extremely high, e.g. with PGAs of 0.5g and 0.9g at the 475-year event and 2475 year event, then the higher initial cost can be justified by less expected losses. Or, if the bridge has higher average daily traffic (e.g. more than 40,000) which indicates significant indirect seismic losses if the bridge is damaged, then the hybrid rocking column option can be more preferable with lower seismicity. Last but not the least, the study assumed that the repair time for the hybrid rocking column is about half of that for the RC column. If in the future, the repair time of the hybrid rocking column can be further reduced, it may become more promising as well.

Chapter 8: Conclusion

8.1 Background

The post-tensioned rocking column is a relatively new structural system in seismic regions and a promising alternative to the traditional reinforced concrete column. The seismic design of the post-tensioned rocking column is not prescribed in the current seismic design codes. However, under the framework of PBD, post-tensioned rocking columns can achieve better results than reinforced concrete columns in terms of serviceability after earthquakes due to their self-centering capacity. This research investigates the seismic behavior of post-tensioned concrete bridge columns from the perspectives of PBD.

This study first reviews the state of the art of PBD development and design codes. A brief comparison of the design codes is conducted. Then, this study reviews and assembles existing experimental studies of rocking columns. The testing result data is collected to perform further data analysis and to propose design equations used in PBD. Subsequently, this study investigates the fundamentals of the rocking column: equations of motion and looks into how different components (e.g. tendon and initial prestressing force) affect the seismic response. Thereafter, finite element models are developed to study the nonlinear response of the rocking column system.

After achieving a good understanding of how the rocking column behaves, this study investigates the drift-based design criteria of the hybrid rocking column and compares it with that of the reinforced concrete column. Design charts that facilitate preliminary engineering design are developed. In the end, a fragility and loss estimate of the hybrid rocking column and reinforced concrete column is conducted and compared.

8.2 Limitations of this study

The limitations of this study are as follows:

- In all the analyses, shallow footing foundations are assumed and the base of the columns are effectively fixed. However, the post-tensioned rocking column system may be used in deep foundations (e.g. shafts) as well. When the foundation is founded on weak soils, the soil-structural interaction would need to be considered.
- Regression equations proposed based on testing data in available literature have relatively low R squares due to the variability in the column details such as different shear keys, steel jackets and unbonded lengths. The obtained data was not enough to include more parameters in the proposed equation to improve accuracy.
- Radiation damping is not included in the dynamic modeling of the columns. In the work conducted by Moustafa and ElGawady, it was shown that radiation damping contributes a notable percentage to total damping. Although ignoring radiation damping is conservative, being able to capture radiation damping in design would improve the seismic response predictions.
- This study mainly focuses on flexural dominant columns, it is assumed that shear failure would be avoided. However, for short columns that are controlled by shear rather than bending moment, some of the conclusions in this study would not apply.
- When comparing the loss estimate of the hybrid rocking column with reinforced concrete columns, the conclusions from the case study may not be generalized, although it can represent a large number of standard highway bridges.
- The columns studied in this project are representative of standard highway bridge columns. For irregular bridges with special considerations such as unequal column heights and torsional responses, more research needs to be conducted.

8.3 Conclusion

The following conclusions can be drawn from this study:

- By comparing design criteria among different codes based on the case study, the Canadian Highway Bridge Design Code 2014 (CSA 2014) has the most stringent criteria. The design criteria from BCMOTI (2016), the Canadian Highway Bridge Design Code 2019 (CSA 2019), are more in line with design requirements from Departments of Transportation in the US. Thus, the criteria from the Canadian Highway Bridge Design Code 2019 (CSA 2019) are used in this study.
- This study categorizes precast columns into three types: emulative column, simple rocking column, and hybrid rocking column. Hybrid rocking columns with ED bar ratios up to 1.7% have been tested by researchers and showed less than 1% residual drift when tested to a 6% maximum column drift. The use of a higher amount of ED bar ratios would need to be carefully examined as more ED bars would make the columns behave as emulative columns.
- Satisfactory performance (positive post-elastic stiffness) is observed for the post-tensioned rocking column with total axial load ratios up to 20%. Although Caltrans (2019) requires an axial load ratio within 15% for reinforced concrete columns, a post-tensioned column could have a more relaxed requirement since the post-tensioning force is different from the dead load and it does not cause additional P-Delta bending moment.
- Based on the review of available testing data in the literature, for columns with the ED bar ratio ranging from 0 to 1.4% and the tendon area ratio ranging from 0.15% to 1%, the cracked to uncracked stiffness ratio ranges from 20% to 40%. When a detailed analysis is not performed, engineers should check both the lower and upper bond stiffness.
- To facilitate engineering designs, regression equations are proposed to calculate residual to maximum drift ratio and to predict the equivalent viscous damping ratio. They are key components of the PBD and should help to simply design work.

- In the developed equations of motion for rocking columns, a parameter q is defined to represent the stiffness of the tendon. When q is zero (no tendon condition), the rocking period increases with the increases in initial rotation amplitude. When q is greater than 0 (with tendon condition), the rocking period increases with the increase in initial rotation amplitude, but the rate is smaller. The increase of tendon stiffness has an effect of increasing rocking frequency.
- This study confirms that the kinematic characteristics of ground motions determine the effectiveness of supplemental damping. It is also found that the effectiveness of tendon stiffness and initial PT force also dependent on the kinematic characteristics. Although when in free vibration, tendon stiffness, initial PT force and supplemental damping are beneficial to the seismic performance, it is not always true when the structure is subject to ground motions.
- Existing literature suggests that using supplemental damping may adversely change the rocking response and increase maximum rocking rotation. This study finds that this effect can be eliminated by using supplemental damping and post-tensioning at the same time. When supplemental damping happens to increase the rocking response by changing its period, other measures such as post-tensioning should be used to control the response.
- One rigid large size and one rigid small size columns are studied considering two ground motions. Rocking spectra are plotted for the two structures considering varying tendon stiffness, initial PT force and supplemental damping. The use of supplemental damping may amplify peak rotation occasionally, in most cases, it reduces the peak rotation response.

- In the nonlinear response of the post-tensioned rocking column, interactions exist between PT levels and PT ratios in determining post-elastic stiffness. This is due to the excessive axial load ratio when both the factors were at high levels.
- Charts correlating drift limits with damage states are presented based on the damage definitions in the Canadian Highway Bridge Design Code (CSA 2019). It is noted that aspect ratios have the most significant impact on drift limits for both reinforced concrete and hybrid rocking columns. The influence of reinforcement ratio and axial load ratio is relatively small.
- Regressions equations correlating residual/max drift ratio and PGA and maximum drift ratio are developed. The residual drift of the RC column is more dependent on the max drift compared with the hybrid rocking column.
- Based on time history analysis results, fragility functions of both systems are developed using the maximum likelihood function fitting methods, the fragility functions show that the hybrid column has less probability of being damaged under all intensity measurements and all damage states.
- Through a loss estimate comparison, it shows that when the seismicity is high, e.g. with PGAs of 0.5g and 0.9g at the 475-year event and 2475-year event, the hybrid rocking column design would be more economical option. Or, if the bridge has higher average daily traffic (e.g. more than 40,000) which indicates significant indirect seismic losses if the bridge is damaged, then the hybrid rocking column option can be more preferable even in moderate seismicity regions.

8.4 Recommendations for future research

- Soil-structure interaction is an important aspect of seismic design. Its effect on the response of post-tensioned rocking should be investigated and that would give practicing engineers more confidence in using the new structural system.

- The damage states of bridge columns are well established in design codes and guidelines, however, the damage states of other structural (e.g. bearings, expansion joints) and non-structural components are not well defined in most of the codes. To properly estimate the repair cost and repair time, a large amount of research data has to be made available.

- The current study and previous studies by others suggest that supplemental damping can increase the rocking response and bring negative effects to the seismic response. This phenomenon is worth more study to determine under what type of motions and for what types of rocking parameters the supplemental damping brings negative effects.

- To fully transfer research results to applications, detailed design standards are to be developed for use by design professionals. Although hybrid PT columns may be used if meeting acceptance criteria in ACI-374 (2014) based on physical testing, this would require significant effort from practitioners and hinder the use of this system.

- Studies on the life-cycle cost of the post-tensioned rocking column system are needed to justify its engineering application. Currently, there is very limited data on the initial cost and maintenance cost for the system. More research on cost analysis is needed before the new system can be widely used.

Bibliography

AASHTO (2013). "AASHTO Guide Specifications for LRFD Seismic Bridge Design." American Association of State Highway and Transportation Officials, Washington, DC.

AASHTO (2020). "AASHTO LRFD Bridge Design Specifications." American Association of State Highway and Transportation Officials, Washington, DC.

ABAQUS (2012). *Abaqus computer software documentation*, Hibbitt, Karlsson and Sorensen Inc., Plymouth, MI.

ACI-318 (2014). *Building code requirements for structural concrete (ACI 318-08) and commentary*, American Concrete Institute, Farmington Hills, MI.

ACI-341 (2014). *Analysis and Design of Seismic-Resistant Concrete Bridge Systems*, American Concrete Institute, Farmington Hills, MI.

ACI-374 (2014). *Acceptance criteria for moment frames based on structural testing and commentary*, American Concrete Institute, Farmington Hills, MI.

ACI-550.3 (2013). *Design Specification for Unbonded Post-Tensioned Precast Concrete Special Moment Frames Satisfying ACI 374.1*, American Concrete Institute, Farmington Hills, MI.

Ahn, I.-S., Chen, S. S., and O'Connor, J. S. (2006). "Accelerated Bridge Pier Construction in the US: Seismic Implications." *Structures Congress* St. Louis, Missouri, 1-10.

Akiyama, M., Frangopol, D., Deodatis, G., Ellingwood, B., and Frangopol, D. (2013). "Life-cycle design of bridges under multiple hazards: Earthquake, tsunami, and continuous deterioration." *Safety, Reliability, Risk and Life-Cycle Performance of Structures and Infrastructure*, 3-16.

Alam, M. S., Nehdi, M., and Youssef, M. A. (2009). "Seismic performance of concrete frame structures reinforced with superelastic shape memory alloys." *Smart Struct Syst*, 5(5), 565-585.

Alam, M. S., Youssef, M. A., and Nehdi, M. L. (2010). "Exploratory investigation on mechanical anchors for connecting SMA bars to steel or FRP bars." *Materials and Structures*, 43(1), 91-107.

Ameli, M., Brown, D. N., Parks, J. E., and Pantelides, C. P. (2016). "Seismic column-to-footing connections using grouted splice sleeves." *ACI Structural Journal*, 113(5), 1021.

Ameli, M., Parks, J., Brown, D., and Pantelides, C. (2014). "Grouted splice sleeve connection alternatives for precast reinforced concrete bridge piers in moderate-to-high seismic regions." *10th US National Conference on Earthquake Engineering: Frontiers of Earthquake Engineering*, Earthquake Engineering Research Institute, Anchorage, Alaska.

Andreaus, U., and Casini, P. (1999). "Dynamics of three‐block assemblies with unilateral deformable contacts. Part 2: actual application." *Earthquake engineering & structural dynamics*, 28(12), 1637-1649.

Ardakani, S. S., and Saiidi, M. S. (2018). "Simple method to estimate residual displacement in concrete bridge columns under near-fault earthquake motions." *Engineering Structures*, 176, 208-219.

Aslam, M., Scalise, D. T., and Godden, W. G. (1980). "Earthquake rocking response of rigid bodies." *Journal of the Structural Division*, 106(2), 377-392.

ATC-58 (2019). "*Seismic Performance Assessment of Buildings*." Applied Technology Council Redwood City, California.

ATC (1985). "Earthquake damage evaluation data for California." Applied Technology Council Redwood City, California.

Atkinson, G. M., and Boore, D. M. (2006). "Earthquake ground-motion prediction equations for eastern North America." *Bulletin of the Seismological Society of America*, 96(6), 2181-2205.

Baker, J. W. (2007). "Quantitative classification of near-fault ground motions using wavelet analysis." *Bulletin of the Seismological Society of America*, 97(5), 1486-1501.

Baker, J. W. (2008). "An introduction to probabilistic seismic hazard analysis." *Report for the US Nuclear Regulatory Commission*, 1.

Baker, J. W. (2015). "Efficient analytical fragility function fitting using dynamic structural analysis." *Earthquake Spectra*, 31(1), 579-599.

Barthes, C. B. (2012). *Design of earthquake resistant bridges using rocking columns*, University of California, Berkeley.

BCMOTI (2016). "British Columbia Supplement to CHBDC S6-14." British Columbia Ministry of Transportation and Infrastructure.

BCMOTI (2013). "CONSTRUCTION AND REHABILITATION COST GUIDE." Ministry of Transportation and Infrastructure, BC, Canada.

Bendimerad, F. (2001). "Loss estimation: a powerful tool for risk assessment and mitigation." *Soil Dynamics and Earthquake Engineering*, 21(5), 467-472.

Berry, M., and Eberhard, M. (2003). "Performance models for flexural damage in reinforced concrete columns." *Report PEER 2003/18, Pacific Earthquake Engineering Center, University of California Berkeley*.

Billah, A., and Alam, M. (2015). "Seismic fragility assessment of highway bridges: a state-of-the-art review." *Structure and Infrastructure Engineering*, 11(6), 804-832.

Billah, A. M., and Alam, M. S. (2012). "Seismic performance of concrete columns reinforced with hybrid shape memory alloy (SMA) and fiber reinforced polymer (FRP) bars." *Construction and Building Materials*, 28(1), 730-742.

Billah, A. M., and Alam, M. S. (2014). "Performance-based prioritisation for seismic retrofitting of reinforced concrete bridge bent." *Structure and Infrastructure Engineering*, 10(8), 929-949.

Billah, A. M., and Alam, M. S. (2016). "Performance-based seismic design of shape memory alloy–reinforced concrete bridge piers. I: Development of performance-based damage states." *Journal of Structural Engineering*, 142(12), 04016140.

Billah, A. M., and Alam, M. S. (2016). "Performance-based seismic design of shape memory alloy–reinforced concrete bridge piers. I: Development of performance-based damage states." *Journal of Structural Engineering*, 04016140.

Billah, A. M., and Alam, M. S. (2016). "Performance-Based Seismic Design of Shape Memory Alloy–Reinforced Concrete Bridge Piers. II: Methodology and Design Example." *Journal of Structural Engineering*, 04016141.

Billah, A. M., Alam, M. S., and Bhuiyan, M. R. (2012). "Fragility analysis of retrofitted multicolumn bridge bent subjected to near-fault and far-field ground motion." *Journal of Bridge Engineering*, 18(10), 992-1004.

Billah, A. M., and Shahria Alam, M. (2014). "Seismic fragility assessment of concrete bridge pier reinforced with superelastic shape memory alloy." *Earthquake Spectra*.

Billington, S. L., and Yoon, J. (2004). "Cyclic response of unbonded posttensioned precast columns with ductile fiber-reinforced concrete." *Journal of Bridge Engineering*, 9(4), 353-363.

Bormann, P., Baumbach, M., Bock, G., Grosser, H., Choy, G. L., and Boatwright, J. (2002). "Seismic sources and source parameters." *IASPEI new manual of seismological observatory practice*.

Boulanger, R. W., Curras, C. J., Kutter, B. L., Wilson, D. W., and Abghari, A. (1999). "Seismic soil-pile-structure interaction experiments and analyses." *Journal of Geotechnical and Geoenvironmental Engineering*, 125(9), 750-759.

Bu, Z.-Y., Ou, Y.-C., Song, J.-W., and Lee, G. C. (2016). "Hysteretic modeling of unbonded posttensioned precast segmental bridge columns with circular section based on cyclic loading test." *Journal of Bridge Engineering*, 21(6), 04016016.

Bu, Z.-Y., Ou, Y.-C., Song, J.-W., Zhang, N.-S., and Lee, G. C. (2015). "Cyclic loading test of unbonded and bonded posttensioned precast segmental bridge columns with circular section." *Journal of Bridge Engineering*, 21(2), 04015043.

Bu, Z., Guo, J., Zheng, R., Song, J., and Lee, G. C. (2016). "Cyclic performance and simplified pushover analyses of precast segmental concrete bridge columns with circular section." *Earthquake Engineering and Engineering Vibration*, 15(2), 297-312.

Burak, R., and Seraderian, R. (2010). "Accelerated Bridge Construction – On the Fast Track to Success." *2010 Annual Conference of the Transportation Association of Canada*Halifax, Nova Scotia.

Cai, Z.-K., Wang, Z., and Yang, T. Y. (2019). "Cyclic Load Tests on Precast Segmental Bridge Columns with Both Steel and Basalt FRP Reinforcement." *Journal of Composites for Construction*, 23(3), 04019014.

Caltrans (2013). "Caltrans Seismic Design Criteria." California Department of Transportation, CA.

Caltrans (2019). "Caltrans Seismic Design Criteria." California Department of Transportation, CA.

Calvi, G., Priestley, M., and Kowalsky, M. "Displacement-based seismic design of structures." *Proc., 3rd National Conference on Earthquake Engineering and Engineering Seismology*.

Chang, S. E., and Shinozuka, M. (1996). "Life-cycle cost analysis with natural hazard risk." *journal of infrastructure systems*, 2(3), 118-126.

Cheng, C.-T. (2008). "Shaking table tests of a self-centering designed bridge substructure." *Engineering Structures*, 30(12), 3426-3433.

Cheng, H., Li, H., Wang, D., Sun, Z., Li, G., and Jin, J. (2016). "Research on the influencing factors for residual displacements of RC bridge columns subjected to earthquake loading." *Bulletin of Earthquake Engineering*, 14(8), 2229-2257.

China-MOC (2008). "Chinese Guidelines for Seismic Design of Highway Bridges ".

Choi, E., DesRoches, R., and Nielson, B. (2004). "Seismic fragility of typical bridges in moderate seismic zones." *Engineering Structures*, 26(2), 187-199.

Choi, H., Saiidi, M. S., Somerville, P., and El-Azazy, S. (2010). "Experimental Study of Reinforced Concrete Bridge Columns Subjected to Near-Fault Ground Motions." *ACI Structural Journal*, 107(1).

Chou, C.-C., Chang, H.-J., and Hewes, J. T. (2013). "Two-plastic-hinge and two dimensional finite element models for post-tensioned precast concrete segmental bridge columns." *Engineering Structures*, 46, 205-217.

Chou, C. C., and Chen, Y. C. (2006). "Cyclic tests of post‐tensioned precast CFT segmental bridge columns with unbonded strands." *Earthquake engineering & structural dynamics*, 35(2), 159-175.

Chou, C. C., and Hsu, C. P. (2008). "Hysteretic model development and seismic response of unbonded post‐tensioned precast CFT segmental bridge columns." *Earthquake Engineering & Structural Dynamics*, 37(6), 919-934.

Christopoulos, C., Pampanin, S., and Nigel Priestley, M. (2003). "Performance-based seismic response of frame structures including residual deformations part i: Single-degree of freedom systems." *Journal of Earthquake Engineering*, 7(01), 97-118.

Cohagen, L. S., Pang, J. B., Stanton, J. F., and Eberhard, M. O. (2008). *A precast concrete bridge bent designed to re-center after an earthquake*, TransNow, Seattle, Washington.

CSA (2014). *Canadian Highway Bridge Design Code*, Canadian Standards Association, Ontario, Canada.

CSA (2019). *Canadian Highway Bridge Design Code*, Canadian Standards Association, Ontario, Canada.

Culmo, M. P. (2009). "Connection details for prefabricated bridge elements and systems."

Culmo, M. P. (2011). "Accelerated Bridge Construction - Experience in Design, Fabrication and Erection of Prefabricated Bridge Elements and Systems ", The Federal Highway Administration.

Dash, S. R., Bhattacharya, S., Blakeborough, A., and Hyodo, M. (2008). "PY curve to model lateral response of pile foundations in liquefied soils." *The 14th World Conference on Earthquake Engineering* Beijing, China, 04-01.

Davis, P. M., Janes, T. M., Haraldsson, O. S., Eberhard, M. O., and Stanton, J. F. (2017). "Unbonded pretensioned columns for accelerated bridge construction in seismic regions." *Journal of Bridge Engineering*, 22(5), 04017003.

Dawood, H., ElGawady, M., and Hewes, J. (2011). "Behavior of segmental precast posttensioned bridge piers under lateral loads." *Journal of Bridge Engineering*, 17(5), 735-746.

Dawood, H., Elgawady, M., and Hewes, J. (2014). "Factors affecting the seismic behavior of segmental precast bridge columns." *Frontiers of Structural and Civil Engineering*, 8(4), 388-398.

Dawood, H. M., and ElGawady, M. (2013). "Performance-based seismic design of unbonded precast post-tensioned concrete filled GFRP tube piers." *Composites Part B: Engineering*, 44(1), 357-367.

de Normalisation, C. E. (1998). "Eurocode 8–Design of Structures for earthquake resistance." *European Standard NF EN*, 1.

DeJong, M. J., and Dimitrakopoulos, E. G. (2014). "Dynamically equivalent rocking structures." *Earthquake engineering & structural dynamics*, 43(10), 1543-1563.

Dong, Y., and Frangopol, D. M. (2015). "Risk and resilience assessment of bridges under mainshock and aftershocks incorporating uncertainties." *Engineering Structures*, 83, 198-208.

Doolen, T., Saeedi, A., and Emami, S. (2011). "Accelerated bridge construction (ABC) decision making and economic modeling tool."

Dowdell, D. J., and Hamersley, B. A. "Lions' Gate Bridge North Approach: Seismic retrofit." *Proc., Behaviour of Steel Structures in Seismic Areas: Proc., 3rd Int. Conf.: STESSA 2000*, Balkema, 319-326.

Ebrahimpour, A., Earles, B. E., Maskey, S., Tangarife, M., and Sorensen, A. D. (2016). "Seismic performance of columns with grouted couplers in Idaho accelerated bridge construction applications." Idaho. Transportation Dept.

EGBC (2018). "The Professional Practice Guidelines – Performance Based Seismic Design of Bridges in British Columbia." ENGINEERS AND GEOSCIENTISTS BC, Vancouver.

ElGawady, M., Booker, A. J., and Dawood, H. M. (2010). "Seismic behavior of posttensioned concrete-filled fiber tubes." *Journal of Composites for Construction*, 14(5), 616-628.

ElGawady, M. A., and Dawood, H. M. (2012). "Analysis of segmental piers consisted of concrete filled FRP tubes." *Engineering Structures*, 38, 142-152.

ElGawady, M. A., and Sha'lan, A. (2010). "Seismic behavior of self-centering precast segmental bridge bents." *Journal of Bridge Engineering*, 16(3), 328-339.

Elwood, K. J., and Moehle, J. P. (2005). "Axial capacity model for shear-damaged columns." *ACI Structural Journal*, 102(4), 578.

Eom, T.-S., Park, H.-G., Hwang, H.-J., and Kang, S.-M. (2015). "Plastic Hinge Relocation Methods for Emulative PC Beam–Column Connections." *Journal of Structural Engineering*, 142(2), 04015111.

Erochko, J., Christopoulos, C., Tremblay, R., and Choi, H. (2011). "Residual drift response of SMRFs and BRB frames in steel buildings designed according to ASCE 7-05." *Journal of Structural Engineering*, 137(5), 589-599.

FEMA (2000). "Commentary for the Seismic Rehabilitation of Buildings." *FEMA-356, Federal Emergency Management Agency, Washington, DC*.

FEMA (2012). *Seismic Performance Assessment of Buildings*, FEMA P-58-1, Washington, D.C., U.S.

Feng, Y., Kowalsky, M. J., and Nau, J. M. (2014). "Effect of seismic load history on deformation limit states for longitudinal bar buckling in RC circular columns." *Journal of Structural Engineering*, 141(8), 04014187.

FHWA-NHI (2014). *LRFD Seismic Analysis and Design of Bridges Reference Manual*, U.S. Department of Transportation Federal Highway Administration, Publication No. FHWA-NHI-15-004.

FHWA (2017). "Accelerated Bridge Construction." <https://www.fhwa.dot.gov/bridge/abc/>. (Accessed January 5, 2019).

fib (2010). "The International Federation for Structural Concrete." *Struct. Concr.*, 2, 312.

Finn, W., and Fujita, N. (2002). "Piles in liquefiable soils: seismic analysis and design issues." *Soil Dynamics and Earthquake Engineering*, 22(9), 731-742.

Finn, W., Pandey, B. H., and Ventura, C. E. (2011). "Modeling soil–foundation–structure interaction." *The Structural Design of Tall and Special Buildings*, 20(S1), 47-62.

FIU (2018). "ABC-UTC Project & Research Databases." <https://abc-utc.fiu.edu/technology-transfer/project-research-databases/>. (Accessed May 5, 2018).

Floren, A., and Mohammadi, J. (2001). "Performance-based design approach in seismic analysis of bridges." *Journal of Bridge Engineering*, 6(1), 37-45.

Fowler, J. R., and Eng, P. "Accelerated Bridge Construction." *Proc., Annual Conference & Exhibition of the Transportation Association of Canada, 2006. Congres et exposition annuels de l'Association des transport du Canada, 2006. Transportation Association of Canada*.

Freyermuth, C. L. (1969). "Design of continuous highway bridges with precast, prestressed concrete girders." PCI Journal 14(2), 14–39.

GangaRao, H. V., and Moulton, L. K. (1981). "Tolerable movement criteria for highway bridges." *Public Roads*, 44(4).

Gardoni, P., Der Kiureghian, A., and Mosalam, K. M. (2002). "Probabilistic capacity models and fragility estimates for reinforced concrete columns based on experimental observations." *Journal of Engineering Mechanics*.

Ghobarah, A. (2001). "Performance-based design in earthquake engineering: state of development." *Engineering structures*, 23(8), 878-884.

Ghobarah, A. "On drift limits associated with different damage levels." *Proc., International workshop on performance-based seismic design*, Dept. of Civil Engineering, McMaster University.

Gibson, E. (1982). "Working with the performance approach in building." *Rotterdam: CIB Report Publication*.

Gidaris, I., Padgett, J. E., Barbosa, A. R., Chen, S., Cox, D., Webb, B., and Cerato, A. (2016). "Multiple-hazard fragility and restoration models of highway bridges for regional risk and resilience assessment in the United States: state-of-the-art review." *Journal of structural engineering*, 04016188.

Giouvanidis, A. I., and Dong, Y. (2020). "Seismic loss and resilience assessment of single-column rocking bridges." Bulletin of earthquake engineering, 18, 4481-4513.

Gutenberg, B., and Richter, C. F. (1944). "Frequency of earthquakes in California." *Bulletin of the Seismological Society of America*, 34(4), 185-188.

Haber, Z. B., Saiidi, M. S., and Sanders, D. H. (2014). "Seismic performance of precast columns with mechanically spliced column-footing connections." *ACI Structural Journal*, 111(3), 639-650.

Hamburger, R., Rojahn, C., Heintz, J., and Mahoney, M. "FEMA P58: Next-generation building seismic performance assessment methodology." *Proc., 15th world conference on earthquake engineering*.

Hamburger, R., Rojahn, C., Moehle, J., Bachman, R., Comartin, C., and Whittaker, A. "The ATC-58 project: development of next-generation performance-based earthquake engineering design criteria for buildings." *Proc., The 13th World Conference on Earthquake Engineering*, 1-15.

Han, L. H. (2000). "Concrete filled steel tubular structures." *Beijing: Science Press*, 17(21), 101-136.

Han, Q., Du, X., Liu, J., Li, Z., Li, L., and Zhao, J. (2009). "Seismic damage of highway bridges during the 2008 Wenchuan earthquake." *Earthquake Engineering and Engineering Vibration*, 8(2), 263-273.

Haraldsson, O. S., Janes, T. M., Eberhard, M. O., and Stanton, J. F. (2013). "Precast bent system for high seismic regions: Laboratory tests of column-to-footing socket connections."

Haraldsson, O. S., Janes, T. M., Eberhard, M. O., and Stanton, J. F. (2013). "Seismic resistance of socket connection between footing and precast column." *Journal of Bridge Engineering*, 18(9), 910-919.

HAZUS (2010). " Multi-hazard loss estimation methodology—earthquake model (technical manual)." Federal Emergency Management Agency, Washington.

Hazus, E. L. E. M. (1997). "Technical manual." *National Institute of Building for the Federal Emergency Management Agency, Washington (DC)*.

Hedayati Dezfuli, F., and Alam, M. S. (2016). "Effect of different steel‐reinforced elastomeric isolators on the seismic fragility of a highway bridge." *Structural Control and Health Monitoring*.

Hewes, J. T., and Priestley, M. N. (2002). "Seismic design and performance of precast concrete segmental bridge columns." *Report No. SSRP 2001/25*University of California San Diego, La Jolla, CA.

Hieber, D. G., Wacker, J. M., Eberhard, M. O., and Stanton, J. F. (2005). "Precast concrete pier systems for rapid construction of bridges in seismic regions." Washington State Department of Transportation.

Hogan, S. (1990). "The many steady state responses of a rigid block under harmonic forcing." *Earthquake Engineering & Structural Dynamics*, 19(7), 1057-1071.

Holden, T., Restrepo, J., and Mander, J. B. (2003). "Seismic performance of precast reinforced and prestressed concrete walls." *Journal of Structural Engineering*, 129(3), 286-296.

Housner, G. W. (1963). "The behavior of inverted pendulum structures during earthquakes." *Bulletin of the seismological society of America*, 53(2), 403-417.

Hung, H.-H., Sung, Y.-C., Lin, K.-C., Jiang, C.-R., and Chang, K.-C. (2017). "Experimental study and numerical simulation of precast segmental bridge columns with semi-rigid connections." *Engineering Structures*, 136, 12-25.

Hwang, H., Liu, J. B., and Chiu, Y.-H. (2001). "Seismic fragility analysis of highway bridges." *Mid-America Earthquake Center CD Release 01-06*.

Ichikawa, S., Matsuzaki, H., Moustafa, A., ElGawady, M. A., and Kawashima, K. (2016). "Seismic-resistant bridge columns with ultrahigh-performance concrete segments." *Journal of Bridge Engineering*, 21(9), 04016049.

Iowa-DOT (2009). *ABC - achieving the need for speed*, Iowa Department of Transportation, Ames, IA, USA.

Ishiyama, Y. (1982). "Motions of rigid bodies and criteria for overturning by earthquake excitations." *Earthquake Engineering & Structural Dynamics*, 10(5), 635-650.

Issa, M. A., Idriss, A. T., Kaspar, I. I., and Khayyat, S. Y. (1995). "Full depth precast and precast, prestressed concrete bridge deck panels." *PCI journal*, 40(1), 59-80.

Itani, R. (2003). "Effects of retrofitting applications on reinforced concrete bridges." Washington State Department of Transportation. Pullman, Washington.

ITG-5.1 (2008). "Acceptance Criteria for Special Unbonded Post-Tensioned Precast Structural Walls Based on Validation Testing." American Concrete Institute: Farmington Hills, MI.

ITG-5.2 (2009). "Requirements for Design of a Special Unbonded Post-Tensioned Precast Shear Wall Satisfying ACI ITG-5.1 and Commentary." American Concrete Institute: Farmington Hills, MI.

Jacqueline, G. (1999). "The future for precast concrete in low-rise housing." *Precast Housing Feasibility Study Group, UK*.

Jeong, H. I. (2007). *Evaluation of self-centering reinforced concerete columns by shaking table tests and numerical simulations*, University of California, Berkeley.

Jeong, H. I., Sakai, J. i., Mahin, S. A., and Center, P. E. E. R. (2008). *Shaking table tests and numerical investigation of self-centering reinforced concrete bridge columns*, Pacific Earthquake Engineering Research Center.

JRC-Ispra (2012). "Seminar 'Bridge Design with Eurocodes'." *European Commission*. (2015).

Kameshwar, S., and Padgett, J. "Towards Risk-Based, Multi-Hazard-Resistant Design of Bridges." *Proc., Structures Congress 2014*, ASCE, 2318-2329.

Kapur, J., and Khaleghi, B. (2009). "Use of Precast Bridge Members in Areas of High or Moderate Seismicity." *Transportation Research Record: Journal of the Transportation Research Board*(2131), 101-109.

Kapur, J., Yen, W. P., Dekelbab, W., Bardow, A., Keever, M., Sletten, J., Tobias, D., and Saiidi, M. S. (2012). "Best practices regarding performance of ABC connections in bridges subjected to multihazard and extreme events."

Kausel, E. (2010). "Early history of soil–structure interaction." *Soil Dynamics and Earthquake Engineering*, 30(9), 822-832.

Kawashima, K. (2000). "Seismic design and retrofit of bridges." *Bulletin of the New Zealand Society for Earthquake Engineering*, 33(3), 265-285.

Kawashima, K., MacRae, G. A., Hoshikuma, J.-i., and Nagaya, K. (1998). "Residual displacement response spectrum." *Journal of Structural Engineering*, 124(5), 523-530.

Kawashima, K., Takahashi, Y., Ge, H., Wu, Z., and Zhang, J. (2009). "Reconnaissance report on damage of bridges in 2008 Wenchuan, China, earthquake." *Journal of Earthquake Engineering*, 13(7), 965-996.

Kawashima, K., Unjoh, S., Hoshikuma, J.-I., and Kosa, K. (2011). "Damage of bridges due to the 2010 Maule, Chile, earthquake." *Journal of Earthquake Engineering*, 15(7), 1036-1068.

Khaleghi, B. (2005). "Use of precast concrete members for accelerated bridge construction in Washington State." *Transportation Research Record: Journal of the Transportation Research Board*, 11(1), 187-196.

Khan, M. A. (2014). *Accelerated Bridge Construction: Best Practices and Techniques*, Elsevier.

Kim, S.-H., and Feng, M. Q. (2003). "Fragility analysis of bridges under ground motion with spatial variation." *International Journal of Non-Linear Mechanics*, 38(5), 705-721.

Kirchsteiger, C. (1999). "On the use of probabilistic and deterministic methods in risk analysis." *Journal of Loss Prevention in the Process Industries*, 12(5), 399-419.

Kowalsky, M. J. (2000). "Deformation limit states for circular reinforced concrete bridge columns." *Journal of Structural Engineering*, 126(8), 869-878.

Kurama, Y., Sause, R., Pessiki, S., and Lu, L.-W. (1999). "Lateral load behavior and seismic design of unbonded post-tensioned precast concrete walls." *ACI Structural Journal*, 96(4).

Kurama, Y. C., and Shen, Q. (2004). "Posttensioned hybrid coupled walls under lateral loads." *Journal of structural Engineering*, 130(2), 297-309.

Kurama, Y. C., Sritharan, S., Fleischman, R. B., Restrepo, J. I., Henry, R. S., Cleland, N. M., Ghosh, S., and Bonelli, P. (2018). "Seismic-Resistant Precast Concrete Structures: State of the Art."

Kuwabara, T., Tamakoshi, T., Murakoshi, J., Kimura, Y., Nanazawa, T., and Hoshikuma, J.-i. (2013). "Outline of Japanese Design Specifications for Highway Bridges in 2012." *The 44thMeeting, Joint Panel on Wind and Seismic Effects (UJNR), UJNR Gaithersburg*.

Kwan, W.-P., and Billington, S. L. (2003). "Unbonded posttensioned concrete bridge piers. I: Monotonic and cyclic analyses." *Journal of Bridge Engineering*, 8(2), 92-101.

Kwan, W.-P., and Billington, S. L. (2003). "Unbonded posttensioned concrete bridge piers. II: Seismic analyses." *Journal of Bridge Engineering*, 8(2), 102-111.

Larkin, A. S., Sanders, D. H., and Saiidi, M. S. (2012). "Unbonded Prestressed Columns for Earthquake Resistance." *Structures Congress 2012*, 539-548.

Larkin, A. S., Sanders, D. H., and Saiidi, M. S. "Unbonded prestressed columns for earthquake resistance." *Proc., Structures Congress*, 539-548.

Lee, W. K. (2007). "Simulation and performance-based earthquake engineering assessment of self-centering post-tensioned concrete bridge systems." Stanford University.

Lee, W. K., and Billington, S. L. (2010). "Modeling residual displacements of concrete bridge columns under earthquake loads using fiber elements." *Journal of Bridge Engineering*, 15(3), 240-249.

Lee, W. K., and Billington, S. L. (2011). "Performance‐based earthquake engineering assessment of a self‐centering, post‐tensioned concrete bridge system." *Earthquake engineering & structural dynamics*, 40(8), 887-902.

Lehman, D., Moehle, J., Mahin, S., Calderone, A., and Henry, L. (2004). "Experimental evaluation of the seismic performance of reinforced concrete bridge columns." *Journal of Structural Engineering*, 130(6), 869-879.

Li, C., Hao, H., and Bi, K. (2017). "Numerical study on the seismic performance of precast segmental concrete columns under cyclic loading." *Engineering Structures*, 148, 373-386.

Li, S., Dezfuli, F. H., Wang, J.-q., and Alam, M. S. (2020). "Seismic vulnerability and loss assessment of an isolated simply-supported highway bridge retrofitted with optimized superelastic shape memory alloy cable restrainers." *Bulletin of Earthquake Engineering*, 1-32.

Long, M., and Narciso, J. (1999). "Probabilistic Design Methodology for Composite Aircraft Structures." DTIC Document.

Lu, J., Mackie, K. R., and Elgamal, A. (2011). "BridgePBEE: OpenSees 3D pushover and earthquake analysis of single-column 2-span bridges, User Manual, Beta 1.0."

Lu, X., Han, B., Hori, M., Xiong, C., and Xu, Z. (2014). "A coarse-grained parallel approach for seismic damage simulations of urban areas based on refined models and GPU/CPU cooperative computing." *Advances in Engineering Software*, 70, 90-103.

Mackie, K.-R., and Stojadinović, B. (2005). "Fragility basis for California highway overpass bridge seismic decision making."

Mackie, K., and Stojadinovic, B. "Residual displacement and post-earthquake capacity of highway bridges." *Proc., Proceedings of the Thirteenth World Conference on Earthquake Engineering*.

Mackie, K., and Stojadinović, B. (2003). *Seismic demands for performance-based design of bridges*, Pacific Earthquake Engineering Research Center Berkeley.

Mackie, K., and Stojadinović, B. (2005). *Fragility basis for California highway overpass bridge seismic decision making*, Pacific Earthquake Engineering Research Center, College of Engineering, University of California, Berkeley.

Mackie, K., and Stojadinović, B. (2007). "Performance‐based seismic bridge design for damage and loss limit states." *Earthquake engineering & structural dynamics*, 36(13), 1953-1971.

Mackie, K. R., and Stojadinovic, B. "Residual displacement and post-earthquake capacity of highway bridges." *Proc., Proceedings of the Thirteenth World Conference on Earthquake Engineering*.

Mackie, K. R., and Stojadinović, B. (2005). *Fragility basis for California highway overpass bridge seismic decision making*, Pacific Earthquake Engineering Research Center, College of Engineering, University of California, Berkeley.

Mackie, K. R., Wong, J.-M., and Stojadinovic', B. (2008). *Integrated probabilistic performance-based evaluation of benchmark reinforced concrete bridges*, Pacific Earthquake Engineering Research Center.

Mackie, K. R., Wong, J. M., and Stojadinović, B. (2008). "Integrated probabilistic performance-based evaluation of benchmark reinforced concrete bridges." Pacific Earthquake Engineering Research Center.

Madhusudhanan, S., and Sideris, P. (2018). "Capacity Spectrum Seismic Design Methodology for Bridges with Hybrid Sliding-Rocking Columns." *Journal of Bridge Engineering*, 23(8), 04018052.

Maeda, M., Nakano, Y., and Lee, K. S. "Post-earthquake damage evaluation for R/C buildings based on residual seismic capacity." *Proc., 13th World Conference on Earthquake Engineering, Vancouver*.

Maheshwari, B., and Sarkar, R. (2011). "Seismic behavior of soil-pile-structure interaction in liquefiable soils: Parametric study." *International Journal of Geomechanics*, 11(4), 335-347.

Makris, N., and Aghagholizadeh, M. (2019). "Effect of supplemental hysteretic and viscous damping on rocking response of free-standing columns." *Journal of Engineering Mechanics*, 145(5), 04019028.

Makris, N., and Konstantinidis, D. (2003). "The rocking spectrum and the limitations of practical design methodologies." *Earthquake engineering & structural dynamics*, 32(2), 265-289.

Makris, N., and Vassiliou, M. F. (2013). "Planar rocking response and stability analysis of an array of free‐standing columns capped with a freely supported rigid beam." *Earthquake Engineering & Structural Dynamics*, 42(3), 431-449.

Makris, N., and Vassiliou, M. F. (2015). "The dynamics of the rocking frame." *Seismic Assessment, Behavior and Retrofit of Heritage Buildings and Monuments*, Springer, 37-59.

Mander, J. B., and Cheng, C.-T. (1997). "Seismic resistance of bridge piers based on damage avoidance design." In Seismic resistance of bridge piers based on damage avoidance design(pp. 109-109), New York

Mander, J. B., Priestley, M. J., and Park, R. (1988). "Theoretical stress-strain model for confined concrete." *Journal of structural engineering*, 114(8), 1804-1826.

Marriott, D., Pampanin, S., Bull, D., and Palermo, A. (2008). "Dynamic testing of precast, post-tensioned rocking wall systems with alternative dissipating solutions." Bulletin of the New Zealand Society for Earthquake Engineering 41(2):90–103.

Marriott, D., Pampanin, S., and Palermo, A. (2009). "Quasi‐static and pseudo‐dynamic testing of unbonded post‐tensioned rocking bridge piers with external replaceable dissipaters." *Earthquake engineering & structural dynamics*, 38(3), 331-354.

Marriott, D., Pampanin, S., and Palermo, A. (2011). "Biaxial testing of unbonded post‐tensioned rocking bridge piers with external replacable dissipaters." *Earthquake Engineering & Structural Dynamics*, 40(15), 1723-1741.

Marsh, M. L. (2011). *Application of accelerated bridge construction connections in moderate-to-high seismic regions*, Transportation Research Board.

Marsh, M. L. (2013). *Performance-based Seismic Bridge Design*, Transportation Research Board.

Marsh, M. L., and Stringer, S. J. (2013). *Performance-based Seismic Bridge Design*, Transportation Research Board.

Mashal, M., Aguilar, I., Ebrahimpour, A., and Ruminski, L. "Accelerated Bridge Construction (ABC) in Idaho: The State-of-the-Art Bridge Technologies, Current Practice and Future Research." *Proc., IABSE Symposium Report*, International Association for Bridge and Structural Engineering, 2642-2650.

Mashal, M., and Palermo, A. "High-damage and low-damage seismic design technologies for accelerated bridge construction." *Proc., Structures Congress 2015*, 549-560.

Mashal, M., White, S., and Palermo, A. "Quasi-static cyclic tests of Emulative Precast Segmental Bridge Piers (E-PSBP)." *Proc., 2013 NZSEE Conference, Wellington, New Zealand*.

Massachusetts-DOT (2013). *LRFD Bridge Manual, Part III – Prefabricated Elements*, Massachusetts Department of Transportation, Boston, MA, USA.

McCormack, T. C., and Rad, F. N. (1997). "An earthquake loss estimation methodology for buildings based on ATC-13 and ATC-21." *Earthquake Spectra*, 13(4), 605-621.

McCormick, J., Aburano, H., Ikenaga, M., and Nakashima, M. "Permissible residual deformation levels for building structures considering both safety and human elements." *Proc., Proceedings of the 14th world conference on earthquake engineering*, Seismological Press Beijing, 12-17.

McGuire, R. K. (2001). "Deterministic vs. probabilistic earthquake hazards and risks." *Soil Dynamics and Earthquake Engineering*, 21(5), 377-384.

Mehrsoroush, A., and Saiidi, M. S. "Seismic Performance of Two-Column Bridge Piers with Innovative Precast Members and Pipe Pin Connections." *Proc., Bridge Maintenance, Safety, Management and Life Extension [Proceedings of 7th International Conference on Bridge Maintenance, Safety, and Management (IABMAS)]*, 1472-1479.

Mehrsoroush, A., and Saiidi, M. S. (2016). "Cyclic response of precast bridge piers with novel column-base pipe pins and pocket cap beam connections." *Journal of Bridge Engineering*, 21(4), 04015080.

Mekki, M., Elachachi, S., Breysse, D., Nedjar, D., and Zoutat, M. (2014). "Soil-structure interaction effects on RC structures within a performance-based earthquake engineering framework." *European Journal of Environmental and Civil Engineering*, 18(8), 945-962.

Metelli, G., Beschi, C., and Riva, P. (2011). "Cyclic behaviour of a column to foundation joint for concrete precast structures." *European Journal of Environmental and Civil Engineering*, 15(9), 1297-1318.

Michigan-DOT (2013). *Bridge Design Manual for the Michigan Department of Transportation.*, Michigan Department of Transportation, Michigan, USA.

Mitchell, D., Bruneau, M., Saatcioglu, M., Williams, M., Anderson, D., and Sexsmith, R. (1995). "Performance of bridges in the 1994 Northridge earthquake." *Canadian Journal of Civil Engineering*, 22(2), 415-427.

Moehle, J., and Deierlein, G. G. "A framework methodology for performance-based earthquake engineering." 13th World Conference on Earthquake Engineering.

Mohebbi, A., Saiidi, M. S., and Itani, A. M. (2018). "Shake Table Studies and Analysis of a PT-UHPC Bridge Column with Pocket Connection." *Journal of Structural Engineering*, 144(4), 04018021.

Montgomery, D. C. (2008). *Design and analysis of experiments*, John Wiley & Sons.

Moon, D. Y., Roh, H., and Cimellaro, G. P. (2015). "Seismic performance of segmental rocking columns connected with NiTi martensitic SMA bars." *Advances in Structural Engineering*, 18(4), 571-584.

Moore, J., Kiremidjian, A., and Chiu, S. "Seismic risk model for a designated highway system: Oakland/San Francisco Bay area." *Proc., PEER Rep. No. 2002/02, US–Japan Workshop on the Effects of Near-Field Earthquake Shaking*, 71-75.

Motaref, S., Saiidi, M. S., and Sanders, D. (2013). "Shake table studies of energy-dissipating segmental bridge columns." *Journal of Bridge Engineering*, 19(2), 186-199.

Motaref, S., Saiidi, M. S., and Sanders, D. H. (2011). "Seismic response of precast bridge columns with energy dissipating joints." University of Nevada, Reno, Univ. of Nevada, Reno, NV.

Moustafa, A., and ElGawady, M. A. (2018). "Shaking Table Testing of Segmental Hollow-Core FRP-Concrete-Steel Bridge Columns." *Journal of Bridge Engineering*, 23(5), 04018020.

Murphy, T. P., Marsh, L., Bennion, S., Buckle, I. G., Luco, N., Anderson, D., Kowalsky, M., and Restrepo, J. (2020). "Proposed AASHTO Guidelines for Performance-Based Seismic Bridge Design."

Mylonakis, G., and Gazetas, G. (2000). "Seismic soil-structure interaction: beneficial or detrimental?" *Journal of Earthquake Engineering*, 4(03), 277-301.

Nagae, T., Tahara, K., Fukuyama, K., Matsumori, T., Shiohara, H., Kabeyasawa, T., Kono, S., Nishiyama, M., Moehle, J., and Wallace, J. "Test results of four-story reinforced concrete and post-tensioned concrete buildings: The 2010 E-Defense shaking table test." *Proc., Proceedings of the 15th World Conference on Earthquake Engineering*.

NCHRP (2002). *Comprehensive specification for the seismic design of bridges*, National Academy Press.

Negro, P., Bournas, D. A., and Molina, F. J. (2013). "Pseudodynamic tests on a full-scale 3-storey precast concrete building: global response." *Engineering structures*, 57, 594-608.

NEHRP (2012). "Soil-structure interaction for building structures." *NIST GCR*.

Nguyen, W., Trono, W., Panagiotou, M., and Ostertag, C. P. (2017). "Seismic response of a rocking bridge column using a precast hybrid fiber-reinforced concrete (HyFRC) tube." *Composite Structures*, 174, 252-262.

Nikbakht, E., Rashid, K., Hejazi, F., and Osman, S. A. (2015). "Application of shape memory alloy bars in self-centring precast segmental columns as seismic resistance." *Structure and Infrastructure Engineering*, 11(3), 297-309.

Nikoukalam, M., and Sideris, P. (2017). "Resilient Bridge Rocking Columns with Polyurethane Damage-Resistant End Segments and Replaceable Energy-Dissipating Links." *Journal of Bridge Engineering*, 22(10), 04017064.

NRC "Fifth Generation Seismic Hazard Model for Canada." Geological Survey of Canada, Open File, 7893(2015), 26.

NYSDOT (2015). New York State Department of Transportation LRFD, New York, United States.

NZS (2006). "New Zealand Concrete Structures Standard." New Zealand.

NZT (2018). "*New Zealand Bridge Manual*." Transit New Zealand.

ODOT (2016). *Bridge Design and Drafting Manual*, Oregon Department of Transportation, Salem, Oregon.

Ou, Y.-C. (2007). "Precast segmental post-tensioned concrete bridge columns for seismic regions." State University of New York at Buffalo.

Ou, Y.-C., Chiewanichakorn, M., Aref, A. J., and Lee, G. C. (2007). "Seismic performance of segmental precast unbonded posttensioned concrete bridge columns." *Journal of structural engineering*, 133(11), 1636-1647.

Ou, Y.-C., Oktavianus, Y., and Tsai, M.-S. (2013). "An emulative precast segmental concrete bridge column for seismic regions." *Earthquake Spectra*, 29(4), 1441-1457.

Ou, Y.-C., Pratiwi, A. Y., and Song, J. (2018). "Pseudodynamic Testing and Inelastic Displacement Ratios of Self-Centering Precast Concrete Segmental Bridge Columns." *Journal of Structural Engineering*, 144(9), 04018158.

Ou, Y.-C., Wang, P.-H., Tsai, M.-S., Chang, K.-C., and Lee, G. C. (2009). "Large-scale experimental study of precast segmental unbonded posttensioned concrete bridge columns for seismic regions." *Journal of structural engineering*, 136(3), 255-264.

Ou, Y., Chiewanichakorn, M., Aref, A. J., and Lee, G. C. (2007). "Seismic performance of segmental precast unbonded posttensioned concrete bridge columns." *Journal of structural engineering*, 133(11), 1636-1647.

Ou, Y., Chiewanichakorn, M., Aref, A. J., and Lee, G. C. (2009). "Large-scale experimental study of precast segmental unbonded posttensioned concrete bridge columns for seismic regions." *Journal of structural engineering*, 136(3), 255-264.

Ou, Y. C., Tsai, M. S., Chang, K. C., and Lee, G. C. (2010). "Cyclic behavior of precast segmental concrete bridge columns with high performance or conventional steel reinforcing bars as energy dissipation bars." *Earthquake Engineering & Structural Dynamics*, 39(11), 1181-1198.

Padgett, J. E., and DesRoches, R. (2009). "Retrofitted bridge fragility analysis for typical classes of multispan bridges." *Earthquake Spectra*, 25(1), 117-141.

Palermo, A., and Mashal, M. (2012). "Accelerated bridge construction (ABC) and seismic damage resistant technology: a New Zealand challenge." *Bulletin of the New Zealand Society for Earthquake Engineering*, 45(3), 123-134.

Palermo, A., and Pampanin, S. "Analysis and simplified design of precast jointed ductile connections." *Proc., The 14th World Conference on Earthquake Engineering*.

Palermo, A., Pampanin, S., and Calvi, G. M. (2005). "Concept and development of hybrid solutions for seismic resistant bridge systems." *Journal of Earthquake Engineering*, 9(06), 899-921.

Palermo, A., Pampanin, S., and Marriott, D. (2007). "Design, modeling, and experimental response of seismic resistant bridge piers with posttensioned dissipating connections." *Journal of Structural Engineering*, 133(11), 1648-1661.

Palermo, A., Wotherspoon, L., Wood, J., Chapman, H., Scott, A., Hogan, L., Kivell, A., Camnasio, E., Yashinsky, M., and Bruneau, M. (2011). "Lessons learnt from 2011 Christchurch earthquakes: analysis and assessment of bridges." *Bulletin of the New Zealand Society for Earthquake Engineering*, 44(4), 319-333.

Palmeri, A., and Makris, N. (2008). "Response analysis of rigid structures rocking on viscoelastic foundation." *Earthquake Engineering & Structural Dynamics*, 37(7), 1039-1063.

Pampanin, S., Nigel Priestley, M., and Sritharan, S. (2001). "Analytical modelling of the seismic behaviour of precast concrete frames designed with ductile connections." *Journal of Earthquake Engineering*, 5(3), 329-367.

Pampanin, S., Priestley, M. N., and Sritharan, S. (2001). "Analytical modelling of the seismic behaviour of precast concrete frames designed with ductile connections." *Journal of Earthquake Engineering*, 5(03), 329-367.

Park, J., Bazzurro, P., and Baker, J. (2007). "Modeling spatial correlation of ground motion intensity measures for regional seismic hazard and portfolio loss estimation." *Applications of statistics and probability in civil engineering*, 1-8.

Parks, J. E., Brown, D. N., Ameli, M., and Pantelides, C. P. (2016). "Seismic repair of severely damaged precast reinforced concrete bridge columns connected with grouted splice sleeves." *ACI Structural Journal*, 113(3), 615.

PCI (2006). "Guidelines for Accelerated Bridge Construction using Precast/Prestressed Concrete Components." Report No. PCINER-06-ABC. Precast/Prestressed Concrete Institute, Chicago, IL.

PCI (2011). *Full Depth Deck Panels Guidelines*, Precast/Prestressed Concrete Institute North East, Belmont, MA.

PCI (2017). *Partial Depth Deck Panel Guidelines*, Precast/Prestressed Concrete Institute North East, Belmont, MA.

Perez, F. J., Sause, R., and Pessiki, S. (2007). "Analytical and experimental lateral load behavior of unbonded posttensioned precast concrete walls." *Journal of structural engineering*, 133(11), 1531-1540.

Petrini, L., Maggi, C., Priestley, M. N., and Calvi, G. M. (2008). "Experimental verification of viscous damping modeling for inelastic time history analyzes." *Journal of Earthquake Engineering*, 12(S1), 125-145.

Phan, V., Saiidi, M. S., Anderson, J., and Ghasemi, H. (2007). "Near-fault ground motion effects on reinforced concrete bridge columns." *Journal of structural engineering*, 133(7), 982-989.

Popa, V., Papurcu, A., Cotofana, D., and Pascu, R. (2015). "Experimental testing on emulative connections for precast columns using grouted corrugated steel sleeves." *Bulletin of Earthquake Engineering*, 13(8), 2429-2447.

Porter, K. (2020). "A beginner's guide to fragility, vulnerability, and risk." *Encyclopedia of earthquake engineering*, 235-260.

Priestley, M. (2000). "Performance based seismic design." *Bulletin of the New Zealand Society for Earthquake Engineering*, 33(3), 325-346.

Priestley, M. N., Seible, F., and Calvi, G. M. (1996). *Seismic design and retrofit of bridges*, John Wiley & Sons.

Priestley, M. N., Sritharan, S., Conley, J. R., and Pampanin, S. (1999). "Preliminary results and conclusions from the PRESSS five-story precast concrete test building." *PCI journal*, 44(6), 42-67.

Priestley, N., Calvi, M., Petrini, L., and Maggi, C. "Effects of damping modelling on results of time-history analysis of RC bridges." *Proc., 1st US-Italy Seismic Bridge Workshop, Pavia, Italia*.

Psycharis, I. N. (1990). "Dynamic behaviour of rocking two‐block assemblies." *Earthquake Engineering & Structural Dynamics*, 19(4), 555-575.

Psycharis, I. N., and Jennings, P. C. (1983). "Rocking of slender rigid bodies allowed to uplift." *Earthquake Engineering & Structural Dynamics*, 11(1), 57-76.

Rahmzadeh, A., Alam, M. S., and Tremblay, R. (2018). "Analytical Prediction and Finite-Element Simulation of the Lateral Response of Rocking Steel Bridge Piers with Energy-Dissipating Steel Bars." *Journal of Structural Engineering*, 144(11), 04018210.

Roberts, L., and Misra, A. (2010). "Performance-based design of deep foundation systems in load and resistance factor design framework." *Transportation Research Record: Journal of the Transportation Research Board*(2186), 29-37.

Roberts, L. A., Fick, D., and Misra, A. "Design of bridge foundations using a performance-based soil-structure interaction approach." *Proc., Proceedings of Structures Congress/North American Steel Construction Conference*.

Roddenberry, M. (2012). "Prefabricated/Precast Bridge Elements and Systems (PBES) for Off-System Bridges." Florida. Dept. of Transportation.

Roh, H., and Reinhorn, A. M. (2009). "Analytical modeling of rocking elements." *Engineering structures*, 31(5), 1179-1189.

Roh, H., and Reinhorn, A. M. (2010). "Hysteretic behavior of precast segmental bridge piers with superelastic shape memory alloy bars." *Engineering Structures*, 32(10), 3394-3403.

Rojahn, C., King, S. A., Scholl, R. E., Kiremidjian, A. S., Reaveley, L. D., and Wilson, R. R. (1997). "Earthquake damage and loss estimation methodology and data for Salt Lake County, Utah (ATC-36)." *Earthquake Spectra*, 13(4), 623-642.

Routledge, P., Cowan, M., and Palermo, A. "Low-damage detailing for bridges—a case study of Wigram–Magdala bridge." *Proc., Proceedings, New Zealand society for earthquake engineering 2016 conference. Christchurch*.

Sadrossadat-Zadeh, M., O'Brien, M., and Saiidi, M. S. (2007). "A Study of Concrete Bridge Columns Using Innovative Materials Subjected to Cyclic Loading." (Report No. CCEER-07-01). University of Nevada, Reno, Nevada: CCEER, Department of Civil Engineering.

Saiidi, M. S., Tazarv, M., Nakashoji, B., Varela, S., and Kavianipour, F. (2015). "Resilient and sustainable bridges of the future." *INTERNATIONAL JOURNAL OF BRIDGE ENGINEERING*, 3(2), 37-48.

Saiidi, M. S., Tazarv, M., Varela, S., Bennion, S., Marsh, M. L., Ghorbani, I., and Murphy, T. P. (2017). "Seismic Evaluation of Bridge Columns with Energy Dissipating Mechanisms, Volume 1: Research Overview."

Sakai, J., Jeong, H., and Mahin, S. "Earthquake simulator tests on the mitigation of residual displacements of reinforced concrete bridge columns." *Proc., Proc., 21st US-Japan Bridge Engineering Workshop*.

Sakai, J., Jeong, H., and Mahin, S. A. "Reinforced concrete bridge columns that re-center following earthquakes." *Proc., Proceedings of the 8th US national conference on earthquake engineering*, Citeseer, 18-22.

Sakai, J., and Mahin, S. A. "Mitigation of residual displacements of circular reinforced concrete bridge columns." *Proc., Proceedings, 13th World Conference on Earthquake Engineering*.

Salehi, M., and Sideris, P. "Nonlinear dynamic analysis of hybrid sliding-rocking bridges." *Proc., Geotechnical and Structural Engineering Congress 2016*, 90-102.

SCDOT (2008). "The South Carolina Department of Transportation (SCDOT) Seismic Design Specifications for Highway Bridges (Specifications)." Columbia, SC.

Schanack, F., Valdebenito, G., and Alvial, J. (2012). "Seismic damage to bridges during the 27 February 2010 magnitude 8.8 Chile earthquake." *Earthquake Spectra*, 28(1), 301-315.

SeismoSoft (2020). "A computer program for static and dynamic nonlinear analysis of framed structures."

Shafieifar, M., Farzad, M., and Azizinamini, A. (2018). "New Connection Detail to Connect Precast Column to Cap Beam using Ultra-High-Performance Concrete in Accelerated Bridge Construction Applications." *Transportation Research Record*, 0361198118792766.

Shamsabadi, A., Rollins, K. M., and Kapuskar, M. (2007). "Nonlinear soil–abutment–bridge structure interaction for seismic performance-based design." *Journal of geotechnical and geoenvironmental engineering*.

Shenton III, H. W. (1996). "Criteria for initiation of slide, rock, and slide-rock rigid-body modes." *Journal of Engineering Mechanics*, 122(7), 690-693.

Shim, C. S., Chung, C.-H., and Kim, H. H. (2008). "Experimental evaluation of seismic performance of precast segmental bridge piers with a circular solid section." *Engineering Structures*, 30(12), 3782-3792.

Shinozuka, M., Feng, M. Q., Kim, H.-K., and Kim, S.-H. (2000). "Nonlinear static procedure for fragility curve development." *Journal of Engineering Mechanics*.

Shinozuka, M., Feng, M. Q., Lee, J., and Naganuma, T. (2000). "Statistical analysis of fragility curves." *Journal of Engineering Mechanics*, 126(12), 1224-1231.

Shome, N. (1999). *Probabilistic seismic demand analysis of nonlinear structures*. Report No. RMS-35, RMS Program, Stanford University, Stanford, 1999

Sideris, P., Aref, A. J., and Filiatrault, A. (2014). "Large-scale seismic testing of a hybrid sliding-rocking posttensioned segmental bridge system." *Journal of Structural Engineering*, 140(6), 04014025.

Sideris, P., Aref, A. J., and Filiatrault, A. (2015). "Experimental seismic performance of a hybrid sliding–rocking bridge for various specimen configurations and seismic loading conditions." *Journal of Bridge Engineering*, 20(11), 04015009.

Somerville, P. G. (1997). *Development of ground motion time histories for phase 2 of the FEMA/SAC steel project*, SAC Joint Venture.

Spanos, P. D., and Koh, A.-S. (1984). "Rocking of rigid blocks due to harmonic shaking." *Journal of Engineering Mechanics*, 110(11), 1627-1642.

Spanos, P. D., Roussis, P. C., and Politis, N. P. (2001). "Dynamic analysis of stacked rigid blocks." *Soil Dynamics and Earthquake Engineering*, 21(7), 559-578.

Stein, S. M., Young, G. K., Trent, R. E., and Pearson, D. R. (1999). "Prioritizing scour vulnerable bridges using risk." *Journal of Infrastructure Systems*, 5(3), 95-101.

Steuck, K. P., Cohagen, L., Stanton, J. F., and Eberhard, M. O. (2008). "Rapidly Constructible Large-Bar Precast Bridge-Bent Seismic Connection." Washington, DC United States.

Stewart, J. P., Comartin, C., and Moehle, J. P. "Implementation of soil-structure interaction models in performance based design procedures." *Proc., Proc. 13th World Conf. Earthquake Engrg*.

Tang, L., Ling, X., Xu, P., Gao, X., and Wang, D. (2010). "Shake table test of soil-pile groups-bridge structure interaction in liquefiable ground." *Earthquake Engineering and Engineering Vibration*, 9(1), 39-50.

Tazarv, M., and Saiid Saiidi, M. (2016). "Low-damage precast columns for accelerated bridge construction in high seismic zones." *Journal of Bridge Engineering*, 21(3), 04015056.

Tazarv, M., and Saiidi, M. S. "Emulative moment-resistant RC bridge column-footing connection for accelerated bridge construction in high seismic zone." *Proc., Proceedings of the 7th National Seismic Conference on Bridges & Highways*.

Tazarv, M., and Saiidi, M. S. (2015). "design and construction of precast bent caps with pocket connections for high seismic regions." Center For Civil Engineering Earthquake Research, Department Of Civil and Environmental Engineering, University of Nevada, Reno, Nevada, Report No. CCEER-15-06, August 2015.

Tazarv, M., and Saiidi, M. S. (2015). "UHPC-filled duct connections for accelerated bridge construction of RC columns in high seismic zones." *Engineering Structures*, 99, 413-422.

Terzic, V., and Stojadinovic, B. (2010). "Post-earthquake traffic capacity of modern bridges in California." (No. CA/PEER/2010-103). California. Dept. of Transportation. Division of Research and Innovation.

Thonstad, T., Mantawy, I. M., Stanton, J. F., Eberhard, M. O., and Sanders, D. H. (2016). "Shaking table performance of a new bridge system with pretensioned rocking columns." *Journal of Bridge Engineering*, 21(4), 04015079.

Tobolski, M. J., Ralls, M. L., Matsumoto, E. E., and Restrepo, J. I. "State-of-Practice of Precast Bent Cap Systems." *Proc., Structures Congress 2006: Structural Engineering and Public Safety*, 1-10.

Tran, H., Eberhard, M., Stanton, J., and Marsh, L. (2014). "seismic-resistant, abc connection between precast concrete columns and drilled shafts." Seattle, Washington: University of Washington.

Tran, H. V., Stanton, J. F., and Eberhard, M. O. (2013). "Precast bent system for high seismic regions: Laboratory tests of column-to-drilled shaft socket connections." Seattle, Washington: University of Washington.

Trono, W., Jen, G., Panagiotou, M., Schoettler, M., and Ostertag, C. P. (2014). "Seismic response of a damage-resistant recentering posttensioned-HYFRC bridge column." *Journal of Bridge Engineering*, 20(7), 04014096.

Trono, W. D. (2014). "Earthquake resilient bridge columns utilizing damage resistant hybrid fiber reinforced concrete." UC Berkeley.

Turner, J. (2006). "Rock-socketed shafts for highway structure foundations: a synthesis of highway practice. NCHRP Synthesis 360. National Cooperative Highway Research Program (NCHRP)." *Transportation Research Board, Washington, DC*.

UDOT (2015). "Utah DOT Structures Design and Detailing Manual." *Utah Department of Transportation*.

Varela, S., and Saiidi, M. (2017). "Resilient deconstructible columns for accelerated bridge construction in seismically active areas." *Journal of Intelligent Material Systems and Structures*, 28(13), 1751-1774.

Vassiliou, M. F., and Makris, N. (2015). "Dynamics of the vertically restrained rocking column." *Journal of Engineering Mechanics*, 141(12), 04015049.

Vassiliou, M. F., Truniger, R., and Stojadinović, B. (2015). "An analytical model of a deformable cantilever structure rocking on a rigid surface: development and verification." *Earthquake Engineering & Structural Dynamics*, 44(15), 2775-2794.

Wang, J., Wang, Z., Tang, Y., Liu, T., and Zhang, J. (2018). "Cyclic loading test of self-centering precast segmental unbonded posttensioned UHPFRC bridge columns." *Bulletin of Earthquake Engineering*, 1-29.

Wang, J. C., Ou, Y. C., Chang, K. C., and Lee, G. C. (2008). "Large‐scale seismic tests of tall concrete bridge columns with precast segmental construction." *Earthquake Engineering & Structural Dynamics*, 37(12), 1449-1465.

Wang, Z., Padgett, J. E., and Dueñas-Osorio, L. (2014). "Toward a uniform seismic risk design of reinforced concrete bridges: A displacement-based approach." *Structural Safety*, 50, 103-112.

Wang, Z., Wang, J.-Q., Tang, Y.-C., Liu, T.-X., Gao, Y.-F., and Zhang, J. (2018). "Seismic behavior of precast segmental UHPC bridge columns with replaceable external cover plates and internal dissipaters." *Engineering Structures*, 177, 540-555.

Weatherill, G., Silva, V., Crowley, H., and Bazzurro, P. (2015). "Exploring the impact of spatial correlations and uncertainties for portfolio analysis in probabilistic seismic loss estimation." *Bulletin of Earthquake Engineering*, 13(4), 957-981.

Wen, Y. (2001). "Minimum lifecycle cost design under multiple hazards." *Reliability Engineering & System Safety*, 73(3), 223-231.

White, S., and Palermo, A. (2016). "Quasi-static testing of posttensioned nonemulative column-footing connections for bridge piers." *Journal of Bridge Engineering*, 21(6), 04016025.

Whitman, R. V., Anagnos, T., Kircher, C. A., Lagorio, H. J., Lawson, R. S., and Schneider, P. (1997). "Development of a national earthquake loss estimation methodology." *Earthquake Spectra*, 13(4), 643-661.

Winkler, T., Meguro, K., and Yamazaki, F. (1995). "Response of rigid body assemblies to dynamic excitation." *Earthquake Engineering and Structural Dynamics*, 24(10), 1389-1408.

WisDOT (2017). "WisDOT Bridge Manual." *Wisconsin Department of Transportation*.

Wong, I. G., Silva, W., Olig, S., Thomas, P., Wright, D., Ashland, F., Gregor, N., Pechmann, J., Dober, M., and Christenson, G. (2002). *Earthquake scenario and probabilistic ground shaking maps for the Salt Lake City, Utah, metropolitan area*, Utah Geological Survey.

WSDOT (2016). "Bridge Design Manual LRFD." Washington State *Department of Transportation (WSDOT)*.

WSDOT (2017). "Bridge Design Manual (LRFD)." *Washington State Department of Transportation (WSDOT)*.

Xiang, N., and Alam, M. S. (2019). "Displacement-based seismic design of bridge bents retrofitted with various bracing devices and their seismic fragility assessment under near-fault and far-field ground motions." *Soil Dynamics and Earthquake Engineering*, 119, 75-90.

Yamane, T., Tadros, M. K., Badie, S. S., and Baishya, M. C. (1998). "Full depth precast, prestressed concrete bridge deck system." *PCI Journal*, 43(3).

Yamashita, R., and Sanders, D. H. (2009). "Seismic performance of precast unbonded prestressed concrete columns." *ACI Structural Journal*, 106(06).

Yang, C., and Okumus, P. (2017). "Ultrahigh-Performance Concrete for Posttensioned Precast Bridge Piers for Seismic Resilience." *Journal of Structural Engineering*, 143(12), 04017161.

Yazgan, U., and Dazio, A. (2011). "Simulating maximum and residual displacements of RC structures: I. Accuracy." *Earthquake Spectra*, 27(4), 1187-1202.

Yim, C. S., Chopra, A. K., and Penzien, J. (1980). "Rocking response of rigid blocks to earthquakes." *Earthquake Engineering & Structural Dynamics*, 8(6), 565-587.

Yousif, A. A. (1995). "Field performance of full depth precast concrete panels in bridge deck reconstruction." University of Illinois at Chicago Chicago, Illinois.

Zatar, W. A., and Mutsuyoshi, H. (2002). "Residual displacements of concrete bridge piers subjected to near field earthquakes." *Structural Journal*, 99(6), 740-749.

Zhang, J., and Makris, N. (2001). "Rocking response of free-standing blocks under cycloidal pulses." *Journal of Engineering Mechanics*, 127(5), 473-483.

Zhang, N., Lan, H., Gao, W., Tang, G., and Lee, G. (2014). "Shake Table Study of Bridge with Precast Post-Tensioned Segmental Columns." *Challenges and Advances in Sustainable Transportation Systems*, 555-562.

Zhang, Q., and Alam, M. S. "The Dynamics of Precast Post-Tensioned Rocking Columns." *Proc., Structures Congress*.

Zhang, Q., Alam, M. S., Khan, S., and Jiang, J. (2016). "Seismic performance comparison between force-based and performance-based design as per Canadian Highway Bridge Design Code (CHBDC) 2014." *Canadian Journal of Civil Engineering*(ja).

Zhang, Q., Alam, M. S., Khan, S., and Jiang, J. (2016). "Seismic performance comparison between force-based and performance-based design as per Canadian Highway Bridge Design Code (CHBDC) 2014." *Canadian Journal of Civil Engineering*, 43(8), 741-748.

Zohrevand, P., and Mirmiran, A. (2011). "Cyclic behavior of hybrid columns made of ultra high performance concrete and fiber reinforced polymers." *Journal of Composites for Construction*, 16(1), 91-99.

Appendices

Appendix A

Design example of hybrid rocking column

A design example using the proposed equations in this thesis and displacement-based design method is presented in this appendix. It is assumed that the bridge is located in Vancouver, BC, Canada with a site condition of Class E Soil as defined in the Canadian Highway Bridge Design Code (CSA, 2014). The acceleration response spectra are downloaded from Natural Resources Canada, which is shown in Figure 82 (with 5% damping). Acceleration response spectra are converted to displacement response spectra using Equation 71 and the displacement response spectra are shown in Figure 83.

The bridge is 11 m wide and 145 m long with three continuous spans. The span lengths are 30 m, 70 m and 45 m. The superstructure is composed of a concrete deck and three lines of steel plate girders. The weight of the superstructure is approximately 80 kN/m. Bridge bearings are used at piers to release rotations and at abutments to release rotations and longitudinal translation. Two 9.5 m tall columns will be designed to support the bridge under seismic loadings. The columns provide both longitudinal and transverse seismic load paths and the abutments only provide transverse seismic load paths. Assume the design criterion is to limit the longitudinal and transverse column drifts to 3% at a 2475-year earthquake. A screenshot of the bridge model is shown in Figure 84.

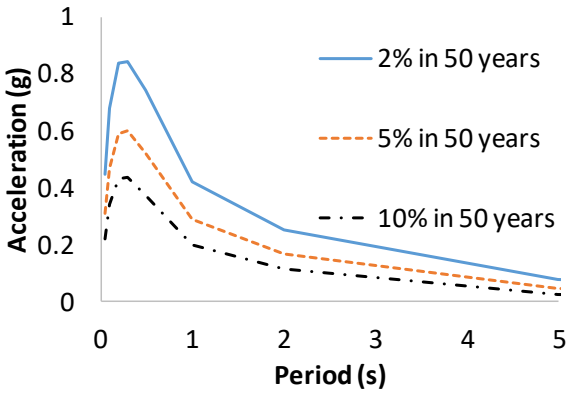

Figure 82 Acceleration spectra (Class C, 5% damping)

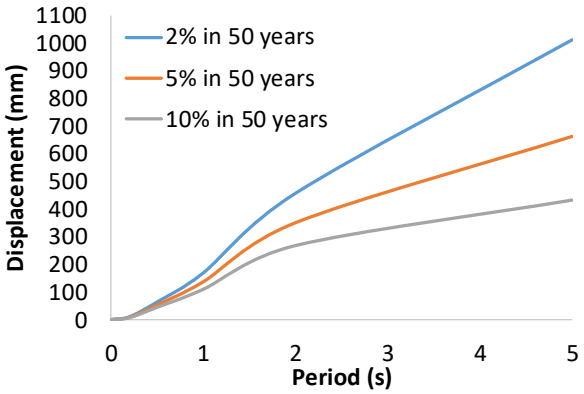

Figure 83 Displacement spectra (Class C, 5% damping)

$$S_d(T) = 250 \times S(T) \times T^2$$ Equation 71

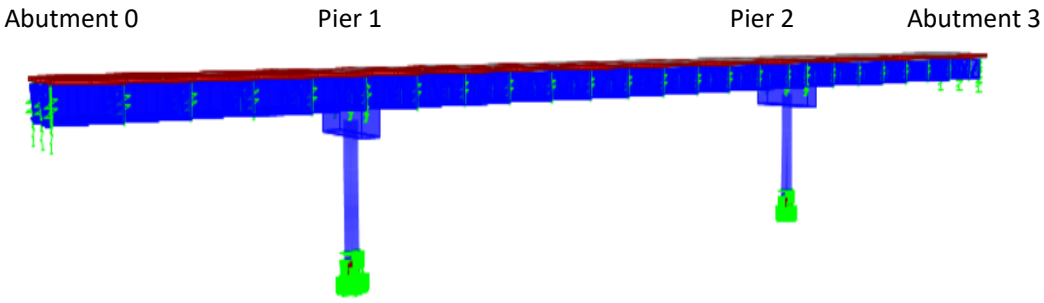

Figure 84 Three-span bridge model screenshot

Based on the design criterion of 3% drift, the column maximum displacement limit is about 0.285 m in both longitudinal and transverse directions. In displacement-based design, the bridge system is simplified to an equivalent single degree of freedom system. In the longitudinal direction, the system displacement is equal to the column displacement as the two columns deform simultaneously. The effective mass in the longitudinal direction is equal to the total mass of the bridge. In the transverse direction, a parabolic deformed shape is assumed, therefore, it is likely that Pier 2 governs the design. When Pier 2 deforms 0.285 m, the corresponding Pier 1 displacement is about 0.22 m. In the preliminary design, it is assumed that the abutments are relatively stiff and the displacement at the maximum design earthquake is 0.01 m. Meanwhile, as suggested by Chen and Duan (2014), it is assumed that the abutments take about 50% of the total transverse seismic forces in the first iteration. The effective design displacement of the system can be calculated using Equation 72 and the effective mass can be calculated using Equation 73. In the bridge transverse direction, the effective displacement is 0.26 m and the effective mass is 886,900 kg.

$$\Delta \mathrm{d} = \frac{\sum_{i=1}^{n}(m_i \Delta_i^2)}{\sum_{i=1}^{n}(m_i \Delta_i\ )} \qquad \text{Equation 72}$$

$$\mathrm{m}_e = \frac{\sum_{i=1}^{n}(m_i \Delta_i\ )}{\Delta_d} \qquad \text{Equation 73}$$

In displacement-based design, equivalent viscous damping is incorporated so that the design displacement is smaller than that corresponding to 5% damping. The equivalent viscous damping is usually calculated as a function of displacement ductility demand. However, for hybrid rocking columns, it is more complicated to determine the ductility demand as it is related to a number of variables such as ED bar strength, ED bar debonding length, PT strand design and so on. It is first assumed that yielding occurs at 1.0% drift in preliminary design. Therefore, the design displacement ductility corresponding to 3% would be a displacement ductility factor of 3. The equivalent viscous damping can be estimated using Equation 74. In this equation, the

equivalent viscous damping is a function of ductility and recentering ratio. Recentering ratio is defined in Equation 75, which describes the relative magnitude of dead load, the strength of PT and ED bars. The higher the ratio is, the less permanent deformation there would be. In the calculation of equivalent viscous damping, the recentering factor is assumed to be 1.3, which is equal to the overstrength factor in the Canadian Highway Bridge Design Code (CSA, 2014). Thus, Equation 74 yields viscous damping of 10%. The displacement response spectra for 5% damping can be reduced to spectra for 10% damping using Equation 76 (Chen and Duan, 2014), which is shown in Figure 85.

$$\vartheta = 0.05 + \frac{0.16}{\lambda_{\mathrm{re}}} \times \left(1 - \frac{1}{\sqrt{\mathrm{R}}}\right) \quad \text{Equation 74}$$

$$\lambda_{re} = \frac{D + A_p f_{pi}}{A_s f_y} \quad \text{Equation 75}$$

$$R = \left(\frac{0.07}{0.02 + \vartheta}\right) \quad \text{Equation 76}$$

where ϑ is the equivalent viscous damping ratio, λ_{re} is the recentering ratio, R is the displacement ductility, D is dead load, Ap is tendon area; f_{pi} is tendon initial stress, A_s is ED bar area, f_y is the yield strength of ED bar.

By entering the displacement response spectra with 0.285 m and 0.260 m in Figure 14, the corresponding longitudinal and transverse structural periods are 1.70 s and 1.55 s. Based on the effective period, transverse and longitudinal stiffnesses can be calculated using Equation 77. In the longitudinal direction, the two piers take 50% of seismic forces each since they have the same height, and abutments do not participate in the longitudinal seismic load path. In the transverse direction, it is assumed that the two piers take 50% of overall seismic force and the abutments take the rest of 50% seismic force. The two piers would take a different amount of force due to unequal span arrangement. However, in the first iteration, it is simply assumed that each pier takes 25% of the total seismic forces. The transverse and longitudinal shear demands

of each pier are approximately 900 kN and 2100 kN, respectively. A summary of the calculation results is shown in Table 26 for the convenience of readers.

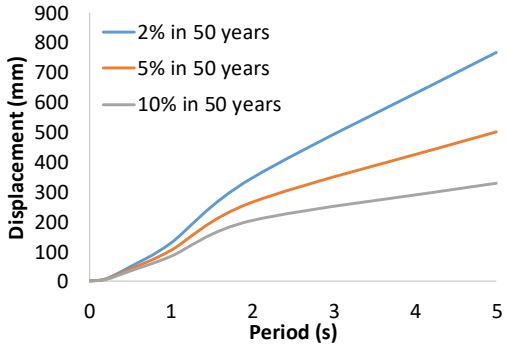

Figure 85 Displacement spectra for Class C soil (10% damping)

$$K_e = \frac{4\pi^2 m_e}{T_e^2}$$ Equation 77

In seismic regions, columns are generally sized such that the axial dead load to capacity ratio is about 10%. Based on a static analysis of dead load, Pier 1 takes 4611 kN vertical dead load and Pier 2 takes 5062 kN dead load. Considering a concrete strength of 35 MPa, the approximate circular column size is 1.5 m, which results in axial load ratios of 7% and 8% for Pier 1 and Pier 2, respectively.

Table 26 Displacement-based design calculation summary

	Transverse	Longitudinal
Effective design displacement, m	0.260	0.285
Effective mass, kg	886,908	1,183,673
Effective stiffness, kN/m	3,886	3,811
Total seismic force, kN	993	1,086
Column shear demand, kN	250	550

In terms of the reinforcement design, the prestressing force after losses should be large enough to generate a re-centering factor greater than 1.3. In the meantime, it should not be excessive to cause high axial force which would reduce the post-elastic stiffness under seismic events. In this design example, the longitudinal ED bars are set to 1% of the column section area, which is to meet the minimum rebar requirement from most design codes. Then, based on 1% ED bar

which yields at 400 MPa, the prestressing force is set to be 4050 kN such that the recentering factor is 1.3. The prestressing force is provided by two tendons with 19-15mm strands and 1860 MPa ultimate strength. A simplified equation (Equation 78) can be used to calculate the tendon elongation caused by the rocking response. For a drift of 3%, the corresponding tendon strain is 0.002, conservatively assuming c is 0. The total tendon stress is the prestressing stress plus the additional stress caused by rocking. The prestressing force of 4050 kN corresponds to a stress of 760 MPa. Therefore, the total tendon stress is about 1235 MPa, which is 67% of tendon's ultimate strength.

$$\Delta_{pt} = \theta\left(\frac{h}{2} - c\right) \qquad \text{Equation 78}$$

where Δ_{pt} is tendon elongation due to rotation (θ), h is the total depth of the section and c is the neutral axis depth.

To summarize the design outcome, the above calculations generate the following preliminary design results in Table 27.

Table 27 Design results

Design inputs	Concrete (f_c)	Reinforcing steel (f_y)	Strands (f_{pu})	Axial load ratio	
	35 MPa	400 MPa	1860 MPa	7% and 8%	
Parameter	Column height	Column Diameter	Longitudinal Rebar ratio	Tendon	Effective prestress
Results	9.5 m	1.5m	1%	2 tendons 19-15mm strands	67% f_{pu}

Appendix B

		Basic design					Generaterd from Basic design		H/D		ρs		ρl		ADLR		h/D		fp		f´c	
Experiment	Column stiffness	H/D	ρs	ρl	ALR	h/D	fp	f´c	a	a	b	b	c	c	d	d	e	e	f	f	g	g
No.	N/mm	A	B	C	D	E	F=ABCD	G=ABDE	1	-1	1	-1	1	-1	1	-1	1	-1	1	-1	1	-1
1	49723	-1	-1	-1	-1	-1	1	1	0	49723	0	49723	0	49723	0	49723	0	49723	49723	0	49723	0
2	6961	1	-1	-1	-1	-1	-1	-1	6961	0	0	6961	0	6961	0	6961	0	6961	0	6961	0	6961
3	37118	-1	1	-1	-1	-1	-1	-1	0	37118	37118	0	0	37118	0	37118	0	37118	0	37118	0	37118
4	12015	1	1	-1	-1	-1	1	1	12015	0	12015	0	0	12015	0	12015	0	12015	12015	0	12015	0
5	44982	-1	-1	1	-1	-1	-1	1	0	44982	0	44982	44982	0	0	44982	0	44982	0	44982	44982	0
6	9113	1	-1	1	-1	-1	1	-1	9113	0	0	9113	9113	0	0	9113	0	9113	9113	0	0	9113
7	42849	-1	1	1	-1	-1	1	-1	0	42849	42849	0	42849	0	0	42849	0	42849	42849	0	0	42849
8	8312	1	1	1	-1	-1	-1	1	8312	0	8312	0	8312	0	0	8312	0	8312	0	8312	8312	0
9	35250	-1	-1	-1	1	-1	-1	-1	0	35250	0	35250	0	35250	35250	0	0	35250	0	35250	0	35250
10	10708	1	-1	-1	1	-1	1	1	10708	0	0	10708	0	10708	10708	0	0	10708	10708	0	10708	0
11	51041	-1	1	-1	1	-1	1	1	0	51041	51041	0	0	51041	51041	0	0	51041	51041	0	51041	0
12	7458	1	1	-1	1	-1	-1	-1	7458	0	7458	0	0	7458	7458	0	0	7458	0	7458	0	7458
13	36895	-1	-1	1	1	-1	1	-1	0	36895	0	36895	36895	0	36895	0	0	36895	36895	0	0	36895
14	10783	1	-1	1	1	-1	-1	1	10783	0	0	10783	10783	0	10783	0	0	10783	0	10783	10783	0
15	44827	-1	1	1	1	-1	-1	1	0	44827	44827	0	44827	0	44827	0	0	44827	0	44827	44827	0
16	9137	1	1	1	1	-1	1	-1	9137	0	9137	0	9137	0	9137	0	0	9137	9137	0	0	9137
17	39817	-1	-1	-1	-1	1	1	-1	0	39817	0	39817	0	39817	0	39817	39817	0	39817	0	0	39817
18	10523	1	-1	-1	-1	1	-1	1	10523	0	0	10523	0	10523	0	10523	10523	0	0	10523	10523	0
19	55978	-1	1	-1	-1	1	-1	1	0	55978	55978	0	0	55978	0	55978	55978	0	0	55978	55978	0
20	9464	1	1	-1	-1	1	1	-1	9464	0	9464	0	0	9464	0	9464	9464	0	9464	0	0	9464
21	33975	-1	-1	1	-1	1	-1	-1	0	33975	0	33975	33975	0	0	33975	33975	0	0	33975	0	33975
22	9118	1	-1	1	-1	1	1	1	9118	0	0	9118	9118	0	0	9118	9118	0	9118	0	9118	0
23	50434	-1	1	1	-1	1	1	1	0	50434	50434	0	50434	0	0	50434	50434	0	50434	0	50434	0
24	6808	1	1	1	-1	1	-1	-1	6808	0	6808	0	6808	0	0	6808	6808	0	0	6808	0	6808
25	49176	-1	-1	-1	1	1	-1	1	0	49176	0	49176	0	49176	49176	0	49176	0	0	49176	49176	0
26	7327	1	-1	-1	1	1	1	-1	7327	0	0	7327	0	7327	7327	0	7327	0	7327	0	0	7327
27	29574	-1	1	-1	1	1	1	-1	0	29574	29574	0	0	29574	29574	0	29574	0	29574	0	0	29574
28	11588	1	1	-1	1	1	-1	1	11588	0	11588	0	0	11588	11588	0	11588	0	0	11588	11588	0
29	50178	-1	-1	1	1	1	1	1	0	50178	0	50178	50178	0	50178	0	50178	0	50178	0	50178	0
30	8632	1	-1	1	1	1	-1	-1	8632	0	0	8632	8632	0	8632	0	8632	0	0	8632	0	8632
31	37111	-1	1	1	1	1	-1	-1	0	37111	37111	0	37111	0	37111	0	37111	0	0	37111	0	37111
32	11562	1	1	1	1	1	1	1	11562	0	11562	0	11562	0	11562	0	11562	0	11562	0	11562	0
Sum of highs and lows									149508	688929	425276	413161	414715	423722	411246	427190	421264	417172	428956	409481	480949	357488
Difference of high and low/ overall difference of high and low									0.75		0.02		0.01		0.02		0.01		0.03		0.17	

		Basic design					erateerd from Basic de		H/D		ρs		ρl		ADLR		h/D		fp		f´c	
		H/D	ρs	ρl	ALR	h/D	fp	f´c	a	a	b	b	c	c	d	d	e	e	f	f	g	g
Experiment No.	Yield force N	A	B	C	D	E	F=ABCD	G=ABDE	1	-1	1	-1	1	-1	1	-1	1	-1	1	-1	1	-1
1	197395.1783	-1	-1	-1	-1	-1	1	1	0	197395.2	0	197395.2	0	197395.2	0	197395.2	0	197395.2	197395.2	0	197395.2	0
2	54379.46626	1	-1	-1	-1	-1	-1	-1	54379.47	0	0	54379.47	0	54379.47	0	54379.47	0	54379.47	0	54379.47	0	54379.47
3	99199.23529	-1	1	-1	-1	-1	-1	-1	0	99199.24	99199.24	0	0	99199.24	0	99199.24	0	99199.24	0	99199.24	0	99199.24
4	105217.248	1	1	-1	-1	-1	1	1	105217.2	0	105217.2	0	0	105217.2	0	105217.2	0	105217.2	105217.2	0	105217.2	0
5	123516.3383	-1	-1	1	-1	-1	-1	1	0	123516.3	0	123516.3	123516.3	0	0	123516.3	0	123516.3	0	123516.3	123516.3	0
6	86210.10714	1	-1	1	-1	-1	1	-1	86210.11	0	0	86210.11	86210.11	0	0	86210.11	0	86210.11	86210.11	0	0	86210.11
7	168566.8899	-1	1	1	-1	-1	1	-1	0	168566.9	168566.9	0	168566.9	0	0	168566.9	0	168566.9	168566.9	0	0	168566.9
8	67902.42291	1	1	1	-1	-1	-1	1	67902.42	0	67902.42	0	67902.42	0	0	67902.42	0	67902.42	0	67902.42	67902.42	0
9	248772.7813	-1	-1	-1	1	-1	-1	-1	0	248772.8	0	248772.8	0	248772.8	248772.8	0	0	248772.8	0	248772.8	0	248772.8
10	192617.7698	1	-1	-1	1	-1	1	1	192617.8	0	0	192617.8	0	192617.8	192617.8	0	0	192617.8	192617.8	0	192617.8	0
11	445720.7081	-1	1	-1	1	-1	1	1	0	445720.7	445720.7	0	0	445720.7	445720.7	0	0	445720.7	445720.7	0	445720.7	0
12	132743.2295	1	1	-1	1	-1	-1	-1	132743.2	0	132743.2	0	0	132743.2	132743.2	0	0	132743.2	0	132743.2	0	132743.2
13	280357.3664	-1	-1	1	1	-1	1	-1	0	280357.4	0	280357.4	280357.4	0	280357.4	0	0	280357.4	280357.4	0	0	280357.4
14	176058.5177	1	-1	1	1	-1	-1	1	176058.5	0	0	176058.5	176058.5	0	176058.5	0	0	176058.5	0	176058.5	176058.5	0
15	399389.0979	-1	1	1	1	-1	-1	1	0	399389.1	399389.1	0	399389.1	0	399389.1	0	0	399389.1	0	399389.1	399389.1	0
16	140711.1552	1	1	1	1	-1	1	-1	140711.2	0	140711.2	0	140711.2	0	140711.2	0	0	140711.2	140711.2	0	0	140711.2
17	160557.1022	-1	-1	-1	-1	1	1	-1	0	160557.1	0	160557.1	0	160557.1	0	160557.1	160557.1	0	160557.1	0	0	160557.1
18	68641.6865	1	-1	-1	-1	1	-1	1	68641.69	0	0	68641.69	0	68641.69	0	68641.69	68641.69	0	0	68641.69	68641.69	0
19	120672.2632	-1	1	-1	-1	1	-1	1	0	120672.3	120672.3	0	0	120672.3	0	120672.3	120672.3	0	0	120672.3	120672.3	0
20	91769.44535	1	1	-1	-1	1	1	-1	91769.45	0	91769.45	0	0	91769.45	0	91769.45	91769.45	0	91769.45	0	0	91769.45
21	95628.36889	-1	-1	1	-1	1	-1	-1	0	95628.37	0	95628.37	95628.37	0	0	95628.37	95628.37	0	0	95628.37	0	95628.37
22	109572.6798	1	-1	1	-1	1	1	1	109572.7	0	0	109572.7	109572.7	0	0	109572.7	109572.7	0	109572.7	0	109572.7	0
23	197381.3841	-1	1	1	-1	1	1	1	0	197381.4	197381.4	0	197381.4	0	0	197381.4	197381.4	0	197381.4	0	197381.4	0
24	55992.92474	1	1	1	-1	1	-1	-1	55992.92	0	55992.92	0	55992.92	0	0	55992.92	55992.92	0	0	55992.92	0	55992.92
25	367929.3743	-1	-1	-1	1	1	-1	1	0	367929.4	0	367929.4	0	367929.4	367929.4	0	367929.4	0	0	367929.4	367929.4	0
26	144221.4436	1	-1	-1	1	1	1	-1	144221.4	0	0	144221.4	0	144221.4	144221.4	0	144221.4	0	144221.4	0	0	144221.4
27	318232.5955	-1	1	-1	1	1	1	-1	0	318232.6	318232.6	0	0	318232.6	318232.6	0	318232.6	0	318232.6	0	0	318232.6
28	193424.5819	1	1	-1	1	1	-1	1	193424.6	0	193424.6	0	0	193424.6	193424.6	0	193424.6	0	0	193424.6	193424.6	0
29	386563.4004	-1	-1	1	1	1	1	1	0	386563.4	0	386563.4	386563.4	0	386563.4	0	386563.4	0	386563.4	0	386563.4	0
30	110873.1573	1	-1	1	1	1	-1	-1	110873.2	0	0	110873.2	110873.2	0	110873.2	0	110873.2	0	0	110873.2	0	110873.2
31	251114.048	-1	1	1	1	1	-1	-1	0	251114	251114	0	251114	0	251114	0	251114	0	0	251114	0	251114
32	203780.0742	1	1	1	1	1	1	1	203780.1	0	203780.1	0	203780.1	0	203780.1	0	203780.1	0	203780.1	0	203780.1	0
Sum of highs and lows									1934116	3860996	2991817	2803295	2853618	2941494	3992509	1802603	2876355	2918758	3228875	2566237	3355783	2439329
Difference of high and low/ overall difference of high and low									0.32		0.03		0.01		0.36		0.01		0.11		0.15	

Appendix C

Hysteretic curves of hybrid rocking columns under the ground motion recorded at El Centro Array #9 during 1968 Borrego Mountain earthquake event. The columns are named as L(ED bar ratio)A(axial load ratio) D(column diameter). For instance, L0.5A10D0.6 is a column with longitudinal ED bar ratio of 0.5%, axial load ratio of 10% and column diameter of 0.6m.

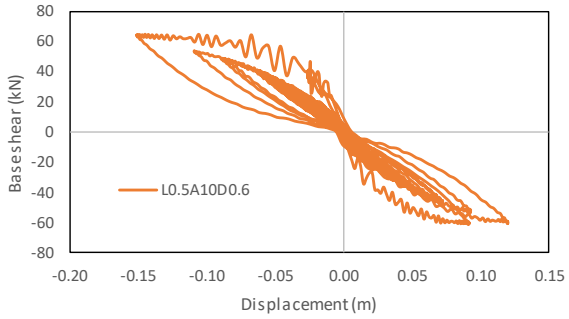

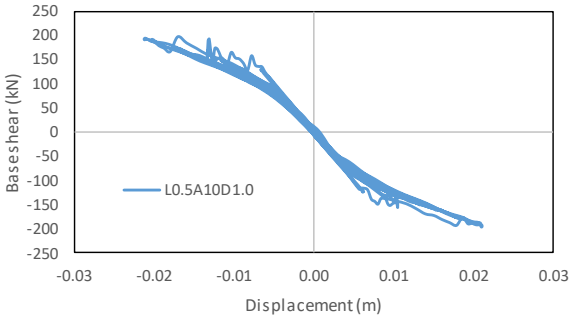

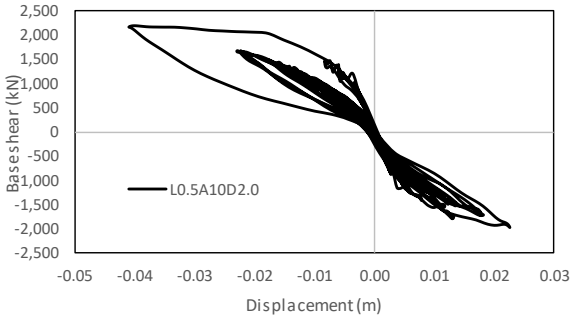

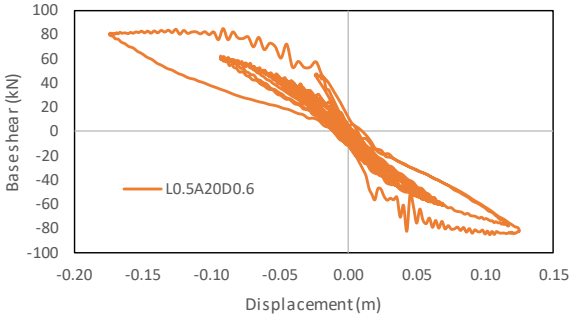

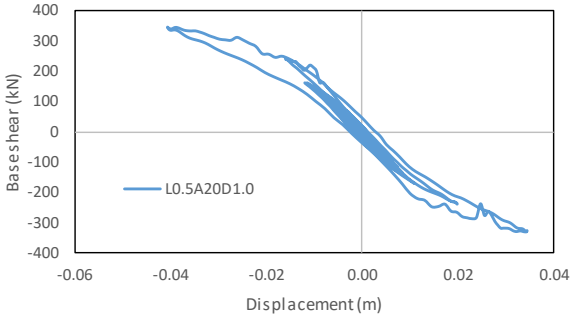

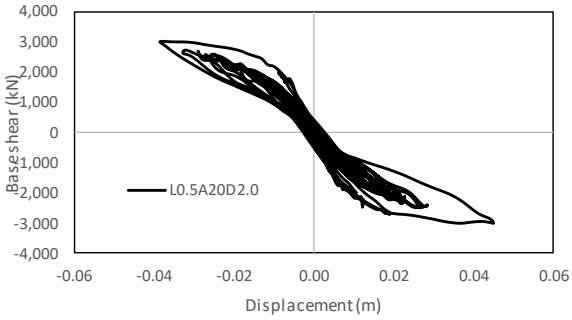

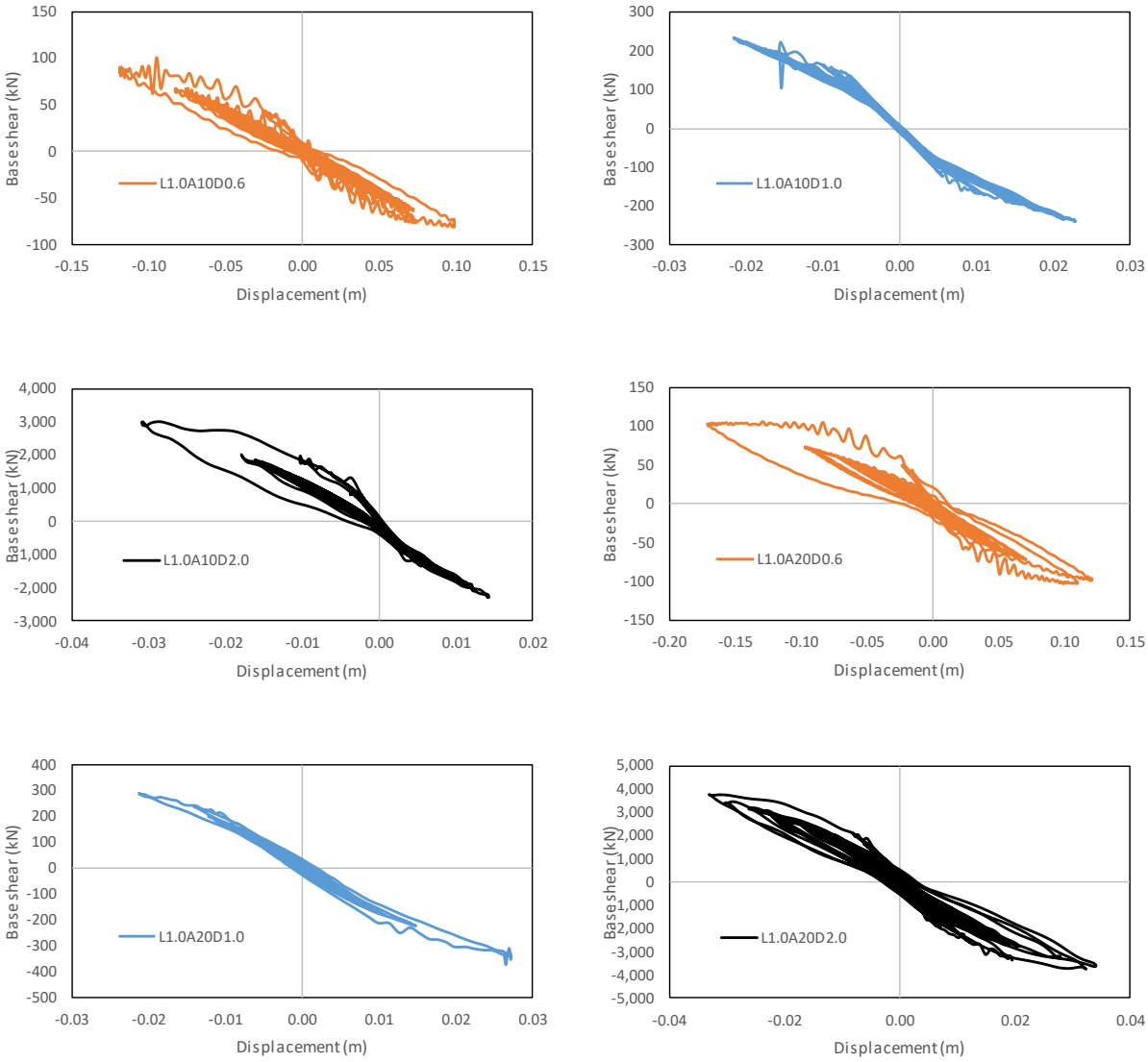

Figure 86 Hysteretic curves of hybrid columns, 1968 Borrego Mountain earthquake event